

©Copyright 2016

Ryan M. Ziels

Recovering biomethane from fats, oils, and greases:  
Examining the impacts of microbial ecology on anaerobic codigester stability and bioconversion  
kinetics

Ryan M. Ziels

A dissertation

submitted in partial fulfillment of the  
requirements for the degree of

Doctor of Philosophy

University of Washington

2016

Reading Committee:

H. David Stensel, Chair

David Stahl

David Beck

Program Authorized to Offer Degree:

Civil and Environmental Engineering

University of Washington

**Abstract**

Recovering biomethane from fats, oils, and greases: Examining the impacts of microbial ecology on anaerobic codigester stability and bioconversion kinetics

Ryan M. Ziels

Chair of the Supervisory Committee:  
Professor H. David Stensel  
Civil and Environmental Engineering

Recovering biomethane with anaerobic digestion is of global interest to reduce carbon footprints and improve process economics for the treatment of organic wastes. Fats, oils, and greases (FOG) are desirable co-substrates for biomethane recovery because they have a substantially higher energy density than wastewater treatment solids or livestock manure. Yet, biomethane recovery from FOG codigestion at wastewater treatment plants or agricultural digesters can be limited due to process inhibition caused by long-chain fatty acids (LCFA) accumulation.

Currently, there is a lack of understanding regarding the role of anaerobic digester microbial communities in maintaining efficient conversion of LCFA into biomethane. The ultimate goal of this research was to improve the reliability of biomethane recovery during FOG codigestion by elucidating relationships between microbial community composition and LCFA bioconversion kinetics.

The ability to accurately monitor LCFA-degrading populations in anaerobic digesters was obtained by developing and validating quantitative PCR (qPCR) assays for the syntrophic LCFA

$\beta$ -oxidizing genera of *Syntrophomonas* and *Syntrophus*. These qPCR assays were then utilized to measure population changes in a codigester treating FOG and municipal wastewater treatment solids at increasing FOG loadings for over 150 days. A relationship was developed that correlated higher effluent LCFA concentrations with higher influent FOG loading rates normalized to digester *Syntrophomonas* 16S rRNA gene concentrations. Subsequently, the impacts of LCFA feeding strategy on LCFA bioconversion kinetics were investigated using bench-scale codigesters that were either pulse-fed every two days or continuously-fed daily with oleate. The results showed that *Bacteria* and *Archaea* community compositions in the codigesters diverged based on LCFA feeding frequency and LCFA loading. Predictive models for LCFA bioconversion kinetics were developed as a function of absolute concentrations of selected *Syntrophomonas* taxa. DNA-stable isotope probing (SIP) based metagenomics confirmed that different LCFA-degrading syntrophic bacteria were selected with different codigester LCFA feeding frequencies. Taken together, the results of this study demonstrate that higher codigester FOG loadings can be achieved by developing a higher biomass concentration of LCFA-degrading syntrophic consortia, and that the codigester feeding strategy can be adjusted to biologically select for LCFA-degrading populations with higher LCFA bioconversion kinetics at high FOG loadings.

# TABLE OF CONTENTS

List of Figures .....	vi
List of Tables .....	xii
Chapter 1. Overview .....	15
Chapter 2. Literature Background.....	20
2.1 Resource recovery potential of fats, oils, and grease by anaerobic treatment .....	20
2.2 Characteristics of Long-chain Fatty Acids .....	21
2.3 Bioconversion of Long-chain Fatty Acids Into Methane .....	24
2.4 Inhibition of Long-chain Fatty Acid Degradation During Anaerobic Digestion.....	30
2.5 Microbial Ecology of Long-chain Fatty Acid Degradation.....	33
2.6 Effect of Microbial Community Diversity and Ecological Stability on Anaerobic Digester Performance .....	38
Chapter 3. Monitoring the dynamics of syntrophic beta-oxidizing bacteria during anaerobic degradation of oleic acid by quantitative PCR .....	41
3.1 Abstract.....	41
3.2 Introduction.....	42
3.3 Materials And Methods .....	45
3.3.1 Batch-fed Methanogenic Bioreactors Degrading Oleic Acid .....	45
3.3.2 Extraction and Quantification of Genomic DNA .....	47
3.3.3 Design and Validation of qPCR Primer and Probe Sets .....	47
3.3.4 Quantitative PCR (qPCR).....	50

3.3.5	High-Throughput Amplicon Sequencing of Bacterial 16S rRNA Genes .....	52
3.3.6	Analytical Methods .....	54
3.3.7	Statistical Analysis .....	55
3.4	Results .....	56
3.4.1	Validation of Syntrophomonas and Syntrophus Genus-Level qPCR Assays .....	56
3.4.2	Specific Mineralization Rates of Oleic Acid in Methanogenic Bioreactors .....	58
3.4.3	Quantitative Dynamics of Syntrophic $\beta$ -Oxidizing Bacteria by qPCR .....	59
3.4.4	Quantitative Dynamics of Methanogenic Archaea by qPCR .....	62
3.4.5	Dynamics of Bacterial Community by High-throughput Amplicon Sequencing of 16S rRNA Genes .....	64
3.5	Discussion .....	66
3.6	Supplemental Information Available .....	71
Chapter 4. Microbial community adaptation influences long-chain fatty acid conversion during anaerobic codigestion of fats, oils, and grease with municipal sludge .....		72
4.1	Abstract .....	72
4.2	Introduction .....	73
4.3	Materials and Methods .....	76
4.3.1	Digester Operation .....	76
4.3.2	Batch Methanogenic Activity Assays .....	78
4.3.3	Analysis of Microbial Community Structure .....	80
4.4	Results .....	83
4.4.1	FOG codigestion led to enhanced methane production and higher LCFA conversion kinetics .....	83

4.4.2 FOG codigestion selected for syntrophic $\beta$ -oxidizing bacteria and specific methanogenic archaea partners .....	86
4.4.3 Microbial community structure was related to reactor performance during FOG codigestion .....	92
4.5 Discussion .....	95
4.6 Conclusions.....	99
4.7 Supplemental Information Available.....	100
Chapter 5. Syntrophic community structure and biokinetics driven by long-chain fatty acid feeding strategy in anaerobic codigestion.....	
5.1 Abstract.....	101
5.2 Introduction.....	102
5.3 Materials and Methods.....	106
5.3.1 Anaerobic Digester Description and Operation:.....	106
5.3.2 Oleate Bioconversion Kinetics .....	110
5.3.3 Oleate Inhibition of Aceticlastic Methanogenic Activity .....	110
5.3.4 Analytical Methods.....	111
5.3.5 DNA Extraction and Quantification .....	112
5.3.6 Quantitative PCR .....	112
5.3.7 16S rRNA Gene Amplicon Sequencing .....	112
5.3.8 Bioinformatics.....	113
5.3.9 Regression Analysis.....	114
5.4 Results.....	114
5.4.1 Effect of LCFA OLR and feeding frequency on codigester performance .....	114

5.4.2	Impacts of LCFA OLR and feeding frequency on LCFA and acetate bioconversion kinetics .....	116
5.4.3	Microbial community structure and diversity was altered by the codigester feeding pattern	119
5.4.4	Oleate and acetate bioconversion kinetics were correlated to syntrophic and methanogenic community abundance .....	125
5.5	Discussion .....	127
5.5.1	Codigester stability and bioconversion kinetics were impacted by LCFA feeding pattern	127
5.5.2	Codigester feeding pattern drove biological selection of syntrophic bacteria and methanogen population structures .....	128
5.5.3	Relating bioconversion kinetics to microbial community structure .....	130
5.6	Conclusions.....	131
5.7	Supplemental Information Available.....	132
Chapter 6. DNA-stable isotope probing based metagenomics identifies key long-chain fatty acid degrading populations in parallel anaerobic codigesters with different oleate feeding strategies .....		133
6.1	Abstract.....	133
6.2	Introduction.....	134
6.3	Materials and Methods.....	137
6.3.1	Anaerobic Bioreactor Operation .....	137
6.3.2	Stable Isotope Probing Incubations with Anaerobic Digester Sludge .....	138
6.3.3	DNA Extraction and Density Gradient Centrifugation.....	139



6.3.4	Quantitative PCR .....	140
6.3.5	16S rRNA Amplicon Sequencing.....	141
6.3.6	Metagenomic Sequencing, Assembly, and Annotation .....	142
6.3.7	Metagenomic Binning.....	142
6.3.8	Statistical Analysis.....	143
6.4	Results.....	144
6.4.1	Conversion of Oleate into Methane and Enrichment of <sup>13</sup> C DNA .....	144
6.4.2	16S rRNA Amplicon Sequencing of DNA-SIP Samples .....	147
6.4.3	DNA-SIP Metagenomic Sequencing .....	149
6.5	Discussion.....	154
6.6	Supplemental Information Available.....	160
Chapter 7. Conclusions and Future Outlook.....		161
7.1	Major Findings and Engineering Significance .....	162
7.2	Future Outlooks .....	164
Bibliography .....		168
Appendix A.....		A1
Appendix B.....		B1
Appendix C.....		C1
Appendix D.....		D1

## LIST OF FIGURES

Figure 2-1 Chemical structures of various LCFA commonly found in wastewater sources (adapted from Sousa et al. 2009) .....	23
Figure 2-2 Potential trophic interactions during conversion of LCFA into methane in anaerobic digesters. ....	25
Figure 2-3 LCFA metabolism and its regulation through the <i>fad</i> regulon (adapted from Fujita et al., 2007). ....	27
Figure 3-1 Changes in 16S rRNA gene concentrations of (A) <i>Syntrophomonas</i> and (B) <i>Syntrophus</i> in methanogenic bioreactors; Ratio of 16S rRNA gene concentrations of (C) <i>Syntrophomonas</i> and (D) <i>Syntrophus</i> to that of total <i>Bacteria</i> in bioreactors. Error bars indicate one standard deviation based on biological (n=3) and technical replicates (n=2). ....	60
Figure 3-2 Correlation between the initial specific methane production rate during the oleic acid batch degradation periods and the average relative abundance of (A) <i>Syntrophomonas</i> 16S rRNA genes in bacterial community, and (B) methanogenic archaea 16S rRNA genes in prokaryotic community. The total methanogenic archaea gene concentration was determined as the sum of all methanogen target groups, and the prokaryotic gene concentration was determined as the sum of methanogenic archaea and total <i>Bacteria</i> gene counts. Error bars for the specific methane production rate indicate one standard deviation based on biological replicates (n=3), and error bars for relative abundance values indicate one standard deviation based on biological (n=3) and technical replicates (n=2). ....	61
Figure 3-3 (A) Change in the 16S rRNA gene concentration of the sum of all methanogenic archaea targets in bioreactors degrading oleic acid; (B) Relative abundance of the 16S rRNA gene concentration of each methanogenic target group relative to the sum of methanogenic archaea targets; (■) = <i>Methanomicrobiales</i> ; (●) = <i>Methanosaetales</i> ; (◆) = <i>Methanobacteriales</i> ; (^) = <i>Methanosarcinales</i> . <i>Methanobacteriales</i> and <i>Methanosarcinales</i> remained below 1% relative abundance, while <i>Methanococcales</i> was	

not detected by qPCR of the bioreactor samples. Error bars indicate one standard deviation based on biological (n=3) and technical replicates (n=2). ..... 63

Figure 3-4 Change in the relative abundance of each OTU that accounted for 1% or more of the bacterial community during the bioreactor operation relative to initial conditions, as determined by high-throughput amplicon sequencing of 16S rRNA genes. The left axis shows a phylogenetic clustering of the OTU's based on sequence alignment with MUSCLE (<http://www.ebi.ac.uk>). The right axis shows the genus level classification of each representative OTU sequence. The scale on the color key is relative to the entire community (e.g., an increase in relative abundance from 1% to 5% would be shown as +4%). The relative abundance change of each OTU is shown for all reactor replicates (e.g. 1, 2, 3) at days 7, 14, 21, 28, and 35. .... 65

Figure 3-5 Relative abundance of bacterial groups based on high-throughput amplicon sequencing of 16S rRNA genes from bioreactor samples taken on days 0, 7, 14, 21, 28, and 35 showing (A) the 12 most abundant bacterial orders, and (B) the 20 most abundant genera. The groups were ranked based on their maximum observed relative abundances, and all other groups were combined and are shown as “Other”. The abundances of groups shown at each time point represent an average of the triplicate bioreactors..... 66

Figure 4-1 Comparison of the FOG codigester and the control digester performance over experimental period, based on (A) daily volatile solids loading rate, (B) daily methane production, (C) digester pH, and (D) effluent LCFA concentrations. The LCFA concentrations shown in (D) were calculated as the sum of palmitate, stearate, and oleate in the digester effluent solids (error bars represent one standard deviation with n=4). 85

Figure 4-2 Maximum methane production rate in batch assays fed with (A) oleate and (B) acetate, as determined by fitting the Gompertz growth model to observed methane production in triplicate biological replicates. Error bars represent the standard error based on the non-linear regression model fitting (n=3). ..... 86

Figure 4-3 Relative fraction of 16S rRNA genes of the  $\beta$ -oxidizing bacterial genera, (A) *Syntrophomonas* and (B) *Syntrophus*, within the total *Bacteria* 16S rRNA gene concentration in the FOG codigester and control digester over the experimental period, as

determined by qPCR. Error bars represent a standard deviation based on DNA extraction replicates (n=3) and qPCR technical replicates (n=2) for each time point. .... 88

Figure 4-4 Relative sequence fraction of the 13 most abundant genera within the FOG codigester and control digester libraries produced from Illumina MiSeq sequencing of *Bacteria* 16S rRNA gene amplicons. The triplicate bars shown for each sample day represent replicate DNA extractions. The relative sequence fraction of all other genera were summed, and are shown here as “Other”. .... 89

Figure 4-5 Change in the relative fraction of methanogenic *Archaea* 16S rRNA genes in prokaryotic community of the control digester and FOG codigester. The total methanogenic *Archaea* 16S rRNA gene concentration was determined as the sum of all methanogen groups targeted in qPCR, and the prokaryotic gene concentration was determined as the sum of methanogenic *Archaea* and total *Bacteria* 16S rRNA gene concentrations. .... 91

Figure 4-6 Relative sequence fraction of the 13 most abundant genera within the FOG codigester and control digester libraries produced from Illumina MiSeq sequencing of *Archaea* 16S rRNA gene amplicons. The triplicate bars shown at each sample day represent replicate DNA extractions. The relative sequence fraction of all other genera were summed, and are shown here as “Other”. .... 91

Figure 4-7 Canonical correspondence analysis (CCA) plots based on (A) *Bacteria* and (B) *Archaea* scaled OTU sequence counts in the codigester and control digester samples, constrained by the four highest-scoring environmental gradients: daily methane production, maximum methane production from oleate ( $q_{max,oleate}$ ), maximum methane production from acetate ( $q_{max,acetate}$ ), and time (experimental days). The color of the outer circles represents the sample digester source and the color of the inner circles represents the sample collection day. The triplicate samples shown for each sample day are from replicate DNA extractions. The length and direction of each arrow represents the scaling used for that environmental gradient in the CCA model. .... 93

Figure 4-8 Specific effluent LCFA concentration of the FOG codigester versus the FOG to syntroph feed ratio ( $F:M_{Syn}$ ). The exponential trend line was fitted with a non-linear regression method in R v. 3.0.2. Error bars represent one standard deviation. .... 94

Figure 5-1 Comparison of (A) daily methane production and organic loading rate (OLR) for Phase I experimental digesters; (B) daily methane production and OLR for Phase II experimental digesters; (C) digester effluent acetate concentrations during Phase I; and (D) digester effluent acetate concentrations during Phase II. Error bars represent one standard deviation with  $n=4$ . ..... 118

Figure 5-2 Relative read fractions of the (A) 12 most abundant *Bacteria* genera, and (B) 10 most abundant *Archaea* genera in the 16S rRNA amplicon sequence libraries for the digesters during Phase I. Genus abundance profiles from triplicate DNA extractions are shown for each time point. .... 120

Figure 5-3 Concentration of 16S rRNA genes in the Phase I digesters for (A) *Bacteria*, (B) *Archaea*, and (C) *Syntrophomonas*, and in the Phase II digesters for (D) *Bacteria*, (E) *Archaea*, and (F) *Syntrophomonas*. Error bars represent one standard deviation based on triplicate DNA extractions and duplicate qPCR technical replicates. .... 121

Figure 5-4 Correspondence analysis (CA) plots based on (A) *Bacteria* and (B) *Archaea* normalized OTU sequence counts in the codigester and control digester samples collected throughout Phases I and II. The color of each marker represents the sample collection day and the shape of each marker represents the digester sludge source. The triplicate samples shown for each sample day are from replicate DNA extractions. The percentage shown along each axis represents the fraction of variance explained by that CA axis. .... 122

Figure 5-5 Relative read fractions of the (A) 12 most abundant *Bacteria* genera, and (B) 10 most abundant *Archaea* genera in the 16S rRNA amplicon sequence libraries for the digesters during Phase II. Genus abundance profiles from triplicate DNA extractions are shown for each time point. .... 122

Figure 5-6 Relative read fractions of the 13 most abundant OTUs classified within the *Syntrophomonas* genus of the digesters during Phases I and II based on 16S rRNA amplicon sequencing. OTU abundance profiles from triplicate DNA extractions are shown at each time point. .... 124

Figure 5-7 Linear regression of observed  $q_{max,oleate}$  values versus (A) the total *Syntrophomonas* 16S rRNA gene concentration; and (B) predicted  $q_{max,oleate}$  values from a multiple-linear

regression model based on inferred 16S rRNA gene concentrations of 6 selected *Syntrophomonas* OTUs. Inferred absolute abundances were calculated by multiplying the relative fraction of each OTU within total *Syntrophomonas* read counts by the total *Syntrophomonas* 16S rRNA gene concentration. Error bars represent one standard deviation..... 126

Figure 6-1 Cumulative methane production (minus blank controls) for the microcosms fed with <sup>12</sup>C- and <sup>13</sup>C-labeled oleate over three repeated batch feeding periods. The number above each plot indicates the batch oleate feed round. The black dashed line shows the theoretical methane potential of the added oleate (25.5 mL CH<sub>4</sub>; based on 2.9 g COD/g oleate, 8 mM concentration, and 35 °C temperature). The black solid line represents the predicted methane production based on non-linear model fitting with a modified Gompertz equation (see Supplemental Table D1)..... 145

Figure 6-2 Total copies of *Syntrophomonas* 16S rRNA genes measured by qPCR for each density gradient fraction recovered from isopycnic separation of DNA from <sup>13</sup>C-incubated microcosms and <sup>12</sup>C-controls for both anaerobic codigesters. The filled circles indicate gradient fractions that were pooled for subsequent 16S rRNA amplicon sequencing and metagenomic sequencing. Both biological replicates are shown, and each point represents an average of duplicate technical replicates..... 146

Figure 6-3 Principle coordinate analysis (PCA) plot of OTU read counts from 16S rRNA amplicon sequencing after regularized log transformation with DESeq2 (Love et al., 2014). The different shapes indicate the codigestion reactor biomass source, and the colors represent the isotope of oleate (<sup>13</sup>C or <sup>12</sup>C) fed to the microcosms. Biological duplicate samples are shown. .... 147

Figure 6-4 Cumulative read counts of the 11 most abundant genera in the heavy gradient fractions of <sup>13</sup>C-incubated samples and <sup>12</sup>C-controls for both codigester sample sets, based on 16S rRNA amplicon sequencing. Normalized read counts for all OTUs were calculated with DESeq2 (Love et al., 2014) to correct for differences in sequencing depths between samples, and were then aggregated at the genus level..... 149

Figure 6-5 Phylogenetic overview of differentially abundant genome bins identified in both anaerobic codigester DNA-SIP metagenomes. The tree was constructed based on a

concatenated alignment of conserved marker genes within the metagenomic contigs of each bin using PhyloPhlAn (Segata et al., 2013). The color of each genome bin node represents the codigester biomass source, and the height of the outer bars represent the genome bin coverage in the heavy gradient fractions of the <sup>13</sup>C-incubated samples and <sup>12</sup>C-controls. The tree was illustrated using GraPhLan (Asnicar et al., 2015). ..... 152

Figure 6-6 Cumulative coverage values of KEGG ECs potentially involved in LCFA degradation (KEGG map 00071), based on the coverage of all differentially abundant genome bins in the <sup>13</sup>C-incubated DNA-SIP metagenomes. Values from duplicate biological replicates are shown for both codigesters, and the size of each marker is proportional to the log<sub>10</sub> of the EC read coverage. .... 154

## LIST OF TABLES

Table 2-1 LCFA composition of common raw materials and wastewater sources (shown as % of LCFA present) (adapted from (Alves et al., 2009) .....	23
Table 2-2 Stoichiometry and free energy for the conversion of palmitate and oleate into methane (adapted from (Schink, 1997; Sousa et al., 2007a; Thauer et al., 1977).....	28
Table 2-3 Substrate utilization of isolated syntrophic bacteria capable of degrading C <sub>4</sub> -C <sub>18</sub> fatty acids (adapted from Sousa <i>et al.</i> , 2009).....	37
Table 3-1 Operating conditions and performance characteristics of methanogenic bioreactors degrading oleic acid. ( <i>n</i> =3) .....	46
Table 3-2 Characteristics of qPCR primers and hydrolysis probes developed to target <i>Syntrophomonas</i> and <i>Syntrophus</i> genera.....	49
Table 4-1 Total influent volatile solids loading rate (VSLR), FOG VSLR, and the percent of FOG VS in the feed versus time for the FOG codigester. Values in parentheses indicate one standard deviation. ....	77
Table 5-1 Summary of oleate feed and total feed characteristics to the codigesters during Phase I and II. Values in parentheses represent one standard deviation. ....	109
Table 5-2: Maximum conversion rates for oleate ( $q_{max,oleate}$ ) and acetate ( $q_{max,acetate}$ ) observed in the batch kinetic assays with digester sludges collected throughout Phases I and II.	119
Table 6-1 Taxonomic classification and characteristics for genome bins that were significantly enriched ( $p < 0.01$ ) in <sup>13</sup> C metagenomes relative to <sup>12</sup> C-controls for both codigester sample sets. Only genome bins that were above 40% completion are included. ....	150



## ACKNOWLEDGEMENTS

This dissertation represents a period in my life filled with independent exploration, discovery, and learning, which was supported by the help of many amazing people. Firstly, I give deep thanks to my advisor, Dr. David Stensel, for his incredible mentorship, encouragement, and guidance throughout my academic and personal pursuits. He taught me to think critically and analytically, as well as how to enjoy a nice glass of wine when the day's work is over. I am also grateful for the opportunity to collaborate and work with my other committee members, Dr. David Stahl and Dr. David Beck, who provided me with extremely helpful guidance throughout this work. I also would like to thank my 'host' advisors from the international NSF GROW programs, Dr. Bo Svensson and Dr. Diana Sousa—as they took on extra responsibilities to mentor me, and I am deeply appreciative of their hospitality and guidance.

I was also very fortunate to receive amazing help from Masters research assistants throughout this research. Songlin Wang was truly our 'lab Mother', and I thank her for her determination and generosity—it was a blessing to have her help. I also appreciate the hard work of Xumo Chen toward this research.

I would also like to thank all of my colleagues from Civil and Environmental Engineering (and beyond) for many great scientific discussions and fun times, including (in no particular order): Mariko Lust, Bryce Figdore, Dr. Mari Winkler, Wei Qin, Stephany Wei, Kathryn Cogert,

Nicolette Zhou, Peiran Zhou, Tess Young, Sudarshan Shetty, Jueeli Vaidya, Dr. Nejc Stopnisek, Dr. Frederick von Netzer, Dr. Stuart Strand, and any others I may have forgotten.

I also would like to thank the continued support and involvement of the King County Department of Natural Resources and Parks, Wastewater Treatment Division including John Smyth, Bob Bucher, and Pardi Sukapanpotharam.

This research was supported by numerous funding sources including: the U.S. National Science Foundation Graduate Research Fellowship, the U.S. National Science Foundation Graduate Research Opportunities Worldwide Fellowship, the University of Washington Valle Fellowship, the Water Environment Federation Canham Scholarship, the Department of Energy Joint Genome Institute Community Science Program, and the U.S. EPA Grant STAR\_N3R14A.

I am also grateful for the constant encouragement from my family and friends, who have all put up with my lengthy talks about microbes and bioenergy during this time. And last but most importantly, I would like to thank the unconditional support and love from my wife, Meika. She has been my pillar of strength, and if it were not for her great patience (and awesome cooking skills), this dissertation work would not have been possible.

## Chapter 1. OVERVIEW

Energy recovery through the conversion of organic waste into biomethane with anaerobic digestion is of great interest due to improved economics as well as smaller carbon footprints in comparison to aeration and oxidation based treatment processes. The interest in utilizing fats, oils, and greases (FOG) as co-substrates for anaerobic digestion is growing due to their higher potential methane yield in comparison to waste primary sludge and waste activated sludge typically fed to municipal wastewater sludge digesters, or dairy manure fed to agricultural digesters. Thus, codigesting waste FOG with wastewater treatment sludge or livestock manure has the potential to significantly increase biomethane recovery from existing anaerobic digester operations. However, the long-chain fatty acids (LCFA) released during FOG hydrolysis are a major concern for codigester stability due to their ability to inhibit methanogenic activity. Microbial inhibition by LCFA could limit the maximum methane production obtainable during FOG codigestion, or even result in digester failure. Therefore, understanding the factors influencing LCFA conversion during FOG codigestion is important for determining maximum allowable FOG loading rates that permit stable digester operation with enhanced biomethane recovery. Currently, there is a lack of understanding regarding the role of anaerobic digester microbial communities in maintaining efficient LCFA conversion into biomethane. The ultimate goal of this research project was to improve the reliability of biomethane recovery during FOG codigestion by elucidating relationships between microbial ecology and LCFA bioconversion kinetics and digester stability.

When this research project began, there was a lack of molecular tools available to accurately monitor the abundance of LCFA-degrading bacteria in anaerobic digesters, since they can be present in digester sludge at concentrations below the detection limits of FISH and membrane hybridization probes (Stams et al., 2012). Based on this knowledge gap, the initial research objective was to develop sensitive molecular tools to quantify and monitor the growth dynamics of syntrophic  $\beta$ -oxidizing bacteria during LCFA degradation. Quantitative PCR (qPCR) assays were developed and validated to target the syntrophic LCFA-degrading bacterial genera *Syntrophomonas* and *Syntrophus*. The assays were applied to measure the growth of syntrophic  $\beta$ -oxidizing bacteria in oleate-fed microcosms inoculated with anaerobic digester sludge. This is the topic of the research paper in **Chapter 3**: “Monitoring the dynamics of syntrophic  $\beta$ -oxidizing bacteria during anaerobic degradation of oleic acid by quantitative PCR.”

Once the ability to monitor absolute abundances of syntrophic LCFA-degrading bacteria was established, the objective of the next research phase was to examine potential relationships between LCFA removal efficiency and the concentration of syntrophic  $\beta$ -oxidizing bacteria during FOG codigestion with municipal wastewater sludge. Such relationships are investigated in **Chapter 4**: “Microbial community adaptation influences long-chain fatty acid conversion during anaerobic codigestion of fats, oils, and grease with municipal sludge.” Microbial community structure was monitored in a codigester treating waste restaurant oil and municipal wastewater treatment sludge in parallel with a control digester for over 150 days. A relationship was established between effluent LCFA concentrations and the FOG loading rate normalized to *Syntrophomonas* 16S rRNA genes within the codigester.

The finding that effluent LCFA concentrations were positively correlated to the ratio of the FOG loading rate to *Syntrophomonas* 16S rRNA gene concentrations during codigestion indicated that the overall LCFA bioconversion rate of syntrophic bacteria and methanogenic archaea together could establish the permissible FOG loading rate that prevents inhibitory LCFA accumulation. However, it remained unknown whether different communities of syntrophic bacteria and methanogenic archaea with different LCFA bioconversion kinetics could be biologically selected in codigesters at high FOG loadings, and whether the codigester LCFA feeding frequency could impact the LCFA-degrading community. Thus, the objective of the next phase of research was to investigate the effects of the codigester LCFA feeding frequency on LCFA bioconversion kinetics, codigester stability, and the composition of syntrophic LCFA-degrading consortia. A secondary research objective was to develop predictive models for LCFA-conversion kinetics based on syntrophic LCFA-degrading bacteria community structure and abundance. LCFA bioconversion kinetics and microbial community structure were compared in two parallel anaerobic codigesters receiving oleate (C<sub>18:1</sub> LCFA) in either a pulse-fed or a continuous-fed regime. These objectives are addressed in **Chapter 5**: “Syntrophic community structure and bioconversion kinetics are driven by long chain fatty acid feeding strategy in anaerobic codigestion.”

The results in Chapter 5 showing that the codigester LCFA feeding frequency impacted the fine-scale composition of  $\beta$ -oxidizing *Syntrophomonas* communities were based on time-series 16S rRNA gene amplicon sequencing analysis. However, a comparison of the active LCFA-degrading populations between the codigesters was lacking, and was necessary to address the mechanism in which digester feeding strategies impacted LCFA-degradation biokinetics. The

objective of the next phase of research was thus to apply DNA-SIP combined with metagenomic sequencing to conduct a genomic-based comparison of the active oleate degrading populations in the two parallel codigesters fed with LCFA at different frequencies. This research objective is addressed in **Chapter 6**: “DNA-stable isotope probing based metagenomics identifies key long-chain fatty acid degrading populations in parallel anaerobic codigesters with different oleate feeding strategies.” A comparison of active syntrophic population genome bins between the codigesters was conducted using differential coverage binning on DNA-SIP  $^{13}\text{C}$  and  $^{12}\text{C}$  metagenomes, and the results were also validated with 16S rRNA gene amplicon sequencing. The results showed that *Syntrophomonas* were predominantly enriched in the metagenomes and 16S rRNA sequence libraries of the  $^{13}\text{C}$ -incubated samples, and phylogenetically distinct *Syntrophomonas* were observed within each codigester.

**Chapter 2** provides an overview of relevant literature for this research project, including an introduction to the importance of energy recovery through anaerobic wastewater treatment, the current state of understanding on LCFA inhibition and microbial LCFA conversion, and implications of microbial ecology and stability for anaerobic digester performance. The methods, results, and conclusions of this study are presented in Chapters 3-4 as published papers, and in Chapters 5-6 as manuscripts prepared for submission. Future research needs to develop biokinetic models for FOG codigestion based on ecological principles and thermodynamics are discussed in Chapter 7. Supplemental data for the research presented in Chapters 3-6 is presented in Appendices A-D.

The publication associated with the research in **Chapter 3** is:

Ziels, R. M., Beck, D. A., Martí, M., Gough, H. L., Stensel, H. D., & Svensson, B. H. (2015). Monitoring the dynamics of syntrophic  $\beta$ -oxidizing bacteria during anaerobic degradation of oleic acid by quantitative PCR. *FEMS microbiology ecology*, *91*(4), doi: <http://dx.doi.org/10.1093/femsec/fiv028>

The publication associated with the research in **Chapter 4** is:

Ziels, R.M., Karlsson, A., Beck, D.A., Ejlertsson, J., Yekta, S.S., Bjorn, A., Stensel, H.D. & Svensson, B.H., (2016). Microbial community adaptation influences long-chain fatty acid conversion during anaerobic codigestion of fats, oils, and grease with municipal sludge. *Water Research*, *103*, doi:<http://dx.doi.org/10.1016/j.watres.2016.07.043>

The planned publication associated with the research in **Chapter 5** is:

Ziels, R.M., Beck, D.A., Stensel, H.D. (2016). Syntrophic community structure and biokinetics driven by long-chain fatty acid feeding strategy in anaerobic codigestion. *Prepared for submission to Water Research*.

The planned publication associated with the research in **Chapter 6** is:

Ziels, R.M., Beck, D.A., Stensel, H.D. (2016). DNA-stable isotope probing based metagenomics identifies key long-chain fatty acid degrading populations in parallel anaerobic codigesters with different oleate feeding strategies. *Prepared for submission to Environmental Microbiology*.

## Chapter 2. LITERATURE BACKGROUND

### 2.1 RESOURCE RECOVERY POTENTIAL OF FATS, OILS, AND GREASE BY ANAEROBIC TREATMENT

Anaerobic digestion is commonly used at municipal wastewater treatment plants (WWTPs) as well as agricultural dairy operations to process waste solids and generate renewable energy as biomethane. A growing worldwide interest in anaerobic digestion has led to the implementation of approximately 9,000 full-scale facilities in Europe and over 3,000 facilities in the U.S. by 2012 (Guo et al., 2015). Approximately 9.1 billion kW-h of electricity was generated from biogas in the U.S. in 2012, with approximately 47 to 95 billion kW-h of electricity generated worldwide (Guo et al., 2015).

The combination of multiple organic waste streams and feedstocks in the influent to an anaerobic digester is termed *codigestion*. More recently, codigesting exogenous organic wastes with municipal sludge or dairy manure is gaining interest for increased biomethane recovery and improved process economics (Bishop and Shumway, 2009). Lipid-rich waste streams, such as fats, oils, and greases (FOG) originating from municipal sewer grease traps or industrial processes, are desirable substrates for anaerobic codigestion due to their high energy content (Labatut et al., 2011). The impact of FOG codigestion on renewable energy recovery and carbon footprints of municipalities is thus worth consideration. A city of 500,000 persons is expected to produce approximately 90 million pounds of waste FOG annually (Wiltsee, 1998). Assuming a specific biological methane yield of 0.4 L-CH<sub>4</sub>/g for FOG (Labatut et al., 2011), the above production of FOG would correspond to a potential of 10.3 MW if only 50% of the waste FOG were sent to anaerobic digesters, which is roughly enough to power 10,000 homes per year (U.S.



DOE, 2010) or ~6% of the population with 3 persons per home. Importantly, this renewable methane recovery also would reduce CO<sub>2</sub> emissions by 16,000 tons/year by replacing fossil fuel-derived natural gas (U.S. DOE, 2010). Since waste FOG has 30-50 times the energy density (per volume) as traditional anaerobic digester feed sludge sources (Labatut et al., 2011), the increased reactor volume capacity required for codigestion is negligible. Previous work has demonstrated the potential for substantial increases in digester methane production of 2.6- to 7.3-times with FOG addition from 30 to 60% (v/v) of the feed volatile solids (Kabouris et al., 2009; Luostarinen et al., 2009; Wan et al., 2011; Wang et al., 2013). Therefore, waste FOG represents a valuable energy-rich resource that could be effectively recovered as renewable biomethane with little impact on the solids processing capacity of existing anaerobic digesters.

In addition to increasing renewable methane production, disposing of FOG through codigestion would also alleviate wastewater treatment systems of a major nuisance product. FOG is known to accumulate and congeal on pipe walls, contributing to the obstruction of sewer collection lines (He et al., 2011). Approximately 50-75% of reported sewer overflows were caused by FOG accumulation within the collection system (Keener et al., 2008). FOG from municipal grease traps is typically disposed via landfilling (Davidsson et al., 2008). Codigesting trapped FOG with municipal sludge or dairy manure at existing digestion facilities could help to recover resources (energy) from a problematic waste stream that currently hinders sewer collection infrastructure.

## 2.2 CHARACTERISTICS OF LONG-CHAIN FATTY ACIDS

Lipids are comprised of long-chain fatty acids (LCFA) that are linked to glycerol, alcohols, or other groups (i.e. sugars and sterols) with an ether or ester bond. Fats and oils are a subgroup of

lipids that have their alcohol group (glycerol) esterified with LCFA, and take the form of triglycerides (a glycerol backbone esterified with 3 LCFA) (Alves et al., 2009). *Fats* are triglycerides that are solid at room temperature, while *oils* are triglycerides that are liquid at room temperature. The size and structure of the LCFA in the triglyceride dictate whether it takes the form of a fat or an oil.

LCFA are organic molecules that include a carboxylic head and an aliphatic tail. LCFA are typically defined as carboxylic acids with more than 12 carbon atoms (Sousa et al., 2009). LCFA comprise a major component of fats, accounting for up to 90% of the total organic carbon (Hanaki et al., 1981), and are also major ingredients in soaps due to their surfactant properties (Johansson and Svensson, 2001). The LCFA-composition of typical lipid containing wastewaters and raw materials is summarized in Table 2-1. Palmitic, stearic, oleic, and linoleic acids are the most abundant saturated and unsaturated LCFA in wastewaters and food sources (Table 2-1). Oleic acid is the most common LCFA found in domestic wastewater (Table 2-1). These LCFA commonly found in wastewater sources are depicted in Figure 2-1.

**Table 2-1** LCFA composition of common raw materials and wastewater sources (shown as % of LCFA present) (adapted from (Alves et al., 2009))

Raw material or wastewater source	Saturated LCFA				Unsaturated LCFA		
	Lauric (C12:0)	Myristic (C14:0)	Palmitic (C16:0)	Stearic (C18:0)	Palmitoleic (C16:1)	Oleic (C18:1)	Linoleic (C18:2)
Palm oil <sup>a</sup>	ND	1.4	42.9	4.8	0.7	39	10
Olive oil <sup>a</sup>	ND	ND	14.3	2.4	1.4	71.4	5.5
Soybean oil <sup>a</sup>	ND	1	11	4.8	ND	21.9	49
Cotton seed oil <sup>a</sup>	ND	1.4	25.7	2.9	1	15.2	51.9
Cocoa butter <sup>a</sup>	ND	ND	26.7	32.9	0.5	33.8	4.3
Whole milk <sup>b</sup>	7	6	21	6	2	39	13
Chicken fat <sup>a</sup>	ND	1.4	21	4.3	6.7	42.4	20
Beef tallow <sup>a</sup>	1	2.6	28.1	20	3.8	37.6	2.9
Domestic sewage <sup>c</sup>	ND	2.2	16.4	8.1	0.9	30.5	29.2
Dairy wastewater <sup>d</sup>	ND	ND	27	7	ND	37	13

<sup>a</sup> – (Alves et al., 2009) <sup>b</sup> – (Hanaki et al., 1981) <sup>c</sup> – (Quéméneur and Marty, 1994) <sup>d</sup> – (Kim et al., 2004)

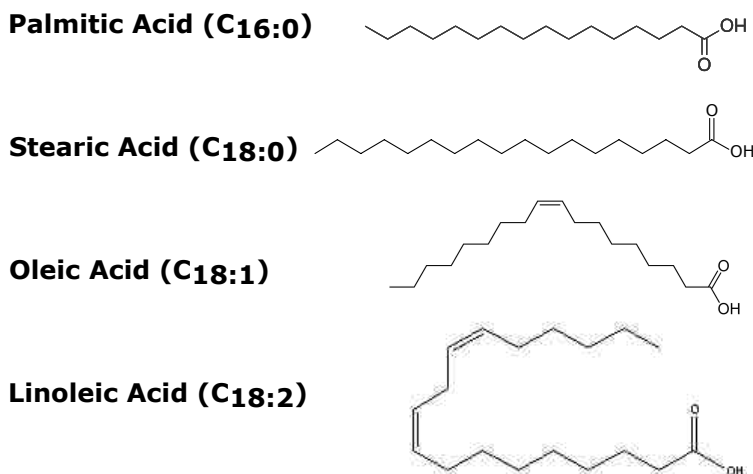


**Figure 2-1** Chemical structures of various LCFA commonly found in wastewater sources (adapted from Sousa et al. 2009)

The number of double bonds in the aliphatic tail determines the degree of saturation for LCFA. If double bonds are absent, the LCFA is *saturated*, whereas the LCFA is *unsaturated* if double

bonds are present. Commonly, the double bonds in LCFA found in nature are in the *cis* configuration (Sousa et al., 2009). The addition of a double bond to the alkyl chain limits the flexibility of the LCFA relative to its saturated counterpart (Kanicky and Shah, 2002). For instance, stearic acid, a C<sub>18</sub> saturated fatty acid, has a limiting area of 21 Å<sup>2</sup>, while oleic acid, a C<sub>18</sub> unsaturated fatty acid, has a limiting area of 32 Å<sup>2</sup> (Kanicky and Shah, 2002). The *pKa* of LCFA is also affected by the degree of saturation as well as chain length. As the alkyl chain length increases, the van der Waals interactions between adjacent LCFA molecules increases, thus bringing their carboxylic heads closer in proximity and shielding hydrogen atoms from protonating the acids (Kanicky and Shah, 2002). *pKa* values measured by titration range from 8.6 in palmitic acid (C<sub>16:0</sub>) to 9.0 for stearic acid (C<sub>18:0</sub>), thus demonstrating the effect of chain length on *pKa* (Christodoulou and Rosano, 1968; Kanicky et al., 2000). It was also shown that the larger limiting areas of LCFA with double bonds causes the *pKa* to decrease, as oleic acid (C<sub>18:1</sub>) and linoleic acid (C<sub>18:2</sub>) had lower *pKa* than stearic acid (C<sub>18:0</sub>) (Kanicky and Shah, 2002). The aqueous solubilities of LCFA are low and are also impacted by the alkyl chain length, with longer chain lengths leading to lower solubility. Double bonds present in LCFA also increase the solubility. The aqueous solubility of the saturated LCFA palmitic (C<sub>16:0</sub>) and stearic (C<sub>18:0</sub>) acids are 7.2 and 2.9 mg/L at 20 °C, respectively (Ralston and Hoerr, 1942), while the unsaturated linoleic acid (C<sub>18:2</sub>) has a solubility of 160 mg/L (Mabrouk and Jr, 1961).

### 2.3 BIOCONVERSION OF LONG-CHAIN FATTY ACIDS INTO METHANE

*Syntrophy* is a thermodynamically-based mutualistic partnership between two different species in which the pool of intermediate metabolites must be kept at a very low concentration in order for growth of the two partners to occur. LCFA are converted into methane through a syntrophic partnership between acetogenic  $\beta$ -oxidizing bacteria and methanogenic archaea (Schink, 1997;

Sousa et al., 2009). Interspecies hydrogen/formate transfer between syntrophic bacteria and methanogenic archaea plays an important role in the degradation of LCFA in methanogenic environments (Schink, 1997). Beta-oxidation involves the cleavage of acetate, hydrogen and/or formate from the fatty acid, producing ATP through substrate-level phosphorylation (Schink, 1997). An overall scheme showing the steps involved in converting LCFA into methane is shown in Figure 2-2.

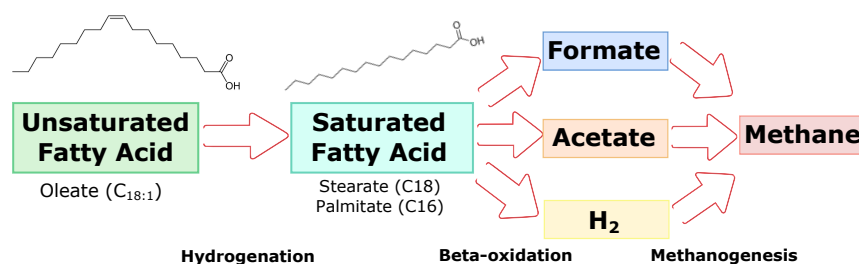


**Figure 2-2** Potential trophic interactions during conversion of LCFA into methane in anaerobic digesters.

The regulation of bacterial LCFA fatty acid metabolism has been mainly studied using the model organism *Escherichia coli* (Fujita et al., 2007). *E. coli* is capable of utilizing fatty acids with various chain lengths as the sole carbon and energy sources, yet it requires a terminal respiratory electron acceptor such as oxygen or nitrate for growth (Campbell et al., 2003; Fujita et al., 2007). After uptake, *E. coli* either degrades LCFA via  $\beta$ -oxidation or utilizes the fatty acids as precursors for membrane phospholipid biosynthesis (Fujita et al., 2007). The *fad* regulon encodes for enzymes utilized in the LCFA degradation pathway, including the transport and activation of fatty acids, as well as their activation and cleavage via  $\beta$ -oxidation into acetyl-CoAs (Figure 2-3). Briefly, LCFA are transported across the cell via an outer membrane protein, FadL, and an acyl-CoA synthetase, FadD (Campbell et al., 2003). *E. coli* contains a single acyl-CoA synthetase (FadD) that has a broad substrate specificity, whereas eukaryotic systems possess

multiple acyl-CoA synthetases with different fatty acid chain length specificities (Campbell et al., 2003; Fujita et al., 2007). In the initial step of LCFA degradation, acyl-CoA is converted to enoyl-CoA via the acyl-CoA dehydrogenase, FadE (Campbell et al., 2003). The remaining steps of LCFA degradation involves hydration, oxidation and thiolitic cleavage by the tetrameric complex consisting of two copies each of FadB and FadA (Pramanik et al., 1979). The  $\beta$ -oxidation pathway acts in a cyclic manner, with each cycle shortening the input acyl-CoA by two carbon atoms to give acetyl-CoA (Figure 2-3).

The metabolic pathway for the degradation of unsaturated fatty acids by  $\beta$ -oxidation differs slightly from saturated fatty acids. After a given number of cycles through the  $\beta$ -oxidation pathway, the double bond present in unsaturated fatty acids must be removed before subsequent hydration, oxidation and thiolitic cleavage in the  $\beta$ -oxidation cycle. Two pathways have been proposed for the degradation of double bonds during LCFA  $\beta$ -oxidation: (1) the isomerase-dependent pathway involves one auxiliary enzyme,  $\Delta^3, \Delta^2$ -enoyl-CoA isomerase (enoyl-CoA isomerase); (2) the reductase-dependent pathway requires three auxiliary enzymes, enoyl-CoA isomerase, 2,4-dienoyl-CoA reductase, and  $\Delta^{3,5}, \Delta^{2,4}$ -dienoyl-CoA isomerase (dienoyl-CoA isomerase) (Ren et al., 2004). In *E. coli*, the isomerase-dependent pathway is thought to be dominant pathway for double bond removal during oleate degradation (Ren et al., 2004). In addition to double bond removal coupled to the classical LCFA  $\beta$ -oxidation pathway, another possible mechanism for the saturation of LCFA (length  $C_n$ ) was shown to be coupled to the production of a  $C_{n-2}$  saturated fatty acid (Cavaleiro et al., 2016). This alternative pathway was found to be independent of hydrogen partial pressure and methanogenesis, suggesting that non-

syntrophic organisms could execute double bond saturation prior to syntrophic conversion of the excreted  $C_{n-2}$  saturated fatty acid (Cavaleiro et al., 2016).

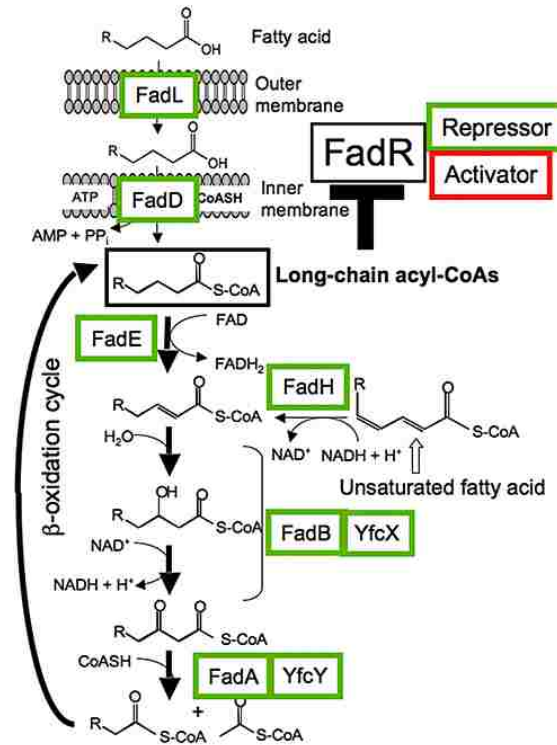


**Figure 2-3** LCFA metabolism and its regulation through the *fad* regulon (adapted from Fujita et al., 2007).

As mentioned, the formation of methane from LCFA involves a syntrophic partnership of proton-reducing acetogenic bacteria, which utilize the  $\beta$ -oxidation pathway to convert LCFA into acetate and formate/hydrogen (Weng and Jeris, 1976), along with aceticlastic and hydrogenotrophic methanogenic archaea (Schink, 1997; Sousa et al., 2009). The consumption of hydrogen and/or formate is essential to maintain favorable thermodynamics of LCFA conversion (Schink, 1997), as well as prevent hydrogenase inhibition from hydrogen accumulation (Garcia et al., 2000). The Gibbs free energies of LCFA conversion into methane are shown below in Table 2-2, and demonstrate the importance of low hydrogen concentrations for maintaining energy-yielding conditions.

**Table 2-2** Stoichiometry and free energy for the conversion of palmitate and oleate into methane (adapted from (Schink, 1997; Sousa et al., 2007a; Thauer et al., 1977))

LCFA	Equation	$\Delta G^{\circ\prime}$ (kJ/mole) <sup>a</sup>	$\Delta G'$ (kJ/mole) <sup>b</sup>
Palmitate	$C_{16}H_{31}O_2^- + 14H_2O \rightarrow 8C_2H_3O_2^- + 14H_2 + 8H^+$	+419	-81
Oleate	$C_{18}H_{33}O_2^- + 16H_2O \rightarrow 9C_2H_3O_2^- + 14H_2 + 9H^+$	+391	-131
Methanogenic Substrate	Equation	$\Delta G^{\circ\prime}$ (kJ/mole) <sup>a</sup>	$\Delta G'$ (kJ/mole) <sup>b</sup>
Acetate	$C_2H_3O_2^- + H_2O \rightarrow HCO_3^- + CH_4$	-31	-19
Hydrogen and CO <sub>2</sub>	$4H_2 + HCO_3^- + H^+ \rightarrow CH_4 + 3H_2O$	-136	-20

<sup>a</sup> - Gibbs free energies (at 25°C) under standard conditions (solute concentrations of 1 M and gas partial pressure of 1 atm).

<sup>b</sup> - Gibbs free energies (at 25°C) for environmental conditions with 1 mM LCFA, 10 mM acetate, and gas partial pressure of 1 Pa).

The biochemical mechanisms involved in LCFA degradation have not been well studied for microorganisms growing in methanogenic environments (Sousa et al., 2009). However, the mechanisms involved in the syntrophic  $\beta$ -oxidation of butyrate (C<sub>4:0</sub>) have been better characterized, and may be analogous to  $\beta$ -oxidation pathways of LCFA degradation. Similar to LCFA, the production of hydrogen or formate with electrons derived from butyrate oxidation is energetically unfavorable under standard conditions. If the methanogenic partner organisms keep the hydrogen concentration below 10<sup>-4</sup> atm, the midpoint potential of the proton/hydrogen couple is raised to -300 to -250 mV (Schink, 1997; Sieber et al., 2012). This potential can then be matched by electrons delivered from NADH ( $E^{0'} = -320$  mV) (Thauer et al., 1977). It was shown that NAD<sup>+</sup> is the electron acceptor involved in the second oxidation step of the butyrate pathway, from 3-hydroxybutyryl-CoA to acetoacetyl-CoA (Gustafson et al., 1986). However, at 1 Pa hydrogen partial pressure, two electrons are released at a much higher redox potential in the first oxidation step of the butyrate pathway ( $E^{0'} = -10$  mV), from butyryl-CoA to crotonyl-CoA



(Sieber et al., 2012). To release these electrons as hydrogen or formate ( $E^{\circ} = -260$  mV), it is assumed that the syntrophic bacteria invests energy through a process called *reverse electron transport* (Sieber et al., 2012).

Several recent studies utilized transcriptomics and proteomics to analyze the metabolic pathways involved in butyrate  $\beta$ -oxidation by *Syntrophomonas wolfei* (Schmidt et al., 2013; Sieber et al., 2015, 2014). The genome sequence of *S. wolfei* has been thoroughly analyzed and annotated to understand how butyrate oxidation is coupled to the formation of hydrogen/formate (Sieber et al., 2010). The *S. wolfei* genome contains a cluster of five formate dehydrogenases (FDH-1 - FDH-5), and three hydrogenases (HYD-1 – HYD-3) (Sieber et al., 2010). To identify enzymes involved in syntrophic butyrate degradation, proteins were extracted and compared from *S. wolfei* grown on butyrate in co-culture with *Methanospirillum hungatei* (syntrophic) and in pure-culture on crotonate (non-syntrophic) (Schmidt et al., 2013; Sieber et al., 2015). Formate dehydrogenases were predominant proteins expressed by *S. wolfei* during butyrate degradation in co-culture with *M. hungatei*, but were not expressed in pure-culture growth on crotonate (Schmidt et al., 2013). Hydrogenase activity was not detected in the proteome of *S. wolfei* during butyrate degradation with *M. hungatei* (Schmidt et al., 2013). In contrast to these findings, another study revealed that butyrate metabolism was limited by hydrogenase inhibitors (cyanide and carbon monoxide), but not by a formate dehydrogenase inhibitor (hypophosphite) in washed cell suspensions of *S. wolfei* and *M. hungatei* (Sieber et al., 2014). Reverse-transcription quantitative PCR confirmed that the expression of hydrogenases *hydA1* and *hydA2* was 50-fold greater than formate dehydrogenases *fdhA1*- *fdhA5* in *S. wolfei* during syntrophic butyrate degradation with *M. hungatei* (Sieber et al., 2014).

Interestingly, the different findings from these proteomic- and transcriptomic- based studies of butyrate degradation by *S. wolfei* and *M. hungatei* were attributed to different cultivation conditions, such as: the presence of yeast extract in the growth medium, iron concentration of the growth medium, incubation temperature, and the size of the incubation bottles (Sieber et al., 2014). It was reported that membranes of *S. wolfei* cells retrieved from a larger incubation vessel (250-L) with butyrate had high levels of formate-dehydrogenase activity but low levels of hydrogenase activity (Sieber et al., 2014). Thus, the metabolic pathways involved in syntrophic  $\beta$ -oxidation by *S. wolfei* appear to be flexible and dependent upon environmental conditions.

## 2.4 INHIBITION OF LONG-CHAIN FATTY ACID DEGRADATION DURING ANAEROBIC DIGESTION

Despite the high methane yield potential of FOG, the LCFA released during lipid hydrolysis are a major concern for the stability of anaerobic digestion, due to the inhibitory effects of LCFA on anaerobic microorganisms (Koster & Cramer 1987; Rinzema *et al.* 1994; Lalman & Bagley 2000). Microbial inhibition by LCFA could limit the maximum methane production obtainable during FOG codigestion, or even result in digester failure. Problematic digester performance issues associated with LCFA accumulation involve: (1) sludge foaming due to the surfactant properties of LCFA (Long et al., 2012); (2) sludge floatation and washout due to LCFA adsorption onto biomass (Hwu et al., 1998), and (3) the inhibition of methanogenic activity (Davidsson et al., 2008; Hwu and Lettinga, 1997; Lalman and Bagley, 2001, 2000; Luostarinen et al., 2009; Wang et al., 2013). The accumulation of LCFA may interfere with microbial activity by disrupting the cell plasma membrane (Koster and Cramer, 1987). It has also been suggested

that substrate transport is limited when LCFA adsorbs onto the biomass surface (Pereira et al., 2005), as adsorbed LCFA can interfere with cell membrane transport activities (Soliva et al., 2004). LCFA can also disrupt cellular energy production mechanisms by disrupting the electron transport chain and uncoupling oxidative phosphorylation (Desbois and Smith, 2010).

LCFA inhibition of methanogenic communities was shown to be a reversible phenomenon, with methane production resuming after a lag phase (Pereira et al., 2005). This suggested that perceived LCFA inhibition of methanogenic communities might be attributed to temporary transport limitations from adsorption, rather than true substrate toxicity. However, at very high concentrations, LCFA can solubilize large segments of the plasma membrane (Desbois and Smith, 2010), which may lead to direct cell toxicity and lysis (Hanaki et al., 1981; Rinzema et al., 1994). Therefore, it appears that LCFA toxicity can depend on concentration and adaptation time.

LCFA could slow biological conversion by toxic inhibition of methanogenic archaea, syntrophic bacteria, and hydrolytic bacteria. Both acetoclastic and hydrogenotrophic methanogens can be affected by LCFA. The concentration of oleate that led to 50% inhibition of activity (i.e.  $IC_{50}$ ) for acetoclastic methanogens ranged from 0.5 – 2.3 mM at 40°C for anaerobic sludge collected from a mesophilic digester (Hwu and Lettinga, 1997). The  $IC_{50}$  of oleate for pure-cultures of the hydrogen-utilizing methanogens *Methanospirillum hungatei* and *Methanobacterium formicicum* was reported to be 0.3 mM and 1.0 mM, respectively (Sousa et al., 2013). While the  $IC_{50}$  for oleate towards the acetoclastic methanogens *Methanosaeta concilii* and *Methanosarcina mazei* was about 0.5 mM, the  $IC_{50}$  for palmitate was ~3 mM for *M. concilii* and ~1.5 mM for *M. mazei*

(Silva et al., 2016). These findings suggest that different methanogenic archaeal species can be affected by LCFA to varying degrees, which has been attributed to differences in cell wall structure and membrane lipid composition (Sousa et al., 2013). Although acetoclastic methanogens have been purported to be more susceptible to LCFA toxicity than hydrogenotrophic methanogens (Hwu and Lettinga, 1997; Lalman and Bagley, 2001), the above findings also indicate that LCFA inhibition of hydrogenotrophic and acetoclastic methanogens can occur within a similar concentration range (Hwu and Lettinga, 1997; Silva et al., 2016; Sousa et al., 2013). With regards to LCFA impacting other microbial populations, the addition of LCFA up to ~0.5 mM had little effect on the fermentation of glucose by an anaerobic digester sludge (Lalman and Bagley, 2002). In contrast, butyrate degradation by the anaerobic sludge was inhibited by 75% with the addition of ~0.5 mM LCFA (Lalman and Bagley, 2002). Thus, it appears that the accumulation of LCFA within a digester would not limit the rate of hydrolysis/fermentation, but rather the kinetics of syntrophic acetogenesis and methanogenesis.

Reported threshold values for FOG loading that led to process inhibition in municipal sludge codigestion have ranged from 30% to 71% of the total feed VS (w/w) (Davidsson et al., 2008; Luostarinen et al., 2009; Silvestre et al., 2011; Wan et al., 2011; Wang et al., 2013; Yalcinkaya and Malina, 2015). Higher threshold values for FOG loading have been proposed for digester biomass previously exposed to lipids (Silvestre et al., 2011; Wang et al., 2013). Silvestre *et al.* (2011) suggested that step-wise increases in the FOG loading allowed for a gradual increase in acetogenic activity in the anaerobic sludge. Methanogenic processes were also observed to develop increased tolerances toward LCFA over time, with increased substrate-conversion activity after pulse (Nielsen & Ahring, 2006; Cavaleiro *et al.*, 2008; Palatsi *et al.*, 2009) and

continuous feeding (Pereira *et al.*, 2005; Cavaleiro *et al.*, 2009; Baserba *et al.*, 2012). However, the relationship between microbial community structure and the maximum loading rate of FOG during codigestion has not been characterized. Additionally, it is unknown whether ‘indicator’ populations can be used to assess the level of LCFA adaptation in an anaerobic digester community. Therefore, understanding the relationships between LCFA accumulation and changes in the microbial population during FOG codigestion may be important for determining maximum allowable FOG loading rates with stable digester operation for enhanced methane production.

## 2.5 MICROBIAL ECOLOGY OF LONG-CHAIN FATTY ACID DEGRADATION

As previously mentioned, LCFA are converted into methane by a syntrophic partnership between obligate hydrogen producing acetogens and methanogens (Schink, 1997). To date, 15 bacteria have been isolated that are capable of anaerobically degrading C<sub>4</sub> – C<sub>18</sub> fatty acids in pure culture or co-culture with hydrogen-utilizing microorganisms (Table 2-3). All of these isolates belong to the two families of syntrophic bacteria, *Syntrophomonadaceae* (Hatamoto *et al.*, 2007a; McInerney, 1992; Sousa *et al.*, 2007b; Wu *et al.*, 2007; F. Zhang *et al.*, 2012) and *Syntrophaceae* (Jackson *et al.*, 1999). Bacteria capable of utilizing LCFA (i.e. greater or equal to 12 carbons in length) include *Syntrophomonas sapovorans*, *Syntrophomonas saponavida*, *Syntrophomonas curvata*, *Syntrophomonas zehnderi*, *Thermosyntrophica lipolytica*, *Thermosyntrophica tengcongensis*, and *Syntrophus aciditrophicus* (Table 2-3).

Syntrophic  $\beta$ -oxidizing bacteria are thought to be slow growing, with maximum growth rates near 0.06 d<sup>-1</sup> reported for butyrate-degrading co-cultures (Beaty and McInerney, 1987;

McInerney et al., 1979). However, the growth of syntrophic LCFA degrading bacteria in environmental systems, such as anaerobic digesters, has not been well characterized. Membrane hybridization probes and fluorescent in-situ hybridization (FISH) probes have been developed to target members of the  $\beta$ -oxidizing *Syntrophomonadaceae* family (H. Ariesyady et al., 2007; Hansen et al., 1999; Menes and Travers, 2006), and were used to detect *Syntrophomonadaceae* bacteria within full-scale anaerobic digesters and laboratory-scale digesters at relative abundances up to 1.75% of the bacteria community (Hansen et al., 1999; McMahon, 2001; McMahon et al., 2004). The abundance of the genus *Syntrophomonas* was quantified at 1.5% of the bacterial population using FISH in a full-scale mesophilic anaerobic digester treating domestic wastewater sludge (H. Ariesyady et al., 2007). Members of *Syntrophomonadaceae* were detected with FISH up to 3% of the bacterial population of a full-scale mesophilic digester treating edible tallow refinery wastewater (Menes and Travers, 2006). Yet, butyrate-degrading syntrophic bacteria were not detected in sludges of 4 full-scale anaerobic digesters using RNA-cleavage probes (Narihiro et al., 2012). These findings suggest that characterized syntrophic  $\beta$ -oxidizing bacteria are present at relatively low abundances in anaerobic digester communities, often below the detection limits of membrane hybridization and FISH probes (Stams et al., 2012). More accurate and sensitive quantification techniques, such as quantitative PCR, may therefore be needed to monitor their growth dynamics during LCFA degradation.

The use of culture-independent molecular fingerprinting techniques to monitor changes in microbial community structure has led to somewhat contradictory results about the key populations involved in LCFA degradation (Baserba et al., 2012; Hatamoto et al., 2007c; Palatsi et al., 2010; Sousa et al., 2007a). Sousa *et al.* (2007a) used PCR-denaturing gradient gel

electrophoresis (DGGE) to study the microbial communities of an anaerobic bioreactor fed oleate (C<sub>18:1</sub>) and palmitate (C<sub>16:0</sub>) followed by batch degradation. The bacterial communities shifted toward more *Syntrophomonadaceae*-affiliated organisms that were not detectable in the initial inoculum. Hatamoto *et al.* (2007c) used RNA-based stable isotope probing (SIP) to identify palmitate (C<sub>16:0</sub>)-degrading bacteria in methanogenic sludges from commercial upflow anaerobic sludge blanket (UASB) reactors. *Syntrophomonadaceae*-affiliated sequences were only detected in half of the <sup>13</sup>C-RNA clone libraries (2 of the 4 reactor libraries), whereas sequences from *Syntrophus* were highly abundant in the clone libraries (Hatamoto *et al.*, 2007c). The observed differences in bacterial community structure shifts during LCFA degradation were hypothesized to be influenced by the degree of saturation of the LCFA used for growth; a clade of *Deltaproteobacteria* (i.e. *Syntrophus*) were associated more with saturated LCFA DNA sequence libraries, while a clade of *Syntrophomonadaceae* were more associated with unsaturated LCFA incubations (Sousa *et al.*, 2009). Conversely, Palatsi *et al.* (2010) found no significant changes in the bacterial community structure using PCR-DGGE on sludge from an anaerobic bioreactor subjected to repeated pulses of LCFA, even though increases in hydrogenotrophic and  $\beta$ -oxidation activities were observed. Recently, a metagenomic assessment of microbial biodiversity based on differential coverage binning in parallel anaerobic digesters led to the recovery of 48 *Syntrophomonas* draft population genomes (Campanaro *et al.*, 2016; Treu *et al.*, 2016b). Yet, metatranscriptomic mapping of mRNA reads to the draft population genomes revealed that only two *Syntrophomonas* bins showed significant response to LCFA addition (Treu *et al.*, 2016a). Thus, it remains uncertain whether the increased tolerance of anaerobic communities to LCFA is a result of the growth of specialized degrading populations (Sousa *et al.*, 2007b; Hatamoto *et al.*, 2007b; Baserba *et al.*, 2012), or rather to changes in the

physiology of existing populations (Palatsi *et al.*, 2010). Therefore, additional ecological understanding of the microorganisms responsible for degrading LCFA in methanogenic communities is needed.



**Table 2-3** Substrate utilization of characterized syntrophic bacteria capable of degrading C<sub>4</sub>-C<sub>18</sub> fatty acids (adapted from Sousa *et al.*, 2009)

Organism	Fatty acid utilized in co-culture with H <sub>2</sub> -utilizing partner										Reference
	Butyrate (C4:0)	Caproate (C6:0)	Caprylate (C8:0)	Caprate (C10:0)	Laurate (C12:0)	Myristate (C15:0)	Palmitate (C16:0)	Stearate (C18:0)	Oleate (C18:1)	Linoleate (C18:2)	
<i>Syntrophomonas bryantii</i>	+	+	+	+	-	-	-	-	ND	ND	(Wu et al., 2007)
<i>Syntrophomonas cellicola</i>	+	+	+	-	-	-	ND	ND	ND	ND	(Wu et al., 2007)
<i>Syntrophomonas curvata</i>	+	+	+	+	+	+	+	+	+	-	(Zhang et al., 2004)
<i>Syntrophomonas erecta erecta</i>	+	+	+	-	-	-	-	-	-	-	(Zhang et al., 2005)
<i>Syntrophomonas erecta sporosyntropha</i>	+	+	+	-	-	-	-	-	-	-	(Wu et al., 2006)
<i>Syntrophomonas palmitatica</i>	+	+	+	+	+	+	+	+	-	-	(Hatamoto et al., 2007a)
<i>Syntrophomonas saponavida</i>	+	+	+	+	+	+	+	+	-	-	(Lorowitz et al., 1989)
<i>Syntrophomonas sapovorans</i>	+	+	+	+	+	+	+	+	+	+	(Zhang et al., 2005)
<i>Syntrophomonas wolfei methylbutyratica</i>	+	+	+	-	-	-	-	-	ND	ND	(Wu et al., 2007)
<i>Syntrophomonas wolfei wolfei</i>	+	+	+	-	-	-	-	-	-	-	(McInerney, 1992)
<i>Syntrophomonas zehnderi</i>	+	+	+	+	+	+	+	+	+	+	(Sousa et al., 2007b)
<i>Syntrophus aciditrophicus</i>	+	+	+	ND	ND	ND	+	+	ND	ND	(Jackson et al., 1999)
<i>Syntrophothermus lipocalidus</i>	+	+	+	+	-	-	-	-	-	-	(Sekiguchi et al., 2000)
<i>Thermosyntropha lipolytica</i>	+	+	+	+	+	+	+	+	+	+	(Svetlitsnyi et al., 1996)
<i>Thermosyntropha tengcongensis</i>	+	+	+	+	+	+	+	+	+	+	(F. Zhang et al., 2012)

+, utilized; -, not utilized; ND, not determined or reported

## 2.6 EFFECT OF MICROBIAL COMMUNITY DIVERSITY AND ECOLOGICAL STABILITY ON ANAEROBIC DIGESTER PERFORMANCE

Advances in molecular microbiology techniques over the past two decades have permitted a closer examination of the microbial communities present in wastewater treatment process biomass (Rittmann et al., 2006). Such investigations have contributed evidence suggesting that microbial communities in biological treatment processes can have high levels of ecological biodiversity (T. Zhang et al., 2012) and display dynamic patterns of community composition over time (Ju and Zhang, 2015; Wittebolle et al., 2008). The vast microbial biodiversity of wastewater treatment biomass is in conflict with traditional biokinetic models used for predicting treatment process performance, such as the IWA Anaerobic Digester Model 1 (ADM1), which assume uniform biomass compositions (Rittmann et al., 2006). Improving our understanding of the relationships between microbial community composition and function within biological wastewater treatment processes thus has potential to revise existing engineering design approaches by incorporating ecological theory to achieve better treatment performance (McMahon et al., 2007).

The *functional stability* of the anaerobic digestion process is often characterized by efficient methane production without VFA or LCFA accumulation (Briones and Raskin, 2003), and has been related to the resilience, resistance, and redundancy of the microbial populations within the various trophic levels (i.e. functional guilds) of the digester microbial food web (Carballa et al., 2015; Werner et al., 2011). *Resistance* refers to the degree in which a community composition remains unchanged during a disturbance; *resilience* indicates to the rate at which the microbial community returns to its original composition following a disturbance; and *functional*

*redundancy* refers to the potential for various microbial taxa to process the same substrate (Allison and Martiny, 2008). Community stability has been related to levels of biodiversity, as indicated by the species *richness* (number of different species) (Elsas et al., 2012; Johnson et al., 2014) and/or the community *evenness* (equality of species abundance) (Wittebolle et al., 2009); although general diversity-stability relationships remain unclear (Shade, 2016). Determining which metrics of diversity and/or ecological stability are important drivers of digester performance is thus a major challenge for the development of predictive treatment models that incorporate ecological principles (McMahon et al., 2007).

In anaerobic digesters, hydrolytic bacteria are thought to have a high degree of functional redundancy (Carballa et al., 2015; Vanwonterghem et al., 2014), whereas syntrophic bacteria and methanogens are thought to be more metabolically specialized (Briones and Raskin, 2003; McInerney et al., 2009) and less likely to undergo competition (Werner et al., 2011). Thus, anaerobic digester biomass may be inherently uneven based on a comparison of functional clades (Briones and Raskin, 2003). Yet, the metabolically-specialized microbes that convert fatty acids, hydrogen, acetate, and carbon dioxide into methane are considered keystone species (Briones and Raskin, 2003), and maintaining their metabolic roles has implications for the efficiency of methane recovery from organic waste. For instance, the discovery of syntrophic acetate oxidation (Lee and Zinder, 1988; Schnürer et al., 1996) demonstrated a new pathway for methanogenesis from acetate, which could afford a digester with greater functional flexibility to convert acetate under stressful conditions (Werner et al., 2014). The reported flexible metabolism of *Methanosarcina* species to use both hydrogen and acetate for growth (Phelps et al., 1985) could also allow for multiple pathways of methanogenesis within an anaerobic digester population. The

ability to enrich for *Methanosarcina* species over *Methanosaeta* species by changing the digester feeding pattern (Conklin et al., 2006) indicated that it may be possible to impact the functional redundancy of keystone functional groups by adjusting digester operating conditions. Similarly, it was observed that four distinct clades of syntrophic propionate oxidizing bacteria (POB) were enriched in an anaerobic digester operated in fill-and-draw mode, and the coexistence of multiple syntrophic POB groups was attributed to the different biokinetic characteristics of the POB clades and the periodic changes in propionate concentration with batch feeding (H. D. Ariesyady et al., 2007). Distinct syntrophic POB populations with different biokinetic parameters were also detected in the first and second phases of a thermophilic phased-digester based on differences in organic loading (Zamanzadeh et al., 2013). However, Werner *et al.* (2011) observed that the same syntrophic populations rebounded after periods of starvation in full-scale digesters treating distillery waste, and thus concluded that syntrophic populations were resilient rather than functionally redundant. If different syntrophic and methanogenic consortia could have different rates of fatty acid conversion (e.g. functional redundancy), then biological selective pressures could potentially be incorporated into FOG codigester operating strategies to favorably steer the LCFA-degrading community toward a composition with higher bioconversion kinetics. Thus, the effects of codigester operating conditions on the resistance, resilience, and functional redundancy of syntrophic and methanogenic consortia warrant further investigation to facilitate appropriate strategies to maximize biomethane recovery.

# Chapter 3. MONITORING THE DYNAMICS OF SYNTROPHIC BETA-OXIDIZING BACTERIA DURING ANAEROBIC DEGRADATION OF OLEIC ACID BY QUANTITATIVE PCR

**This work is published as:**

Ziels, R. M., Beck, D. A., Martí, M., Gough, H. L., Stensel, H. D., & Svensson, B. H. (2015). Monitoring the dynamics of syntrophic  $\beta$ -oxidizing bacteria during anaerobic degradation of oleic acid by quantitative PCR. *FEMS microbiology ecology*, *91*(4), doi: <http://dx.doi.org/10.1093/femsec/fiv028>

## 3.1 ABSTRACT

The ecophysiology of long-chain fatty acid (LCFA)-degrading syntrophic  $\beta$ -oxidizing bacteria has been poorly understood due to a lack of quantitative abundance data. Here, TaqMan quantitative PCR (qPCR) assays targeting the 16S rRNA gene of the known mesophilic syntrophic  $\beta$ -oxidizing bacterial genera *Syntrophomonas* and *Syntrophus* were developed and validated. Microbial community dynamics were followed using qPCR and Illumina-based high throughput amplicon sequencing in triplicate methanogenic bioreactors subjected to five consecutive batch feedings of oleic acid. With repeated oleic acid feeding, the initial specific methane production rate significantly increased along with the relative abundances of *Syntrophomonas* and methanogenic archaea in the bioreactor communities. The novel qPCR assays showed that *Syntrophomonas* increased from 7% to 31% of the bacterial community 16S rRNA gene concentration, whereas that of *Syntrophus* decreased from 0.02% to less than 0.005%. High throughput amplicon sequencing also revealed that *Syntrophomonas* became the dominant genus within the bioreactor microbiomes. These results suggest that increased specific mineralization rates of oleic acid were attributed to quantitative shifts within the microbial

communities toward higher abundances of syntrophic  $\beta$ -oxidizing bacteria and methanogenic archaea. The novel qPCR assays targeting syntrophic  $\beta$ -oxidizing bacteria may thus serve as monitoring tools to indicate the fatty acid  $\beta$ -oxidization potential of anaerobic digester communities.

### 3.2 INTRODUCTION

Anaerobic digestion (AD) is an attractive biotechnology used to treat organic wastes and produce renewable energy as methane. Co-digesting energy-rich wastes with municipal sludge or manure has gained increased interest due to observed improvements in bioreactor methane production (Davidsson et al., 2008; Luostarinen et al., 2009; Wang et al., 2013). Lipid-rich wastes are desirable co-substrates for AD due to their relatively high specific methane yield (Cavaleiro et al., 2008; Palatsi et al., 2010). However, the long-chain fatty acids (LCFA) produced during lipid hydrolysis have been shown to inhibit anaerobic microorganisms (Angelidaki and Ahring, 1992; Hanaki et al., 1981; Koster and Cramer, 1987; Lalman and Bagley, 2000; Rinzema et al., 1994). Achieving efficient degradation of LCFA by anaerobic microorganisms is therefore critical to obtain stable and elevated methane production during the AD of lipid-rich wastes.

Under anaerobic conditions, LCFA are primarily degraded through  $\beta$ -oxidation to yield hydrogen and acetate (Weng and Jeris, 1976). Methane formation from LCFA occurs through a syntrophic partnership between LCFA  $\beta$ -oxidizing acetogenic bacteria and methanogenic archaea, which are responsible for maintaining low concentrations of acetate and hydrogen (Schink, 1997; Sousa et al., 2009). Currently, all of the bacterial species that have been characterized to grow on LCFA in syntrophic partnership with methanogens belong to the families of *Syntrophomonadaceae*

within the class of *Clostridia* (Hatamoto et al., 2007a; McInerney, 1992; Sousa et al., 2009, 2007b; Wu et al., 2007; Zhao et al., 1993), or *Syntrophaceae* within the subclass of *Deltaproteobacteria* (Jackson et al., 1999).

The effect of LCFA exposure on methanogenic activity has been observed to vary with contact time, and has been attributed to either microbial acclimation to LCFA or adaptation through changes in the microbial community composition. Despite early reports of bactericidal (Rinzema et al., 1994) and permanent toxic effects of LCFA (Angelidaki and Ahring, 1992), LCFA inhibition was shown to be reversible with anaerobic microorganisms capable of mineralizing biomass-sorbed LCFA after a lag period (Pereira et al., 2005, 2004, 2003). Methanogenic communities were also observed to develop an increased tolerance toward LCFA after pulse (Cavaleiro et al., 2008; Nielsen and Ahring, 2006; Palatsi et al., 2009) and continuous feeding (Baserba et al., 2012; Cavaleiro et al., 2009; Pereira et al., 2005). However, the use of culture-independent molecular fingerprinting techniques (Baserba et al., 2012; Hatamoto et al., 2007c; Palatsi et al., 2010; Sousa et al., 2007a) led to contradictory results regarding the changes in microbial community structure during LCFA degradation. Sousa *et al.* (2007a) used PCR-denaturing gradient gel electrophoresis (DGGE) to study the microbial communities of an anaerobic bioreactor fed oleate (C18:1) and palmitate (C16:0) followed by batch degradation. The bacterial communities shifted toward more *Syntrophomonadaceae*-affiliated organisms that were not detectable in the initial inoculum. Conversely, Palatsi *et al.* (2010) found no significant changes in the bacterial community structure using PCR-DGGE on sludge from an anaerobic bioreactor subjected to repeated pulses of LCFA, even though improvements in hydrogenotrophic and  $\beta$ -oxidation activities were observed. Thus, it remains uncertain whether

the increased tolerance of anaerobic communities to LCFA is a result of the proliferation of specialized degrading populations (Baserba et al., 2012; Hatamoto et al., 2007c; Sousa et al., 2007a), or rather to changes in the physiology of existing populations (Palatsi et al., 2010). Additional ecological understanding of the microorganisms responsible for degrading LCFA in methanogenic communities is thus needed.

The ability to quantify syntrophic  $\beta$ -oxidizing bacteria could offer new insight into their ecophysiology during the degradation of LCFA. Membrane hybridization (Hansen et al., 1999) and cleavage (Narihiro et al., 2012) probes have been previously developed targeting the mesophilic syntrophic  $\beta$ -oxidizing genera *Syntrophomonas* and *Syntrophus*. Yet, poor detection has been reported when employing these methods due to the potentially low concentrations of  $\beta$ -oxidizing bacteria in anaerobic bioreactors (Menes and Travers, 2006; Narihiro et al., 2012), thus calling for a more sensitive quantification technique. Quantitative PCR (qPCR) is a widely employed method that uses DNA primer sets to obtain rapid and highly-sensitive detection of specific microorganisms (Bustin et al., 2009), and has proven to be a powerful tool for monitoring microbial populations in the complex communities of anaerobic bioreactors (Hori et al., 2006; Lee et al., 2009; Westerholm et al., 2011; Yu et al., 2005). The use of a dual-labeled fluorogenic hydrolysis probe in the qPCR assay (TaqMan qPCR) may offer a higher level of specificity in comparison to SYBR Green assays (Wittwer et al., 1997). Currently, there have been no qPCR primer and TaqMan hydrolysis probe sets designed to quantify mesophilic syntrophic LCFA  $\beta$ -oxidizing bacteria.



The objective of this study was to develop and validate TaqMan qPCR assays targeting the known mesophilic syntrophic LCFA  $\beta$ -oxidizing genera *Syntrophomonas* and *Syntrophus*, and to apply the newly developed qPCR assays to monitor changes in the abundance of the syntrophic  $\beta$ -oxidizing groups in methanogenic bioreactors that were batch-fed with oleic acid. High-throughput amplicon sequencing of the bacterial 16S rRNA gene was also conducted on time-series samples from the bioreactors to further examine microbial community dynamics.

### 3.3 MATERIALS AND METHODS

#### 3.3.1 *Batch-fed Methanogenic Bioreactors Degrading Oleic Acid*

Triplicate bioreactors (330 mL Pyrex glass serum bottles) were initially purged with N<sub>2</sub>/CO<sub>2</sub> (80:20, 1atm) and sealed with butyl rubber septa. The bioreactors were seeded with sludge (21 g VS L<sup>-1</sup>) from a mesophilic laboratory-scale complete-mix AD bioreactor co-digesting grease waste with primary and waste activated sludge. The seed sludge was diluted 50:50 with anaerobic basal medium prepared according to Karlsson *et al.* (1999). The bioreactors were initially incubated at 37°C for seven days until methane production ceased from the background substrate in the seed sludge. After this period, sludge samples for DNA extraction (10 mL), total solids and volatile solids (TS/VS) (8 mL), volatile fatty acids (VFA) (1 mL), and LCFA (3 mL) analyses were withdrawn to characterize the initial conditions.

The bioreactors were incubated without shaking in a 37°C environmental chamber during five consecutive batch-feedings of oleic acid. The bioreactors were fed with oleic acid (80% purity, VWR) every 7th day using a needle and syringe to obtain the target initial concentrations given in Table 3-1. The liquid volume that was removed for liquid sampling throughout the batch

degradation period (42 mL) was replaced with anaerobic basal medium during each subsequent batch feeding to maintain an initial working volume of 120 mL. This operation resulted in the replacement of approximately two reactor liquid volumes throughout the experimental period, and thus promoted the washout of the initial inoculum over time. Liquid samples were withdrawn with a needle and syringe for analysis of VFA (1 mL) and LCFA (3 mL) six times during each batch degradation period. Sludge samples for DNA extraction (10 mL) and TS/VS and pH (8 mL) were withdrawn at the end of each batch period before the subsequent feeding. The bioreactor headspace was purged with N<sub>2</sub>/CO<sub>2</sub> (80:20, 1 atm) prior to the addition of new substrate at the start of each batch-feeding period. The bioreactor conditions during each batch degradation period are summarized in Table 3-1.

**Table 3-1** Operating conditions and performance characteristics of methanogenic bioreactors degrading oleic acid. (*n*=3)

Parameter	Batch Cycle				
	1	2	3	4	5
VS (g L <sup>-1</sup> ) <sup>a</sup>	7.8 ± 0.3	4.9 ± 0.2	3.5 ± 0.1	2.1 ± 0.2	1.2 ± 0.1
pH	7.3 ± 0.03	7.3 ± 0.01	7.2 ± 0.03	7.2 ± 0.01	7.1 ± 0.01
Oleic Acid Added (mM)	2.9	4.0	5.0	5.0	6.6
Initial Oleic Acid to Solids Ratio (mg g VS <sup>-1</sup> ) <sup>b</sup>	100 ± 4	230 ± 10	410 ± 7	670 ± 65	1570 ± 130
Initial Specific Methane Production Rate (mL CH <sub>4</sub> g VS <sup>-1</sup> d <sup>-1</sup> )	57 ± 3	85 ± 2	130 ± 1	170 ± 7	260 ± 24

<sup>a</sup> Average of the levels at the beginning and end of each batch degradation period

<sup>b</sup> Based on the amount of oleic acid added and the VS concentration in each vial, since the LCFA did not accumulate above 0.15 mM at the end of each batch period (see Table A2)

Biogas volume and composition were measured daily throughout the bioreactor operation. The initial specific methane production rates in each batch period were determined by dividing the

initial slope of the methane production curve (in mL CH<sub>4</sub> L<sup>-1</sup> d<sup>-1</sup>) by the average volatile solids (in g VS L<sup>-1</sup>) of each vial, and were expressed as mL CH<sub>4</sub> g VS<sup>-1</sup> d<sup>-1</sup>.

### 3.3.2 *Extraction and Quantification of Genomic DNA*

Bioreactor samples for DNA extraction were immediately centrifuged at 10,000 x g at 4°C for 10 min, decanted, and stored at -20°C. Genomic DNA was isolated from approximately 0.2 g of wet solids using the PowerSoil® RNA/DNA Isolation Kit (MO BIO, Inc, Carlsbad, California) according to the manufacturer instructions. This DNA extraction protocol was chosen due to its use of phenol-chloroform, which can help to ensure efficient recovery of high-quality archaeal and bacterial DNA (Urakawa et al., 2010). The concentration of extracted DNA was immediately measured with the Quant-IT dsDNA High Sensitivity Assay Kit with a Qubit 2.0 fluorometer, according to the manufacturer's instructions (Invitrogen, Carlsbad, California). Extracted DNA was stored in nuclease-free water at -20°C.

### 3.3.3 *Design and Validation of qPCR Primer and Probe Sets*

16S rRNA gene sequences of strains belonging to the genera *Syntrophomonas* and *Syntrophus* were obtained from the National Center for Biotechnology Information (NCBI) GenBank database (<https://www.ncbi.nlm.nih.gov/genbank/>, retrieved July, 2013) and separately aligned using the Clustal package in Jalview software (v. 2.8) (Waterhouse et al., 2009). Sequence regions of high similarity within the multiple gene alignments were identified, and were used to design potential hybridization sites for primers and probes. Primer sequences were designed to meet the following criteria: minimal dimer formation, a guanine + cytosine (GC) content of 40% to 70%, minimal repeats of guanine and cytosine, an amplicon fragment length less than 150 bp, and the fewest degenerate nucleotides possible. Hydrolysis (TaqMan) probes were designed

based on: a 5' location as close to the forward primer as possible, less than 30 nucleotides in length, minimal self- and cross- annealing, no terminal guanine base at the 5' end, a melting temperature 5°C to 10°C above the associated primer pair, and minimal degenerate nucleotides. All hydrolysis probes were labeled with 6-FAM at the 5' end and BHQ-1 at the 3' end.

The optimal qPCR primer and probe sets were chosen based on their adherence to the above criteria, as well as their target group specificity and coverage. The specificity and group coverage of each primer and probe set was tested *in silico* by conducting searches with: BLAST of the GenBank Database (<http://blast.ncbi.nlm.nih.gov/>); the Ribosomal Database Project ProbeMatch software (Cole et al., 2009); and the SILVA TestPrime 1.0 and TestProbe 3.0 programs (Klindworth et al., 2013). Potential false-positive targets were identified by increasing the number of allowed sequence mismatches in the *in silico* database searches. Organisms with three or more mismatches within each of the three oligonucleotide sequences ( $\geq 9$  mismatches total) were excluded from the analysis due to their low probability of amplification (Yu et al., 2005). The optimal primer/probe sets targeting *Syntrophomonas* and *Syntrophus* 16S rRNA genes are given in Table 3-2 along with their respective target group coverage.

**Table 3-2** Characteristics of qPCR primers and hydrolysis probes developed to target *Syntrophomonas* and *Syntrophus* genera

Oligo. Name <sup>a</sup>	Target Group	Position <sup>b</sup>	Oligo. Sequence (5' to 3')	Expected Length (bp)	T <sub>m</sub> (°C) <sup>c</sup>	Target Group Coverage (%) <sup>d</sup>
Symm-678 (F)		678-691	CCWGGTGTAGCGGT		60.3	97
Symm-696 (P)	<i>Syntrophomonas</i>	696-722	TGCGTAGAAATCAGGAGGAAYACCAGT	75	70.0	90
Symm-738 (R)		738-752	TCAGGGYCAGTCCAG		61.5	97
Syntr-441 (F)		441-459	GGTGGGAAGAAATGTATKGA		61.6	88
Syntr-462 (P)	<i>Syntrophus</i>	462-487	TTAAYAGCCTTTGTAAGTACCGGTAC	137	66.8	88
Syntr-559 (R)		559-576	CTCTTACGCCCAATGAT		60.1	88

<sup>a</sup> F = forward primer; P = hydrolysis probe; R = reverse primer

<sup>b</sup> According to *Escherichia coli* J01695 numbering

<sup>c</sup> Calculated using nearest-neighbor method with the OligoAnalyzer 3.1 program (<http://www.idtdna.com>), using the model inputs: 200nM probe, 500nM primer, 200mM monobasic salt

<sup>d</sup> Calculated as the ratio of matches with sequences from isolated organisms within the target group over the total number of sequences from isolated organisms in that group. The ratios were calculated based on available sequences in the Ribosomal Database Project using the Probe Match program (<http://rdp.cme.msu.edu/probematch>) with inputs: Quality="Good", Size ≥ 1200bp, Source="Isolates", Mismatches=0.

In addition to the *in silico* analysis, the specificities of the qPCR assays were tested empirically using genomic DNA from pure cultures. Positive controls included genomic DNA from: *Syntrophomonas wolfei subsp. saponavida* (DSM 4212), *Syntrophomonas palmitatica* (DSM 18709), *Syntrophomonas zehnderi* OL-4, *Syntrophus aciditrophicus* (DSM 26646), and *Syntrophus gentianae* (DSM 8423). Negative controls to test for non-specific amplification included DNA from: *Syntrophobacter wolinii*, *Syntrophobacter pfennigii*, *Pelotomaculum propionicum*, *Desulfotomaculum kuznetsovii* (DSM 6115), *Desulfomonile tiedjei* (DSM 6799), *Desulfovibrio desulfuricans* (DSM 642), *Clostridium ultunense*, *Clostridium acidurici* (DSM 604), *Enterococcus faecalis*, *Streptococcus pyogenes*, *Escherichia coli*, *Pseudomonas aeruginosa*, *Methanosaeta concilii* (DSM 3671), *Methanospirillum hungatei* (DSM 864), *Methanococcus voltae* (DSM 1537), *Methanosarcina barkeri* (DSM 800), and *Methanobacterium formicicum* (DSM 1535). Most genomic DNA samples of pure-culture

isolates were purchased from the Deutsche Sammlung von Mikroorganismen und Zellkulturen GmbH (DSMZ) (Braunschweig, Germany). Additional genomic DNA samples from isolated strains were obtained from collections at Wageningen University (Wageningen, Netherlands), Linköping University (Linköping, Sweden) and the Swedish University of Agricultural Sciences (Uppsala, Sweden). Approximately 0.5-2 ng DNA of each pure-culture DNA sample was loaded in the qPCR reaction for specificity testing.

#### 3.3.4 *Quantitative PCR (qPCR)*

qPCR targeting partial 16S rRNA gene sequences was performed using a LightCycler 480 system (Roche Diagnostics GmbH, Mannheim, Germany). Each 20  $\mu$ L reaction mix contained 5  $\mu$ L DNA template, 2  $\mu$ L PCR-grade water (Roche Diagnostics GmbH), 500 nM of each forward and reverse primers, 200 nM of hydrolysis probe, and 10  $\mu$ L LightCycler 480 Probes Master mix (2X, Roche Diagnostics GmbH). All samples were analyzed in duplicate. No-template controls (NTCs) were included with each qPCR run to ensure that no contamination occurred.

In addition to the *Syntrophomonas* and *Syntrophus* genus-level qPCR assays developed in this study (Table 3-2), qPCR analysis was also conducted targeting 16S rRNA genes of the domain Bacteria, the methanogenic archaeal orders of *Methanomicrobiales*, *Methanobacteriales*, *Methanococcales*, and the methanogenic archaeal families of *Methanosarcinaceae* and *Methanosaetaceae* using previously developed primer/probe sets (Yu et al., 2005). The details of all primer/probe sets used for qPCR in this study are provided in Table A1 (Supplemental Information). The amplification procedure for all qPCR assays consisted of an initial denaturation at 95°C for 10 min, followed by 42 cycles of 95°C for 10 s, and annealing and

extension at 60°C for 30 s. The only exception was the *Methanomicrobiales* assay, which had the annealing and extension step at 63°C for 30 s (Yu et al., 2005).

DNA samples for calibration standards were prepared by cloning the target PCR amplicon fragment of each primer set into a pUC57 plasmid (GeneScript, Piscataway, New Jersey). The strains from which 16S rRNA gene sequences were used to construct the calibration standards for each target group are given in Table A1 (Supplemental Information). Plasmids containing the target PCR amplicon sequence were linearized with XbaI (FastDigest®, Thermo Scientific, Waltham, Massachusetts) according to the manufacturer's instructions, and were quantified by Qubit. Gene copy numbers were calculated from the measured DNA concentration and the molecular weight of the ligated plasmid containing the PCR amplicon insert. Calibration standards for each qPCR primer/probe set were constructed from the linearized plasmids in a dilution series ranging from 25 to 10<sup>8</sup> gene copies (9 calibration standard concentrations total). Calibration standards were run in duplicate, and were included in each qPCR run for all target groups. The average slopes and intercepts of the qPCR calibration standard curves for the various targets are given in Table A1 (Supplemental Information).

Extracted DNA from the bioreactors was diluted 1:10 in nuclease-free water to prevent PCR inhibition. A four-fold series of 1:10 dilutions of a randomly selected experimental DNA sample was included with each qPCR run to ensure that the PCR efficiency of the experimental samples was similar to the calibration standards (efficiency values were within 10% of standards). The gene copy numbers were normalized to the amount of DNA loaded in the PCR reaction (ng) in order to correct for any variation in DNA extraction efficiencies between samples.

### 3.3.5 High-Throughput Amplicon Sequencing of Bacterial 16S rRNA Genes

All DNA extracts were processed for high-throughput amplicon sequencing on the Illumina MiSeq platform. Two-step nested PCR was conducted prior to sequencing to improve PCR sensitivity. The primers used in the initial PCR were a modified 341F (CCTAYGGGRBGCASCAG) and a modified 806R (GGACTACNNGGGTATCTAAT) (Sundberg et al., 2013), which targeted a 465 bp DNA fragment flanking the V3 and V4 regions of the 16S rRNA gene of *Bacteria* and *Archaea*. The initial PCR was performed in a total volume of 20  $\mu$ L containing: 5  $\mu$ L of sample DNA extract (diluted 1:10), 500 nM of each of the primers 341F and 806R, 0.2 mM dNTPs mixture, 0.4 U of Phusion High Fidelity DNA Polymerase (Finnzymes, Finland), 1X Phusion High-Fidelity Buffer (Finnzymes), and PCR grade water. The PCR amplification was performed with an initial incubation at 98°C for 30 s, followed by 35 cycles of 98°C for 5 s, annealing at 60°C for 20 s, extension at 72°C for 20 s, and a final extension step at 72°C for 5 min. PCR was run in duplicate for each DNA sample and then subsequently pooled. PCR products were purified using the High-Pure PCR Cleanup Kit (Roche Diagnostics GmbH, Mannheim, Germany) according to the manufacturer's instructions. DNA concentrations of the purified PCR product were subsequently quantified using the Quant-IT dsDNA High Sensitivity Assay Kit and a Qubit fluorometer, and amplicon size was verified by gel electrophoresis. Addition of adapters and indices to DNA fragments was done in a second PCR using the modified primers 515F (GTGCCAGCMGCCGCGGTAA) and 806R. The second PCR was performed in a total volume of 20  $\mu$ L containing: 2  $\mu$ L AccuPrime™ PCR Buffer (10X, Invitrogen), 0.24 U AccuPrime™ Taq DNA Polymerase High-Fidelity (Invitrogen), 500 nM each of the fusion primers 515F and 806R with indexes, 2  $\mu$ L of 1:10 diluted PCR product from the first PCR, and PCR grade water. The second PCR was run with the following



conditions: 94°C for 2 min, followed by 15 cycles of 94° C for 20 s, 56°C for 30 s and 68°C for 40 s, and a final extension at 68°C for 5 min. PCR amplicons were purified using Agencourt AMPure XP (Agencourt Bioscience Corporation, MA, USA) and the concentration was measured using PicoGreen staining (Invitrogen), according to the manufacturer protocols. The sample amplicons were pooled at equimolar concentrations, and subjected to high-throughput sequencing on the Illumina MiSeq platform at the University of Copenhagen Molecular Microbial Ecology Lab according to MiSeq Reagent Kit Preparation Guide (Illumina, Inc., San Diego, CA, USA). Sequences were submitted to the NCBI Sequence Read Archive as BioProject PRJNA262832.

Sequences were processed and analyzed using QIIME version 1.8.0 (Caporaso et al., 2010b). Paired-end sequences were joined using the fastq-join method (Aronesty, 2013) within the QIIME script *join\_paired\_ends.py* with a minimum overlap of 100 bp and a zero percent difference allowed in the overlap region. Sequences shorter than 220 bp and with quality scores less than 20 were filtered using the *split\_libraries\_fastq.py* script in QIIME. Sequence chimeras were identified and filtered with USEARCH61 (Edgar, 2010; Edgar et al., 2011). Filtered sequences were clustered into operational taxonomic units (OTU's) based on 3% sequence divergence using USEARCH61 (Edgar, 2010). Representative sequences of each OTU were identified based on the cluster seed, and were classified using a naïve Bayesian algorithm with the Ribosomal Database Project (RDP) Classifier program version 2.2 (Wang et al., 2007). Archaeal sequences were removed from the sequence libraries prior to further analysis of the bacterial community. The representative sequences were aligned to the Greengenes core reference alignment (DeSantis et al., 2006) using PyNAST (Caporaso et al., 2010a). Weighted

UniFrac distances (Lozupone and Knight, 2005) were calculated with QIIME to determine changes in phylogenetic community structure over time. Community richness was determined by rarefying each sample based on the lowest number of sequences observed in a single sample, and the community evenness was estimated with the Gini coefficient (Wittebolle et al., 2009).

### 3.3.6 *Analytical Methods*

The total gas production was measured based on the pressure increase in the bioreactors using a handheld pressure transducer (Testo 3123, Testo, Sparta, New Jersey). The change in headspace volume over time within the batch vials due to liquid sampling was accounted for when determining the total gas production. The methane content of the headspace was measured in triplicate by GC-FID (Hewlett Packard, 5880 A) at each gas pressure sampling point. All measured gas volumes are reported at standard temperature and pressure (1 atm pressure and 0°C). The pH of bioreactor samples was measured using an Inolab pH 7310 meter (WTW, Weilheim, Germany). TS and VS were determined according to Standard Methods (Eaton & Franson, 2005). VFA (acetate, propionate, butyrate, iso-butyrate, valerate, iso-valerate, capronate and iso-capronate) were analyzed by GC-FID (HP 6890, Hewlett Packard), and were separated with a BP21 (FFAP) column (30m x 0.32mm x 0.25µm, SGE Analytical Science) as described previously (Jonsson and Borén, 2002).

The protocol for LCFA extraction and analysis was adapted from Lalman and Bagley (2000). Bioreactor sludge samples were stored at -20°C and thawed at 4°C prior to LCFA extraction. 1 mL of sample was transferred to a 10 mL glass vial, and the following were added: 100 µL of 10 g L<sup>-1</sup> pentadecanoic acid (>99% purity, Sigma Aldrich, St. Gallen, Switzerland) in methanol as internal standard (IS), 200 µL of 250 g L<sup>-1</sup> sodium chloride in MilliQ water, two drops of 50%

sulfuric acid, and 2 mL of 1:1 hexane:methyl-tert-butylether (MTBE). Samples were then sealed with Teflon-lined caps, vortexed to mix, placed on an orbital shaker at 250 rpm for 20 minutes before centrifuging at  $4,500 \times g$  for 10 minutes. The organic supernatant was decanted for analysis by GC-FID (Clarus 580, Perken-Elmer) with a split/splitless injector. LCFA were separated with a BP21 (FFAP) column (30m x 0.32mm x 0.25 $\mu$ m, SGE Analytical Science), with He as the carrier-gas at a flow of 2 mL min<sup>-1</sup> and a split-ratio of 1:10. The injector temperature was 250°C and the injection volume was 1  $\mu$ L. The detector temperature was 280°C and the detector flow was comprised of 45 mL min<sup>-1</sup> H<sub>2</sub> and 450 mL min<sup>-1</sup> air. The oven temperature was initially 160°C with a 20°C min<sup>-1</sup> ramp to 225°C, isothermal for 15 minutes, then a final 5°C min<sup>-1</sup> ramp to 240°C. Calibration standards included 10, 25, 50, 100, 250, 500, and 1000 mg L<sup>-1</sup> of palmitic, stearic, and oleic acids (>99% purity, Sigma Aldrich), each containing 500 mg L<sup>-1</sup> of pentadecanoic acid (IS) dissolved in 1:1 hexane:MTBE. The average recovery of palmitic acid, stearic acid, and oleic acid was 88%, 87%, and 102%, respectively.

### 3.3.7 *Statistical Analysis*

Changes in abundance based on qPCR data were determined using two-tailed t-tests with biological ( $n=3$ ) and technical replicates ( $n=2$ ). Changes in abundance and microbial community structure parameters (i.e. Unifrac distances, evenness, richness) based on high throughput amplicon sequencing data were determined using two-tailed t-tests with biological replicates ( $n=3$ ).

## 3.4 RESULTS

### 3.4.1 Validation of *Syntrophomonas* and *Syntrophus* Genus-Level qPCR Assays

The qPCR primer and probe sets developed for *Syntrophomonas* and *Syntrophus* successfully detected all species belonging to the respective target groups during the specificity testing with pure-culture DNA (Figures A1 and A2, Supplemental Information). Moreover, the *in silico* analysis of the *Syntrophus* and *Syntrophomonas* qPCR assays showed that between 88% and 97% of target 16S rRNA gene sequences in the RDP database matched the corresponding primers and probe sets (Table 3-2), indicating that false-negative results were minimized due to the high target group coverage of the assays. Slopes of the calibration dilution series were calculated by performing linear regressions on plots of  $C_t$  values versus the  $\log_{10}$  of the template concentrations. The reproducibility of the qPCR assays was tested by generating 8 standard calibration curves over approximately 4 months, yielding average slopes of -3.30 and -3.32 for the *Syntrophomonas* and *Syntrophus* sets, respectively. These average qPCR calibration slopes for the *Syntrophomonas* and *Syntrophus* assays corresponded to average PCR efficiencies of 101% and 100%, respectively. The relative standard deviations of the slopes and intercepts of standard calibration curves were less than 3%. The linear dynamic range of both primer/probe sets was between 25 to  $10^8$  gene copies (Figures A3 and A4, Supplemental Information).

The *in silico* testing of the *Syntrophomonas* qPCR assay identified potential false-positive 16S rRNA gene sequences from non-target organisms. Potentially interfering sequences with 4 to 5 total mismatches within the primer and probe oligonucleotide sequences aligned to the genera: *Desulfotomaculum*, *Desulfitibacter*, *Syntrophothermus*, *Thermosyntropha*, *Thermoanaerobacter*, *Halomonas*, and *Chromohalobacter*. Sequences from the genus *Pelospira* were also identified as

potential false-positives with less than 4 total mismatches in the primer and probe sequences of the *Syntrophomonas* qPCR assay. Yet, *Syntrophothermus*, *Thermosyntropha*, and *Thermoanaerobacter* are thermophilic (Sekiguchi et al., 2000; Svetlitsnyi et al., 1996; F. Zhang et al., 2012), while *Halomonas* and *Chromohalobacter* species thrive in hypersaline environments (Arahal and Ventosa, 2006; Mata et al., 2002), and are thus not expected to be present in the study bioreactors. Moreover, no sequences aligning to *Desulfotomaculum*, *Halomonas*, *Chromohalobacter*, and *Thermoanaerobacter* were detected by high-throughput amplicon sequencing of the bioreactor samples, while sequences aligning to *Desulfitibacter* and *Syntrophothermus* were detected below 0.1% relative abundance and *Thermosyntropha* and *Pelospora* sequences remained below 0.5% relative abundance. It is therefore unlikely that DNA from the above groups interfered with the specificity of the *Syntrophomonas* qPCR assay applied to the mesophilic bioreactors. Moreover, the specificity of the *Syntrophomonas* qPCR assay was verified with no observed amplification of *Desulfitibacter alkalitolerans* DNA (5 total mismatches), and minimal amplification of *Desulfotomaculum kuznetsovii* DNA (4 total mismatches) (Figure A1, Supplemental Information). The potential for interference with the *Syntrophomonas* qPCR assay due to the presence of *Desulfotomaculum* DNA was further negated by demonstrating that the addition of *D. kuznetsovii* DNA (0.6 ng) to each standard in the calibration curve had no significant impact on the slope of the standard curve between 100 to 10<sup>8</sup> gene copies (Figure A5, Supplemental Information). The *Syntrophomonas* 16S rRNA gene concentration in the bioreactor DNA samples also showed no significant change when spiked with 10<sup>6</sup> to 10<sup>7</sup> 16S gene copies of *D. kuznetsovii* (Figure A6, Supplemental Information) ( $p > 0.10$ ), and testing of all other pure-culture isolates with the *Syntrophomonas* qPCR assay showed no amplification of non-target DNA (Figure A1, Supplemental Information). The

*Syntrophomonas* qPCR assay was therefore highly specific for *Syntrophomonas* 16S rRNA genes.

No potential non-target 16S rRNA gene sequences were found with less than 2 mismatches in each of the three oligonucleotides in the *Syntrophus* primer/probe set (up to 6 mismatches total) during the *in-silico* database searches. Furthermore, the specificity testing showed that the *Syntrophus* primer/probe set did not amplify DNA from *Desulfomonile tiedjei* (Figure A2, Supplemental Information), a species that also belongs to the family *Syntrophaceae*, nor was amplification observed with other non-target DNA samples (Figure A2, Supplemental Information). The effect of non-target DNA on the efficiency of the *Syntrophus* primer/probe set was assessed by spiking each standard in the calibration curve with *D. tiedjei* DNA (0.5 ng DNA), which had no significant impact on the PCR slope or linear dynamic range between 25 to 10<sup>8</sup> gene copies (Figure A7, Supplemental Information). Thus, false-positive results were minimized by the high target specificity of the *Syntrophus* qPCR assay.

### 3.4.2 Specific Mineralization Rates of Oleic Acid in Methanogenic Bioreactors

The amount of oleic acid added to the bioreactors during batch feeding was more than doubled by the fifth batch degradation cycle (Table 3-1), and for all degradation cycles most of the oleic acid was metabolized (Table A2, Supplemental Information). The detection of stearic, palmitic, and acetic acids as intermediates from oleic acid (Table A2, Supplemental Information) indicated that  $\beta$ -oxidation was the primary degradation pathway for oleic acid metabolism (Lalman and Bagley, 2001; Pereira et al., 2002; Weng and Jeris, 1976). While the VS concentration decreased in each consecutive batch cycle due to the replacement of a fraction of the liquid volume with anaerobic basal medium during feeding, the initial specific methane production rate (normalized

to VS) increased after each batch feeding (Table 3-1). This observation suggested an increase in the fraction of LCFA  $\beta$ -oxidizing consortia, as discussed below.

### 3.4.3 Quantitative Dynamics of Syntrophic $\beta$ -Oxidizing Bacteria by qPCR

The newly developed qPCR assays targeting the  $\beta$ -oxidizing genera of *Syntrophomonas* and *Syntrophus* were applied to the triplicate bioreactors degrading oleic acid. Changes in the 16S rRNA gene concentration of the syntrophic bacterial groups are shown in Figure 3-1A and Figure 3-1B. The *Syntrophomonas* 16S rRNA gene concentration significantly increased from  $4.2 \times 10^4$  to  $22 \times 10^4$  copies  $\text{ng}^{-1}$  DNA during the bioreactor operation ( $p=1\text{E-}11$ ; Figure 3-1A), while the *Syntrophus* 16S rRNA gene concentration significantly decreased from 90 to 9 copies  $\text{ng}^{-1}$  DNA ( $p=2\text{E-}10$ ; Figure 3-1B). The 16S rRNA gene concentration of the Bacteria domain slightly increased throughout the bioreactor operation from  $5.9 \times 10^5$  to  $7.1 \times 10^5$  copies  $\text{ng}^{-1}$  DNA ( $p=0.002$ ). The gene copy levels of the two syntrophic  $\beta$ -oxidizing groups were normalized to that of the Bacteria domain to assess the relative abundances of the groups over time (Figure 3-1C and Figure 3-1D). Figure 3-1C illustrates the significant increase in *Syntrophomonas* abundance from 7% of the bacterial 16S rRNA gene concentration initially to approximately 31% after the last batch feeding of oleic acid. The average relative abundance of *Syntrophomonas* in each batch degradation period correlated strongly with the initial specific methane production rate from oleic acid (Pearson's coefficient = 0.99; Figure 3-2A). In contrast, the *Syntrophus* 16S rRNA gene was quantified at an initial relative abundance of 0.015% and decreased to 0.001% of the bacterial 16S rRNA gene concentration by the end of bioreactor operation (Figure 3-1D). These results indicated that *Syntrophomonas* species, but not *Syntrophus* species, were actively growing from the degradation of oleic acid in the bioreactors.

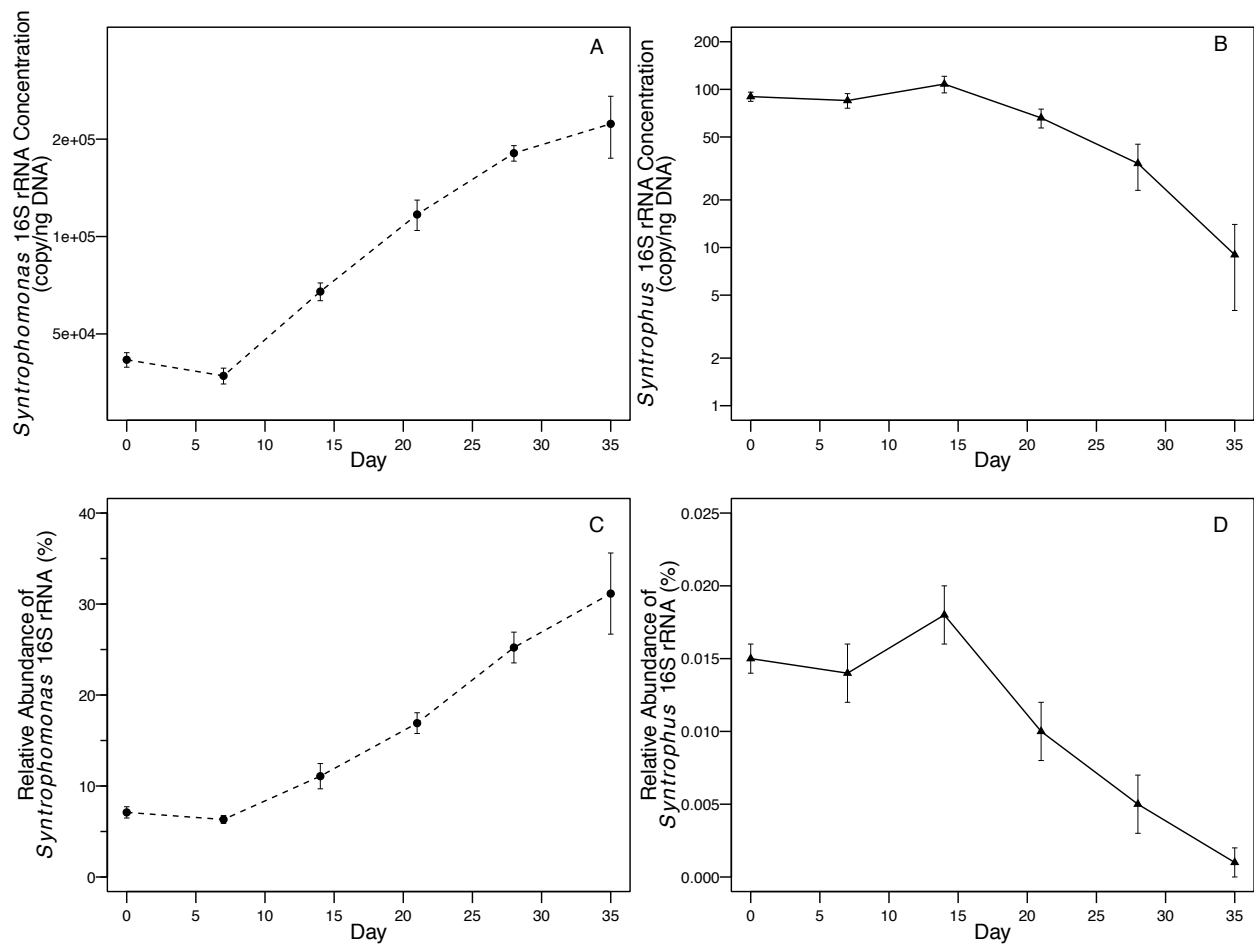


**Figure 3-1** Changes in 16S rRNA gene concentrations of (A) *Syntrophomonas* and (B) *Syntrophus* in methanogenic bioreactors; Ratio of 16S rRNA gene concentrations of (C) *Syntrophomonas* and (D) *Syntrophus* to that of total *Bacteria* in bioreactors. Error bars indicate one standard deviation based on biological (n=3) and technical replicates (n=2).



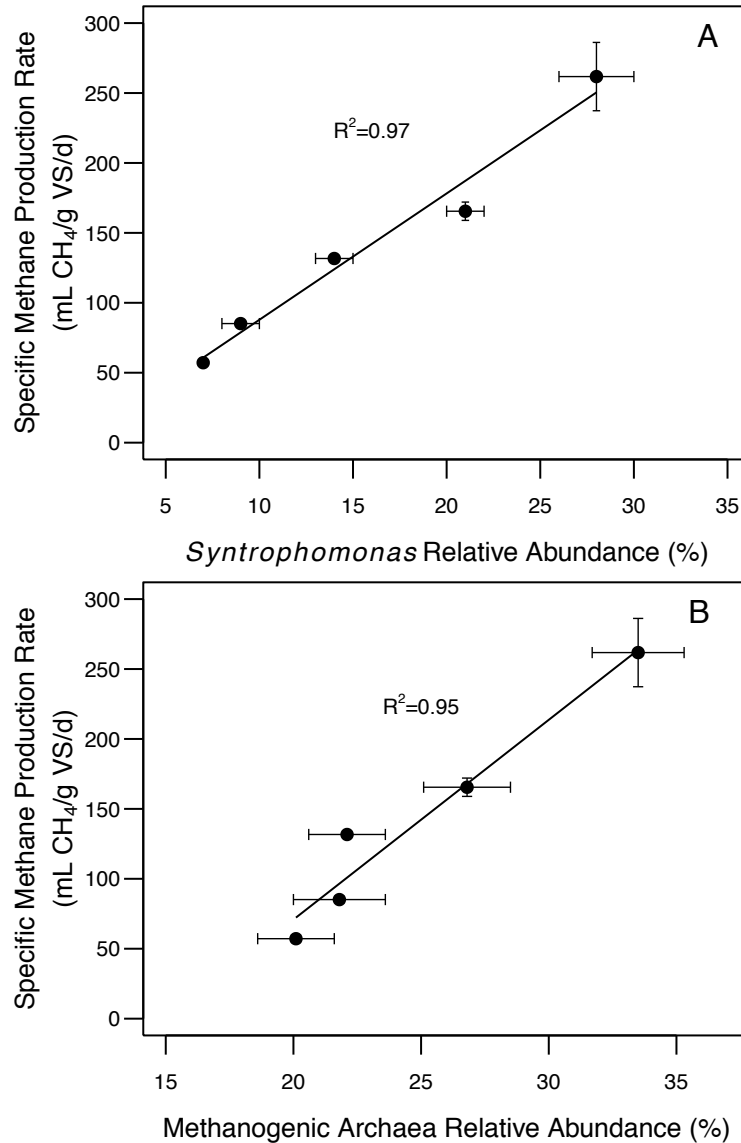


**Figure 3-2** Correlation between the initial specific methane production rate during the oleic acid batch degradation periods and the average relative abundance of (A) *Syntrophomonas* 16S rRNA genes in bacterial community, and (B) methanogenic archaea 16S rRNA genes in prokaryotic community. The total methanogenic archaea gene concentration was determined as the sum of all methanogen target groups, and the prokaryotic gene concentration was determined as the sum of methanogenic archaea and total *Bacteria* gene counts. Error bars for the specific methane production rate indicate one standard deviation based on biological replicates (n=3), and error bars for relative abundance values indicate one standard deviation based on biological (n=3) and technical replicates (n=2).

#### 3.4.4 Quantitative Dynamics of Methanogenic Archaea by qPCR

The sum of the 16S rRNA gene concentrations of all methanogenic archaeal target groups increased 2.8-fold throughout the bioreactor operation, from  $1.4 \times 10^5$  to  $3.9 \times 10^5$  copies  $\text{ng}^{-1}$  DNA ( $p=0.001$ ; Figure 3-3A). Correspondingly, the ratio of the total methanogenic archaea 16S rRNA gene concentration to that plus the Bacteria domain (representing the total prokaryotic community) significantly increased from 19% to 35% throughout bioreactor operation ( $p=0.0004$ ). The relative abundance of the total methanogenic archaea 16S rRNA gene concentration in the prokaryotic community correlated strongly with the initial specific methane production rate from oleic acid (Pearson's coefficient = 0.97; Figure 3-2B). The change in 16S rRNA gene concentration of each targeted methanogenic group is shown in Figure A8 (Supplemental Information). The 16S rRNA gene concentration of each methanogenic archaea group was normalized to the sum of all methanogenic archaea targets to infer their relative abundances over time, as shown in Figure 3-3B. The methanogenic archaeal community composition stayed relatively stable over time, with the hydrogenotrophic order of *Methanomicrobiales* accounting for 70% of the methanogenic archaeal 16S rRNA gene concentration and the acetoclastic family of *Methanosaetacea* accounting for 30% (Figure 3-3B). The order of *Methanobacteriales* and family of *Methanosarcinaceae* comprised less than 1% of the methanogenic archaeal 16S rRNA gene concentration throughout bioreactor operation, while the order of *Methanococcales* was not detected by the qPCR assay (Figure 3-3B).

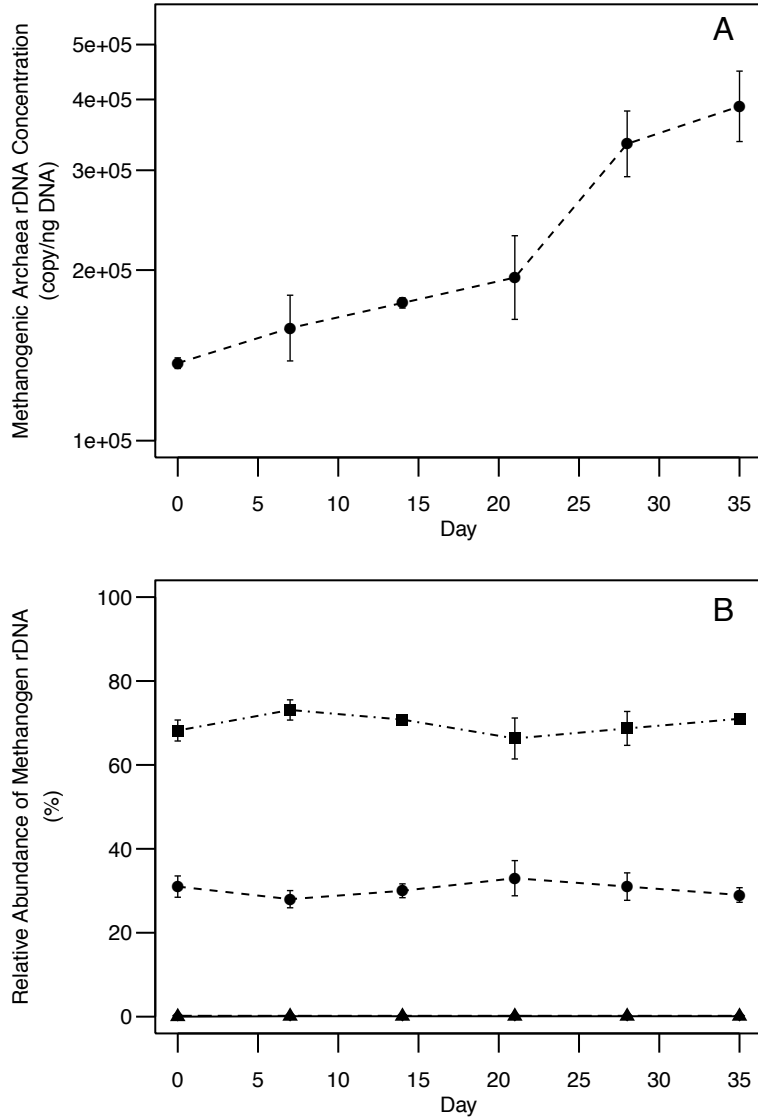


**Figure 3-3** (A) Change in the 16S rRNA gene concentration of the sum of all methanogenic archaea targets in bioreactors degrading oleic acid; (B) Relative abundance of the 16S rRNA gene concentration of each methanogenic target group relative to the sum of methanogenic archaea targets; (■) = *Methanomicrobiales*; (●) = *Methanosaetaceae*; (♦)=*Methanobacteriales*; (^)=*Methanosarcinaceae*. *Methanobacteriales* and *Methanosarcinaceae* remained below 1% relative abundance, while *Methanococcales* was not detected by qPCR of the bioreactor samples. Error bars indicate one standard deviation based on biological (n=3) and technical replicates (n=2).

### 3.4.5 *Dynamics of Bacterial Community by High-throughput Amplicon Sequencing of 16S rRNA Genes*

Bacterial community dynamics in the triplicate bioreactors were monitored using Illumina-based high-throughput amplicon sequencing of 16S rRNA genes for 18 biomass samples, which produced a total of 1,180,000 non-chimeric bacterial sequence reads and an average of 68,000 sequences per sample. The bacterial community structure of the bioreactors significantly changed over time, while similar community structures were maintained between the triplicate bioreactors. This result was apparent by the significant increase in phylogenetic structure differences within the bioreactor microbiomes (determined by weighted UniFrac distances) relative to the initial conditions ( $p=0.0002$ ; Figure A9, Supplemental Information), and by the similar dynamics within the OTU sets of the triplicate bioreactors (Figure 3-4). The richness of the bacterial community significantly decreased throughout the bioreactor operation ( $p=0.005$ ), as did the community evenness ( $p=0.007$ ; Figure A9, Supplemental Information). These observed changes in the diversity and phylogenetic structure within the bacterial communities indicated that a specialized population of bacteria developed during the degradation of oleic acid and its byproducts, during which non-growing bacterial groups were washed out of the bioreactors.

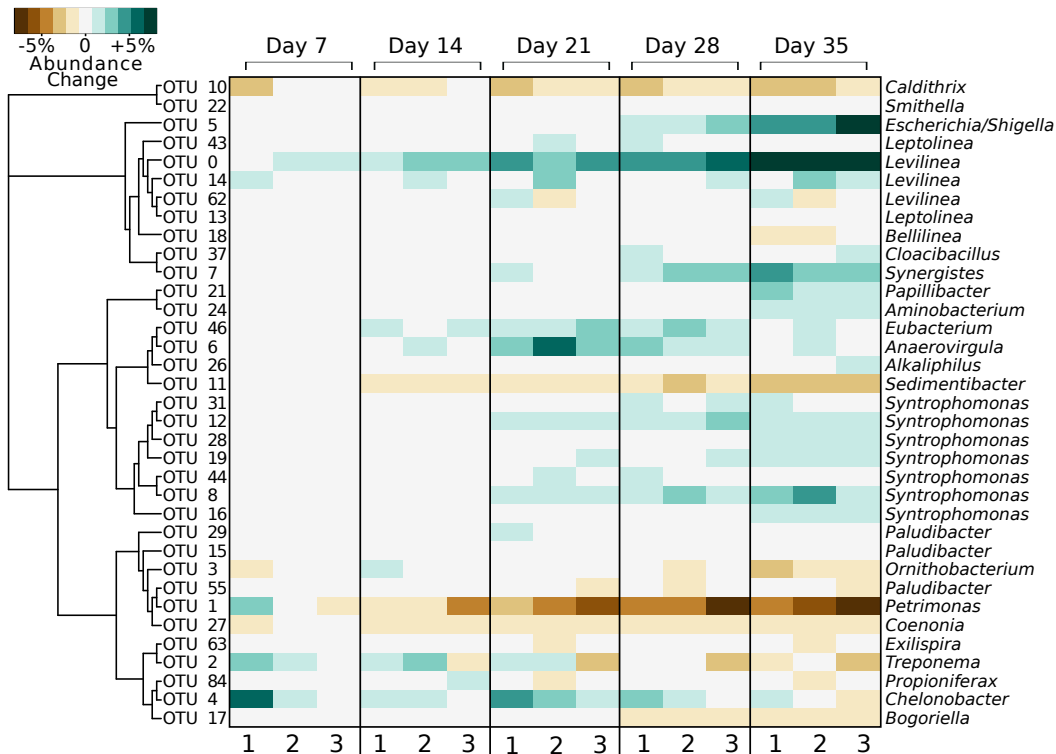


**Figure 3-4** Change in the relative abundance of each OTU that accounted for 1% or more of the bacterial community during the bioreactor operation relative to initial conditions, as determined by high-throughput amplicon sequencing of 16S rRNA genes. The left axis shows a phylogenetic clustering of the OTU's based on sequence alignment with MUSCLE (<http://www.ebi.ac.uk>). The right axis shows the genus level classification of each representative OTU sequence. The scale on the color key is relative to the entire community (e.g., an increase in relative abundance from 1% to 5% would be shown as +4%). The relative abundance change of each OTU is shown for all reactor replicates (e.g. 1, 2, 3) at days 7, 14, 21, 28, and 35.

The growth dynamics of all OTU's representing more than 1% relative abundance are shown in Figure 3-4. The bacterial communities were dominated primarily by the orders *Clostridiales* and *Anaerolineales*, which together accounted for over 55% of the population by the end of bioreactor operation (Figure 3-5A) and were comprised mainly of the genera *Syntrophomonas* and *Levilinea*, respectively (Figure 3-5B). *Syntrophomonas* became the most abundant genus within the bacterial communities by the end of the experiment, increasing in relative abundance from 6% to 19% of sequence reads (Figure 3-5B). *Syntrophomonas*-affiliated OTU's that were detected above 1% relative sequence abundance (7 OTU's total) all showed general patterns of

increased abundance within the bioreactor microbiomes over time (Figure 3-4). Other bacterial orders that experienced growth in the bioreactor microbiomes included *Synergistales* and *Enterobacteriales*, which were comprised mainly of the genera *Synergistes* and *Escherichia/Shigella*, respectively (Figure 3-4 and Figure 3-5A). Notably, no *Syntrophus* sequences were detected above 0.3% relative abundance throughout the bioreactor operation (data not shown), which is consistent with the results of the qPCR assay.

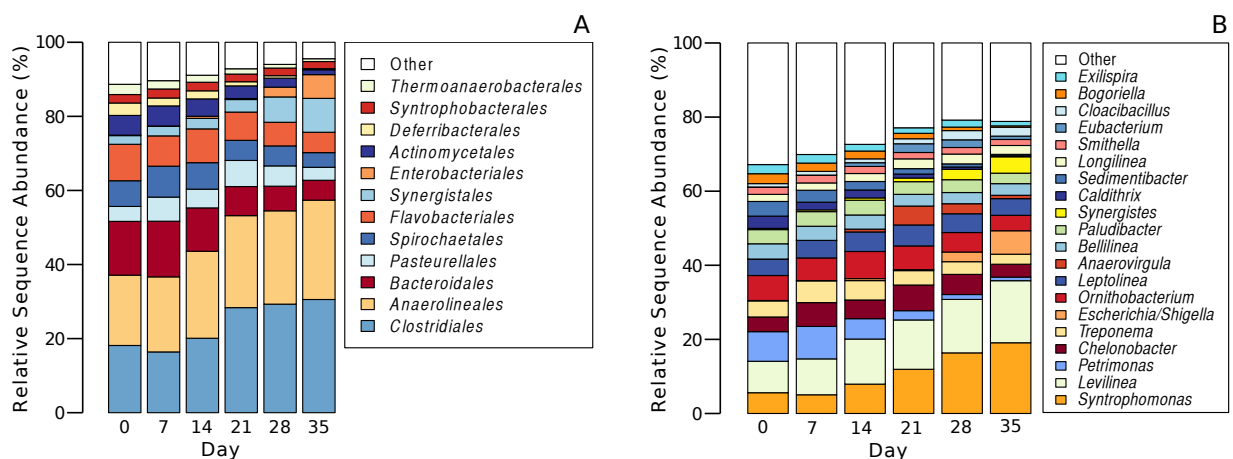


**Figure 3-5** Relative abundance of bacterial groups based on high-throughput amplicon sequencing of 16S rRNA genes from bioreactor samples taken on days 0, 7, 14, 21, 28, and 35 showing (A) the 12 most abundant bacterial orders, and (B) the 20 most abundant genera. The groups were ranked based on their maximum observed relative abundances, and all other groups were combined and are shown as “Other”. The abundances of groups shown at each time point represent an average of the triplicate bioreactors.

### 3.5 DISCUSSION

The dynamics and ecological role of syntrophic  $\beta$ -oxidizing bacteria in methanogenic bioreactors has been poorly understood due to a relative lack of information regarding the concentration of these groups within anaerobic communities (H. Ariesyady et al., 2007; Hansen et al., 1999; McMahon, 2001; McMahon et al., 2004; Narihiro et al., 2012). The application of the newly developed TaqMan qPCR assays in combination with high-throughput amplicon sequencing of

bacterial 16S rRNA genes proved to be a valuable approach to monitor the quantitative dynamics of syntrophic  $\beta$ -oxidizing communities in bioreactors mineralizing oleic acid. Thus, the combination of these assays may provide a platform for analyzing and surveying microorganisms in anaerobic digesters degrading lipid rich wastes.

The increase in the initial specific methane production rate by 4.6-times throughout the experimental period showed that the bioreactor communities developed a greater capacity to convert oleic acid into methane, which was likely caused by the growth of LCFA-degrading consortia within the community. The increase in the relative abundance of *Syntrophomonas* species in the bioreactors to over 30% of the bacterial community determined by qPCR (Figure 3-1C) showed that this group was actively growing through oleic acid  $\beta$ -oxidation. The strong correlation between the relative abundance of *Syntrophomonas* species and the initial specific methane production rate from oleic acid (Figure 3-2A) further suggested that *Syntrophomonas* species contributed to the increase in mineralization rates of the LCFA observed in the bioreactors at higher oleic acid loadings. High-throughput amplicon sequencing corroborated the observed growth of *Syntrophomonas* species by predicting that *Syntrophomonas*-affiliated sequences increased to approximately 20% of the bioreactor communities (Figure 3-5B). The various extent of growth observed within the *Syntrophomonas*-affiliated OTU's (Figure 3-4) suggested that different *Syntrophomonas* ecotypes may express different physiological capacities to degrade oleic acid. A phylogenetic comparison of 16S rRNA gene sequences of characterized *Syntrophomonas* species with that of the most abundant *Syntrophomonas*-affiliated OTU's indicated that the enriched OTU's were distributed throughout the genus (Figure A10, Supplemental Information). The importance of *Syntrophomonadaceae* species in anaerobic

communities degrading LCFA has been implicated in prior studies based on molecular fingerprinting techniques (Baserba et al., 2012; Sousa et al., 2007a). Yet, the quantitative results provided by the newly developed qPCR assays, in combination with high throughput amplicon sequencing, further showed that increased oleic acid degradation rates could be obtained with higher relative abundances of  $\beta$ -oxidizing *Syntrophomonas* species. Thus, the abundance of syntrophic  $\beta$ -oxidizing bacteria, as measured by the novel qPCR assays, may be used to indicate the capacity of anaerobic digester communities to  $\beta$ -oxidize fatty acids, in part involving LCFA.

In contrast to *Syntrophomonas*, the relative abundance of the *Syntrophus* genus was much lower in the initial seed and decreased throughout the bioreactor operation as measured by qPCR. The high-throughput amplicon sequencing results also indicated that *Syntrophus*-affiliated sequences decreased in relative abundance. These results suggest that *Syntrophus* species were not growing through oleic acid  $\beta$ -oxidation either due to out-competition by other populations or to LCFA inhibition. The ability of *Syntrophus* species to degrade oleate remains to be determined (Sousa et al., 2009), and their inability to do so could have also contributed to their observed washout. The disappearance of *Proteobacteria*-related species has been previously reported based on PCR-DGGE profiles of anaerobic communities degrading oleic acid in batch (Sousa et al., 2007a) and continuous (Baserba et al., 2012) modes. It has also been suggested that *Deltaproteobacteria* were more strongly associated with the degradation of saturated versus unsaturated LCFA (Hatamoto et al., 2007c; Sousa et al., 2009). The high-throughput amplicon sequencing indicated that *Smithella*, a genus also within the *Syntrophaceae* family that is phylogenetically closely related to *Syntrophus* (Gray et al., 2011), maintained a stable abundance in the bacterial microbiomes over time (Figures 3-4 and 3-5B). *Smithella* species have been



associated with syntrophic degradation of long-chain alkanes (Embree et al., 2014; Gray et al., 2011), yet it is unclear if members of *Smithella* take part in  $\beta$ -oxidizing LCFA. However, a partial genome of an uncultured *Smithella* species obtained from an enriched methanogenic hexadecane-degrading community showed that the bacterium contained genes involved in LCFA  $\beta$ -oxidation (Embree et al., 2014). The saturated LCFA produced during oleic acid degradation (Table A2, Supplemental Information) therefore may have supported the population of *Smithella* in the bioreactors. Thus, despite the high target group coverage of the *Syntrophus* qPCR assay developed in this study (Table 3-2), it is possible that other members of the *Syntrophaceae* family not targeted by the qPCR assay, such as *Smithella*, were involved in LCFA degradation within the bioreactors.

While previous studies have hypothesized a toxicity of LCFA towards methanogenic archaea (Angelidaki and Ahring, 1992; Hanaki et al., 1981; Koster and Cramer, 1987), the observed increase in the abundance of hydrogenotrophic and acetoclastic methanogens (Figure 3-3) suggests that oleic acid and its intermediate degradation products did not exhibit a permanent toxic effect on the targeted methanogenic groups. The strong correlation between the initial specific methane production rate and the abundance of methanogenic archaea (Figure 3-2B) further showed that higher concentrations of syntrophic  $\beta$ -oxidizing consortia resulted in more efficient LCFA mineralization in the anaerobic bioreactors. The stable abundance of *Methanosaetaceae* in the bioreactors revealed that this acetoclastic group was growing on the acetate produced through oleic acid  $\beta$ -oxidation (Table A2, Supplemental Information), even though oleic acid has been shown to inhibit acetoclastic methanogens (Hanaki et al., 1981; Hwu and Lettinga, 1997; Koster and Cramer, 1987; Sousa et al., 2013). Salvador *et al.* (2013) showed

with PCR-DGGE that *Methanosaeta* was the dominant acetoclastic genus in continuously fed bioreactors treating oleate-based waste with LCFA loadings greater than 10 g COD L<sup>-1</sup> day<sup>-1</sup>. Yet, it was recently shown that oleate was more toxic than palmitate to the acetoclastic methanogens *Methanosaeta concilii* and *Methanosarcina mazei* (Sousa et al., 2013). The results of this study provide quantitative evidence suggesting that both hydrogenotrophic and acetoclastic methanogenic groups remained active during oleic acid degradation.

To the best of our knowledge, this is the first application of a high-throughput amplicon sequencing approach to characterize anaerobic LCFA-degrading bacterial communities. The changes in relative abundance of *Syntrophomonas* and *Syntrophus* sequences correlated with the levels predicted by the respective qPCR assays (Pearson's coefficients of 0.99, 0.93, respectively; Figure A11, Supplemental Information), implying that this technique can be used to complement novel qPCR assays applied to complex environmental samples. The significant difference in phylogenetic structure (weighted UniFrac distances) in the bacterial microbiomes over time (Figure A9, Supplemental Information) showed that growth on oleic acid selected for specialized bacterial populations, which in this case were dominated by *Syntrophomonas* species (Figures 3-1, 3-4, 3-5). The high-throughput sequencing also detected the growth of bacterial groups not previously characterized to participate in syntrophic LCFA  $\beta$ -oxidation (Figure 3-4). For instance, *Escherichia coli* is known to  $\beta$ -oxidize LCFA anaerobically with nitrate as a terminal electron acceptor (Campbell et al., 2003); yet the cause of the increase in relative abundance of *Escherichia/Shigella*-affiliated sequences to 5% in these methanogenic bioreactors (Figure 3-5B) is not known. Moreover, increases in the relative abundance of sequences aligning with *Synergistes* and *Levilinea* (Figures 3-4 and 3-5), members of which have been respectively

associated with syntrophic short chain fatty acid (Ito et al., 2011) and protein degradation (Yamada and Sekiguchi, 2009), suggested that the microbial oleic acid-degrading food web was potentially complex. The increased abundance of these groups might be attributable to growth on endogenous decay products and/or on byproducts of LCFA  $\beta$ -oxidization. However, the ecological role of these groups in oleic acid-degrading communities warrants further investigation.

Collectively, the results of this study contributed new evidence to show that increased mineralization rates of LCFA were a result of quantitative shifts within the microbiome towards a higher abundance of LCFA-degrading *Syntrophomonas* bacteria and methanogenic archaea. The newly developed qPCR assays may thus serve as a novel method to determine the fatty acid  $\beta$ -oxidization potential of AD reactors based on the concentration of syntrophic  $\beta$ -oxidizing bacteria within the community. Such an approach may lead to better anaerobic digester feeding strategies that result in stable elevated methane production from waste fats, oils, and grease.

### 3.6 SUPPLEMENTAL INFORMATION AVAILABLE

The Supplemental Information for this Chapter is available online at (<http://dx.doi.org/10.1093/femsec/fiv028>), and is included in this document as Appendix A.

# Chapter 4. MICROBIAL COMMUNITY ADAPTATION INFLUENCES LONG-CHAIN FATTY ACID CONVERSION DURING ANAEROBIC CODIGESTION OF FATS, OILS, AND GREASE WITH MUNICIPAL SLUDGE

## **This work is published as:**

Ziels, R.M., Karlsson, A., Beck, D.A., Ejlertsson, J., Yekta, S.S., Bjorn, A., Stensel, H.D. & Svensson, B.H., (2016). Microbial community adaptation influences long-chain fatty acid conversion during anaerobic codigestion of fats, oils, and grease with municipal sludge. *Water Research*, 103, doi:<http://dx.doi.org/10.1016/j.watres.2016.07.043>

## 4.1 ABSTRACT

Codigesting fats, oils, and greases with municipal wastewater sludge can greatly improve biomethane recovery at wastewater treatment facilities. Process loading rates of fats, oils, and greases have been previously tested with little knowledge of the digester microbial community structure, and high transient fat loadings have led to long chain fatty acid (LCFA) accumulation and digester upsets. This study utilized recently-developed quantitative PCR assays for syntrophic LCFA-degrading bacteria along with 16S amplicon sequencing to relate changes in microbial community structure to LCFA accumulation during transient loading increases to an anaerobic codigester receiving waste restaurant oil and municipal wastewater sludge. The 16S rRNA gene concentration of the syntrophic  $\beta$ -oxidizing genus *Syntrophomonas* increased to ~15% of the Bacteria community in the codigester, but stayed below 3% in the control digester that was fed only wastewater sludge. *Methanosaeta* and *Methanospirillum* were the dominant methanogenic genera enriched in the codigester, and together comprised over 80% of the *Archaea* community by the end of the experimental period. Constrained ordination showed that

changes in the codigester *Bacteria* and *Archaea* community structures were related to measures of digester performance. Notably, the codigester LCFA concentration was positively correlated to the specific loading rate of waste oil normalized to the *Syntrophomonas* 16S rRNA concentration in the codigester. Specific loading rates of 0 to  $1.5 \times 10^{-12}$  g VS oil/16S gene copies-day resulted in LCFA concentrations below 30 mg/g TS, whereas LCFA accumulated up to 104 mg/g TS at higher transient loading rates. Based on the community-dependent loading limitations found, enhanced biomethane production from high loadings of fats, oils and greases can be achieved by promoting a higher biomass of slow-growing syntrophic consortia, such as with longer digester solids retention times. This work also demonstrates the potential for controlling the loading rate of fats, oils, and greases based on the analysis of the codigester community structure, such as with quantitative PCR measurements of syntrophic LCFA-degrading bacteria abundance.

## 4.2 INTRODUCTION

Anaerobic digestion is commonly used at municipal wastewater treatment plants (WWTPs) to process waste sludge and recover renewable energy as biomethane. Fats, oils, and greases (FOG) are desirable substrates for enhancing biomethane recovery through codigestion because they have a methane yield potential per g VS that is 250% to 350% greater than the wastewater sludge typically fed to municipal digesters (Davidsson et al., 2008; Girault et al., 2012; Luostarinen et al., 2009). Reported increases in digester methane production from 140% to 620% during FOG codigestion with wastewater sludge (Wan et al., 2011; Wang et al., 2013) have demonstrated the potential to significantly improve economics and reduce energy footprints of municipal WWTPs with FOG codigestion.

When fats and oils are added to the anaerobic digestion process, they are rapidly hydrolyzed into their major constituents of glycerol and long-chain fatty acids (LCFA) (Hanaki et al., 1981). After lipid hydrolysis, most of the energy content resides in LCFA, which can comprise over 90% of the chemical oxygen demand of the original lipid molecule (Sousa et al., 2009). The formation of methane from LCFA involves a syntrophic partnership of proton-reducing acetogenic bacteria, which utilize the  $\beta$ -oxidation pathway to convert LCFA into acetate and formate/hydrogen, along with aceticlastic and hydrogenotrophic methanogenic archaea (Schink, 1997; Sousa et al., 2009; Weng and Jeris, 1976). All of the isolated bacterial species known to  $\beta$ -oxidize LCFA syntrophically belong to two families, *Syntrophomonadaceae* and *Syntrophaceae* (Hatamoto et al., 2007a; Jackson et al., 1999; McInerney, 1992; Sousa et al., 2007b; Wu et al., 2006). Generally, the conversion of LCFA into methane is considered the rate-limiting step for lipid degradation in anaerobic digesters (Cirne et al., 2007).

Process failures observed at elevated FOG loading rates have impeded the ability to fully exploit higher biomethane production during FOG codigestion with municipal wastewater sludge (Davidsson et al., 2008; Girault et al., 2012; Luostarinen et al., 2009; Noutsopoulos et al., 2013; Wan et al., 2011; Wang et al., 2013). Specifically, the LCFA released during lipid hydrolysis can inhibit anaerobic microorganisms at high concentrations (Angelidaki and Ahring, 1992; Koster and Cramer, 1987; Lalman and Bagley, 2000; Rinzema et al., 1994), thereby limiting their bioconversion into methane. Causes of inhibition have been attributed to LCFA adsorption onto cell surfaces, which can lead to direct toxicity (Hanaki et al., 1981; Rinzema et al., 1994) and/or substrate transport limitations (Pereira et al., 2005). While aceticlastic methanogens are believed to be the most sensitive group to LCFA toxicity (Koster and Cramer, 1987; Lalman and Bagley,

2001, 2000; Rinzema et al., 1994), the inhibition of hydrogenotrophic methanogens and syntrophic bacteria by LCFA has also been suggested (Hanaki et al., 1981; Lalman and Bagley, 2002; Pereira et al., 2005; Roy et al., 1985). Reported threshold values for FOG loading that led to decreased methane yields during codigestion with municipal wastewater sludge ranged from ~0.4 to 2.1 g VS/L-d (Girault et al., 2012; Luostarinen et al., 2009; Noutsopoulos et al., 2013; Wan et al., 2011; Wang et al., 2013). However, these empirical FOG loading thresholds do not account for digester microbial populations and their role in LCFA conversion, and are thus of limited use for predicting the response of a digester following transient increases in FOG loading. An improved understanding of the relationship between digester biomass composition and LCFA accumulation is needed to develop operational strategies for stable codigester operation with increased FOG loadings and enhanced methane recovery.

The importance of biomass adaptation for stable FOG digestion has been indicated by previous studies. Silvestre et al. (2011) observed that stepwise increases in FOG loading led to the development of biomass with higher LCFA  $\beta$ -oxidation and methanogenic activities during codigestion with municipal sludge. Alves et al. (2001) found that both the tolerance to LCFA toxicity as well as the LCFA-biodegradation activity increased with long-term exposure to lipids in an anaerobic fixed-bed bioreactor. Similarly, long-term acclimation was identified as a key factor influencing the resilience to LCFA toxicity in a series of digester sludges exposed to skim milk and oleate based wastewaters (Silva et al., 2014). While these results collectively indicated that biomass adaptation could affect the efficiency of FOG conversion, the microbial community structures of these digester sludges were not assessed. The dynamics of LCFA-degrading microbial communities have been previously studied using highly enriched systems with LCFA

as the primary carbon source (Salvador et al., 2013; Shigematsu et al., 2006; Sousa et al., 2007a; Ziels et al., 2015). However, the relationship between the LCFA conversion efficiency and microbial community structure during FOG codigestion with municipal wastewater sludge has received little attention. The changes in LCFA-degrading community structure caused by transient increases in FOG loading therefore need further study to enable better predictions of acceptable FOG loadings during codigestion.

The main objective of this study was to elucidate the relationship between digester biomass composition and LCFA conversion rates and removal efficiency during FOG codigestion with municipal wastewater treatment sludge. Quantitative PCR targeting LCFA-degrading syntrophic bacteria and methanogenic archaea was conducted along with Illumina 16S rRNA gene amplicon sequencing of *Bacteria* and *Archaea* communities to monitor microbial population structure changes in a FOG codigester and control digester treating municipal wastewater solids. The specific goals were to: (1) determine the effects of FOG addition on the digester microbial community structure, and (2) examine relationships between microbial community structure and LCFA removal following transient variations in FOG loading.

## 4.3 MATERIALS AND METHODS

### 4.3.1 *Digester Operation*

Two semi-continuous complete-mix anaerobic digesters (4L working volume) were operated at 37°C with a 20-day hydraulic retention time (HRT) for 198 days. The digesters were mixed with axial flow impellers at 275-325 rpm. They were started with anaerobic digester sludge collected from Henriksdal WWTP in Stockholm, Sweden, and were fed with a mixture of waste primary



sludge (WPS) and waste activated sludge (WAS) collected from the same plant throughout the experiment. The WAS+WPS was collected biweekly and stored at 4°C. The digesters were manually fed once daily by withdrawing the volume of reactor liquid corresponding to the volume of the feed prior to addition. The average feed WPS+WAS volatile solids (VS) concentration was  $28 \pm 2$  g VS/L and the feed sludge VS loading rate (VSLR) for both digesters averaged  $1.4 \pm 0.1$  g VS/L-day over the course of the experiment. After an initial startup period of 53 days of only feeding WPS+WAS, waste cooking oil (hereby referred to as FOG) from a nearby restaurant was added to one of the digesters for codigestion. The start of FOG codigestion was defined as day 1 of the experimental period (Table 4-1). The FOG VS content was ~99%, and its addition to the codigester was increased in a stepwise manner over time to 1.5 g VS/L-d (52% of the total feed VS) by day 94 (Table 4-1).

**Table 4-1** Total influent volatile solids loading rate (VSLR), FOG VSLR, and the percent of FOG VS in the feed versus time for the FOG codigester. Values in parentheses indicate one standard deviation.

Days	Total VSLR (g VS/L-day)	FOG VSLR (g VS/L-day)	% FOG in Feed (VS-basis)
-53 - 0	1.4 (0.2)	0	0
1 - 9	1.9 (0.1)	0.25	13
10 - 37	1.8 (0.1)	0.5	27
38 - 72	2.1 (0.1)	0.75	36
73 - 79	2.4 (0.0)	1.0	41
80 - 93	2.6 (0.1)	1.25	47
94 - 145	2.9 (0.1)	1.5	52

Digester performance was monitored with daily biogas production, methane content, pH, effluent volatile fatty acid (VFA), effluent LCFA, total solids (TS), and VS. Biogas production was measured with tipping bucket displacement gas meters (MilliGascounters, Ritter, Germany). The biogas composition was analyzed weekly for methane, carbon dioxide, oxygen, and hydrogen

sulfide using a portable gas analyzer (Biogas Check, Geotech, UK). All measured gas volumes are reported at standard temperature and pressure (1 atm pressure and 0°C). The TS and VS contents of the sludge were determined according to Swedish Standard Method SS028311. The pH of the digesters was measured using an Inolab pH 7310 meter (InoLab, Wissenschaftlich-Technische Werkstätten, Germany) immediately after withdrawing sludge from the reactors. VFA (acetate, propionate, butyrate, iso-butyrate, valerate, iso-valerate, capronate and iso-capronate) were analyzed by GC-FID (HP 6890, Hewlett Packard), and were separated with a BP21 (FFAP) column (30 m × 0.32 mm × 0.25 μm, SGE Analytical Science) as described previously (Jonsson and Borén, 2002). LCFA were measured according Ziels et al. (2015) with minor modifications. Briefly, 10 mL of digester sludge was centrifuged at 10,000 x g for 10 min, and immediately decanted. Approximately 0.2 g of pelleted sludge was transferred to a pre-weighed glass extraction vial, which was then dried at 80°C for 15 hr, allowed to cool, and reweighed. 1 mL of water was then added to the sample, and the subsequent LCFA extraction and quantification was conducted as described by Ziels et al. (2015). The average recovery of palmitate (C<sub>16:0</sub>), stearate (C<sub>18:0</sub>), and oleate (C<sub>18:1</sub>) spiked to digester sludge samples was 100%, 92%, and 83%, respectively.

#### 4.3.2 *Batch Methanogenic Activity Assays*

Batch methanogenic activity tests were conducted with biomass from both digesters in order to determine the maximum conversion kinetics of acetate and oleate on days 0, 65, and 135, according to the protocol by Karlsson et al. (2012). Briefly, 15 mL digester sludge aliquots (0.17-0.19 g VS) were directly transferred into 160 mL glass serum bottles containing 130 mL of anaerobic basal medium prepared according to Karlsson et al. (2012), and were then sealed with butyl rubber septa. The bottles were flushed with a mixture of O<sub>2</sub>-free 80:20 N<sub>2</sub>:CO<sub>2</sub> to ensure

anaerobic conditions. Substrate (either sodium acetate or oleic acid) was then added to an initial concentration of 5 mM. Control vials without any added substrate were also included in each batch test. All treatments were run in triplicate, and were maintained at 37°C for approximately 260 h without mixing. The gas production was measured based on the pressure increase in the bottles using a handheld pressure transducer (Testo 3123, Testo, Sparta, New Jersey). The methane content of the headspace was measured in triplicate by GC-FID (Hewlett Packard, 5880 A) at each gas pressure sampling point. The methane production in the control vials was subtracted from the substrate-amended vials to determine the methane production attributed to substrate conversion.

A modified Gompertz equation was used to describe the inoculum-corrected methane production curves in the batch kinetic assays, as proposed by Palatsi et al. (2012) and Silva et al. (2014):

$$M(t) = P \cdot \exp \left[ -\exp \left[ \frac{q_{max} \cdot e}{P} (\lambda - t) + 1 \right] \right]$$

where  $M$  is the accumulated methane (mL CH<sub>4</sub>/L) at time =  $t$  (days),  $P$  is the maximum cumulative methane production (mL CH<sub>4</sub>/L),  $q_{max}$  is the maximum methane production rate (mL CH<sub>4</sub>/L-day),  $e$  is 2.7182818, and  $\lambda$  is the lag-phase time (days). All methane generation terms are in reference to standard temperature and pressure. The model fitting and parameter standard error estimation was conducted with nonlinear regression in R version 3.0.2.

### 4.3.3 *Analysis of Microbial Community Structure*

#### 4.3.3.1 *DNA Extraction and Quantification*

Digester biomass samples were collected for DNA analysis on days 0, 37, 51, 64, 114 and 138 from the FOG codigester and on days 0, 64, 86 and 138 from the control. The samples were prepared by transferring 10 mL of digester sludge aliquots directly into sterile 15 mL tubes, immediately centrifuging at 10,000 x g for 10 min at 4°C, carefully decanting the supernatant, and storing the remaining pellet at -20°C. DNA was isolated from approximately 0.2 g of wet solids using the PowerSoil® RNA/DNA Isolation Kit (MO BIO, Inc, Carlsbad, California) according to the manufacturer's instructions. The concentration of extracted DNA was immediately measured with the Quant-IT dsDNA High Sensitivity Assay Kit with a Qubit 2.0 flourometer (Invitrogen, Carlsbad, California). Triplicate DNA extractions were analyzed at each sampling date to estimate variance in population abundances and ensure that observed changes in community structure were not due to technical error. Extracted DNA was stored in nuclease-free water at -20°C.

#### 4.3.3.2 *Quantitative PCR (qPCR)*

Reaction contents and thermocycling conditions for qPCR analysis were as described by Ziels et al. (2015). qPCR analysis on syntrophic LCFA  $\beta$ -oxidizing bacteria was conducted targeting 16S rRNA genes of the genera *Syntrophomonas* and *Syntrophus* using the primers and probes developed by Ziels et al. (2015), as these primers/probes were the only established TaqMan qPCR assays targeting these syntrophic  $\beta$ -oxidizing bacterial groups at this time. Additionally, qPCR analysis was conducted targeting the domain *Bacteria*, the methanogenic archaeal orders of *Methanomicrobiales*, *Methanobacteriales*, *Methanococcales*, and the methanogenic archaeal families of *Methanosarcinaceae* and *Methanosaetaceae* using previously developed

primer/probe sets (Yu et al., 2005). Further details on the qPCR primer/probe sets used in this study are provided in Supplemental Table B1. All samples were analyzed in duplicate. No-template controls (NTCs) were included with each qPCR run. Extracted DNA from the digester biomass samples was diluted 1:10 in nuclease-free water to prevent PCR inhibition. Calibration standards for the qPCR assays were prepared as described by Ziels et al. (2015), and were included in duplicate in each qPCR run for all target groups. The strains from which 16S rRNA gene sequences were used to construct the calibration standards are given in Supplemental Table B1, along with the average slopes and intercepts of the qPCR calibration curves.

#### 4.3.3.3 *High-Throughput Amplicon Sequencing of 16S rRNA Genes and Statistics*

Selected DNA extracts were processed for high-throughput amplicon sequencing on the Illumina MiSeq platform, using the protocol described by Ziels et al. (2015). Briefly, two-step nested PCR was conducted prior to sequencing to enhance sensitivity. *Bacteria* and *Archaea* sequence libraries were generated separately for each sample by using different primer sets in the initial PCR. The primers used in the initial PCR for the *Bacteria* sequence library generation were a modified 341F (5'-CCTAYGGGRBGCASCAG-3') and a modified 806R (5'-GGACTACNNGGGTATCTAAT-3') (Sundberg et al., 2013), and for the *Archaea* sequence library the primers Arch-349F (5'-GYGCASCAGKCGMGAAW-3') and Arch-915R (5'-GTGCTCCCCCGCCAATTCCT-3') were used. PCR amplification, purification, and library construction were conducted in accordance to Ziels et al. (2015). Libraries were sequenced with an Illumina MiSeq at the University of Copenhagen Molecular Microbial Ecology Lab. Sequences were submitted to the NCBI Sequence Read Archive as BioProject PRJNA301747.

Paired-end sequences were joined using the fastq-join method (Aronesty, 2013) with a minimum overlap of 100 bp and a zero percent difference allowed in the overlap region. The UPARSE method was used to trim sequences to 298 bp and filter sequences based on a maximum estimated error of 0.05 using USEARCH61 (Edgar, 2010; Edgar et al., 2011). Sequence chimeras were identified against the RDP Gold reference database (v.9) included in the UCHIME distribution (Edgar et al., 2011) within the QIIME pipeline v.1.8.0 (Caporaso et al., 2010b). Filtered sequences were clustered into operational taxonomic units (OTUs) based on 3% sequence divergence using USEARCH61 (Edgar, 2010). Representative sequences of each OTU were identified based on the cluster seed, and were classified using a naïve Bayesian algorithm with the Ribosomal Database Project (RDP) Classifier program version 2.2 (Wang et al., 2007). For the *Bacteria* sequence libraries, *Archaea* sequences were removed prior to further analysis, and similarly *Bacteria* sequences were filtered and removed from *Archaea* sequence libraries. A total of 1,442,363 quality-filtered reads were obtained from the Illumina sequencing of *Bacteria* 16S rRNA gene amplicons ( $n=21$  samples), and 1,312,584 quality-filtered reads were obtained from sequencing of *Archaea* 16S rRNA gene amplicons ( $n=21$  samples).

Multivariate statistical analysis and diversity metrics were calculated using the vegan library version 2.0.10 (Oksanen et al., 2007) in R version 3.0.2. Canonical correspondence analysis (CCA) was performed using sequence counts (scaled to equal reads per sample) for OTUs that were present above 1% of the population in at least one sample. The environmental parameters that maximized the model significance were identified using forward-backward selection based on P-values. Bray-Curtis distance matrices were calculated after rarefying samples to an equal number of reads. Diversity calculations were performed on entire sample sequence libraries

(rarefied to equal reads) excluding singleton OTUs. Richness was calculated as the number of OTUs after rarefying to the smallest number of reads per sample. Hill numbers were used to measure diversity based on effective species numbers ( ${}^qD$ ) at varying orders ( $q=0,1,2$ ) (Hill, 1973; Jost, 2006). Diversity of order 0 (i.e.  ${}^0D$ ) is equal to species richness, while  ${}^1D$  is equal to  $\exp(\text{Shannon entropy})$ , and  ${}^2D$  is equivalent to  $1/(\text{Simpson concentration})$  (Hill, 1973; Jost, 2006). Diversity of order  ${}^1D$  weights species frequencies equally, while diversity of order  ${}^2D$  disproportionally emphasizes dominant species (Jost, 2006; Vuono et al., 2015).

## 4.4 RESULTS

### 4.4.1 *FOG codigestion led to enhanced methane production and higher LCFA conversion kinetics*

Two parallel anaerobic digesters were operated to compare differences in performance between FOG codigestion with WPS+WAS and the digestion of only WPS+WAS for 145 days (Table 4-1). By day 94 after FOG codigestion was commenced, the FOG VSLR reached 1.5 g VS/L-d (52% of the total VSLR w/w), corresponding to an increase in the total VSLR to the codigester of 2.1-times relative to the control (2.9 versus 1.4 g/L-d) (Figure 4-1A). Accordingly, the daily methane production significantly increased by 2.7-times in the FOG codigester (5200 mL CH<sub>4</sub>/d  $\pm$  560) relative to the control (1900 mL CH<sub>4</sub>/d  $\pm$  200) at the highest VSLR ( $p < 1e-3$ , unpaired t-test; Figure 4-1B). Due to the high VS concentration of the added FOG, the HRT of the codigester was only decreased by 3% to 19.4 days at the highest VSLR. Thus, codigesting FOG at a VSLR of 1.5 g FOG VS/L-d resulted in about 2.7-times the daily methane production with no significant process penalty in the digester HRT.

The specific methane yield on a VS-basis also increased by 31% in the FOG codigester (420 mL CH<sub>4</sub>/g VS<sub>fed</sub> ± 40) relative to the control (320 mL CH<sub>4</sub>/g VS<sub>fed</sub> ± 70) at the highest VSLR ( $p < 1e-3$ ), indicating that the added FOG was more biodegradable than the WPS+WAS. The higher degree of biodegradability of the added FOG was further supported by the significantly higher VS reduction in the FOG codigester over the control throughout the experimental period, achieving 63% ± 4 versus 51% ± 5 ( $p < 1e-3$ , unpaired t-test). Assuming that the VS reduction of the feed WPS+WAS in the FOG codigester was similar to the control digester (i.e. 51%), the VS reduction of the feed FOG in the codigester was estimated to be 74% during the highest FOG VSLR. Consequently, the specific LCFA concentration in the codigester effluent increased to a maximum of 104 ± 11 mg LCFA/g TS on day 114 of FOG addition, in comparison to 4 ± 0.5 mg LCFA/g TS in the control (Figure 4-1D). Thus, the 74% reduction in FOG VS at the highest loading rate resulted in LCFA accumulation within the codigester.



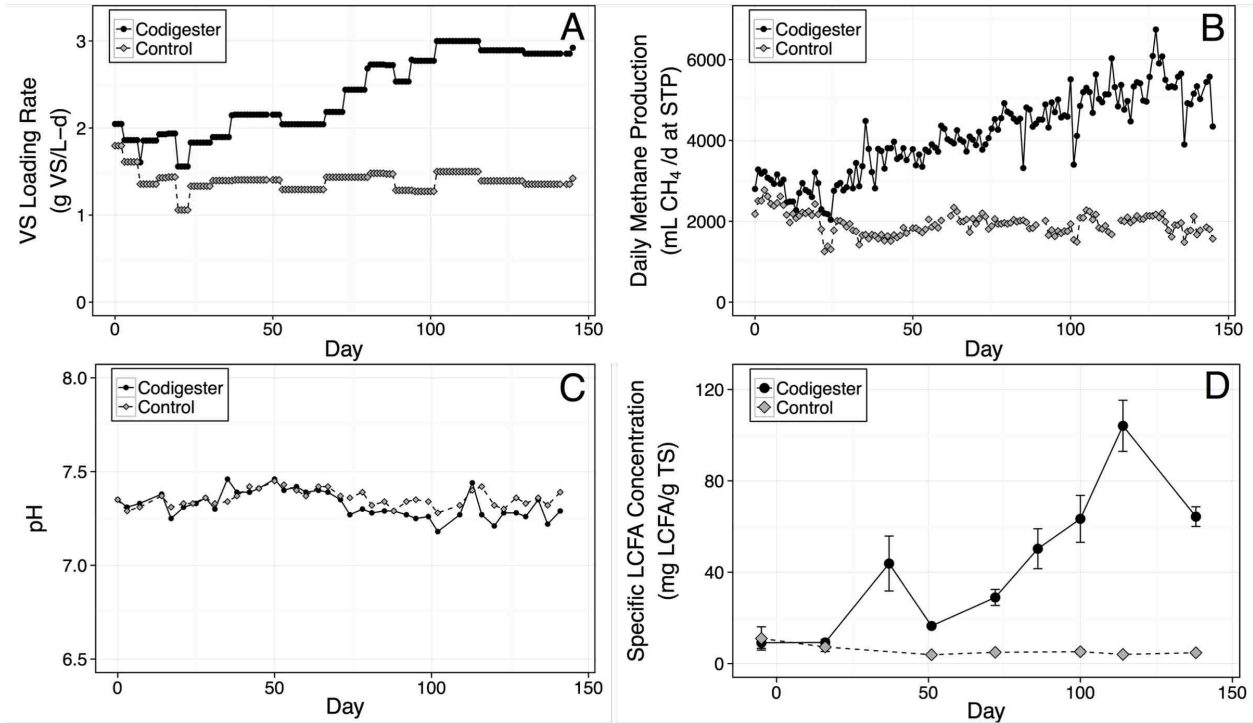


**Figure 4-1** Comparison of the FOG codigester and the control digester performance over experimental period, based on (A) daily volatile solids loading rate, (B) daily methane production, (C) digester pH, and (D) effluent LCFA concentrations. The LCFA concentrations shown in (D) were calculated as the sum of palmitate, stearate, and oleate in the digester effluent solids (error bars represent one standard deviation with  $n=4$ ).

The pH was slightly reduced (Figure 4-1C) after day 50 of FOG codigestion when the LCFA concentration increased (Figure 4-1D). The VFA concentration never exceeded 100 mg/L in both digesters (data not shown), indicating that the codigester had sufficient VFA consumption capacity at the prevailing LCFA conversion rates. LCFA were therefore the major intermediate metabolites that accumulated during FOG degradation (Figure 4-1D). The LCFA in the codigester effluent were comprised of 38% palmitic, 16% stearic, and 46% oleic acids on average (Supplemental Figure B1).

The maximum methane production rates ( $q_{max}$ ) of both digester sludges were determined in batch assays (on days 0, 65, and 135) fed with either acetate or oleate to compare the kinetic capacities

of the digester populations over time. The  $q_{max}$  of oleate-fed batch kinetic assays were significantly increased for the FOG codigester sludge from  $45 \pm 5$  on day zero to  $110 \pm 5$  mL  $\text{CH}_4/\text{L-d}$  by day 65 (Figure 4-2A), corresponding to an increase of 2.4-times relative to the control. Yet, the oleate  $q_{max}$  for the FOG codigester on day 135 was similar to day 65 ( $p > 0.1$ ; Figure 4-2A). Similar  $q_{max}$  values in the acetate-fed batch assays were also observed between the codigester and control for all batch tests (Figure 4-2B); the acetate  $q_{max}$  increased between days zero and 65 and then stabilized for both systems. These results indicate that FOG codigestion resulted in elevated oleate degradation kinetics, and that the codigester community reached a its maximum rate of LCFA conversion by day 65.

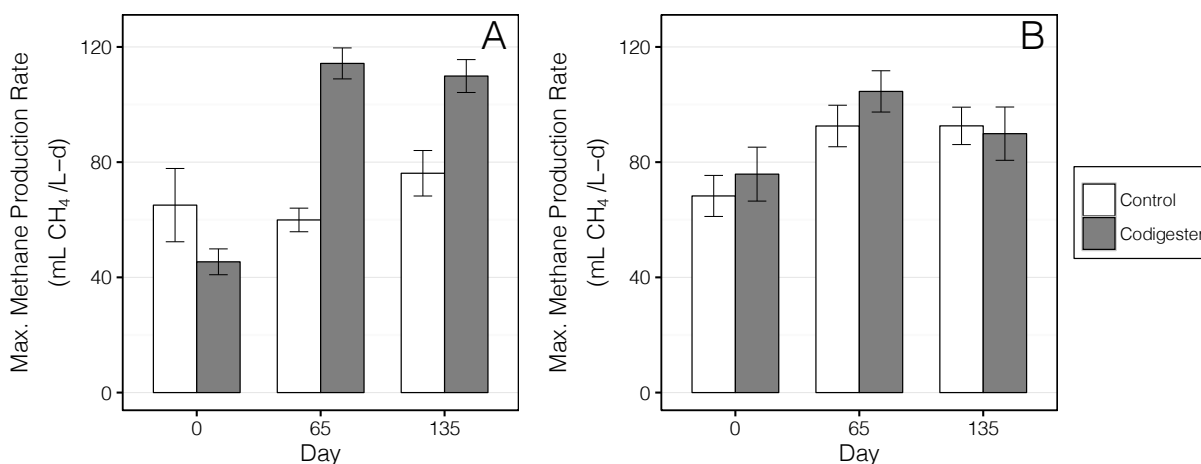


**Figure 4-2** Maximum methane production rate in batch assays fed with (A) oleate and (B) acetate, as determined by fitting the Gompertz growth model to observed methane production in triplicate biological replicates. Error bars represent the standard error based on the non-linear regression model fitting (n=3).

#### 4.4.2 *FOG codigestion selected for syntrophic $\beta$ -oxidizing bacteria and specific methanogenic archaea partners*

Analysis of the *Bacteria* community diversity showed that Hill numbers of orders  ${}^1D$ , and  ${}^2D$  substantially increased in the FOG codigester by the end of the experimental period (Supplemental Figure B2). The taxonomic richness ( ${}^0D$ ) of the *Bacteria* community in the FOG

codigester did not change by day 138 ( $p > 0.1$ , unpaired t-test), while diversities of order  ${}^1D$  and  ${}^2D$  in the FOG codigester increased by 3.0-times and 4.6-times relative to the control, respectively ( $p < 0.001$ , unpaired t-test; Supplemental Figure B2). While it is apparent that the diversity of *Bacteria* was substantially elevated at the orders  ${}^1D$  and  ${}^2D$  in the FOG codigester versus the control, the larger relative increase in diversity of order  ${}^2D$  indicates that the addition of FOG had a larger influence on the diversity of dominant bacterial species.

The increase in the diversity of *Bacteria* in the FOG codigester occurred concomitantly with the significant growth of  $\beta$ -oxidizing *Syntrophomonas* within the *Bacteria* community. *Syntrophomonas* relative abundance in the *Bacteria* community increased to  $14\% \pm 0.7$  in the FOG codigester over the experimental period but remained below 3% relative abundance in the control digester, as measured by qPCR (Figure 4-3A). In contrast, the other known LCFA  $\beta$ -oxidizing genus, *Syntrophus*, was measured by qPCR at less than 0.03% of the *Bacteria* community in both digesters (Figure 4-3B). The *Syntrophus* abundance significantly decreased from day zero to 86 in both digesters ( $p < 1e-3$ ), but returned to its initial level in the FOG codigester by day 138. The enrichment of *Syntrophomonas* within the *Bacteria* community was corroborated by 16S rRNA gene amplicon sequencing, which showed that *Syntrophomonas* became the dominant genus in the *Bacteria* sequence library by day 138 (Figure 4-4). *Syntrophomonas* significantly increased in the FOG codigester *Bacteria* sequence library from  $1.2\% \pm 0.3$  initially to  $9.0\% \pm 1.0$  by day 138 ( $p = 0.009$ , paired t-test), but stayed below 2% in the control (Figure 4-4). *Gelria* was another genus that also increased in the FOG codigester *Bacteria* sequence library relative to the control (Figure 4-4). On the other hand, *Petrimonas* was initially the dominant bacterial genus in both digesters with a relative sequence abundance of

~20%, but had a significantly lower relative sequence abundance in the FOG codigester at  $4.0\% \pm 2.2$  by day 138 ( $p = 0.03$ , paired t-test; Figure 4-4). *Smithella* also significantly decreased from  $6.2\% \pm 0.9$  to  $1.7\% \pm 0.3$  relative sequence abundance in the FOG codigester *Bacteria* community ( $p = 0.01$ , paired t-test), but increased from  $6.7\% \pm 0.1$  to  $12\% \pm 4.5$  in the control (Figure 4-4). Bray-Curtis dissimilarity values relative to the initial *Bacteria* community structure (day zero) significantly increased between days 37 ( $0.44 \pm 0.04$ ) to 138 ( $0.61 \pm 0.03$ ) in the FOG codigester ( $p < 1e-3$ , paired t-test), whereas no significant changes in Bray-Curtis dissimilarity values occurred in the control *Bacteria* community over time ( $p > 0.1$ ; Supplemental Figure B3). These results demonstrate that FOG codigestion resulted in changes in the *Bacteria* community structure, primarily attributed to the growth of the initially rare members of *Syntrophomonas* and *Gelria* and the washout of initially dominant bacterial members such as *Petrimonas* and *Smithella* (Figure 4-4).

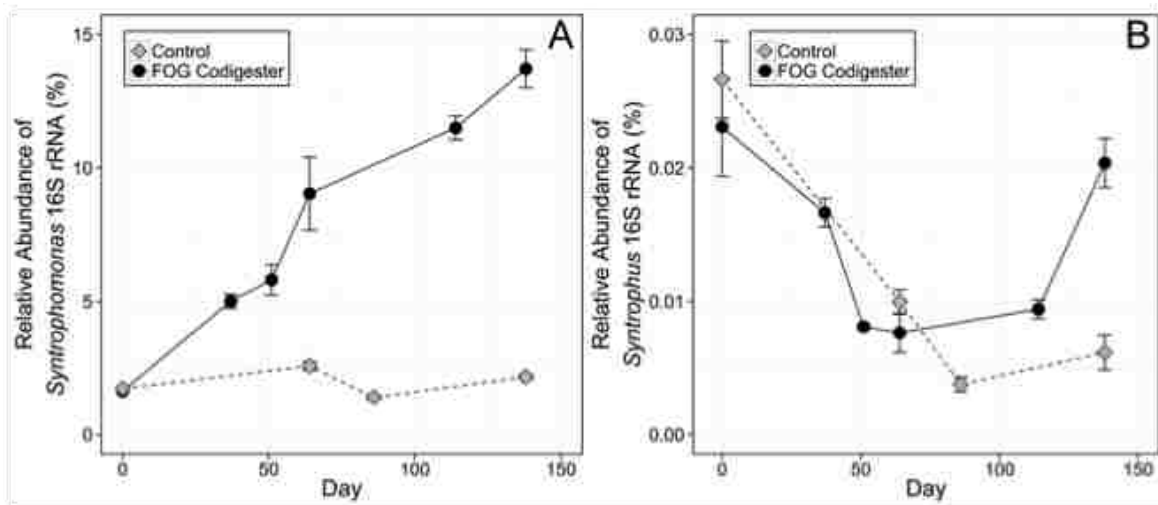


**Figure 4-3** Relative fraction of 16S rRNA genes of the  $\beta$ -oxidizing bacterial genera, (A) *Syntrophomonas* and (B) *Syntrophus*, within the total *Bacteria* 16S rRNA gene concentration in the FOG codigester and control digester over the experimental period, as determined by qPCR. Error bars represent a standard deviation based on DNA extraction replicates ( $n=3$ ) and qPCR technical replicates ( $n=2$ ) for each time point.

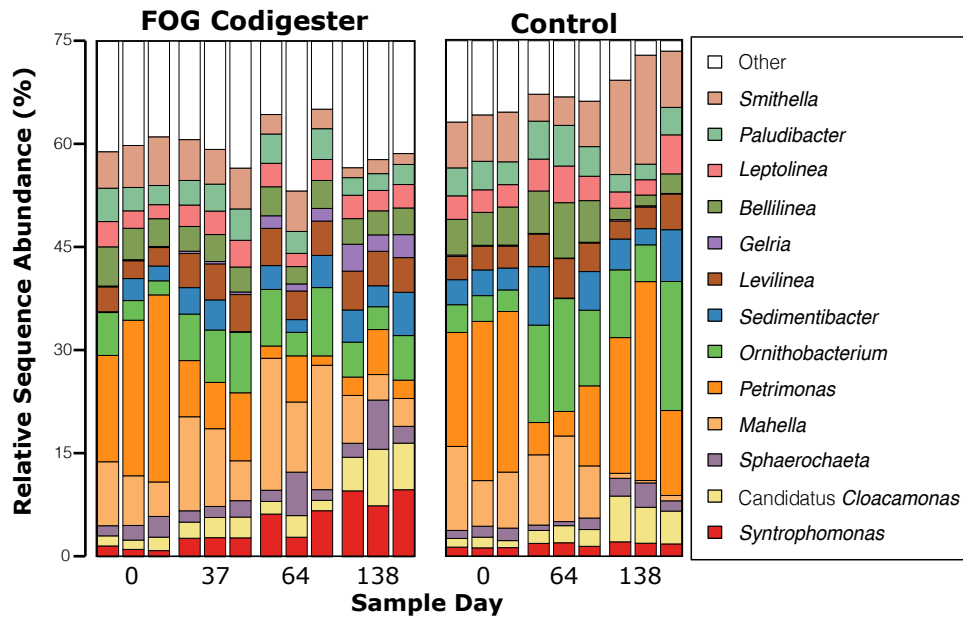


**Figure 4-4** Relative sequence fraction of the 13 most abundant genera within the FOG codigester and control digester libraries produced from Illumina MiSeq sequencing of *Bacteria* 16S rRNA gene amplicons. The triplicate bars shown for each sample day represent replicate DNA extractions. The relative sequence fraction of all other genera were summed, and are shown here as “Other”.

In contrast to changes in *Bacteria* diversity, Hill diversity of orders  $^1D$ , and  $^2D$  for the *Archaea* showed a decreasing trend in the FOG codigester over the experimental period (Supplemental Figure B4). Notably, the diversity of orders  $^1D$ , and  $^2D$  for *Archaea* in the FOG codigester on day 138 were 6% and 8% of that for *Bacteria*, respectively. *Archaea* species richness ( $^0D$ ) for the FOG codigester and control were 34% and 51% of that for *Bacteria* on day 138, respectively. These results indicate that the diversity of *Archaea* was less than that of the *Bacteria* communities in both digesters.

Significant changes in the *Archaea* community structure and abundance were observed with FOG codigestion. The fraction of methanogenic archaea 16S rRNA gene concentration in the prokaryotic community (calculated as the sum of all methanogen groups targeted by qPCR

divided by total methanogens + *Bacteria*) increased 8-times by day 138 in the FOG codigester relative to the control ( $p < 1e-3$ , unpaired t-test; Figure 4-5). The methanogenic archaea 16S rRNA gene concentration comprised over 20% of the prokaryotic community by the end of the experimental period, while that of the control digester was 2.5% (Figure 4-5). Bray-Curtis dissimilarity values relative to the initial *Archaea* community structure significantly increased in the FOG codigester between days 37 ( $0.29 \pm 0.08$ ) and 138 ( $0.62 \pm 0.10$ ) ( $p < 1e-3$ , paired t-test) (Supplemental Figure B5). The increase in Bray-Curtis dissimilarity of the codigester *Archaea* community relative to its initial population reveals that the addition of FOG resulted in changes in the *Archaea* community structure. A significant increase in the hydrogenotrophic *Methanospirillum* relative sequence abundance from  $1.3\% \pm 0.4$  to  $34\% \pm 3.0$  occurred between day zero and 138 in the FOG codigester ( $p = 0.002$ , paired t-test; Figure 4-6). In contrast, *Methanospirillum* stayed below 3% relative sequence abundance in the control digester (Figure 4-6). *Methanosaeta* was the dominant acetoclastic genus within the FOG codigester, increasing from a relative concentration of  $23\% \pm 9$  on day zero to  $46\% \pm 5$  by day 138 ( $p=0.01$ ; Figure 4-6). Pearson correlation coefficients between the average relative sequence abundances of *Methanospirillum* and *Methanosaeta* with *Syntrophomonas* in the FOG codigester were 0.90 and 0.96, respectively. *Methanospirillum* and *Methanosaeta* species were therefore key methanogenic groups growing along with *Syntrophomonas* in the codigester microbiome during the degradation of FOG.

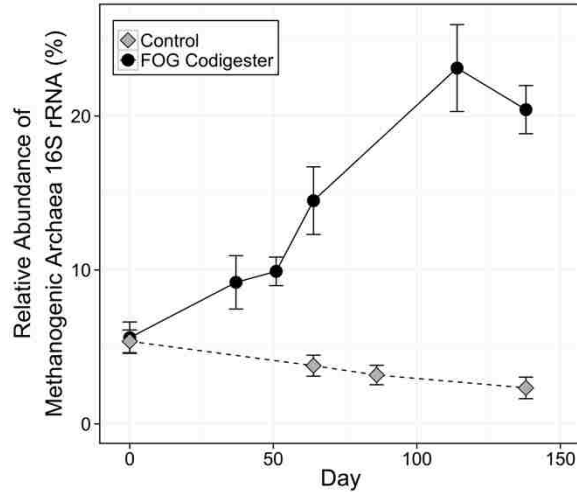


**Figure 4-5** Change in the relative fraction of methanogenic *Archaea* 16S rRNA genes in prokaryotic community of the control digester and FOG codigester. The total methanogenic *Archaea* 16S rRNA gene concentration was determined as the sum of all methanogen groups targeted in qPCR, and the prokaryotic gene concentration was determined as the sum of methanogenic *Archaea* and total *Bacteria* 16S rRNA gene concentrations.

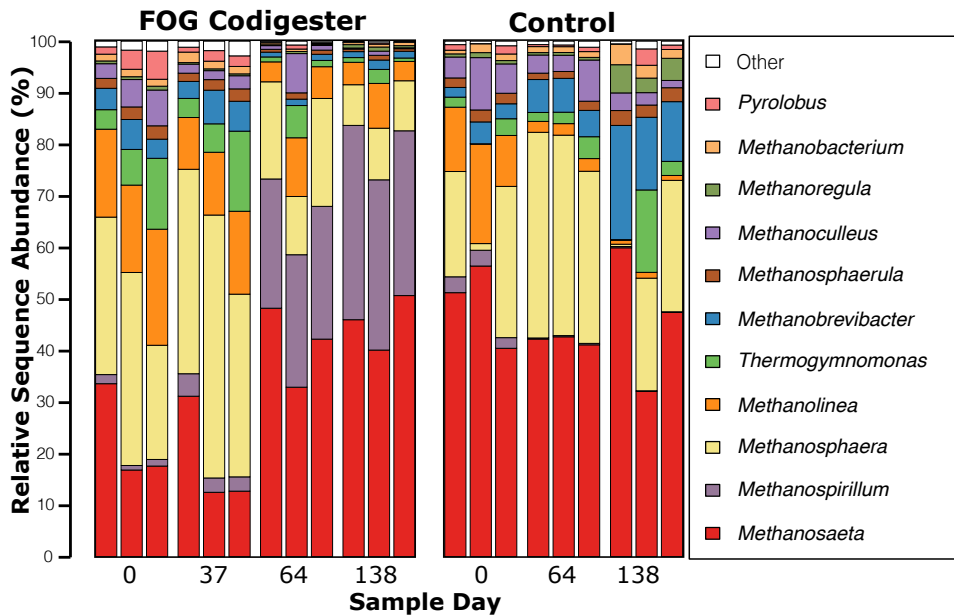


**Figure 4-6** Relative sequence fraction of the 13 most abundant genera within the FOG codigester and control digester libraries produced from Illumina MiSeq sequencing of *Archaea* 16S rRNA gene amplicons. The triplicate bars shown at each sample day represent replicate DNA extractions. The relative sequence fraction of all other genera were summed, and are shown here as “Other”.

#### 4.4.3 *Microbial community structure was related to reactor performance during FOG codigestion*

Canonical correspondence analysis (CCA) was utilized to elucidate potential relationships between environmental and operational digester parameters and *Bacteria* and *Archaea* OTU sequence abundances within the digester samples (Figure 4-7). The four environmental gradients found to be most effective at explaining the community abundance data for *Bacteria* and *Archaea* were: daily methane production rate, maximum methane production rate from oleate ( $q_{max,oleate}$ ), maximum methane production rate from acetate ( $q_{max,acetate}$ ), and time (experimental days). Analysis of variance (ANOVA) on the CCA models showed that the selected environmental variables were significant in constraining both *Bacteria* and *Archaea* OTU abundances ( $p < 0.05$ ). The fractions of the total variability that was explained through the CCA models were 69% and 67% for the *Bacteria* and *Archaea* OTU abundance datasets, respectively.



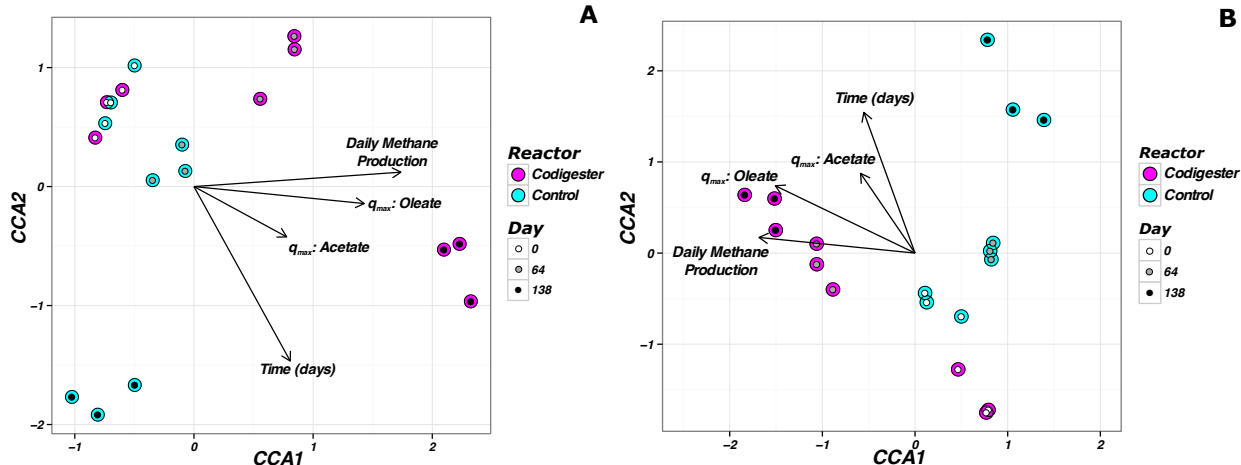


**Figure 4-7** Canonical correspondence analysis (CCA) plots based on (A) Bacteria and (B) Archaea scaled OTU sequence counts in the codigester and control digester samples, constrained by the four highest-scoring environmental gradients: daily methane production, maximum methane production from oleate ( $q_{max,oleate}$ ), maximum methane production from acetate ( $q_{max,acetate}$ ), and time (experimental days). The color of the outer circles represents the sample digester source and the color of the inner circles represents the sample collection day. The triplicate samples shown for each sample day are from replicate DNA extractions. The length and direction of each arrow represents the scaling used for that environmental gradient in the CCA model.

To further evaluate whether microbial community structure was related to system performance during FOG degradation, a parameter was developed to relate the food-to-microorganism ratio ( $F:M$ ) for FOG loading to the LCFA-degrading microbial population within the codigester. Due to the significant increase in *Syntrophomonas* abundance in the codigester relative to the control (Figure 4-3A and Figure 4-4), we investigated whether *Syntrophomonas* abundance could serve as a predictor for LCFA-degradation activity. A parameter termed the FOG-to-syntroph feed ratio ( $F:M_{Synt}$ ) was thereby developed by normalizing the FOG loading to the concentration of *Syntrophomonas* in the digester:

$$F : M_{Synt} = \frac{Q \cdot VS_{FOG}}{V \cdot X_{VS} \cdot f_{Synt}}$$

where:  $Q$  is the daily feed volume (L/d),  $VS_{FOG}$  is the influent FOG VS concentration (g VS/L),  $V$  is the reactor working volume (L),  $X_{VS}$  is the reactor VS concentration (g VS/L), and  $f_{Synt}$  is the

specific concentration of *Syntrophomonas* based on qPCR (16S rRNA copies/g VS). The  $F:M_{Syn}$  was calculated based on a 10-day average of daily FOG VS loading, a 10-day average of the reactor VS concentration, and the specific concentration of *Syntrophomonas* 16S rRNA genes per g VS on the day of the LCFA measurement.

The effluent LCFA concentration in the codigester was positively correlated to the  $F:M_{Syn}$  ( $R^2$  of nonlinear regression = 0.94), indicating that the LCFA removal efficiency was related to the abundance of *Syntrophomonas* biomass within the codigester (Figure 4-8). Specific FOG loading rates of 0 to  $1.5 \times 10^{-12}$  g VS/16S gene copies-day resulted in effluent LCFA concentrations below 30 mg LCFA/g TS, whereas LCFA accumulated up to 104 mg LCFA/g TS at higher  $F:M_{Syn}$  values.

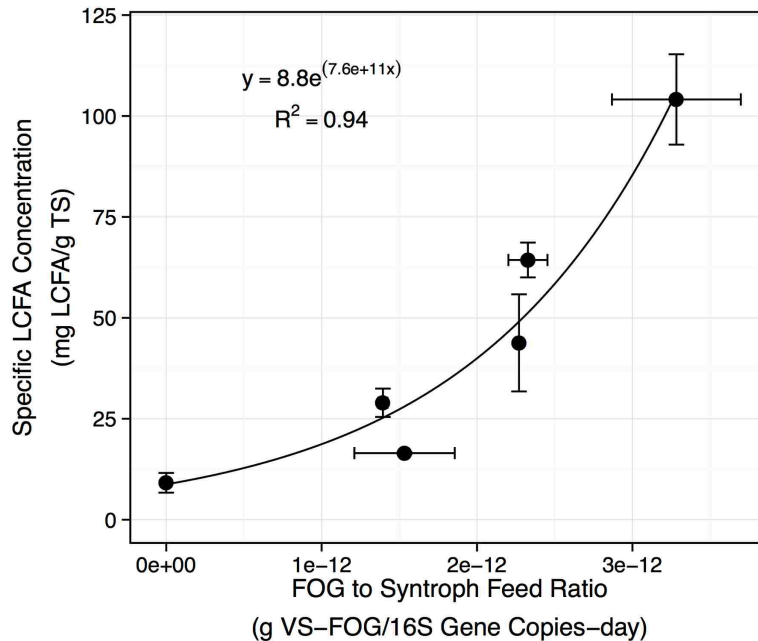


**Figure 4-8** Specific effluent LCFA concentration of the FOG codigester versus the FOG to syntroph feed ratio ( $F:M_{Syn}$ ). The exponential trend line was fitted with a non-linear regression method in R v. 3.0.2. Error bars represent one standard deviation.

## 4.5 DISCUSSION

High FOG loadings during codigestion with municipal sludge have led to process upsets (Davidsson et al., 2008; Girault et al., 2012; Luostarinen et al., 2009; Noutsopoulos et al., 2013; Wang et al., 2013) and even delayed process recovery (Wan et al., 2011). Threshold FOG loading limits for codigestion have been recommended (Noutsopoulos et al., 2013; Wang et al., 2013), but these loading limits have not considered the impacts of microbial community adaptation. In our study, changes in microbial community structure were closely monitored during transient increases in FOG loading, which showed that LCFA accumulation was related to both the FOG loading rate and the abundance of syntrophic  $\beta$ -oxidizing consortia. LCFA accumulated at higher specific loading rates of FOG relative to the abundance of *Syntrophomonas* 16S rRNA genes in the codigester. Thus, previous reports of unstable digester performance at high FOG loadings (Davidsson et al., 2008; Girault et al., 2012; Luostarinen et al., 2009; Noutsopoulos et al., 2013; Wang et al., 2013) could possibly have been attributed to an insufficient abundance of LCFA-degrading syntrophic bacteria, so that LCFA accumulated to a concentration high enough to inhibit methanogenic activity (Angelidaki and Ahring, 1992; Hanaki et al., 1981; Rinzema et al., 1994). The significant growth of LCFA-degrading syntrophic bacteria and methanogenic archaea in the FOG codigester in this study supports previous observations that gradual stepwise increases in FOG loading stimulated higher rates of LCFA  $\beta$ -oxidation and methanogenesis (Silvestre et al., 2011) and that biomass resilience to LCFA was impacted by the exposure time to lipids (Alves et al., 2001; Silva et al., 2014). Our finding that LCFA conversion efficiency depends upon the digester biomass composition may also help to explain some of the variation in reported threshold limits of FOG loading during municipal sludge codigestion, which ranged from ~0.4 to 2.1 g FOG VS/L-d (Girault et al., 2012;

Luostarinen et al., 2009; Noutsopoulos et al., 2013; Silvestre et al., 2011; Wan et al., 2011; Wang et al., 2013). The highest FOG VSLR tested in this study was 1.5 g VS/L-d, which is close to the FOG VSLR threshold of 1.6 g VS/L-d reported previously during FOG codigestion with municipal sludge by Luostarinen et al. (2009). At our highest FOG VSLR, LCFA accumulated to 104 mg LCFA/g TS with no appreciable increase in VFA. This phenomenon was also observed by Silvestre et al. (2014) and Girault et al. (2012) during FOG codigestion with municipal sludge, suggesting that acetogenesis from LCFA can be rate-limiting in such processes. The decrease in effluent LCFA in the codigester on day 138 in our study thus indicates that a higher FOG VSLR may be possible after further time for microbial community adaptation. Overall, these results implicate that the FOG loading threshold during codigestion may be considered a ‘moving target’ that relies upon the degree of microbial community adaptation and the activity within the digester microbiome to degrade LCFA.

This is the first study to monitor changes in syntrophic  $\beta$ -oxidizing bacteria abundance during FOG codigestion by qPCR, which highlighted a differential selection of *Syntrophomonas* over *Syntrophus*. The family of *Syntrophomonadaceae* has been previously identified as key syntrophic bacteria enriched in anaerobic digester biomass during unsaturated LCFA degradation (Baserba et al., 2012; Sousa et al., 2009, 2007a; Ziels et al., 2015). In contrast, *Syntrophaceae* have been detected at higher abundances in anaerobic communities degrading saturated LCFA (Sousa et al., 2009) as well as long-chain alkanes (Gray et al., 2011; Zengler et al., 1999). While the saturated fatty acids of palmitate (C<sub>16:0</sub>) and stearate (C<sub>18:0</sub>) together comprised 54% of the LCFA in the codigester effluent on average (Supplemental Figure B1), it is not known whether the LCFA composition of the influent FOG influenced the selection of *Syntrophomonas* over

*Syntrophus*. It may be also possible that the enrichment of *Syntrophomonas* in the codigester was attributed to specific syntroph-methanogen pairings with *Methanospirillum* and *Methanosaeta*, which were the dominant methanogenic archaeal groups enriched with FOG addition and were strongly correlated with *Syntrophomonas* abundance (i.e. Pearson coefficients > 0.9).

The positive association of the FOG codigester *Bacteria* and *Archaea* community profiles with the constrained gradients of daily methane production and  $q_{max,oleate}$  further confirm that changes in microbial community structure were related to measures of codigester performance. Hill diversity numbers also proved to be effective metrics to capture the alpha and beta components of community structure changes within the digesters, as was similarly found with other biological wastewater treatment processes (Vuono et al., 2015). Diversity numbers of orders  ${}^1D$  and  ${}^2D$  for the *Bacteria* community increased along with measures of reactor performance in the FOG codigester, but the same was not true with species richness ( ${}^0D$ ). This agrees with previous findings indicating that higher order diversity (i.e. evenness) in digester *Bacteria* communities correlated positively with COD removal and methane production, whereas species richness did not (Werner et al., 2011). While the *Bacteria* species richness of the FOG codigester remained stable in this study, the community experienced changes in dominant members (captured by  ${}^2D$ ) that contributed to higher ecosystem function. The higher methane production of the codigester following shifts in dominant *Bacteria* community members (higher  ${}^2D$ ) coincided with the growth of the functionally specific *Syntrophomonas*. The increased biodiversity within the codigester was therefore attributed to the growth of initially rare syntrophic bacteria, which were also a driving force behind improvements in the codigester daily methane production and increased values of  $q_{max,oleate}$ . This finding agrees with previous observations that the abundance

of syntrophic bacteria was linked to anaerobic digester resilience (Regueiro et al., 2015; Werner et al., 2011).

Evaluating the activity of syntrophic fatty acid-oxidizing bacteria has previously been proposed as an alternative approach to gauge the activity of methanogenic pathways, since the metabolism of syntrophic fatty acid-oxidizing bacteria is directly coupled to the activity of methanogens (Smith et al., 2015). Our proposed relationship between LCFA removal and the *Syntrophomonas* 16S rRNA gene concentration was based on the assumption that *Syntrophomonas* was a major syntrophic bacterial group involved in LCFA  $\beta$ -oxidation, and that *Syntrophomonas* biomass could serve as a surrogate measure for the activity of the LCFA-degrading community (syntrophic bacteria + methanogens). This assumption was supported by the observation that LCFA were the primary metabolite of FOG degradation rather than acetate, indicating that LCFA  $\beta$ -oxidation was not likely limited by acetoclastic methanogenesis. Similar to our findings, the concentration of syntrophic bacterial biomass was recently found to be the limiting factor for butyrate conversion via  $\beta$ -oxidation in non-defined methanogenic enrichments (H. Junicke et al., 2016). Ziels et al. (2015) also found that the relative fraction of *Syntrophomonas* in the *Bacteria* community of oleate-fed anaerobic enrichments was positively correlated with the specific methane production rate. Since the thermodynamics of LCFA-degradation hinges upon the activity of methanogenic archaea and syntrophic  $\beta$ -oxidizing bacteria (Schink, 1997), we propose that the FOG-loading capacity of a given digester can be better predicted by closely monitoring the abundance and activity of those populations.

From a process engineering perspective, efficient turnover of LCFA is critical for maintaining the maximum kinetic capacity of the digester community (Pereira et al., 2005). The positive correlation observed between the effluent LCFA concentration and the codigester  $F:M_{Syn}$  suggested that a higher biomass of syntrophic LCFA-degrading consortia could increase the threshold loading rate of FOG during codigestion. A higher biomass of slow growing *Syntrophomonas* has been associated with longer anaerobic digester solids retention times (Hao et al., 2016; Lee et al., 2011). Therefore, the methane production of FOG codigestion processes should be greater with longer solids retention times by allowing a higher mass loading of FOG while maintaining an  $F:M_{Syn}$  that supports low effluent LCFA concentrations. This work also demonstrates the potential to minimize LCFA accumulation by controlling transient FOG loading rates based on the analysis of the codigester community structure, such as with qPCR measurements of syntrophic LCFA-degrading bacteria abundance.

#### 4.6 CONCLUSIONS

Microbial adaptation was important for the conversion of FOG into methane during codigestion with municipal wastewater sludge. *Syntrophomonas* bacteria were the primary syntrophic  $\beta$ -oxidizing group that was enriched in the codigester microbiome. Increases in digester LCFA concentrations occurred when the FOG loading rate relative to *Syntrophomonas* abundance exceeded a threshold value. Changes in the FOG codigester and control digester microbiomes were best explained through constrained ordination by measures of digester function. These results collectively indicate that more efficient LCFA conversion into methane can be achieved by strategically managing transient FOG loadings to allow sufficient time for microbial community adaptation through higher abundances of LCFA-degrading consortia.

#### 4.7 SUPPLEMENTAL INFORMATION AVAILABLE

Supplemental Information for this Chapter is available online at (<http://dx.doi.org/10.1016/j.watres.2016.07.043>), and is included in this document as Appendix B.



# Chapter 5. SYNTROPHIC COMMUNITY STRUCTURE AND BIOKINETICS DRIVEN BY LONG-CHAIN FATTY ACID FEEDING STRATEGY IN ANAEROBIC CODIGESTION

## 5.1 ABSTRACT

This study investigated the impacts of long-chain fatty acid (LCFA) feeding pattern on microbial community structure, bioconversion kinetics, and process stability during anaerobic codigestion. Parallel laboratory-scale anaerobic codigesters were fed with dairy cattle manure, and were either pulse-fed every two days or continuously-fed daily with oleate (C<sub>18:1</sub>) up to a maximum loading of 64% of the influent COD over 200 days. Maximum substrate conversion rates of oleate ( $q_{max,oleate}$ ) and acetate ( $q_{max,acetate}$ ) were significantly higher in the pulse-fed codigester compared to the continuous-fed codigester. The effluent acetate concentration in the continuous-fed codigester exceeded 3,000 mg/L at the highest oleate loading rate, whereas acetate in the pulse-fed codigester remained at low levels. 16S rRNA gene amplicon sequencing showed that *Bacteria* and *Archaea* community profiles diverged based on the codigester LCFA feeding pattern and loading rate. LCFA-degrading *Syntrophomonas* bacteria were significantly enriched in both LCFA codigesters, but the pulse-fed codigester had almost double the fraction of *Syntrophomonas* 16S rRNA genes by the end of the experiment with 43% of *Bacteria* sequences.  $q_{max,oleate}$  and  $q_{max,acetate}$  values were both significantly correlated to absolute concentrations of *Syntrophomonas* and *Methanosaeta* 16S rRNA genes, respectively. Improved quantitative predictions of bioconversion kinetics were achieved with multiple-linear regression models based on the absolute abundance of individual *Syntrophomonas* and *Methanosaeta* taxa. These

results suggest that pulse-feeding LCFA during anaerobic codigestion selected for higher microbial bioconversion kinetics and functional stability, which were related to changes in the physiological diversity and adaptive capacity of syntrophic and methanogenic communities.

## 5.2 INTRODUCTION

Anaerobic digestion of agricultural livestock manure is an attractive solution to minimize carbon footprints by treating the organic waste through the recovery of biomethane. However, the low biomethane potential of animal manures (Labatut et al., 2011) can limit the economic viability of agricultural digesters (Bishop and Shumway, 2009). Codigesting high-strength organic wastes with manure can significantly improve process economics by increasing biomethane recovery as well as provide additional revenue from tipping fees (Bishop and Shumway, 2009). Fats, oils, and greases (FOG) are appealing substrates for codigestion because of their 2.7-times greater biological methane yield per unit mass than that for livestock manures (Labatut et al., 2011). When added to the digestion process, fats and oils are rapidly hydrolyzed into glycerol and long-chain fatty acids (LCFA) (Cirne et al., 2007; Hanaki et al., 1981), with over 90% of the original methane potential of FOG maintained within LCFA (Sousa et al., 2009).

The conversion of LCFA into methane is considered rate-limiting for the ultimate degradation of FOG in anaerobic digesters (Cirne et al., 2007; Hanaki et al., 1981). LCFA-degradation under methanogenic conditions involves an obligatory syntrophic partnership between acetogenic  $\beta$ -oxidizing bacteria and acetate- and hydrogen-utilizing methanogenic archaea (Schink, 1997; Sousa et al., 2009). The bacterial species known to  $\beta$ -oxidize LCFA in syntrophy with a hydrogen- or formate- consuming partner have so far been identified within only two families,

*Syntrophomonadaceae* and *Syntrophaceae* (Sousa et al., 2009). The slower biodegradation of LCFA relative to lipid hydrolysis in anaerobic digesters can lead to LCFA accumulation and process instability, as LCFA are known inhibitors of hydrogenotrophic and acetoclastic methanogenic activity at high concentrations (Hanaki et al., 1981; Hwu and Lettinga, 1997; Rinzema et al., 1994; Silva et al., 2016; Sousa et al., 2013). LCFA accumulation can also limit the kinetics of syntrophic  $\beta$ -oxidizing bacteria (Hanaki et al., 1981). Understanding how to increase the robustness and stability of anaerobic digesters at high FOG loading rates is thus key for improving biomethane recovery from agricultural digesters through codigestion.

The relationship between the LCFA-degrading community structure and LCFA bioconversion kinetics in anaerobic digesters has not been well characterized. Previous efforts have predicted LCFA conversion kinetics in anaerobic digesters using theoretical models, such as ADM1 (Palatsi et al., 2010; Zonta et al., 2013). However, those biokinetic models were based on predictions of biomass composition, instead of calibration with actual measurements of LCFA-degrading bacteria abundance. Such models have also represented LCFA-degrading bacteria as a single homogenous population, whereas it was previously shown that various LCFA-degrading *Syntrophomonas* and *Syntrophus* taxa can coexist in anaerobic digester sludge (Sousa et al., 2007a; Ziels et al., 2015). Different methanogenic archaea species can also have varying degrees of tolerance to LCFA exposure (Silva et al., 2016; Sousa et al., 2013), suggesting that the digester methanogen community structure could be affected by FOG addition. The recent finding that effluent LCFA concentrations were inversely correlated to LCFA-degrading bacteria 16S rRNA gene concentrations during FOG codigestion (Ziels et al., 2016) indicated that the overall LCFA bioconversion rate of syntrophic bacteria and methanogenic archaea within a codigester

could establish the allowable FOG loading rate that prevents inhibitory LCFA accumulation. However, no studies have examined whether different communities of syntrophic bacteria and methanogenic archaea with different LCFA bioconversion kinetics could be biologically selected during FOG codigestion. Additional research is therefore needed to develop predictive models for LCFA conversion kinetics based on the LCFA-degrading community abundance and composition. Such models could then be utilized to identify effective digester operating strategies that promote stable performance at high FOG loading rates.

The stability of the anaerobic digestion process during disturbances has been attributed to the resilience, resistance, and redundancy of the various microbial trophic guilds of the digester food web (Carballa et al., 2015; Werner et al., 2011). *Resistance* refers to the degree in which a community composition remains unchanged during a disturbance; *resilience* indicates to the rate at which the microbial community returns to its original composition following a disturbance; and *functional redundancy* refers to the potential for various microbial taxa to process the same substrate (Allison and Martiny, 2008). In anaerobic digesters, hydrolytic bacteria are thought to have a high degree of functional redundancy (Carballa et al., 2015; Vanwonterghem et al., 2014), whereas syntrophic bacteria are thought to be more metabolically specialized (Briones and Raskin, 2003; McInerney et al., 2009) and less likely to undergo competition (Werner et al., 2011). However, if different syntrophic and methanogenic consortia could have different rates of LCFA conversion, then biological selective pressures could potentially be incorporated into FOG codigester operating strategies to favorably steer the LCFA-degrading community toward a composition with higher bioconversion kinetics. It was observed that four distinct clades of syntrophic propionate oxidizing bacteria (POB) were enriched in an anaerobic digester operated

in fill-and-draw mode, and the presence of multiple syntrophic POB groups was attributed to periodic changes in propionate concentrations with batch feeding along with different biokinetic characteristics of the POB clades (H. D. Ariesyady et al., 2007). Distinct syntrophic POB populations with different biokinetic parameters were also detected in the first and second phases of a thermophilic phased-digester based on differences in organic loading (Zamanzadeh et al., 2013). The digester feeding strategy was also found to impact the methanogen community structure (Conklin et al., 2006) and digester robustness during overloading events (Conklin et al., 2006; De Vrieze et al., 2013; Mulat et al., 2016). With regards to LCFA degradation, pulse-feeding LCFA during codigester startup was suggested to promote greater stability at higher loading rates (Cavaleiro et al., 2009); however, the resulting LCFA-degrading community structure and biokinetics were not compared to a continuous-fed codigester in parallel. Thus, the impact of LCFA feeding frequency on the bioconversion kinetics and community composition of LCFA-degrading syntrophic bacteria and methanogenic archaea during the codigestion of LCFA-rich wastes remains unknown.

The objective of this research was to investigate the effects of LCFA feeding frequency during codigestion on: (1) LCFA bioconversion kinetics, (2) codigester stability and performance, and (3) the composition of syntrophic LCFA-degrading consortia. Additionally, a goal of this study was to develop quantitative models to predict LCFA-conversion kinetics based on syntrophic LCFA-degrading bacteria community structure and abundance. Anaerobic codigesters fed with dairy manure and oleate were operated with either a pulse-fed or a semi-continuous-fed regime to compare their respective substrate conversion kinetics and microbial community structures.

## 5.3 MATERIALS AND METHODS

### 5.3.1 *Anaerobic Digester Description and Operation:*

The three anaerobic digesters operated in this study consisted of 5.5 L glass semi-continuous stirred tank reactors with 4.0 L working volumes. The digesters were configured as shown in Supplemental Figure C1. The digesters were intermittently mixed for 2 minutes every 10 minutes with an axial impeller mixer (5VB, Cleveland Mixer), and temperature was controlled at 35°C in an environmental chamber.

The digesters were inoculated with effluent sludge from a mesophilic anaerobic digester treating dairy manure at a nearby farm. Fresh cow dairy manure feedstock was collected from the influent mixing tank of the same dairy farm digester that supplied the inoculum sludge. The manure feedstock was blended for 1 minute before storing ~1L aliquots at -20°C. Single manure aliquots were thawed at 4°C daily before use. Three batches of manure were collected throughout the entire experimental period. The manure feed was manually added once daily after withdrawing 200 mL of sludge. The total feed volume (manure + oleate) was maintained at 200 mL/day to maintain a 20-day hydraulic retention time (HRT), which was also equal to the solids retention time (SRT). Daily biogas production was measured with wet tip gas meters (Wet Tip Gas Meter Co., Nashville), and the methane composition of the biogas was measured at least twice weekly at the end of the daily feeding cycle. Total COD (TCOD), total solids (TS), and volatile solids (VS) of the manure feed and digester effluents were measured 3-times weekly. Effluent volatile fatty acids (VFA) were measured 3-7 times weekly, and effluent long-chain fatty acids (LCFA) were measured weekly.

Digester operation conditions were varied under three experimental phases: (1) start-up period with manure-only feeding (days -50 to 0); (2) Phase I of oleate codigestion with manure (days 1 to 85); and (3) Phase II of oleate codigestion with manure (days 86 to 204). The manure feed VS loading was maintained at  $1.3 \pm 0.2$  g VS/L-d during all experimental phases.

During Phase I, two of the digesters received an aqueous solution of sodium oleate (>97%, Tokyo Chemical Industry Co.) at 10% of the daily influent feed volume for codigestion, while the third digester was fed only manure as the control. The oleate feed organic loading rate (OLR) for the two codigesters was equal, and was increased over time by increasing the oleate concentration. The oleate feeding frequency was different for the two codigesters. One codigester received the oleate feed every 6-hrs daily, and is hereon referred to as the *continuous-fed codigester* (CF codigester). The other codigester received the oleate feed once every 2-days, and is hereon referred to as the *pulse-fed codigester* (PF codigester). The oleate OLR was almost doubled about every 20-days (equal to SRT/HRT) during Phase I, accounting for up to 27% of the influent feed total COD during the 85 day period (Table 5-1). On day 85, the PF codigester operation was terminated due to accidental damage to the reactor vessel.

During Phase II, two oleate-fed codigesters were operated in parallel: (1) the control digester from Phase I was used for the pulse-fed codigester operation, and is hereon termed *pulse-fed codigester #2* (PF2 codigester); and (2) the operation of the CF codigester from Phase I was continued. The oleate OLR to the PF2 codigester in Phase II was increased about every 10 days and the step increases to the CF codigester remained about every 20 days, such that the oleate accounted for 64% of the total influent COD to both codigesters by day 150 (Table 5-1). Due to

acetate accumulation in the CF codigester at an oleate OLR of 3.8 g COD/L-d, the oleate OLR was reduced to 3.2 g COD/L-d on day 184 (Table 5-1).



**Table 5-1** Summary of oleate feed and total feed characteristics to the codigesters during Phase I and II. Values in parentheses represent one standard deviation.

Step # LCFA increase	Days	Oleate Feed				Total Feed (Manure + Oleate)			
		VS (g/L)	VSLR (g VS/L-d)	COD (g/L)	OLR (g COD/L-d)	VSLR (g VS/L-d)	OLR (g COD/L-d)	% VS as LCFA	% COD as LCFA
<i>Phase I: Pulse-fed and Continuous-Fed Codigesters</i>									
0	-50 - 0	0	0	0	0	1.3 (0.1)	2.4 (0.7)	0%	0%
1	1 - 20	0.7	0.04	2.1	0.1	1.3 (0.1)	2.2 (0.3)	3%	5%
2	21-45	1.5	0.08	4.5	0.2	1.3 (0.1)	3.0 (0.4)	6%	7%
3	46-65	2.5	0.1	7.5	0.4	1.3 (0.1)	2.3 (0.4)	10%	16%
4	66-85	4.8	0.2	14	0.7	1.5 (0.2)	2.7 (0.2)	16%	27%
<i>Phase II: Continuous-Fed Codigester</i>									
5	86 - 106	7.5	0.4	22	1.1	1.7 (0.2)	3.5 (0.2)	22%	32%
6	107 - 126	11.6	0.6	34	1.7	1.8 (0.2)	3.7 (0.3)	32%	47%
7	127 - 149	18.9	0.9	56	2.8	2.1 (0.2)	5.2 (0.3)	45%	54%
8	150 - 183	25.6	1.3	76	3.8	2.6 (0.2)	5.9 (0.3)	50%	64%
9	184 - 204	21.8	1.1	65	3.2	2.3 (0.1)	5.2 (0.4)	48%	62%
<i>Phase II: Pulse-Fed Codigester</i>									
1	104-116	1.5	0.1	4.6	0.2	1.4 (0.2)	2.3 (0.1)	5%	10%
2	117-126	3.5	0.2	10	0.5	1.3 (0.2)	2.4 (0.4)	13%	22%
3	127-137	6	0.3	18	0.9	1.7 (0.3)	3.0 (0.3)	18%	30%
4	138-149	13.6	0.7	40	2.0	1.9 (0.2)	3.9 (0.3)	36%	52%
5	150-183	25.6	1.3	76	3.8	2.6 (0.2)	5.9 (0.4)	50%	64%
6	184-204	21.8	1.1	65	3.2	2.3 (0.1)	5.2 (0.4)	48%	62%

VSLR = volatile solids volumetric loading rate; OLR = COD volumetric loading rate

### 5.3.2 *Oleate Bioconversion Kinetics*

Oleate bioconversion kinetics were measured for each codigester sludge in a series of batch tests conducted on days 0, 41, and 84 during Phase I, and on days 129, 148, 170, and 204 for Phase II. The 30-mL glass serum batch test bottles were purged with N<sub>2</sub>:CO<sub>2</sub> (80:20) before adding 15 mL digester effluent (digestate), sealed with butyl rubber septa and purged again with N<sub>2</sub>:CO<sub>2</sub> (80:20). A 100 g/L aqueous solution of sodium oleate was added to the batch test bottles via syringe for initial oleate concentrations of 0 (control), 100, 175, 350, 750, 1800, and 4500 mg/L. The pH was adjusted to 7.2 with 1 N HCl. Triplicate test bottles were maintained at 35°C on an orbital shaker at 150 rpm. Gas production was measured using a digital manometer (Series 490, Dwyer Instruments, Michigan City) approximately 7 times over 8 hrs. The headspace methane concentration was sampled with each pressure measurement. The background methane production from the control was subtracted from each substrate-amended treatment, and the slope of methane production was determined via linear regression in R version 3.2.1. Methane production rates were adjusted to standard temperature and pressure (STP), and were normalized to the amount of VS added to the vials initially. Batch tests for the PF codigesters were conducted at the end of the 48-hr pulse-feeding cycles to minimize background substrate concentrations.

### 5.3.3 *Oleate Inhibition of Aceticlastic Methanogenic Activity*

To test inhibitory effects of oleate on methanogenic activity, aceticlastic maximum methane production rates ( $q_{max,acetate}$ ) were measured in batch tests with different initial oleate concentrations. The aceticlastic maximum methane production rate was measured according to the procedure described by Conklin et al. (2006). Batch test bottle preparation was conducted as

described above in Section 5.3.2. A series of triplicate bottles received 50 mM sodium acetate in addition to sodium oleate at initial concentrations of 0, 1.5, 4, 8, 12, and 16 g/L. One set of triplicate vials without any added substrate was incubated in parallel to measure background digestate methane production. Methane production was monitored 8-times over a 6-hr period based on headspace pressure and composition. The  $q_{max,acetate}$  was calculated based on linear regression of methane production curves as described by Conklin et al. (2006). Aceticlastic inhibition tests were conducted within 3-days of each oleate bioconversion kinetic tests.

#### 5.3.4 Analytical Methods

TCOD was measured with High-Range COD digestion vials (Hach Co., Loveland, CO) according to Hach Method 8000. TS and VS were measured according to Standard Methods (Eaton and Franson, 2005). Prior to daily wasting and feeding of the digesters, pH was measured (EcoSens pH100A, YSI, Yellow Springs, Ohio) immediately after withdrawing samples.

Effluent sludge samples for volatile fatty acid (VFA) analysis were initially centrifuged at 14,000 g for 10 minutes. The supernatant was serial filtered with 0.45 and 0.22  $\mu\text{m}$  polyethersulfone (PES) syringe filters, and 100  $\mu\text{L}$  of 10% formic acid was then added to 1 mL of filtrate to acidify the sample. VFA were measured with a GC-FID (Shimadzu GC-2010) equipped with a BP-21 column (30 m $\times$ 0.32 mm I.D., 0.25  $\mu\text{m}$  film thickness, SGE). LCFA were extracted from digester effluent according to the protocol described by Ziels et al. (2015), and were analyzed by GC-FID with a BP-21 column (30 m $\times$ 0.32 mm I.D., 0.25  $\mu\text{m}$  film thickness; SGE). Biogas samples (~0.5-1 mL) were collected with a syringe equipped with a Teflon Mininert valve, and the methane composition was analyzed using a SRI 8610C GC-FID with a Supelco Alumina Sulfate Plot column (50 m, 0.53 mm i.d.).

### 5.3.5 DNA Extraction and Quantification

DNA was extracted in triplicate from digester sludge samples collected on the same days as the batch oleate bioconversion kinetic assays. Briefly, ~15 mL of digester sludge was collected via catheter syringe and transferred to pre-purged, O<sub>2</sub>-free centrifuge tubes on ice. The digester sludge was aliquoted into 2 mL microcentrifuge tubes on ice in an anaerobic glove chamber. The 2 mL samples were then centrifuged at 14,000 g for 10 min at 4°C, immediately decanted, and stored at -80°C. DNA was extracted from the pellet using the PowerMicrobiome™ kit (MO BIO Laboratories Inc., Carlsbad, CA) with phenol:chloroform:isoamyl during bead-beating, according to the manufacturer's instructions. Extracted DNA was quantified with the Quant-iT HS DNA kit using a Qubit 2.0 fluorometer (Invitrogen, Carlsbad, CA).

### 5.3.6 Quantitative PCR

Quantitative PCR (qPCR) was conducted in accordance to Ziels et al. (2015) targeting 16S rRNA gene fragments of the syntrophic  $\beta$ -oxidizing bacterial genera of *Syntrophomonas*, as well as the domains *Bacteria* and *Archaea* (Yu et al., 2005). More detailed descriptions of the reaction conditions, primers and probes, and calibration standards are given in the Supplemental Information. qPCR was conducted on triplicate DNA extractions from each sampling point, and gene copy numbers were normalized per g VS of digester biomass.

### 5.3.7 16S rRNA Gene Amplicon Sequencing

Amplicon sequencing of 16S rRNA genes was conducted on triplicate DNA extractions from each sampling point. Briefly, 16S rRNA gene fragments from all samples were amplified with barcoded and indexed universal prokaryotic V4-V5 primers 515F-Y (5'-GTGYCAGCMGCCGCGGTAA) and 926R (5'-CCGYCAATTYMTTTRAGTTT) (Parada et

al., 2015), and the products were pooled and sequenced on a 2x300bp Illumina MiSeq run by the United States Department of Energy Joint Genome Institute. The raw sequence data is available through the JGI Portal (<http://jgi.doe.gov>) under project ID number 1105525.

### 5.3.8 *Bioinformatics*

To obtain a high resolution of the community composition, amplicon reads were denoised into their exact sequences using the DADA2 pipeline (Callahan et al., 2016). Reads were first quality filtered by trimming the first 10 bp from all sequences, truncating forward reads at 265 bp, truncating reverse reads at 180 bp, and filtering all reads based on a maximum expected error of 2 using DADA2. Parameters for the DADA2 error model were initially calculated on dereplicated reads of a random subset of 20 samples, and the estimated error parameters were subsequently used to denoise all dereplicated sample reads into exact sequences. Forward and reverse sequences were then merged with DADA2 using a minimum overlap of 20 bp and zero allowed mismatches. Merged denoised sequences were truncated to 390 bp and clustered into 99.5% OTUs following chimera removal with UPARSE (Edgar, 2013), resulting in 5014 non-singleton OTUs. Representative sequences of the 99.5% OTUs were classified against the SILVA SSU Ref NR dataset (v.123) using the RDP classifier (Wang et al., 2007).

Relative abundance values were calculated based on normalized sequence counts obtained with DESeq2 (Love et al., 2014), which accounted for different sequencing depths among samples. Diversity estimates were based on Hill diversity numbers ( ${}^qD$ ) of orders  $q = 0, 1, \text{ and } 2$  (Jost, 2006) using DESeq2 normalized sequence counts.

### 5.3.9 Regression Analysis

A stepwise regression approach was used to identify a subset of OTUs that significantly explained maximum methane production rates from oleate and acetate ( $p < 0.05$ ). Predictor variables (before stepwise feature selection) for the  $q_{max,oleate}$  regression model included the inferred absolute abundances of 13 dominant *Syntrophomonas* OTUs, and the predictor variables for the  $q_{max,acetate}$  regression model consisted of inferred absolute abundances of 3 dominant *Methanosaeta* OTUs. Inferred absolute abundances were calculated by multiplying each OTU relative abundance value by the target group 16S rRNA gene copies per g VS obtained by qPCR. The triplicate amplicon sequence profiles for each sampling point were included individually in the model development and validation. Prior to model fitting, multicollinearity between OTU abundances was examined using Pearson's correlation, and OTUs with correlation coefficients greater than 0.7 were removed from the dataset. Stepwise feature selection was conducted with the remaining OTU abundance datasets, and model selection was cross-validated based on 10 sub-samplings repeated 10 times using the caret package in R (Kuhn, 2008).

## 5.4 RESULTS

### 5.4.1 Effect of LCFA OLR and feeding frequency on codigester performance

Impacts of LCFA (oleate) feeding frequency on codigester performance and bioconversion kinetics were investigated by increasing the oleate loading in two operational phases over 204 days (Table 5-1). There was no significant effect of the LCFA OLR on codigester effluent VS concentrations, indicating that LCFA addition with both feeding strategies did not impair the manure VS destruction efficiency and that most of the LCFA fed was degraded (Supplemental

Tables C1 and C2). The pH of the codigesters was on average 7.2 and 7.5 by the end of Phase I and II, respectively (Supplemental Tables C1 and C2), indicating sufficient buffering capacity in the codigesters.

During Phase I, the average daily methane production rate was similar for the two codigesters, and increased with each incremental increase in the feed LCFA concentration (Figure 5-1A). By the end of Phase I, the methane production rate for the codigesters was on average 70% higher than that for the manure-fed control (average of 1700 mL/d versus 1000 mL/d). Similar increases in methane production during Phase II were observed with each incremental increase in LCFA loading to the codigesters (Figure 5-1B). At the highest LCFA loading of 64% of the influent COD during Phase II, the daily methane production of both codigesters was on average 440% higher than that for the Phase I manure-fed control (average of 5500 mL/d versus 1000 mL/d). The average specific methane yield was 8% higher for the PF2 codigester relative to the CF codigester at the highest LCFA loading during Phase II, but the difference was not statistically significant due to the large daily variation in gas production with the pulse-feeding regime (Supplemental Table C2).

Acetate was the only VFA that accumulated above 40 mg/L during LCFA codigestion. In Phase I, acetate was always below 40 mg/L (Figure 5-1C), but in Phase II the effluent acetate persisted after the oleate OLR was increased to 64% of the total influent COD ( $3.8 \text{ g COD}_{\text{oleate}}/\text{L-d}$ ) on day 150. After day 180, the effluent acetate concentration in the CF codigester steadily increased to about 3,000 mg/L by the end of the experiment on day 204. During that time, the PF2 codigester effluent acetate concentration was elevated to about 500-1000 mg/L at 24 hrs after LCFA

feeding, but the acetate was consumed to low levels before the next feeding every 48-hrs (Figure 5-1D).

#### 5.4.2 *Impacts of LCFA OLR and feeding frequency on LCFA and acetate bioconversion kinetics*

After the addition of oleate to the codigesters, their  $q_{max,acetate}$  and  $q_{max,oleate}$  values increased with increasing oleate OLRs up to day 170. At the end of Phase I, the CF and PF codigesters had similar  $q_{max,acetate}$  values, but the  $q_{max,oleate}$  value for the PF codigester was 16% higher (Table 5-2). During Phase II, the oleate OLR was increased for the CF codigester from 2.8 to 3.8 g COD/L-d by day 170 (Table 5-1). The PF2 codigester had the same oleate OLR of 3.8 g COD/L-d by day 170, but its OLR had been increased at a faster rate starting from day 104. On day 170, the PF2 codigester had a higher  $q_{max,oleate}$  than the CF codigester by 17%, and a higher  $q_{max,acetate}$  by 28% (Table 5-2). The  $q_{max,acetate}$  and  $q_{max,oleate}$  values for both codigesters decreased between days 170 and 204 in Phase II, but the biokinetics of the PF2 codigester remained faster with 35% and 33% higher  $q_{max,acetate}$  and  $q_{max,oleate}$  values than that of the CF codigester on day 204, respectively (Table 5-2). These results were confirmed by substrate inhibition kinetic modeling (Aiba et al., 1968) described in the Supplemental Information, which showed that the PF and PF2 codigesters had 65% and 27% higher  $q_{max,oleate}$  values than the CF codigester at the end of Phase I and II (Supplemental Table C7). Pulse-feeding oleate during codigestion therefore selected for higher oleate and acetate utilization kinetics.

Tests were conducted to examine the effect of oleate concentration on the maximum acetate utilization rate ( $q_{max,acetate}$ ), and showed that  $q_{max,acetate}$  values were not inhibited by oleate concentrations below 4 g/L until day 204 (Supplemental Table C3). On day 204, the  $q_{max,acetate}$  of



both Phase II codigesters was not inhibited by an oleate concentration of 0.8 g/L, but at 4 g/L oleate it was inhibited by over 60% (Supplemental Table C3). Effluent oleate concentrations for both Phase I and II were below 150 mg/L (Supplemental Tables C4 and C5), which were below these inhibitory concentrations for acetoclastic methanogenesis. Yet, a decreased acetoclastic tolerance to oleate on day 204 was indicated by lower total  $q_{max,acetate}$  values in both codigesters (Table 5-2), as well as acetate accumulation within the CF codigester (Figure 5-1D).

Until day 84 in Phase I, the rate of oleate bioconversion in the batch tests with both codigester sludges was inhibited above 350 mg/L oleate, as indicated by lower methane production rates at higher oleate concentrations (Supplemental Table C6). On day 84 in Phase I, the rate of oleate conversion in PF codigester batch tests was not inhibited up to 1,800 mg/L oleate, whereas the conversion rate in the CF codigester batch tests was inhibited at 350 mg/L (Supplemental Table C6). During Phase II, the inhibitory oleate concentration increased for both codigesters batch tests toward ~1,800 mg/L until day 204 (Supplemental Table C6). On day 204, oleate bioconversion rates in CF codigester batch tests were inhibited at an oleate concentration of 875 mg/L, whereas the rates in the PF2 codigester batch tests were not inhibited up to 1,800 mg/L. Thus, pulse-feeding LCFA during codigestion led to a higher resistance to oleate inhibition during its biodegradation in comparison to continuous-feeding.

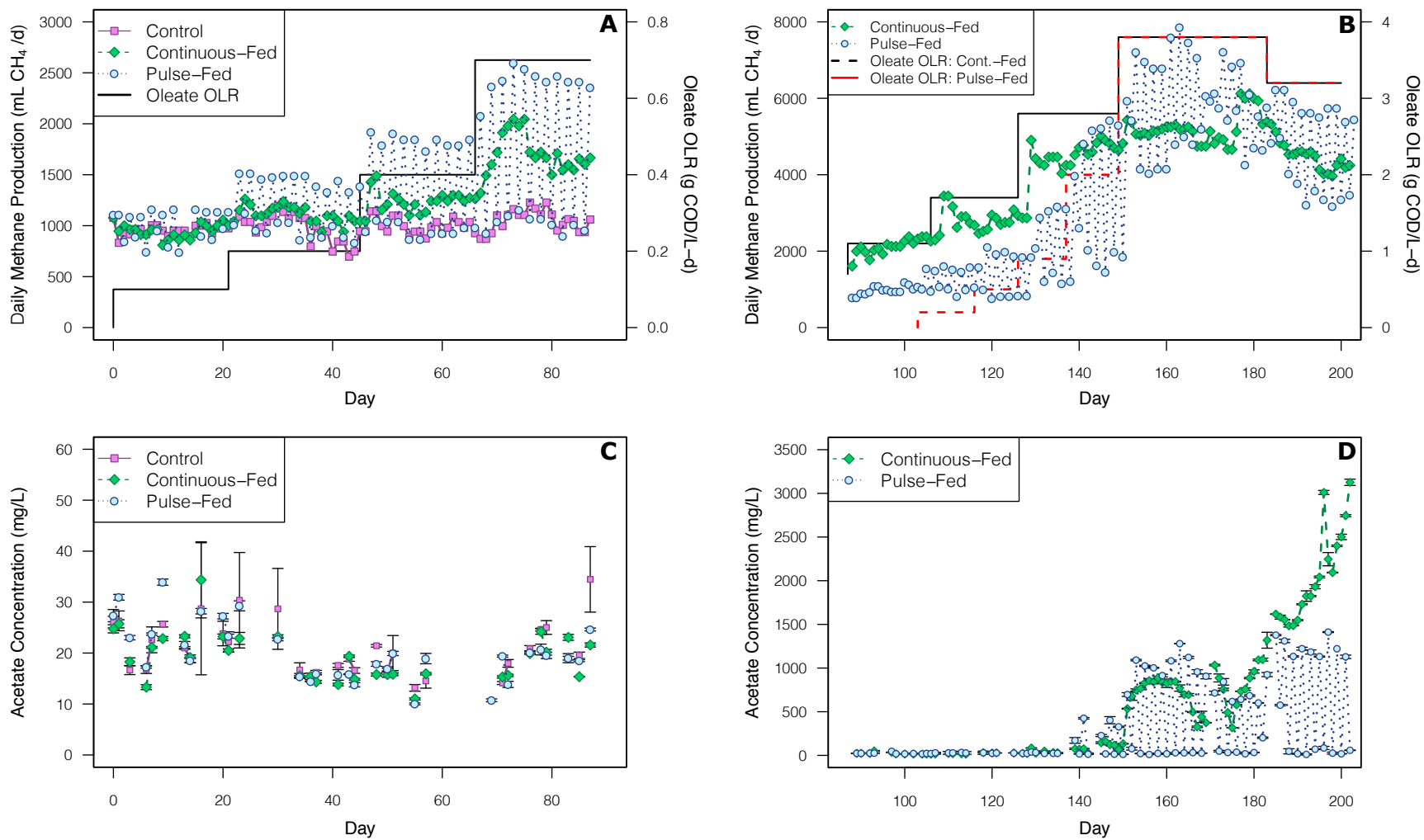


**Figure 5-1** Comparison of (A) daily methane production and organic loading rate (OLR) for Phase I experimental digesters; (B) daily methane production and OLR for Phase II experimental digesters; (C) digester effluent acetate concentrations during Phase I; and (D) digester effluent acetate concentrations during Phase II. Error bars represent one standard deviation with  $n=4$ .

**Table 5-2** Maximum conversion rates for oleate ( $q_{max,oleate}$ ) and acetate ( $q_{max,acetate}$ ) observed in the batch kinetic assays with digester sludges collected throughout Phases I and II.

Day	Oleate $q_{max}$ (mL CH <sub>4</sub> /g VS-d)			Acetate $q_{max}$ (mL CH <sub>4</sub> /g VS-d)		
	Control	CF Codigester	PF Codigester	Control	CF Codigester	PF Codigester
<b>Phase I Digesters</b>						
0	24 (2)	27 (2)	25 (4)	45 (4)	47 (5)	37 (3)
41	11 (0)	34 (1)	23 (1)	35 (4)	40 (3)	32 (2)
84	15 (1)	56 (4)	65 (2)	39 (1)	64 (6)	61 (8)
<b>Phase II Digesters</b>						
129	-	167 (0)	49 (1)	-	137 (11)	88 (8)
148	-	-	124 (9)	-	-	104 (19)
170	-	144 (5)	168 (4)	-	111 (13)	142 (9)
204	-	81 (2)	108 (1)	-	52 (5)	70 (8)

#### 5.4.3 *Microbial community structure and diversity was altered by the codigester feeding pattern*

By the end of Phase I, the *Bacteria* and *Archaea* community profiles were similar between the PF codigester and the CF codigester (Figure 5-2). Yet, sequences of the  $\beta$ -oxidizing *Syntrophomonas* increased to  $9\% \pm 0.2$  and  $4\% \pm 0.1$  of bacterial reads in the PF and CF codigesters by day 84, respectively, which were both significantly higher ( $p < 1e-3$ ) than the control at  $0.5\% \pm 0.04$  (Figure 5-2A). While the fraction of *Syntrophomonas* in the PF codigester was almost double that of the CF codigester by day 84 ( $p < 0.001$ ; Figure 5-2A), the CF codigester had significantly higher absolute concentrations of total *Bacteria* 16S rRNA genes at the end of Phase I ( $p < 0.01$ , respectively; Figure 5-3A). Consequentially, the absolute concentration of *Syntrophomonas* 16S rRNA genes measured by qPCR was similar in the PF and CF codigesters on day 84 (Figure 5-3C). Likewise, the PF codigester had a higher community fraction of aceticlastic *Methanosaeta* on day 84 in Phase I (Figure 5-2B), but the higher total

*Archaea* 16S rRNA concentration in the CF codigester (Figure 5-3B) resulted in similar absolute concentrations of *Methanosaeta* in the two codigesters (Supplemental Figure C2).

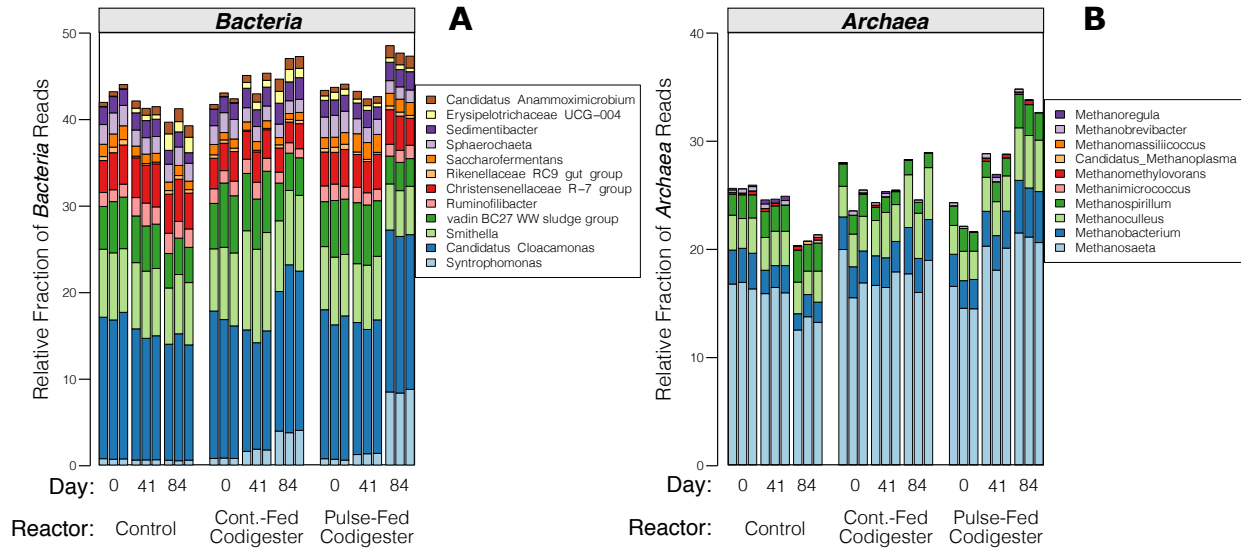


**Figure 5-2** Relative read fractions of the (A) 12 most abundant *Bacteria* genera, and (B) 10 most abundant *Archaea* genera in the 16S rRNA amplicon sequence libraries for the digesters during Phase I. Genus abundance profiles from triplicate DNA extractions are shown for each time point.

Both the microbial community abundance and composition was altered by the LCFA feeding strategy during Phase II. Correspondence analysis revealed that the *Bacteria* and *Archaea* OTU read abundance profiles diverged between the PF2 codigester and CF codigester beginning on day 129 onward (Figure 5-4). On day 170, the PF2 codigester *Archaea* population had significantly higher fractions of *Methanosaeta*, *Methanoculleus*, and *Methanospirillum* sequences compared to the CF codigester ( $p < 0.001$ ; Figure 5-5B), whereas the CF codigester had a significantly higher fraction of *Methanobacterium* ( $p < 0.001$ ). By day 204, the total *Archaea* 16S rRNA gene concentration was similar in both codigesters (Figure 5-3E), indicating that the absolute abundance of *Methanosaeta*, *Methanoculleus*, and *Methanospirillum* was higher in the PF2 codigester (Supplemental Figure C2). The *Bacteria* community of the PF2 codigester had a

significantly higher fraction of  $\beta$ -oxidizing *Syntrophomonas* compared to the CF codigester by day 170 ( $p < 0.001$ ; Figure 5-5A). On day 204, the fraction of *Syntrophomonas* sequences in the PF2 *Bacteria* sequence library increased to  $43\% \pm 2$ , which was almost double that of the CF codigester at  $22\% \pm 0.4$  (Figure 5-5A). The total *Bacteria* 16S rRNA gene concentration reached similar levels in both codigesters by day 204 (Figure 5-3D), indicating that the absolute abundance of *Syntrophomonas* was higher in the PF2 codigester due to its higher community fraction (Figure 5-5A). This result was confirmed with qPCR on total *Syntrophomonas* 16S rRNA genes, which showed a higher concentration in the PF2 codigester relative to the CF codigester on day 204 ( $p < 0.001$ ; Figure 5-3F).

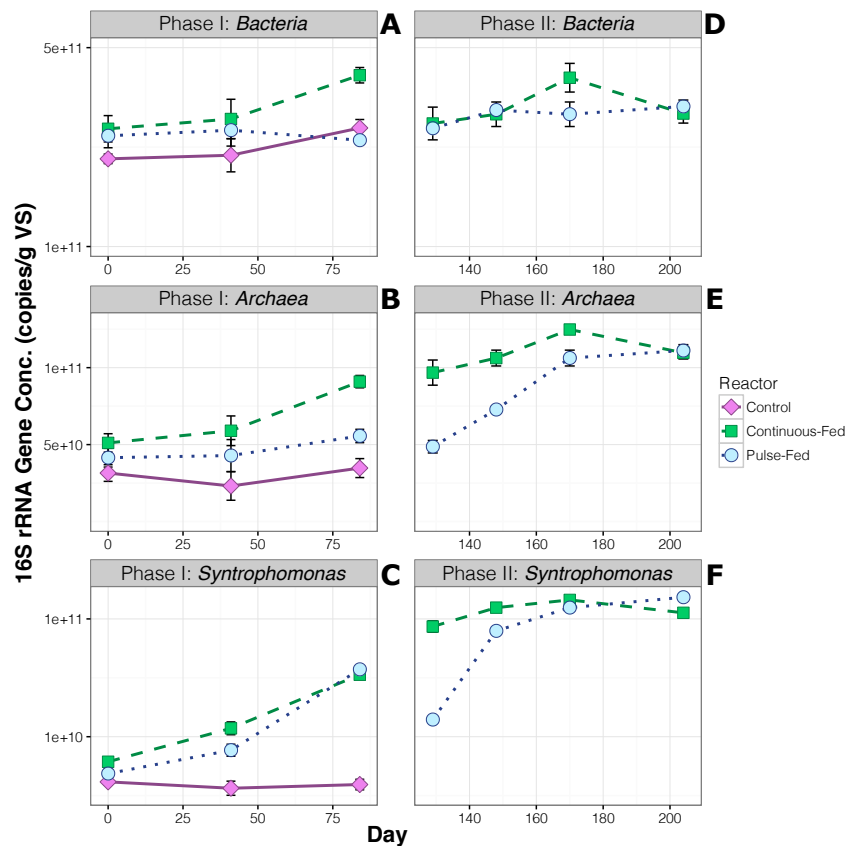


**Figure 5-3** Concentration of 16S rRNA genes in the Phase I digesters for (A) *Bacteria*, (B) *Archaea*, and (C) *Syntrophomonas*, and in the Phase II digesters for (D) *Bacteria*, (E) *Archaea*, and (F) *Syntrophomonas*. Error bars represent one standard deviation based on triplicate DNA extractions and duplicate qPCR technical replicates.

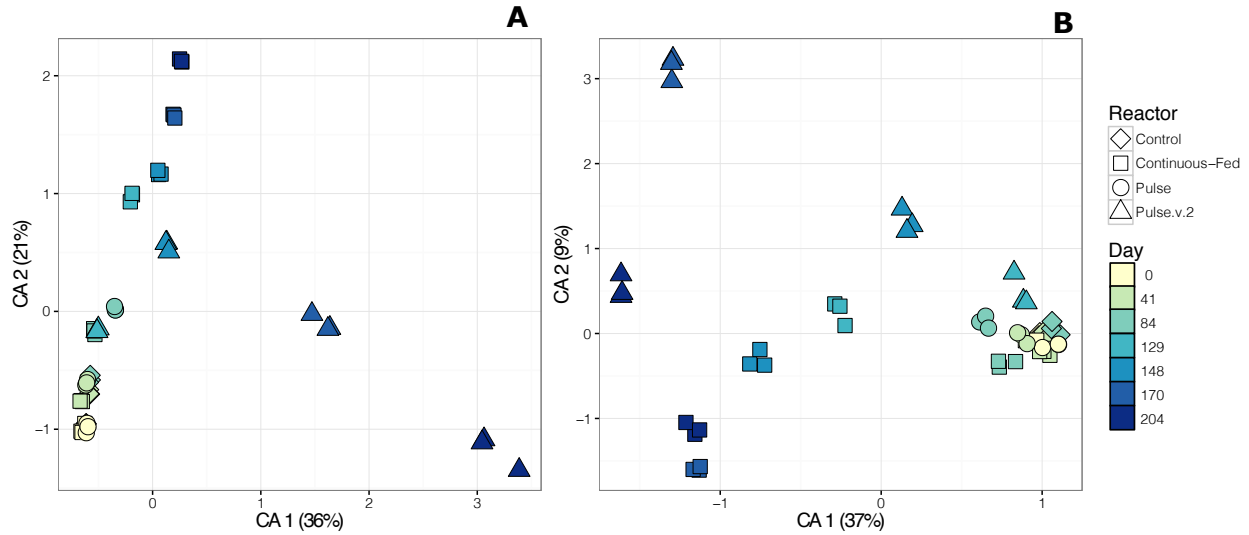


**Figure 5-4** Correspondence analysis (CA) plots based on (A) *Bacteria* and (B) *Archaea* normalized OTU sequence counts in the codigester and control digester samples collected throughout Phases I and II. The color of each marker represents the sample collection day and the shape of each marker represents the digester sludge source. The triplicate samples shown for each sample day are from replicate DNA extractions. The percentage shown along each axis represents the fraction of variance explained by that CA axis.

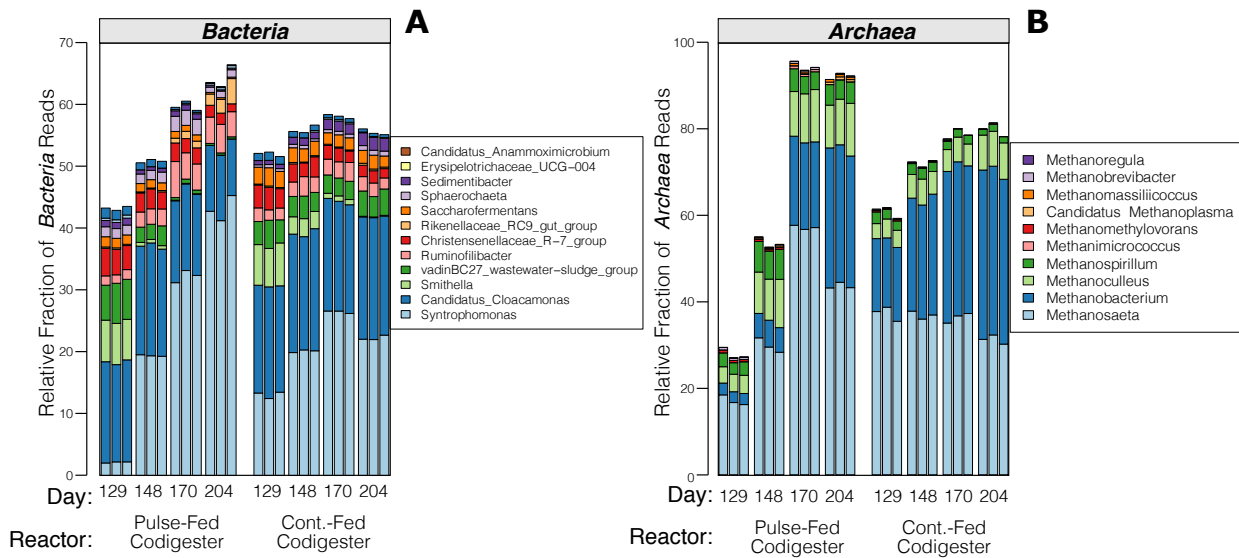


**Figure 5-5** Relative read fractions of the (A) 12 most abundant *Bacteria* genera, and (B) 10 most abundant *Archaea* genera in the 16S rRNA amplicon sequence libraries for the digesters during Phase II. Genus abundance profiles from triplicate DNA extractions are shown for each time point.

In order to obtain a high resolution of digester microbial community compositions, amplicon reads were denoised into their exact sequences with DADA2 (Callahan et al., 2016) prior to clustering into OTUs at a 99.5% similarity. Such high-resolution analysis showed that at least 85% of *Syntrophomonas*-classified sequences were distributed among 13 OTUs (Figure 5-6). Time-series abundance profiles of *Syntrophomonas* OTUs showed divergence based on codigester LCFA feeding patterns by the end of Phases I and II (Figure 5-6). Correspondence analysis of *Syntrophomonas* OTU sequence counts revealed that the genus composition differed based on the codigester LCFA feeding strategy and loading (Supplemental Figure C3). These results indicate that the fine-scale community structure of LCFA  $\beta$ -oxidizing bacteria in the codigesters was impacted by the LCFA feeding frequency. In contrast, over 95% of the sequences classified within the acetoclastic genus of *Methanosaeta* were comprised by only 3 OTUs, which had similar relative abundance profiles between the two codigesters (Supplemental Figure C4). The hydrogen-utilizing genus *Methanobacterium* was represented at over 90% by a single OTU. The biological selective pressure from LCFA feeding frequency therefore had larger impacts on the composition of syntrophic bacteria than selection for different dominant taxa of acetoclastic and hydrogenotrophic methanogens.

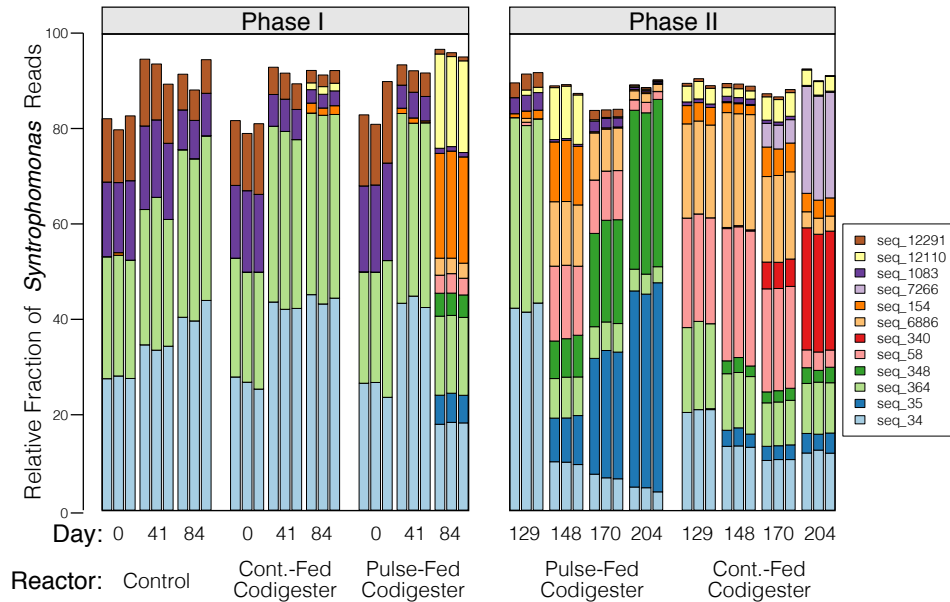


**Figure 5-6** Relative read fractions of the 13 most abundant OTUs classified within the *Syntrophomonas* genus of the digesters during Phases I and II based on 16S rRNA amplicon sequencing. OTU abundance profiles from triplicate DNA extractions are shown at each time point.

The presence of LCFA as a co-substrate in the feed resulted in lower *Bacteria* diversity in both codigesters, while pulse-feeding LCFA during codigestion resulted in higher *Archaea* community diversity. Diversity of the *Bacteria* community at all orders of Hill diversity numbers ( ${}^qD$ ) assessed ( $q = 0, 1, \text{ and } 2$ ) decreased over time for both codigesters during Phases I and II (Supplemental Figure C5). In contrast, *Bacteria* Hill diversity numbers for the Phase I control digester increased over time (Supplemental Figure C5). Despite their decreasing trend in both codigesters during Phase II, *Bacteria* Hill diversity numbers of the orders of  ${}^1D$  and  ${}^2D$  were higher in the PF codigester relative to the CF codigester until day 170, after which  ${}^1D$  and  ${}^2D$  were lower in the PF2 codigester (Supplemental Figure C5). Similarly, diversity numbers of orders  ${}^1D$  and  ${}^2D$  for the *Archaea* community were significantly higher ( $p < 0.01$ ) in the PF codigester relative to the CF codigester at the end of Phase I, and stayed significantly higher ( $p < 0.01$ ) in the PF2 codigester during Phase II (Supplemental Figure C6). Richness (i.e.  ${}^0D$ )



values of the *Archaea* communities were similar between all digesters in Phase I, but were significantly higher ( $p < 0.01$ ) in the PF2 codigester relative to the CF codigester starting at day 170 in Phase II (Supplemental Figure C6).

#### 5.4.4 *Oleate and acetate bioconversion kinetics were correlated to syntrophic and methanogenic community abundance*

A linear regression model was established to examine the relationship between maximum oleate conversion rates ( $q_{max,oleate}$ ) measured during batch kinetic tests with all digester sludges (16 tests total) and the 16S rRNA gene concentration of total *Syntrophomonas* in the sludges (Figure 5-7A). The total *Syntrophomonas* 16S rRNA gene concentration was a significant predictor of  $q_{max,oleate}$  values ( $p < 0.001$ ). The specific slope of the linear regression was  $8.6 \times 10^{-10}$  mL CH<sub>4</sub>/16S rRNA gene-day, and the overall model fit had an  $R^2$  of 0.73.

To examine the importance of syntrophic bacteria community structure, a multiple linear regression model was developed to predict  $q_{max,oleate}$  values based on absolute concentrations of a subset of *Syntrophomonas* OTUs (Figure 5-7B). Feature selection and cross-validation showed that the linear model provided the greatest  $R^2$  by incorporating the absolute concentrations of six *Syntrophomonas* OTUs. All of the six selected *Syntrophomonas* OTUs were significant predictors of  $q_{max,oleate}$  ( $p < 0.05$ ; Supplemental Table C8). The individual OTU correlation coefficients ranged from  $-7.0 \times 10^{-8}$  to  $2.8 \times 10^{-8}$  mL CH<sub>4</sub>/16S rRNA gene-day (Supplemental Table C8). The negative slope contribution found for one OTU suggests that it had an antagonistic effect on oleate conversion. The resulting multiple linear regression model had an improved  $R^2$  of 0.92 in comparison to the linear regression that was dependent only on the total

*Syntrophomonas* 16S rRNA gene concentration (Figure 5-7). A phylogenetic comparison of the six selected *Syntrophomonas* OTUs showed that they were distributed throughout the genus (Supplemental Figure C7).

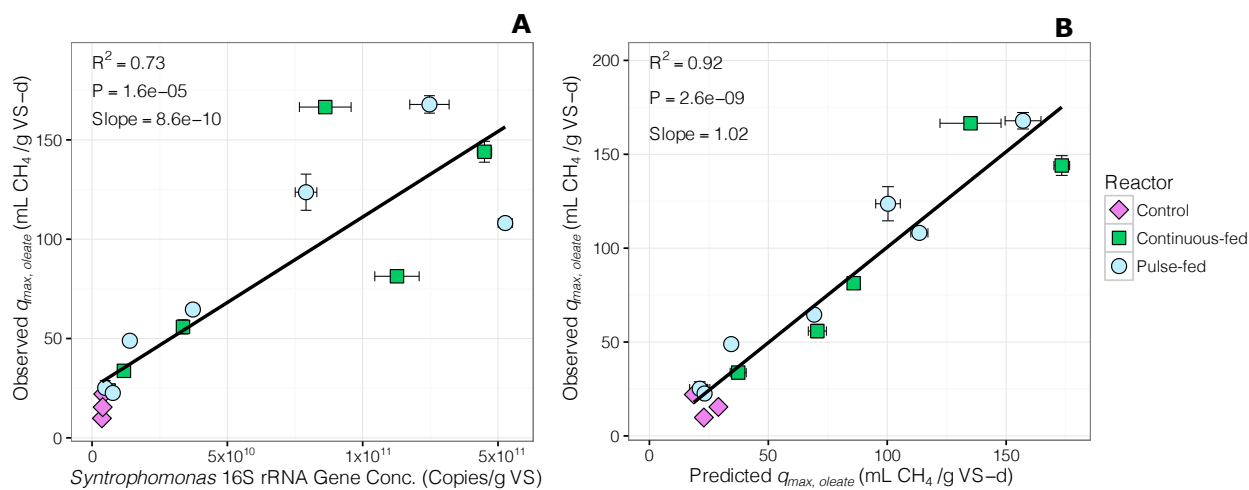


**Figure 5-7** Linear regression of observed  $q_{max,oleate}$  values versus (A) the total *Syntrophomonas* 16S rRNA gene concentration; and (B) predicted  $q_{max,oleate}$  values from a multiple-linear regression model based on inferred 16S rRNA gene concentrations of 6 selected *Syntrophomonas* OTUs. Inferred absolute abundances were calculated by multiplying the relative fraction of each OTU within total *Syntrophomonas* read counts by the total *Syntrophomonas* 16S rRNA gene concentration. Error bars represent one standard deviation.

A similar approach showed that the absolute concentration of total *Methanosaeta* 16S rRNA genes was a significant predictor of the acetate conversion kinetics of the codigester biomasses were both predicted more precisely by incorporating fine-scale syntrophic and methanogenic community structures.

## 5.5 DISCUSSION

### 5.5.1 *Codigester stability and bioconversion kinetics were impacted by LCFA feeding pattern*

The results of this study showed that pulse-feeding oleate during codigestion selected for higher oleate and acetate bioconversion kinetics, as well as more stable digester performance at high LCFA loadings. The improved tolerance to high LCFA loadings was apparent during Phase II, when acetate accumulated to above 3,000 mg/L in the CF codigester but was completely degraded between feedings in the PF2 codigester. Even though the maximum acetate conversion rates ( $q_{max,acetate}$ ) decreased in both codigesters at the high LCFA loadings in Phase II, the PF2 codigester had a higher aceticlastic tolerance by maintaining a higher  $q_{max,acetate}$  than the CF codigester. The higher acetate conversion kinetics in the pulse-fed system may have prevented acetate accumulation at the high LCFA OLRs. These findings agree with previous work showing that daily acetate feeding improved acetate utilization kinetics and digester tolerance to organic overloading in comparison to hourly acetate feeding (Conklin et al., 2006). Pulse-feeding also provided a greater tolerance to organic overloading and ammonia toxicity in comparison to a continuous-fed digester during anaerobic treatment of synthetic wastewater (De Vrieze et al., 2013). Periodic pulse-feeding of LCFA has been suggested as a strategy to enable efficient digester start-up by providing sufficient batch degradation time to consume inhibitory LCFA (Cavaleiro et al., 2009). Yet, this is the first study to operate a continuous-fed codigester in parallel with a pulse-fed codigester for a comparison of stability and LCFA bioconversion kinetics during LCFA codigestion. The mechanism for biological selection imposed by LCFA pulse feeding could have been attributed to transiently high acetate and LCFA concentrations, which could select for more resistant syntrophic and archaeal populations as well as promote higher maximum substrate utilization kinetics. Thus, pulse-feeding LCFA-rich substrates, such

as FOG, may allow for more stable codigester performance at high daily loading rates relative to continuous-fed codigestion systems.

### 5.5.2 *Codigester feeding pattern drove biological selection of syntrophic bacteria and methanogen population structures*

Our results showed that LCFA codigestion promoted the growth of *Syntrophomonas* bacteria as the dominant LCFA  $\beta$ -oxidizing group, with different LCFA feeding patterns resulting in divergent *Syntrophomonas* community composition and absolute abundance. *Syntrophomonas* have been identified by previous studies to play an important role in LCFA  $\beta$ -oxidation in anaerobic digestion systems (Shigematsu et al., 2006; Sousa et al., 2009, 2007a; Ziels et al., 2016, 2015). The maximum relative fraction of *Syntrophomonas* observed in the PF2 codigester of 43% was the largest *Syntrophomonas* community fraction reported for an anaerobic digestion community thus far (Stams et al., 2012; Ziels et al., 2016, 2015). Previous work has suggested that syntrophic bacteria populations are stable and resilient, and are unlikely to undergo competition with different syntrophs that have similar metabolic functions (Werner et al., 2011). The high-resolution 16S rRNA gene amplicon analysis conducted in this study revealed that various *Syntrophomonas* taxa were capable of occupying the same ecological niche within the codigesters, and the resulting *Syntrophomonas* community structure was affected by the digester feeding pattern. Thus, the highly-specialized metabolic role of syntrophic fatty-acid oxidation (McInerney et al., 2009) may have a level of physiological diversity in anaerobic digesters, with multiple syntrophic species/strains capable of contributing to LCFA-degradation. The dynamic LCFA concentrations from pulse-feeding could have possibly promoted competition among syntrophic taxa with different affinities and/or maximum substrate conversion rates, as was

reported for syntrophic propionate oxidation in fill-and-draw anaerobic reactors (H. D. Ariesyady et al., 2007).

The structure of syntrophic communities likely depends on the kinetics of both the syntrophic bacteria and the methanogenic partners, since the metabolism of these communities exists delicately near thermodynamic equilibrium (Stams and Plugge, 2009). The rate of fatty-acid oxidation by syntrophic bacteria was shown to limit fatty-acid conversion when the methanogenic partner maintained low concentrations of acetogenesis products (Junicke et al., 2016), whereas methanogens have also been found to limit syntrophic conversion rates (Warikoo et al., 1996). In our study, higher  $q_{max,oleate}$  values were observed in the PF codigesters, which also had higher values of  $q_{max,acetate}$ . It is plausible that the higher acetate consumption kinetics drove more rapid oleate conversion, since the thermodynamics of oleate conversion into methane relies upon the intermediate acetate concentration (Schink, 1997). Differences in acetate utilization kinetics with pulse- versus continuous-feeding patterns have been attributed to divergent aceticlastic populations, since *Methanosaeta* species have higher affinities for acetate but lower maximum utilization rates in comparison to *Methanosarcina* species (Conklin et al., 2006). In this study, *Methanosaeta* was the dominant aceticlastic group in both codigesters, despite acetate accumulation to over 3,000 mg/L in the CF codigester and periodic acetate accumulation to 500-1,000 mg/L in the PF2 codigester. A higher tolerance to LCFA was reported for pure cultures of *Methanosaeta concilii* in comparison to *Methanosarcina mazei* (Silva et al., 2016), which could explain the dominance of *Methanosaeta* in our study codigesters.

The PF2 codigester had almost twice the *Syntrophomonas* concentration as the CF codigester on day 204 despite similar levels of influent LCFA removal in the two systems, indicating that the LCFA feeding frequency may have altered growth yields or decay rates. Growth yields under anaerobic conditions have been related to thermodynamics, with greater Gibbs free energies supporting higher yields (Kleerebezem and Van Loosdrecht, 2010). High initial oleate concentrations coupled with low digester acetate levels could have promoted more free energy for growth of *Syntrophomonas* in the PF2 codigester (Schink, 1997). In addition to lower acetate, a lower hydrogen concentration would also provide more free-energy for growth via LCFA  $\beta$ -oxidation (Schink, 1997; Stams and Plugge, 2009). Lower hydrogen levels could have been promoted in the PF2 codigester, which had higher concentrations of the hydrogen-utilizing *Methanoculleus* that have higher affinities for hydrogen in comparison to *Methanobacterium* (Chong et al., 2002; Lovley, 1985) that were more abundant in the CF codigester. A more detailed thermodynamic analysis would be needed to elucidate how the LCFA feeding strategy impacted the fluxes of intermediate metabolites during syntrophic conversion, but such work is warranted to improve our understanding of codigester LCFA conversion kinetics and syntrophic community structure.

### 5.5.3 *Relating bioconversion kinetics to microbial community structure*

This study demonstrated that codigester biokinetics were correlated to measurements of community composition. While the  $q_{max,oleate}$  and  $q_{max,acetate}$  both correlated significantly with the absolute concentrations of total *Syntrophomonas* and *Methanosaeta* 16S rRNA genes, respectively, improved model accuracy was obtained by incorporating measurements of fine-scale community composition and absolute abundance measurements. Bocher and colleagues (2015) demonstrated the promising use of multiple-linear regression to predict specific

methanogenic activities from glucose and propionate based on methanogen community descriptors. Yet, the models developed in the latter study utilized relative DGGE band intensities as predictor variables, while the multiple-linear regression models developed in our study utilized absolute concentrations of fine-scale OTUs as predictor variables. Absolute quantification of taxa through the combination of high-throughput 16S amplicon sequencing and quantitative enumeration methods was recently suggested to provide a more comprehensive view of microbial compositional dynamics (Props et al., 2016). Since reactor bioconversion kinetics are dependent on biomass concentrations, we suggest that our predictive modeling approach based on absolute quantification of taxa can be used to identify certain OTUs that contribute to higher bioconversion rates for substrates of interest, such as LCFA and acetate in anaerobic digesters. From a practical perspective, identifying such key microbial taxa could enable more focused monitoring efforts for predicting codigester performance and capacities under dynamic FOG loading situations, leading to improved digester stability and methane recovery.

## 5.6 CONCLUSIONS

This study assessed the impacts of codigester LCFA feeding pattern on microbial community structure and bioconversion kinetics. The following can be concluded from the results of this study:

- Overall *Bacteria* and *Archaea* community composition diverged at high LCFA OLRs in codigesters fed at different frequencies. Thus, LCFA feeding frequency and OLR were biological selective pressures that drove the digester population structure.

- The codigester LCFA feeding strategy impacted the composition of the syntrophic and methanogenic communities. Higher relative and absolute concentrations of *Syntrophomonas* and *Methanosaeta* 16S rRNA genes were observed in the PF2 codigester than the CF codigester in Phase II at high LCFA loadings.
- Higher  $q_{max,oleate}$  values were promoted in the PF codigesters in Phase I and II operation. The  $q_{max,acetate}$  values were also higher in the PF codigester by the end of Phase II operation. These results indicate that the anaerobic codigester oleate feeding pattern influenced microbial bioconversion kinetics for acetate and oleate.
- Both  $q_{max,oleate}$  and  $q_{max,acetate}$  correlated significantly with the concentrations of total *Syntrophomonas* and *Methanosaeta* 16S rRNA genes, respectively.
- Improved predictive accuracy for  $q_{max,oleate}$  and  $q_{max,acetate}$  was obtained through multiple-linear regression based on the absolute concentration of syntrophic and methanogenic taxa. This method could be used to monitor key microbial OTUs that significantly contribute to substrate conversion kinetics in anaerobic digesters.

## 5.7 SUPPLEMENTAL INFORMATION AVAILABLE

The Supplemental Information for Chapter 5 is included in this document as Appendix C.



## Chapter 6. DNA-STABLE ISOTOPE PROBING BASED METAGENOMICS IDENTIFIES KEY LONG-CHAIN FATTY ACID DEGRADING POPULATIONS IN PARALLEL ANAEROBIC CODIGESTERS WITH DIFFERENT OLEATE FEEDING STRATEGIES

### 6.1 ABSTRACT

Recovering biomethane from fats, oils, and greases (FOG) with anaerobic codigestion has considerable potential to reduce energy and carbon footprints of wastewater treatment. Improving our understanding of long-chain fatty acid (LCFA)-degrading microbial communities is key for developing anaerobic digester operating strategies that mitigate inhibitory LCFA accumulation at high FOG loading rates. There is limited information on the impact of anaerobic digester operating conditions on the diversity and genomic potential of LCFA-degrading communities. In this research, DNA stable isotope probing (SIP) was coupled with metagenomic sequencing for a genome-centric comparison of oleate (C<sub>18:1</sub>)-degrading populations in two parallel anaerobic codigesters operated with either a pulse-feeding or continuous-feeding strategy. The pulse-fed codigester SIP microcosms converted oleate into methane at a higher rate than the continuous-fed codigester microcosms. Differential coverage binning was demonstrated for the first time to recover population genome bins (GBs) from DNA-SIP metagenomes. About 70% of the <sup>13</sup>C-enriched GBs were taxonomically classified to the *Syntrophomonas* genus. Phylogenetic comparisons of <sup>13</sup>C-enriched GBs showed that some closely-related *Syntrophomonas* GBs were detected in both codigesters, while other phylogenetically distinct

*Syntrophomonas* GBs were unique to each codigester. 16S rRNA amplicon sequencing of heavy density gradient fractions corroborated the results of metagenomic binning. Overall, these data suggest that syntrophic populations degrading LCFA in anaerobic digesters can be functionally redundant, and different populations may be biologically selected by adjusting the digester feeding strategy to promote favorable biokinetics.

## 6.2 INTRODUCTION

Anaerobic digestion is an attractive biotechnology for recovering renewable energy as biomethane (CH<sub>4</sub>) during organic waste treatment. Worldwide interest in anaerobic digestion has led to the implementation of approximately 9,000 full-scale facilities in Europe and over 3,000 facilities in the U.S. by 2012 (Guo et al., 2015). The conversion of organic matter into biomethane relies upon an intricate balance of multiple microbial trophic groups, including hydrolyzing and fermenting bacteria, syntrophic acetogenic bacteria, and methanogenic archaea (Briones and Raskin, 2003). Despite the relatively widespread adoption of anaerobic digestion, its genomic potential still remains relatively underexplored (Vanwonterghem et al., 2016), owing to the vast phylogenetic and metabolic diversity (Sundberg et al., 2013) and general non-culturability of a majority of the microorganisms present in digesters (Vanwonterghem et al., 2014). An improved understanding of the metabolic capabilities of microbial populations occupying key ecological niches within anaerobic digesters could help to facilitate new process designs and operational strategies that maximize biomethane recovery from organic waste.

Adding fats, oils, and greases (FOG) as a co-substrate in the anaerobic digestion of livestock manure or wastewater treatment solids has gained popularity to increase biomethane recovery due to its higher biological methane potential (Alves et al., 2009; Luostarinen et al., 2009; Wang et al., 2013), which is 2.7 to 3.0-times higher than livestock manure or wastewater treatment solids (Labatut et al., 2011). During anaerobic degradation, FOG is rapidly hydrolyzed into glycerol and long-chain fatty acids (LCFA) (Hanaki et al., 1981). LCFA are biologically converted into methane through a syntrophic partnership between acetogenic  $\beta$ -oxidizing bacteria and methanogenic archaea (Schink, 1997; Sousa et al., 2009). So far, only seven isolated bacterial species are capable of  $\beta$ -oxidizing LCFA ( $> 12$  carbons in length) in syntrophy with a methanogen, and all belong to the families of *Syntrophomonadaceae* and *Syntrophaceae* (Sousa et al., 2009; Zhang et al., 2012). However, the generally slow growth rates of syntrophic bacteria coupled with the toxicity of LCFA has limited the number of cultured representatives obtained (Hatamoto et al., 2007b).

Biomethane recovery from FOG can be limited by the toxicity of LCFA towards microbial activity at high concentrations (Angelidaki and Ahring, 1992; Davidsson et al., 2008; Hanaki et al., 1981; Luostarinen et al., 2009; Rinzema et al., 1994; Wan et al., 2011; Wang et al., 2013). However, recent work showed that the maximum FOG loading rate without LCFA inhibition could be elevated depending on the LCFA-degrading population abundance and specific LCFA bioconversion kinetics (Ziels et al., 2016, Chapter 4). In the work presented in Chapter 5, it was investigated whether the codigester LCFA feeding strategy could select for different LCFA-degrading populations and bioconversion kinetics. The experimental results showed that the LCFA feeding frequency impacted the composition of  $\beta$ -oxidizing *Syntrophomonas* bacteria, and

that pulse-feeding LCFA resulted in higher LCFA bioconversion kinetics in comparison to semi-continuous LCFA feeding (Chapter 5). However, differences in community structure between the codigesters in Chapter 5 were based on time-series 16S rRNA gene amplicon sequencing of total digester biomass, and thus differences in the *active* fraction of LCFA-degrading populations between the systems remain unknown. A comparison of the active LCFA-degrading populations selected with different codigester feeding frequencies could improve our understanding of the level of physiological diversity within digester syntrophic populations.

Stable isotope probing (SIP) is a cultivation-independent method that can be used to elucidate links between microbial activity (function) and identity within environmental samples (Dumont and Murrell, 2005; Radajewski et al., 2000). DNA-SIP relies on the incorporation of ‘heavy’ isotopes (e.g.  $^{13}\text{C}$ ) into microbial DNA during biogrowth on labeled-substrates, and can thus act as a ‘filter’ to enrich the DNA of active populations (Chen and Murrell, 2010). DNA-SIP has been combined with shotgun metagenomic sequencing approaches to discover novel enzymes and operons within microbial communities (Chemerys et al., 2014; Saidi-Mehrabad et al., 2013; Verastegui et al., 2014), and to identify new functional traits of microbial taxa (Eyice et al., 2015). Additionally, the recovery of population genomes from  $^{13}\text{C}$ -enriched metagenome libraries with DNA-SIP has been demonstrated using homology-based binning methods (Grob et al., 2015; Laban et al., 2015). Recently-developed differential coverage binning techniques for recovering population genomes from shotgun metagenomes (Albertsen et al., 2013; Kang et al., 2015; Karst et al., 2016) are amenable to DNA-SIP due to the expected sequence composition divergence between heavy density fractions of  $^{12}\text{C}$ - and  $^{13}\text{C}$ -incubated DNA samples (Coyotzi et

al., 2016). However, there have been no reported studies coupling differential coverage binning with DNA-SIP to recover population genome bins from metagenome sequence data.

The objective of this study was to apply DNA-SIP combined with shotgun metagenomic sequencing for a genome-centric comparison of the active oleate (C<sub>18:1</sub> LCFA) degrading populations in two parallel anaerobic codigesters fed with equal manure loadings but with different oleate feeding frequencies. Differential coverage binning was employed to retrieve population genome bins from the DNA-SIP <sup>13</sup>C and <sup>12</sup>C metagenomes. 16S rRNA gene amplicon sequencing was also conducted on <sup>13</sup>C and <sup>12</sup>C heavy DNA fractions to verify key populations involved in converting oleate into biomethane within the anaerobic codigesters.

## 6.3 MATERIALS AND METHODS

### 6.3.1 *Anaerobic Bioreactor Operation*

The two parallel anaerobic codigesters treating manure and oleate were operated at 35°C for over 200-days, as described previously in Chapter 5. The digesters had a 4-L working volume and a 20-day hydraulic and solids retention time. They were inoculated with anaerobic digester sludge from a mesophilic anaerobic digester treating dairy manure at a nearby farm, and were fed with blended manure feedstock collected from the same dairy farm (Chapter 5). Manure was fed daily at a VS loading rate of  $1.3 \pm 0.2$  g VS/L-d, and an aqueous solution of sodium oleate (>97%, Tokyo Chemical Industry Co.) was added to the influent feed at 10% of the daily feed volume for codigestion. The daily average oleate organic loading rate (OLR) to both codigesters was identical, but their oleate feeding frequency differed. One codigester received the oleate feed semi-continuously every 6-hrs daily, and is termed the *continuous-fed* (CF) codigester. The other

codigester received the oleate feed in a pulse every 2 days, and is termed the *pulse-fed* (PF) codigester. Oleate loading was increased to the codigesters over two experimental phases: in Phase I (days 0-85) the oleate feed reached 27% of the total influent COD, and in Phase II (days 86-204) the oleate loading reached 64% of the influent COD (Chapter 5). After Phase II operation on day 204, the oleate OLR to both codigesters was reduced from 3.2 to 1.8 g COD/L-d for 24 days. During this time, the pH of both codigesters averaged 7.5. The codigesters were not fed between days 228-230 to reduce the level of any background substrates before commencing SIP incubations with  $^{13}\text{C}$ -labeled sodium oleate on day 230. At that time, effluent VFA and LCFA levels were below 70 mg/L.

### 6.3.2 *Stable Isotope Probing Incubations with Anaerobic Digester Sludge*

Sludge was sampled directly from the PF and CF codigesters after 48-hr of starvation on day 230. Microcosms were established in 35 mL glass serum bottles pre-purged with  $\text{N}_2:\text{CO}_2$  (80:20), amended with 10 mL of codigester sludge (0.17 g VS total), sealed and capped with butyl rubber septa, and purged again with  $\text{N}_2:\text{CO}_2$  (80:20). All microcosms were maintained at 35°C, and stirred at 150 rpm on an orbital shaker. Microcosms were grouped into duplicate vials that were supplemented with either  $^{12}\text{C}$ -sodium oleate or  $^{13}\text{C}$ -labeled sodium oleate at an initial concentration of 8 mM. The  $^{13}\text{C}$ -labeled sodium oleate was universally labeled at all 18 carbons (>98% atom purity, Cambridge Isotope Laboratories, Tewksbury, MA). Triplicate un-supplemented controls were incubated in parallel to measure background methane production. Gas production was measured based on the headspace pressure increase using a digital manometer (Series 490A, Dwyer Instruments), and the headspace methane content was measured with a GC-FID (SRI 8610C) equipped with a Supelco Alumina Sulfate Plot column

(50 mL, 0.53 mm i.d.). Headspace pressure and composition were sampled about every 5 hr using sterile syringes.

After the first addition of oleate was converted at >90% into methane over 48 hr (Figure 6-1),  $^{12}\text{C}$ - and  $^{13}\text{C}$ -labeled sodium oleate were re-supplemented separately at 8 mM after purging the headspace with  $\text{N}_2:\text{CO}_2$  (80:20). Following another 48-hrs for oleate conversion into methane, a third supplement of 8 mM  $^{12}\text{C}$ - and  $^{13}\text{C}$ -labeled sodium oleate was added to the microcosms after purging the headspace with  $\text{N}_2:\text{CO}_2$  (80:20). The third incubation lasted 48 hr, after which biomass from all bottles was sacrificed for DNA extraction. In total, 240  $\mu\text{mol}$  of either  $^{12}\text{C}$ - or  $^{13}\text{C}$ -labeled oleate was added to the microcosms over the course of 6-days (144 hr), and was converted into methane at >90% (Figure 6-1).

### 6.3.3 *DNA Extraction and Density Gradient Centrifugation*

Anaerobic codigester sludge samples were collected for DNA extraction at the start of the SIP incubation (time zero), as well as from each SIP microcosm bottle after 6 days of incubation. Briefly, 10 mL sludge was transferred to pre-purged,  $\text{O}_2$ -free 15 mL centrifuge tubes on ice. The 15 mL tubes were then centrifuged at 12,000 g for 10 min at 4°C, immediately decanted, and stored at -80°C. DNA was extracted from the frozen pellet using the PowerMicrobiome™ kit (MO BIO Laboratories Inc., Carlsbad, CA) with phenol:chloroform:isoamyl during bead-beating, according to the manufacturer's instructions. Extracted DNA was suspended in nuclease-free TE buffer, and was quantified with a Quant-iT HS DNA kit on a Qubit 2.0 fluorometer (Invitrogen, Carlsbad, CA).

DNA extracts (5  $\mu\text{g}$  in 500  $\mu\text{L}$  1X TE buffer) from  $^{12}\text{C}$ -oleate and  $^{13}\text{C}$ -oleate fed microcosms after 6 days of incubation were separately combined with 25  $\mu\text{L}$  SYBR Safe DNA Gel Stain (10,000X, ThermoFisher Scientific, Waltham, MA) and 4.4 mL TE/CsCl solution (10mM Tris, 10mM EDTA [pH 8.0], CsCl at a buoyant density of 1.82 g/mL) and loaded into 4.8 mL OptiSeal polyallomer tubes (Beckman Coulter, Brea, CA) for a final buoyant density of 1.71 g/mL. Density gradient centrifugation was performed with a TLA-110 rotor at 55,000 rpm and 20°C for 72 hr in an OptimaMax ultracentrifuge (Beckman Coulter) with vacuum on, maximum acceleration, and no brake on deceleration. Gradients were displaced with MilliQ water pumped into the top of the OptiSeal tube at 425  $\mu\text{L}/\text{min}$  using a Model 11 Plus syringe pump (Harvard Apparatus, Holliston, MA), and 200  $\mu\text{L}$  fractions were collected dropwise from a needle in the bottom of the tube (24 fractions total). The refractive index (nd-TC) of each gradient fraction was immediately measured using an AR200 digital refractometer (Reichert, Ithaca, NY), and the buoyant density (BD) was calculated based on a standard curve of nd-TC versus BD for the TE/CsCl solution (Supplemental Figure D1). DNA was precipitated from each fraction by adding 1  $\mu\text{L}$  of linear polyacrylamide (GenElute LPA, Sigma-Aldrich), 0.3 M sodium acetate, and 70% ethanol and left overnight at 4°C before centrifuging at 16,000 g for 30 min. Pelleted DNA was washed with 1 mL 70% ethanol, centrifuged again for 20 min, air dried and re-suspended in sterile 1X TE buffer (pH 8.0). The concentration of DNA in each fraction was measured with a Quant-iT HS DNA kit to identify shifts in BD in the  $^{13}\text{C}$ -oleate amended microcosms (Supplemental Figure D2).

#### 6.3.4 *Quantitative PCR*

To further detect differences in DNA BD values between the  $^{12}\text{C}$ - and  $^{13}\text{C}$ -incubated microcosms, quantitative PCR (qPCR) was conducted on DNA from gradient fractions with BDs



ranging from 1.68 to 1.75 g/mL. The qPCR targeted 16S rRNA gene fragments of the syntrophic LCFA  $\beta$ -oxidizing bacterial genus of *Syntrophomonas* using primers and probes developed by Ziels et al. (2015). More detailed descriptions of the reaction conditions, primers and probes, and calibration standards are given in the Supplemental Information.

### 6.3.5 *16S rRNA Amplicon Sequencing*

DNA from ‘heavy’ gradient fractions with BDs ranging from 1.70 to 1.73 (4 fractions) were pooled at equal volumes and subjected to 16S rRNA gene amplicon sequencing for each microcosm. Briefly, 16S rRNA gene fragments were amplified with barcoded and indexed universal prokaryotic V4-V5 primers 515F-Y (5'-GTGYCAGCMGCCGCGGTAA) and 926R (5'-CCGYCAATTYMTTTRAGTTT) (Parada et al., 2016), and the products were pooled and sequenced on a 2x300bp Illumina MiSeq run by the United States Department of Energy (DOE) Joint Genome Institute (JGI). Raw sequence data is available through the JGI Portal (<http://jgi.doe.gov>) under project ID number 1105527.

Amplicon reads were denoised into their exact sequences using the DADA2 pipeline (Callahan et al., 2016). Raw reads were filtered by trimming the first 10 bp, truncating forward reads at 265 bp, truncating reverse reads at 180 bp, and filtering all reads based on a maximum expected error of 2 using DADA2. The filtered and trimmed reads were then dereplicated and denoised into exact sequences using estimated error parameters with DADA2. Forward and reverse sequences were then merged with DADA2 using a minimum overlap of 20 bp and zero allowed mismatches. Merged and denoised sequences were then truncated to 390 bp and clustered into OTUs with a 99.5% similarity cutoff following chimera removal with UPARSE (Edgar, 2013).

Representative sequences of the 99.5% OTUs were classified against the SILVA SSU Ref NR dataset (v.123) using the RDP classifier (Wang et al., 2007).

### 6.3.6 *Metagenomic Sequencing, Assembly, and Annotation*

Metagenome library preparation and sequencing were conducted at the DOE JGI according to standard protocols (<http://www.jgi.doe.gov/>). Pooled DNA samples from the heavy gradient fractions as well as codigester DNA samples from time zero were used to generate an Illumina sequence library with an average insert size of 250 bp that was sequenced on an Illumina HiSeq-2500 with paired-end 150 bp reads to a depth of  $88 \pm 11$  M reads (SIP DNA samples) and  $140 \pm 13$  M reads (time zero DNA samples). Reads were trimmed and screened to remove adapters as well as filter sequences with a minimum Phred quality of 12, minimum length of 51, and no ambiguous bases using BBDuk (<https://sourceforge.net/projects/bbmap/>). Trimmed and screened paired-end reads from both codigester time zero metagenomes were individually assembled into contigs using MEGAHIT (v.1.0.3) (D. Li et al., 2015) with default parameters and the kmer list: 23, 43, 63, 83, 103, 123. The assembled contigs were annotated with the Integrated Microbial Genomes Metagenome (IMG/M) platform (Chen et al., 2016) by the DOE JGI, and KEGG annotation information (KO and EC numbers) were extracted. Raw sequence reads and assemblies are available through the DOE JGI portal under project IDs 1105480, 1105482, 1105484, 1105486, 1105488, 1105490, 1105494, 1105496, and 1105498.

### 6.3.7 *Metagenomic Binning*

Quality-filtered reads from all metagenomes, including the heavy gradient fractions of the  $^{12}\text{C}$ - and  $^{13}\text{C}$ -oleate fed microcosms and from codigester time-zero samples, were individually mapped to contigs from the time-zero assemblies using BBMap

(<https://sourceforge.net/projects/bbmap/>) in paired-end mode with default parameters. Metagenome reads were mapped to assemblies separately for both codigester sample sets. SAMtools (Li et al., 2009) was used to sort and index the mapping files and extract contig coverage information across samples. The mapping data and coverage information were used to bin contigs into population genome bins (GBs) separately for each codigester sample set using MetaBat (Kang et al., 2015) in ‘superspecific’ mode. CheckM was used to evaluate the level of bin completeness and contamination based on domain-level single-copy marker genes (Parks et al., 2015). Taxonomic classification of GBs was conducted by extracting a set of 107 conserved marker genes within open reading frames using mmgenome (Karst et al., 2016), running BLASTP on the extracted marker genes against the RefSeq v.52 protein database with a maximum *e*-value cutoff of 1e-5, and finding the least common ancestor (LCA) of the top 5 blast hits for each marker gene with MEGAN v.6.4 (Huson et al., 2007). The finest taxonomic ranking was assigned for which at least 70% of the LCA results agreed. Phylogenetic trees were generated for GBs that were over 40% complete using PhyloPhlAn based on 400 conserved marker genes (Segata et al., 2013), as well as with UPGMA clustering of distance estimates from *in-silico* DNA-DNA hybridization with the Genome-to-Genome Distance Calculator (Auch et al., 2010).

### 6.3.8 *Statistical Analysis*

Statistically significant differences in raw sequence counts of OTUs (from 16S rRNA amplicon libraries) and GBs (from shotgun metagenome libraries) within the <sup>12</sup>C and <sup>13</sup>C DNA-SIP samples were detected with the negative binomial Wald test in DESeq2 separately for each codigester dataset (Love et al., 2014). Raw sequence counts of GBs were obtained from parsing the mapping files. An adjusted *p* value of 0.01 and a log<sub>2</sub> fold change of 2.0 were used to identify

features (e.g. OTUs or GBs) that significantly increased between the  $^{12}\text{C}$  and  $^{13}\text{C}$  DNA-SIP samples.

Normalized sequence counts for 16S RNA amplicon OTUs and GBs were obtained with DESeq2 to account for the different sequencing depths among samples. Coverage values for GBs were calculated based on DESeq2 normalized sequence counts and the GB length. Regularized log-transformed sequence counts of 16S RNA amplicon OTUs were determined with DESeq2 for use in principal coordinate analysis, and permutational multivariate ANOVA (ADONIS) was conducted on Euclidian distance values from transformed sequence counts using the vegan package in R (Oksanen et al., 2007).

## 6.4 RESULTS

### 6.4.1 *Conversion of Oleate into Methane and Enrichment of $^{13}\text{C}$ DNA*

$^{13}\text{C}$ -labeled oleate was fed to a series of microcosms inoculated with sludge from either the PF or CF oleate anaerobic codigesters, respectively.  $^{12}\text{C}$ -oleate was added to a parallel set of microcosms to serve as a control for DNA BD shifts. The  $^{13}\text{C}$ - and  $^{12}\text{C}$ - oleate was fed three times at 8 mM with 48-hr batch incubations to ensure sufficient recovery of labeled biomass. The initial oleate concentration of 8 mM in the microcosms was similar to in situ levels that occurred within the experimental codigesters after feeding (Chapter 5). Metabolism of  $^{12}\text{C}$ - and  $^{13}\text{C}$ -labeled oleate was confirmed with 97% and 95% COD recoveries as methane in the headspace for the PF codigester and CF codigester microcosms, respectively (Figure 6-1). Biokinetic modeling of methane production (described in Supplemental Information) showed that the

maximum methane production rate increased with each subsequent batch feeding of  $^{12}\text{C}$ - and  $^{13}\text{C}$ -labeled oleate (Supplemental Table D1). The maximum methane production rate in the PF codigester microcosms was 26%, 21%, and 17% higher than the CF codigester microcosms for the first, second, and third batch incubation rounds, respectively (Supplemental Table D1).

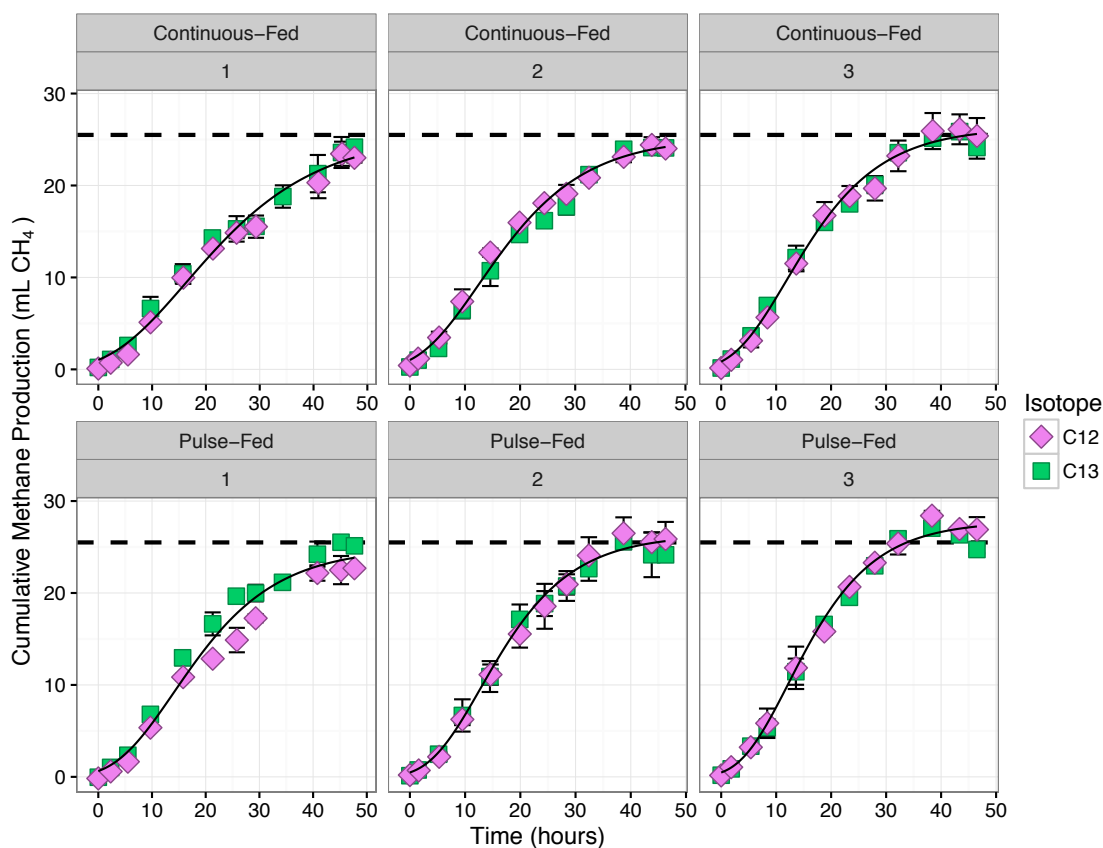


**Figure 6-1** Cumulative methane production (minus blank controls) for the microcosms fed with  $^{12}\text{C}$ - and  $^{13}\text{C}$ -labeled oleate over three repeated batch feeding periods. The number above each plot indicates the batch oleate feed round. The black dashed line shows the theoretical methane potential of the added oleate (25.5 mL  $\text{CH}_4$ ; based on 2.9 g COD/g oleate, 8 mM concentration, and 35 °C temperature). The black solid line represents the predicted methane production based on non-linear model fitting with a modified Gompertz equation (see Supplemental Table D1).

Total DNA concentrations were measured in 24 density gradient fractions to detect BD shifts after the consumption of 240  $\mu\text{mol}$   $^{12}\text{C}$ - or  $^{13}\text{C}$ -labeled oleate after 6 days. The heavy density fractions with BDs from 1.70 to 1.725 g/mL contained 2.2-times and 2.0-times more DNA in the

$^{13}\text{C}$ -incubated samples than in the  $^{12}\text{C}$ -controls for the PF codigester and CF codigester microcosms, respectively (Supplemental Figure D2). To further confirm the enrichment of  $^{13}\text{C}$ -labeled DNA, 16S rRNA genes of the LCFA-degrading bacterial genus *Syntrophomonas* were quantified in density fractions between 1.66 and 1.76 g/mL (Figure 6-2). The four heavy density gradient fractions with BDs ranging from 1.70 to 1.725 g/mL contained over 12-times more *Syntrophomonas* 16S rRNA genes in the  $^{13}\text{C}$ -incubated samples than that in the  $^{12}\text{C}$ -controls for both codigesters (Figure 6-2). The four heavy gradient fractions showing high levels of  $^{13}\text{C}$  incorporation were therefore pooled for each microcosm for subsequent 16S rRNA gene amplicon sequencing and shotgun metagenomic sequencing (Figure 6-2).

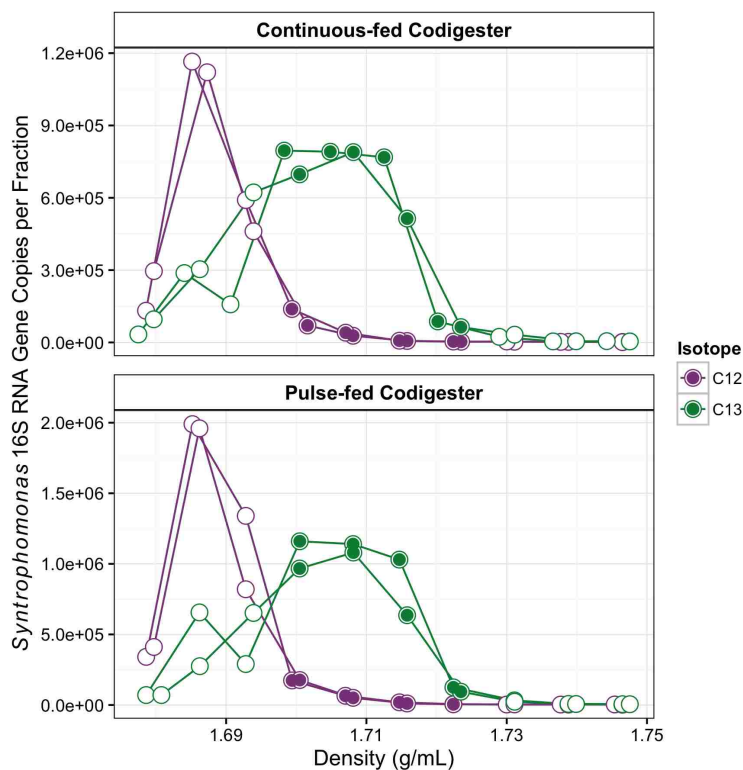


**Figure 6-2** Total copies of *Syntrophomonas* 16S rRNA genes measured by qPCR for each density gradient fraction recovered from isopycnic separation of DNA from  $^{13}\text{C}$ -incubated microcosms and  $^{12}\text{C}$ -controls for both anaerobic codigesters. The filled circles indicate gradient fractions that were pooled for subsequent 16S rRNA amplicon sequencing and metagenomic sequencing. Both biological replicates are shown, and each point represents an average of duplicate technical replicates.

#### 6.4.2 16S rRNA Amplicon Sequencing of DNA-SIP Samples

The microbial community profiles of pooled heavy density gradient fractions (Figure 6-2) were assessed through paired-end 16S rRNA gene amplicon sequencing. After quality-filtering, denoising, and merging paired-end amplicon reads, the number of sequences retained per sample averaged  $164,000 \pm 39,000$ . Principle coordinate analysis (PCA) showed that community profiles of the  $^{12}\text{C}$ - and  $^{13}\text{C}$ -incubated microcosms were distinctly clustered for both codigesters (Figure 6-3). The grouping of community profiles was significant within both codigester sample sets according to the oleate isotope (ADONIS,  $p < 0.05$ ). Additionally, samples within each isotope group were significantly grouped according to the codigester sludge source (ADONIS,  $p < 0.05$ ). These results suggest that microbial community profiles within heavy density gradient fractions were significantly altered by the incorporation of  $^{13}\text{C}$ -labeled oleate, and the community profiles of the  $^{13}\text{C}$ -enriched DNA within both codigester microcosms were also distinct.

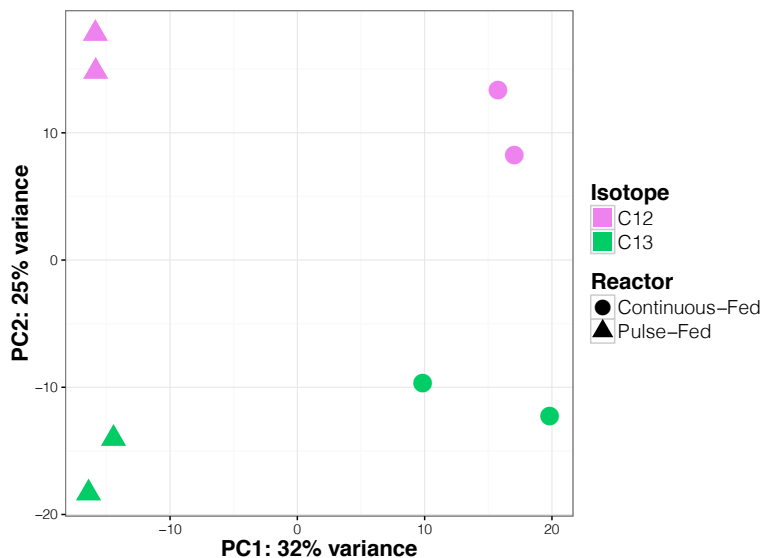


**Figure 6-3** Principle coordinate analysis (PCA) plot of OTU read counts from 16S rRNA amplicon sequencing after regularized log transformation with DESeq2 (Love et al., 2014). The different shapes indicate the codigestion reactor biomass source, and the colors represent the isotope of oleate ( $^{13}\text{C}$  or  $^{12}\text{C}$ ) fed to the microcosms. Biological duplicate samples are shown.

Differential abundance analysis was conducted to detect 16S rRNA OTUs that significantly increased in  $^{13}\text{C}$ -incubated heavy gradient fractions relative to  $^{12}\text{C}$ -controls. A total of 59 differentially abundant OTUs were identified in the PF codigester samples, 42 of which were classified to the *Syntrophomonas* genus (Supplemental Figure D3). Within the CF codigester samples, a total of 40 differentially abundant OTUs were identified, with 36 classified as *Syntrophomonas* (Supplemental Figure D3). Of the total number of differentially abundant *Syntrophomonas* OTUs identified, 19 were found in both codigesters while the remaining OTUs were unique to either codigester (Supplemental Figure D4). Cumulative *Syntrophomonas* genus read counts increased on average 5.0- and 5.5-times in the  $^{13}\text{C}$ -incubated samples relative to the  $^{12}\text{C}$ -controls for the PF codigester and CF codigester, respectively (Figure 6-4). Other bacterial genera that contained differentially abundant OTUs included: *Thermovirga*, *Aminivibrio*, Candidatus *Cloacamonas*, *Anaerofustis*, *Syntrophothermus*, and *Ruminococcaceae* NK4A214 group, along with unclassified members of *Planctomycetes*, *Spirochaetae*, *Synergistes*, *Actinobacteria*, and *Bacterioidetes* (Supplemental Figures D3 and D4). No methanogenic archaeal OTUs were identified as differentially abundant in either codigester sample set. Nonetheless, cumulative read counts of *Methanosaeta* increased by 68% and 170% in the  $^{13}\text{C}$ -incubated samples relative to  $^{12}\text{C}$ -controls for the PF codigester and CF codigester, respectively, and *Methanobacterium* read counts increased by 69% and 90%, respectively (Figure 6-4). These results indicate that *Bacteria* incorporated  $^{13}\text{C}$  into DNA to a greater extent than *Archaea* during the conversion of oleate over 6 days, but some methanogenic archaeal groups showed slight increases in  $^{13}\text{C}$  heavy density gradient profiles (Figure 6-4).



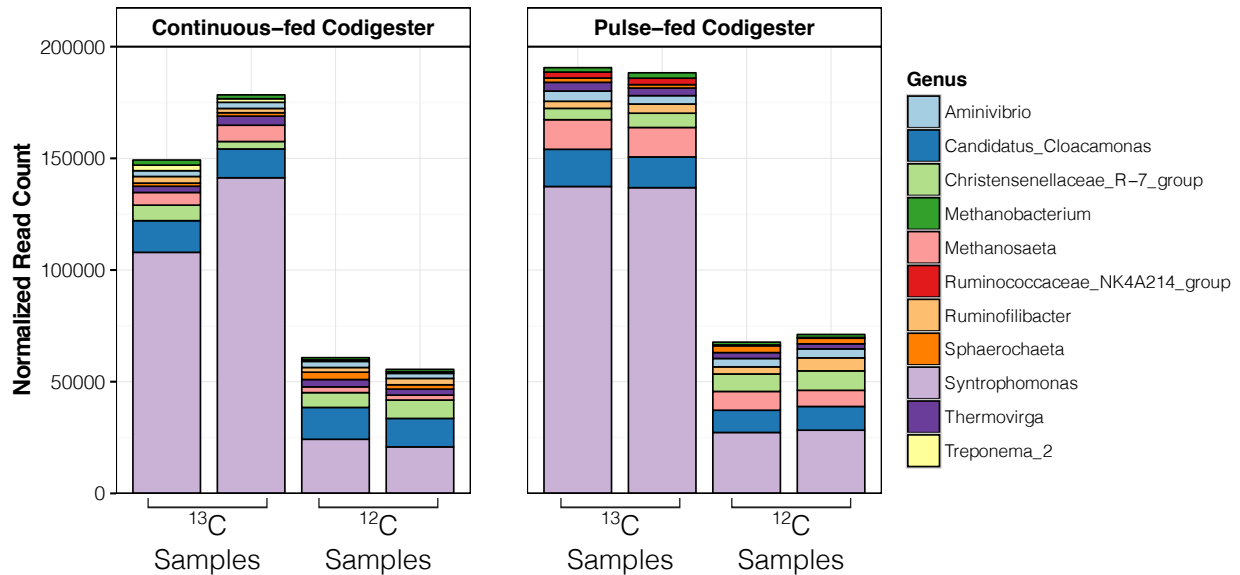


**Figure 6-4** Cumulative read counts of the 11 most abundant genera in the heavy gradient fractions of  $^{13}\text{C}$ -incubated samples and  $^{12}\text{C}$ -controls for both codigester sample sets, based on 16S rRNA amplicon sequencing. Normalized read counts for all OTUs were calculated with DESeq2 (Love et al., 2014) to correct for differences in sequencing depths between samples, and were then aggregated at the genus level.

### 6.4.3 DNA-SIP Metagenomic Sequencing

Metagenomes from the PF and CF codigester sludges before SIP incubation (i.e. time zero) were assembled to produce contigs for genome binning. The PF and CF codigester time-zero metagenome assemblies amounted to 536,947,079 kb and 680,484,169 kb within contigs longer than 1 kb, and had maximum contig lengths of 692,259 kb and 485,835 kb, respectively. Over 200 GBs were recovered through differential coverage binning for each codigester DNA-SIP sample set. Differential abundance analysis of mapped GB read counts with DESeq2 showed that 16 and 18 GBs were significantly enriched in the  $^{13}\text{C}$ -incubated metagenomes of the PF and CF codigesters, respectively (Supplemental Table D2). Due to the low completeness of some enriched GBs (Supplemental Table D2), a threshold of 40% genome completeness was

established for further phylogenetic analysis. Assigned taxonomies and genomic characteristics of differentially abundant GBs with over 40% completeness are summarized in Table 6-1.

**Table 6-1** Taxonomic classification and characteristics for genome bins that were significantly enriched ( $p < 0.01$ ,  $\log_2$  increase  $> 2.0$ ) in  $^{13}\text{C}$  metagenomes relative to  $^{12}\text{C}$ -controls for both codigester sample sets. Only genome bins that were above 40% completion are included.

Genome Bin I.D.	Taxonomy <sup>a</sup>	Assigned Bin 'Species' Name	Completeness <sup>b</sup>	GC	Size (Mbp)	Coding Density <sup>b</sup>
<i>Pulse-fed Codigester Genome Bins</i>						
bin.15	<i>Syntrophomonas</i>	<i>Syntrophomonas</i> sp. PF15	47%	41.4%	1.21	86%
bin.75	<i>Syntrophomonas</i>	<i>Syntrophomonas</i> sp. PF75	90%	41.2%	2.10	89%
bin.62	<i>Syntrophomonas</i>	<i>Syntrophomonas</i> sp. PF62	97%	43.5%	2.66	87%
bin.103	<i>Syntrophomonas</i>	<i>Syntrophomonas</i> sp. PF103	57%	44.6%	1.12	85%
bin.36	<i>Firmicutes</i>	<i>Firmicutes</i> sp. PF103	85%	50.8%	1.60	90%
bin.111	<i>Syntrophomonas</i>	<i>Syntrophomonas</i> sp. PF111	89%	45.7%	3.38	88%
bin.7	<i>Syntrophomonas</i>	<i>Syntrophomonas</i> sp. PF07	74%	49.7%	1.27	89%
bin.128	<i>Syntrophomonadaceae</i>	<i>Syntrophomonadaceae</i> sp. PF128	98%	46.4%	2.71	88%
<i>Continuous-fed Codigester Genome Bins</i>						
bin.22	<i>Syntrophomonas</i>	<i>Syntrophomonas</i> sp. CF22	74%	41.4%	2.00	86%
bin.196	<i>Syntrophomonas</i>	<i>Syntrophomonas</i> sp. CF196	72%	42.9%	2.41	87%
bin.226	<i>Syntrophomonas</i>	<i>Syntrophomonas</i> sp. CF226	98%	47.6%	3.18	88%
bin.14	<i>Syntrophomonas</i>	<i>Syntrophomonas</i> sp. CF14	63%	49.7%	0.78	89%
bin.263	<i>Firmicutes</i>	<i>Firmicutes</i> sp. CF263	83%	50.6%	4.81	92%
bin.250	Candidatus <i>Parcubacteria</i>	Candidatus <i>Parcubacteria</i> sp. CF263	40%	30.8%	0.25	91%
bin.187	<i>Syntrophomonas</i>	<i>Syntrophomonas</i> sp. CF187	86%	45.6%	2.12	89%

<sup>a</sup>Based on LCA of BLAST output; <sup>b</sup>Based on CheckM output

Approximately 75% of the differentially abundant GBs (6 of 8) in the PF codigester samples were taxonomically assigned to the *Syntrophomonas*, along with 71% (5 of 7) of the differentially abundant GBs in the CF codigester (Table 6-1). Both codigesters contained one differentially abundant GB that could only be assigned at the phylum-level to *Firmicutes*. In addition, one differentially abundant GB in the PF codigester was classified to the family-level of *Syntrophomonadaceae*, and one GB in the CF codigester was assigned to the phylum Candidatus *Parcubacteria* (Table 6-1). Multi-gene alignments based on a set of 400 conserved

marker genes showed that some of the differentially abundant GBs in both codigesters were closely clustered (Figure 6-5). GBs that formed sister groups based on both the conserved marker-gene alignments and UPGMA clustering of *in-silico* DNA-DNA hybridization distance values included *Syntrophomonas* sp. PF07 / *Syntrophomonas* sp. CF14, as well as *Syntrophomonas* sp. PF15 / *Syntrophomonas* sp. CF22 (Figure 6-5; Supplemental Figure D6). The GB of *Syntrophomonas* sp. PF103 was consistently clustered with the reference genomes of *Syntrophomonas wolfei* subsp. *wolfei* and *Syntrophomonas wolfei* subsp. *methylbutyrica* (Figure 6-5, Supplemental Figure D6). The *Firmicutes* sp. CF263 GB was placed on a branch outside of *Syntrophomonadaceae*-affiliated genomes based on marker-gene alignments (Figure 6-5), yet it clustered with the reference genome of *Syntrophomonas zehnderi* OL-4 based on *in-silico* DNA-DNA hybridization (Supplemental Figure D6). Both GBs of *Firmicutes* sp. PF36 and Candidatus *Parcubacteria* sp. CF263 were placed as outgroups in both phylogenetic clustering approaches (Figure 6-5, Supplemental Figure D6).

The largest GB coverage fold-change in the <sup>13</sup>C-incubated samples was observed for the sister group of *Syntrophomonas* sp. PF15 / *Syntrophomonas* sp. CF22, which were not closely related to previously-sequenced *Syntrophomonas* isolates (Figure 6-5; Supplemental Figure D2). Other GBs that had high fold-changes in the <sup>13</sup>C-incubated samples ( $\log_2$  change > 3.0) included *Syntrophomonas* sp. PF75, *Syntrophomonas* sp. PF62, *Syntrophomonas* sp. PF103, *Firmicutes* sp. PF103, *Syntrophomonas* sp. PF111, and *Syntrophomonas* sp. CF196 (Figure 6-5; Supplemental Figure D2). In comparison to the CF codigester, the PF codigester had a greater number of GBs that were enriched above a  $\log_2$  change of 3.0 in the <sup>13</sup>C-incubated samples (Figure 6-5).

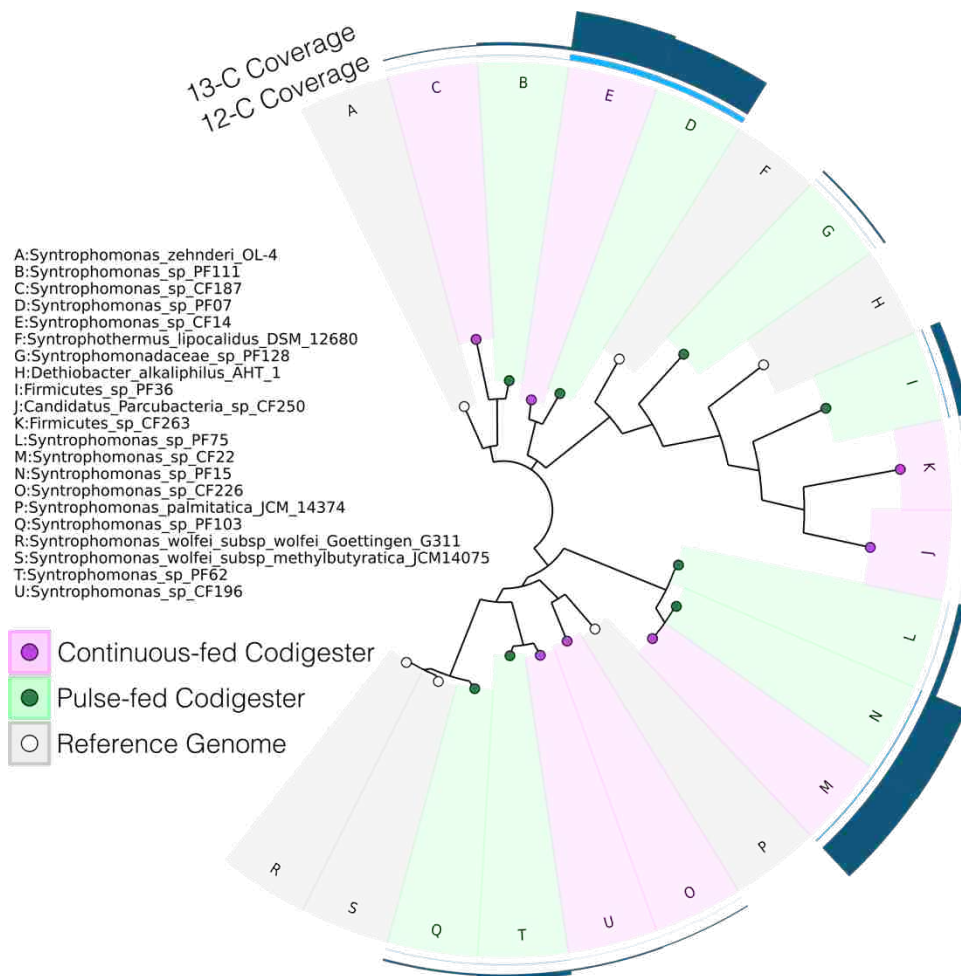


**Figure 6-5** Phylogenetic overview of differentially abundant genome bins identified in both anaerobic codigester DNA-SIP metagenomes. The tree was constructed based on a concatenated alignment of conserved marker genes within the metagenomic contigs of each bin using PhyloPhlAn (Segata et al., 2013). The color of each genome bin node represents the codigester biomass source, and the height of the outer bars represent the genome bin coverage in the heavy gradient fractions of the  $^{13}\text{C}$ -incubated samples and  $^{12}\text{C}$ -controls. The tree was illustrated using GraPhLan (Asnicar et al., 2015).

To assess the functional potential of differentially abundant GBs in  $^{13}\text{C}$ -incubated samples, coverage values were extracted and summarized for KEGG ECs within the LCFA degradation pathway (KEGG Pathway Map 00071). Long-chain fatty acid CoA ligase (EC:6.2.1.3), which is responsible for activating free-fatty acids to acyl-CoA thioesters (Sousa et al., 2009), had the highest EC coverage in differentially abundant GBs within  $^{13}\text{C}$  samples (Figure 6-6). The EC

categories with the next highest coverage were enoyl-CoA hydratase (EC:4.2.1.17) and acetyl-CoA acyltransferase (EC:2.3.1.9). Genes encoding for the entire fatty acid  $\beta$ -oxidation cycle were identified within the differentially abundant GBs for both codigesters (Figure 6-6), but the coverage of acyl-CoA dehydrogenase (fadE, EC:1.3.99.-) differed between the differentially abundant GBs in the two codigesters. Acyl-CoA dehydrogenase (EC:1.3.99) was observed in the PF codigester GBs but not in the CF codigester GBs (Figure 6-6). The GBs in the PF codigester also had substantially higher gene coverage for 3-hydroxyacyl-CoA dehydrogenases (EC:1.1.1.35 and EC:1.1.1.36) in  $^{13}\text{C}$ -incubated samples than the CF codigester GBs (Figure 6-6).

Metabolism of unsaturated fatty acids, like oleate, requires auxiliary enzymes additional to those used in  $\beta$ -oxidation, including:  $\Delta^3, \Delta^2$ -enoyl-CoA isomerase (EC:5.3.3.8),  $\Delta^{3,5}, \Delta^{2,4}$ -dienoyl-CoA isomerase (EC 5.3.3.-), and  $\Delta^2, \Delta^4$ -dienoyl-CoA reductase (EC:1.3.1.34) (Ren et al., 2004). Functional genes encoding for  $\Delta^3, \Delta^2$ -enoyl-CoA isomerase (EC:5.3.3.8) and  $\Delta^{3,5}, \Delta^{2,4}$ -dienoyl-CoA isomerase (EC 5.3.3.-) were not detected in the differentially abundant GBs (Supplemental Figure D3). However, genes encoding for  $\Delta^2, \Delta^4$ -dienoyl-CoA reductase (EC:1.3.1.34) were detected in the differentially abundant GBs for both codigesters, and had a coverage that was an order of magnitude higher in the PF codigester GBs (Supplemental Figure D3).

Syntrophic conversion of LCFA under methanogenic conditions involves interspecies electron transfer between *Bacteria* and *Archaea*, which commonly involves hydrogen and/or formate as electron shuttles (Stams and Plugge, 2009). Several formate dehydrogenases and hydrogenases were detected in the enriched GBs of both codigesters (Supplemental Figure D7). Formate

dehydrogenases were more abundant than hydrogenases within the differentially abundant GBs (Supplemental Figure D7).

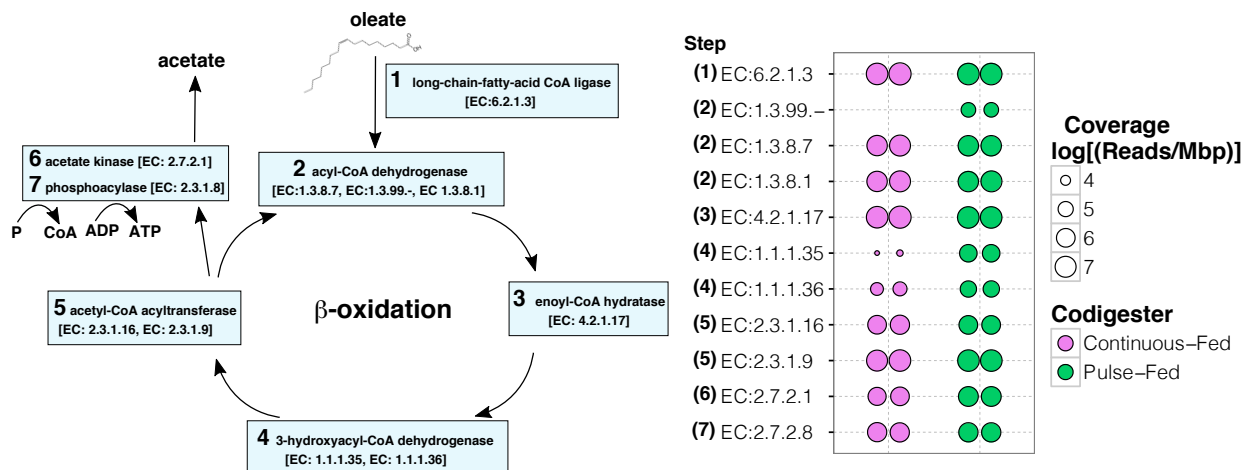


**Figure 6-6** Cumulative coverage values of KEGG ECs potentially involved in LCFA degradation (KEGG map 00071), based on the coverage of all differentially abundant genome bins in the  $^{13}\text{C}$ -incubated DNA-SIP metagenomes. Values from duplicate biological replicates are shown for both codigesters, and the size of each marker is proportional to the  $\log_{10}$  of the EC read coverage.

## 6.5 DISCUSSION

Recovering biomethane from FOG in anaerobic digestion has considerable potential to reduce energy and carbon footprints associated with wastewater treatment (Davidsson et al., 2008; Luostarinen et al., 2009; Wang et al., 2013). Improving our understanding of the microbial communities involved in LCFA degradation within anaerobic digesters is key for identifying operating strategies that can mitigate inhibitory LCFA accumulation at high FOG loading rates. The combination of DNA-SIP with metagenomic sequencing in this study provided novel genomic insights into the active LCFA-degrading populations in anaerobic codigesters, and highlighted the potential for physiological diversity at the trophic level of syntrophy in anaerobic digesters.

In prior research, it was observed that different LCFA-converting syntrophic populations were biologically selected by the frequency of LCFA feeding during codigestion (Chapter 5). Different syntrophic populations between the PF codigester and CF codigester coincided with different LCFA conversion rates, with the PF codigester having significantly higher biokinetics (Chapter 5). In this study, biokinetic modeling of methane production in the DNA-SIP microcosms fed with either  $^{13}\text{C}$ - or  $^{12}\text{C}$ - oleate showed that the PF codigester sludge had higher maximum oleate conversion rates than CF codigester sludge during all three DNA-SIP batch degradation periods. This result further corroborates that biological selection from the LCFA feeding frequency altered LCFA-bioconversion kinetics in the anaerobic codigesters (Chapter 5). Biological selection of different syntrophic populations has also been postulated for anaerobic reactors fed with propionate in a fill-and-draw mode (H. D. Ariesyady et al., 2007). It is plausible that a broad range of fatty-acid concentrations from pulse-feeding could select for multiple syntrophic fatty-acid oxidizers and/or methanogenic archaea that have different substrate affinities and/or maximum substrate utilization rates (H. D. Ariesyady et al., 2007; Conklin et al., 2006).

Near-complete stoichiometric conversion of  $^{13}\text{C}$ -labeled oleate into methane was observed based on high methane COD recoveries in the headspace. Yet, the remaining fraction of  $^{13}\text{C}$  incorporated into microbial biomass was sufficient to identify  $^{13}\text{C}$ -enriched DNA in heavy density gradient fractions based on total DNA and qPCR measurements. Considering that maximum specific growth rates of co-cultures of syntrophic fatty-acid oxidizing bacteria with methanogenic archaea can range from 0.10 to 0.19  $\text{d}^{-1}$  (Stams et al., 2012), the 6-day incubation

time for DNA-SIP may have permitted only a few cell generations. However, longer incubation times in DNA-SIP can be problematic because they can lead to cross-labeling of peripheral populations due to endogenous cell decay (Neufeld et al., 2006). In contrast to our study, previous studies employing DNA-SIP for syntrophic propionate and butyrate degrading communities in soil utilized incubation times ranging from 17 to 69 days (Chauhan and Ogram, 2006; Gan et al., 2012; H. Li et al., 2015; Liu et al., 2011; Lueders et al., 2004). These longer incubation times may have been necessitated due to the low active biomass fractions in soil, which would result in low substrate conversion rates. Thus, the higher active syntrophic biomass fraction in the anaerobic codigester sludges promoted more rapid oleate bioconversion in the DNA-SIP microcosms, which permitted efficient DNA labeling within a 6-day incubation period.

Syntrophic fatty acid conversion requires that free energy from catabolism is shared between syntrophic bacteria and methanogenic archaeal partners (Schink, 1997; Stams and Plugge, 2009). In this study, all of the 16S rRNA OTUs that were differentially abundant in  $^{13}\text{C}$ -incubated DNA-SIP samples for both codigesters belonged to the domain *Bacteria*, while no *Archaea* OTUs were differentially abundant in  $^{13}\text{C}$ -incubated samples. Likewise, all of the differentially abundant GBs recovered from DNA-SIP shotgun metagenomes were assigned to bacterial taxa. However, the higher cumulative 16S rRNA read counts of *Methanosaeta* and *Methanobacterium* in  $^{13}\text{C}$ -incubated samples relative to  $^{12}\text{C}$ -controls indicates that they were likely methanogenic partners involved in syntrophic oleate degradation in both codigesters, but their OTU abundance increases were not statistically significant. The slower incorporation of  $^{13}\text{C}$  into archaeal biomass during syntrophic growth on oleate would suggest that the biomass yield of syntrophic bacteria



was potentially greater than for methanogenic archaea. Yet, the relative fraction of *Bacteria* versus *Archaea* labeling has differed among previous SIP experiments focusing on syntrophic metabolism (Gan et al., 2012; Lueders et al., 2004). Using  $^{13}\text{C}$ -labeled propionate to study syntrophic communities in methanogenic paddy soil, Lueders *et al.* (2004) reported that a 7-week DNA-SIP incubation resulted in no labeled syntrophic bacteria but rather labeled methanogenic archaea. Since microbial growth yields can depend on thermodynamics (Heijnen and Van Dijken, 1992; Kleerebezem and Van Loosdrecht, 2010), it is possible that the relative fraction *Bacteria* versus *Archaea* labeling during SIP with syntrophic communities depended on the free-energy available to each syntrophic partner, which could differ among environmental systems and/or with different microbial substrate affinities.

A large fraction (>70%) of 16S rRNA OTUs significantly enriched in  $^{13}\text{C}$ -samples were assigned to the genus *Syntrophomonas*, which agrees with previous research that identified higher *Syntrophomonas* fractions within anaerobic communities degrading LCFA (Hatamoto et al., 2007b; Shigematsu et al., 2006; Sousa et al., 2009, 2007a; Ziels et al., 2015). However, this is the first study to determine the relative contribution of *Syntrophomonas* toward LCFA degradation using DNA-SIP. The high-resolution amplicon sequence analysis with DADA2 (Callahan et al., 2016) revealed that about half of the significantly enriched *Syntrophomonas* OTUs were shared between the two codigesters, whereas each codigester had a set of unique *Syntrophomonas* OTUs that contributed to oleate conversion. This finding indicates that the codigester LCFA feeding frequency biologically selected for unique active LCFA-degrading syntrophic populations. Other taxonomic groups that contained differentially abundant 16S rRNA OTUs included *Thermovirga*, *Aminivibrio*, *Candidatus Cloacamonas*, *Anaerofustis*, *Ruminococcaceae*

NK4A214 group, *Planctomycetes*, *Spirochaetae*, *Synergistes*, *Actinobacteria*, and *Bacterioidetes*, which do not have characterized species capable of anaerobically degrading LCFA. *Thermovirga lienii* was isolated from a deep-sea oil reservoir, and was characterized to ferment amino acids (Dahle and Birkeland, 2006). Similarly, *Aminivibrio pyruvatiphilus* was isolated from an anaerobic propionate-oxidizing enrichment culture as an amino acid fermenter (Honda et al., 2013). *Ruminococcaceae* have also been implicated with butyrate production from amino acids in the human gut (Vital et al., 2014). It is possible that some of these populations were labeled with  $^{13}\text{C}$  due to interspecies transfer of metabolites, such as amino acids, with syntrophic  $\beta$ -oxidizing bacteria or methanogenic archaea, despite the relatively short DNA-SIP incubation in this study.

To the best of our knowledge, this is the first study to couple DNA-SIP with differential coverage binning to recover population GBs from environmental metagenomes. Differential abundance analysis of GB read counts within the heavy gradient fractions of  $^{13}\text{C}$ -incubated samples versus  $^{12}\text{C}$ -controls was shown to be an effective technique coupled to DNA-SIP metagenomics to identify  $^{13}\text{C}$ -enriched GBs. The taxonomic assignment of differentially abundant GBs agreed with the results of 16S rRNA amplicon sequencing, as over 70% of GBs belonged to the genus *Syntrophomonas*. The finding that some phylogenetically distinct *Syntrophomonas* GBs were unique to each codigester further suggests that microbial communities involved in LCFA conversion can be physiologically diverse. Syntrophic bacteria are considered metabolic-specialists (McInerney et al., 2009; Sieber et al., 2012), which has led to the general conclusion that they have low functional redundancy in anaerobic digesters (Carballa et al., 2015; Werner et al., 2011). A previous genome-centric analysis of anaerobic

digester metagenomes found low diversity within the trophic level of syntrophic acetogenesis (Vanwonterghem et al., 2016). DNA-SIP based metagenomic binning may thus improve our resolution of anaerobic digester trophic groups by enriching metagenome libraries with actively growing population genomes (Coyotzi et al., 2016). The recovery of 236 microbial GBs from anaerobic digester metagenomes led to conclusion that *Syntrophomonas* GBs were among a core essential microbial group that is present independent of digester operational conditions (Treu et al., 2016b). Our finding that the anaerobic digester feeding frequency can impact the genomic composition of *Syntrophomonas* and their biokinetic activities (LCFA bioconversion rates) has implications for developing operating strategies that steer the core digester community to obtain better biokinetics and process stability.

The different oleate bioconversion kinetics between the two codigesters could have been attributed to differences in functional genes of their active LCFA-degrading GBs. The differentially abundant GBs in the PF codigester had more redundant KEGG ECs (e.g. multiple ECs for a single reaction step) in the LCFA-degradation pathway compared to the CF codigester GBs, which could indicate that the PF GBs potentially had a higher level of metabolic flexibility. Using transcriptomic read mapping, Treu *et al.* (2016a) showed that only two *Syntrophomonas* GBs were active after pulsing oleate to an anaerobic digester. In this study, 12 active *Syntrophomonas* GBs were identified with targeted DNA-SIP metagenomic analysis, yet transcriptional expression profiles could be further utilized to identify key biomarker genes for LCFA-degradation. Such genetic biomarkers could then be used to assess the functional potential of anaerobic digesters to convert high loadings of FOG into biomethane.

## 6.6 SUPPLEMENTAL INFORMATION AVAILABLE

The Supplemental Information for Chapter 6 is included in this document as Appendix D.

## Chapter 7. CONCLUSIONS AND FUTURE OUTLOOK

Achieving energy-neutral wastewater treatment is of major importance due to the large carbon and greenhouse gas footprints associated with fossil fuel-derived energy supplies (Singh et al., 2016). This research sought to improve biomethane recovery from anaerobic digestion treatment processes by elucidating relationships between microbial community structure and LCFA bioconversion kinetics during the degradation of fats, oils, and greases (FOG). The objectives of this research therefore align with a broader goal of enhancing wastewater treatment sustainability. To improve our ability to monitor LCFA-degrading populations, quantitative PCR (qPCR) assays were developed and validated in Chapter 3 targeting the syntrophic LCFA-degrading bacterial genera *Syntrophomonas* and *Syntrophus*. In Chapter 4, the qPCR assays were used to monitor changes in LCFA-degrading bacteria during FOG codigestion with municipal wastewater sludge. Chapters 5-6 focus on the impacts of anaerobic codigester feeding on syntrophic LCFA-degrading communities and their associated biokinetics. Overall, this research combined methods from molecular microbiology and process engineering to elucidate the role and effect of microbial community structure in anaerobic FOG conversion. Collectively, the results indicated that higher concentrations of syntrophic LCFA-degrading bacteria were indicators of higher LCFA bioconversion kinetics, which were necessary to maintain stable digester operation at high FOG loading rates without inhibitory LCFA accumulation. The codigester feeding strategy also impacted the syntrophic LCFA-degrading community structure and biokinetics, thus opening a door for the application of digester operating strategies that maximize biomethane recovery from FOG. The key findings of this study along with their engineering significance are presented in more detail below.

## 7.1 MAJOR FINDINGS AND ENGINEERING SIGNIFICANCE

Biokinetic models, such as the IWA Anaerobic Digester Model 1 (ADM1), are commonly used in wastewater treatment process design and analysis to predict performance and capacity under dynamic loading scenarios (Batstone et al., 2015). For accurate predictions of anaerobic digester performance and capacity, such biokinetic models would ideally be calibrated using actual biomass concentrations for the different metabolic guilds (e.g. fermenters, syntrophs, and methanogens) in the mass-balance equations. When this research project began, there was a lack of molecular tools available to accurately monitor the abundance of LCFA-degrading bacteria in anaerobic digesters, because they are generally present in digester sludge at low background concentrations (Stams et al., 2012). Thus, the quantitative molecular tools developed in this research (Chapter 3) are significant advancements for accurately measuring LCFA-degrading biomass in anaerobic digesters. The developed qPCR assays were used to infer three separate relationships between LCFA-degrading bacterial biomass and LCFA conversion rates throughout this research. In Chapter 3, the relative fraction (e.g. percentage) of *Syntrophomonas* within the *Bacteria* community was positively correlated to the methane production rate from oleate in batch enrichment bottles. In Chapter 4, effluent LCFA concentrations were positively correlated to the FOG loading rate normalized to the concentration of *Syntrophomonas* within a codigester. And, in Chapter 5, maximum specific oleate conversion rates ( $q_{max,oleate}$ ) were positively correlated to the concentration of *Syntrophomonas* genes per g VS within codigesters fed with oleate and manure. Therefore, this research identified that the concentration of *Syntrophomonas* 16S rRNA genes could be used as a surrogate biomarker for LCFA conversion rates in anaerobic digesters. The relationship between  $q_{max,oleate}$  and *Syntrophomonas* genes (Chapter 5) could thus

be applied to predict appropriate FOG loading rates that do not cause inhibitory LCFA accumulation in anaerobic digesters.

A key engineering importance of this research is that biomethane recovery was increased by 170% to 440% during FOG codigestion with minimal impacts on the digester SRT. However, microbial adaptation was identified to limit the allowable FOG loading rate. A practical engineering development from these research findings is that the FOG loading rate must be lower than the  $q_{max,LCFA}$  to avoid LCFA accumulation during codigestion. Digester  $q_{max,LCFA}$  values increased as the LCFA-degrading population increased with operating time at each stepwise FOG loading increase. Feeding FOG on a daily or bi-daily basis may promote higher  $q_{max,LCFA}$  values, and thus higher FOG loading rates, compared to continually adding FOG. Full-scale digester operating staff could measure  $q_{max,LCFA}$  in batch kinetic tests using the method outlined in Chapter 5 to determine appropriate FOG loading rates. If measurements of the microbial community are also collected associated with the batch kinetic tests, then modeling approaches could also be developed and implemented that predict  $q_{max,LCFA}$  based on microbial indicators, as is presented in Chapter 5 using *Syntrophomonas* genes. As the price of sequencing continues to decline (Goodwin et al., 2016), the use of molecular markers to predict  $q_{max,LCFA}$  may become less time-consuming and expensive than conducting batch kinetic tests.

This research also found that different syntrophic populations were biologically selected based on the LCFA-feeding frequency during codigestion (Chapter 5). A novel DNA-SIP based metagenomic approach was implemented to compare active LCFA-degraders within pulse- and

continuous fed LCFA codigesters (Chapter 6), and found distinct *Syntrophomonas* genomes within both codigesters. These findings revise previous notions that syntrophic bacteria are not functionally redundant in anaerobic digesters (Werner et al., 2011). The results also showed that pulse-feeding LCFA selected for higher methane production kinetics (Chapter 5). The diversity of *Syntrophomonas* taxa was incorporated into a biokinetic model using multiple-linear regression and stepwise feature selection, which more accurately predicted  $q_{max,oleate}$  values than did total *Syntrophomonas* genes alone (Chapter 5). Therefore, this research employed novel molecular techniques to examine physiological diversity within a metabolic guild of a wastewater treatment process, and demonstrated how to incorporate such microbial biodiversity into biokinetic models. Overall, this research identified digester operating strategies that improved process stability and biokinetics during FOG codigestion, which contributes to the goal of maximizing energy recovery during wastewater treatment.

## 7.2 FUTURE OUTLOOKS

This research showed that syntrophic bacterial biomass could be used as a surrogate for LCFA conversion kinetics in anaerobic digesters. However, as syntrophic metabolism occurs near thermodynamic equilibrium (Schink, 1997), it is likely that the thermodynamic state in an anaerobic digester also affects LCFA conversion kinetics. The thermodynamic state could be altered by hydrogen, formate, and acetate concentrations, which can be governed by the activities and affinities of methanogenic archaea (Schink, 1997). The thermodynamic state has been shown to impact growth yields (Kleerebezem and Van Loosdrecht, 2010) and microbial biokinetics (LaRowe et al., 2012) for low energy-yielding processes like syntrophy. Since methanogenic



archaea grow on acetate and hydrogen produced via the degradation of various substrates in anaerobic digesters, methanogenic biomass levels may be in excess relative to syntrophic LCFA-degrading bacterial biomass in FOG codigesters. Yet, to accurately model LCFA conversion kinetics, more detailed biokinetic models must be developed that incorporate the thermodynamic state (H. Junicke et al., 2016). Currently, existing biokinetic models for LCFA degradation include empirical inhibition constants, such as in Chapter 6 and in the work of Zonta et al. (2013). These models could be revised by relating the Gibbs free energy available from LCFA  $\beta$ -oxidation to growth yields or substrate utilization kinetics (Kleerebezem and Van Loosdrecht, 2010; LaRowe et al., 2012). The tools for quantifying LCFA-degrading bacteria that were developed in this research (Chapter 3) could be utilized to calibrate such thermodynamic-based kinetic growth models, which could then be implemented in widely used design platforms such as the ADM1 model. Thermodynamic-based kinetic models for microbial metabolism could also be used to elucidate shifts in key functional pathways during anaerobic digestion, such shifts from aceticlastic methanogenesis to syntrophic acetate oxidation at high ammonia levels (Werner et al., 2014). Better predictions of microbial metabolism in anaerobic digestion modeling could enable more robust process performance with high-rate methane recovery from organic waste.

While this study revealed that syntrophic populations can be physiologically diverse based on metagenomic sequencing, microbial activity in anaerobic digesters can be better represented by RNA expression in comparison to gene abundance (De Vrieze et al., 2016). Thus, evaluating physiological diversity of a metabolic guild requires information about gene abundance (metagenomics) as well as expression (transcriptomics/proteomics). Future research is therefore needed to evaluate how the anaerobic digester LCFA feeding strategy impacted the diversity of functional genes expressed during LCFA degradation. Information on gene expression could be

obtained by mapping mRNA reads onto metagenome populations bins obtained through the DNA-SIP experiment. Such genetic biomarkers could then be used to assess the functional potential of anaerobic digesters to convert high loadings of FOG into biomethane.

The multiple regression model developed in Chapter 5 for predicting oleate conversion kinetics based on 6 *Syntrophomonas* taxa has implications for improved process monitoring of anaerobic digesters based on real-time measurements of key microbial biomarkers. Such biomarkers used for regression analysis could be based on the taxonomic composition within a functional group (as in Chapter 5), or based on the proportion of functional groups within an entire community (Louca et al., 2016). As the price of molecular sequencing platforms continues to decrease (Goodwin et al., 2016), predictive relationships for wastewater treatment process kinetics and performance based on multi-omic data may be more easily implemented. For instance, the recently-developed MinION sequencer is a small (3 cm x 10cm) mobile USB-based device that is capable of generating ~150 Mbp of DNA sequence data in 24 hrs, although it is currently subject to high error rates (Goodwin et al., 2016). Real-time molecular sequencing data along with treatment process state data (e.g. influent composition, effluent composition, pH, temperature, etc.) could be incorporated into machine-learning based algorithms (Werner et al., 2011) or genome-based process models (Louca and Doebeli, 2015) to accurately predict biological wastewater treatment performance in real-time. The output of such real-time models could identify operational strategies to improve treatment efficiency, and could even be incorporated into ‘smart’ logic controllers (Regmi et al., 2015) for dynamic operational control of biological wastewater treatment processes. Therefore, future research is warranted on novel strategies to incorporate molecular sequence data into real-time biological wastewater treatment

monitoring and control, which could lead to more energy-efficient wastewater treatment and reduce the ecological impacts associated wastewater discharge.

## BIBLIOGRAPHY

- Aiba, S., Shoda, M., Nagatani, M., 1968. Kinetics of product inhibition in alcohol fermentation. *Biotechnol. Bioeng.* 10, 845–864. doi:10.1002/bit.260100610
- Albertsen, M., Hugenholtz, P., Skarshewski, A., Nielsen, K.L., Tyson, G.W., Nielsen, P.H., 2013. Genome sequences of rare, uncultured bacteria obtained by differential coverage binning of multiple metagenomes. *Nat. Biotechnol.* 31, 533–538. doi:10.1038/nbt.2579
- Allison, S.D., Martiny, J.B.H., 2008. Resistance, resilience, and redundancy in microbial communities. *Proc. Natl. Acad. Sci.* 105, 11512–11519. doi:10.1073/pnas.0801925105
- Alves, M.M., Mota Vieira, J.A., Álvares Pereira, R.M., Pereira, M.A., Mota, M., 2001. Effects of lipids and oleic acid on biomass development in anaerobic fixed-bed reactors. Part II: Oleic acid toxicity and biodegradability. *Water Res.* 35, 264–270. doi:10.1016/S0043-1354(00)00242-6
- Alves, M.M., Pereira, M.A., Sousa, D.Z., Cavaleiro, A.J., Picavet, M., Smidt, H., Stams, A.J.M., 2009. Waste lipids to energy: how to optimize methane production from long-chain fatty acids (LCFA). *Microb. Biotechnol.* 2, 538–550. doi:10.1111/j.1751-7915.2009.00100.x
- Angelidaki, I., Ahring, B.K., 1992. Effects of free long-chain fatty acids on thermophilic anaerobic digestion. *Appl. Microbiol. Biotechnol.* 37, 808–812. doi:10.1007/BF00174850
- Arahal, D.R., Ventosa, A., 2006. The Family Halomonadaceae, in: Dr, M.D.P., Falkow, S., Rosenberg, E., Schleifer, K.-H., Stackebrandt, E. (Eds.), *The Prokaryotes*. Springer New York, pp. 811–835.
- Ariesyady, H.D., Ito, T., Yoshiguchi, K., Okabe, S., 2007. Phylogenetic and functional diversity of propionate-oxidizing bacteria in an anaerobic digester sludge. *Appl. Microbiol. Biotechnol.* 75, 673–683. doi:10.1007/s00253-007-0842-y
- Ariesyady, H., Ito, T., Okabe, S., 2007. Functional bacterial and archaeal community structures of major trophic groups in a full-scale anaerobic sludge digester. *Water Res.* 41, 1554–1568. doi:10.1016/j.watres.2006.12.036
- Aronesty, E., 2013. Comparison of sequencing utility programs. *Open Bioinform J* 7, 1–8.
- Asnicar, F., Weingart, G., Tickle, T.L., Huttenhower, C., Segata, N., 2015. Compact graphical representation of phylogenetic data and metadata with GraPhlAn. *PeerJ* 3, e1029. doi:10.7717/peerj.1029
- Auch, A.F., von Jan, M., Klenk, H.-P., Göker, M., 2010. Digital DNA-DNA hybridization for microbial species delineation by means of genome-to-genome sequence comparison. *Stand. Genomic Sci.* 2, 117–134. doi:10.4056/sigs.531120
- Baserba, M.G., Angelidaki, I., Karakashev, D., 2012. Effect of continuous oleate addition on microbial communities involved in anaerobic digestion process. *Bioresour. Technol.* 106, 74–81. doi:10.1016/j.biortech.2011.12.020
- Batstone, D.J., Puyol, D., Flores-Alsina, X., Rodríguez, J., 2015. Mathematical modelling of anaerobic digestion processes: applications and future needs. *Rev. Environ. Sci. Biotechnol.* 14, 595–613. doi:10.1007/s11157-015-9376-4
- Beaty, P.S., McInerney, M.J., 1987. Growth of *Syntrophomonas wolfei* in pure culture on crotonate. *Arch. Microbiol.* 147, 389–393. doi:10.1007/BF00406138

- Bishop, C.P., Shumway, C.R., 2009. The Economics of Dairy Anaerobic Digestion with Coproduct Marketing. *Appl. Econ. Perspect. Policy* 31, 394–410. doi:10.1111/j.1467-9353.2009.01445.x
- Bocher, B.T.W., Cherukuri, K., Maki, J.S., Johnson, M., Zitomer, D.H., 2015. Relating methanogen community structure and anaerobic digester function. *Water Res.* 70, 425–435. doi:10.1016/j.watres.2014.12.018
- Briones, A., Raskin, L., 2003. Diversity and dynamics of microbial communities in engineered environments and their implications for process stability. *Curr. Opin. Biotechnol.* 14, 270–276. doi:10.1016/S0958-1669(03)00065-X
- Bustin, S.A., Benes, V., Garson, J.A., Hellems, J., Huggett, J., Kubista, M., Mueller, R., Nolan, T., Pfaffl, M.W., Shipley, G.L., Vandesompele, J., Wittwer, C.T., 2009. The MIQE Guidelines: Minimum Information for Publication of Quantitative Real-Time PCR Experiments. *Clin. Chem.* 55, 611–622. doi:10.1373/clinchem.2008.112797
- Callahan, B.J., McMurdie, P.J., Rosen, M.J., Han, A.W., Johnson, A.J.A., Holmes, S.P., 2016. DADA2: High-resolution sample inference from Illumina amplicon data. *Nat. Methods* 13, 581–583. doi:10.1038/nmeth.3869
- Campanaro, S., Treu, L., Kougias, P.G., De Francisci, D., Valle, G., Angelidaki, I., 2016. Metagenomic analysis and functional characterization of the biogas microbiome using high throughput shotgun sequencing and a novel binning strategy. *Biotechnol. Biofuels* 9. doi:10.1186/s13068-016-0441-1
- Campbell, J.W., Morgan-Kiss, R.M., E. Cronan, J., 2003. A new *Escherichia coli* metabolic competency: growth on fatty acids by a novel anaerobic  $\beta$ -oxidation pathway. *Mol. Microbiol.* 47, 793–805. doi:10.1046/j.1365-2958.2003.03341.x
- Caporaso, J.G., Bittinger, K., Bushman, F.D., DeSantis, T.Z., Andersen, G.L., Knight, R., 2010a. PyNAST: a flexible tool for aligning sequences to a template alignment. *Bioinformatics* 26, 266–267. doi:10.1093/bioinformatics/btp636
- Caporaso, J.G., Kuczynski, J., Stombaugh, J., Bittinger, K., Bushman, F.D., Costello, E.K., Fierer, N., Peña, A.G., Goodrich, J.K., Gordon, J.I., Huttley, G.A., Kelley, S.T., Knights, D., Koenig, J.E., Ley, R.E., Lozupone, C.A., McDonald, D., Muegge, B.D., Pirrung, M., Reeder, J., Sevinsky, J.R., Turnbaugh, P.J., Walters, W.A., Widmann, J., Yatsunencko, T., Zaneveld, J., Knight, R., 2010b. QIIME allows analysis of high-throughput community sequencing data. *Nat. Methods* 7, 335–336. doi:10.1038/nmeth.f.303
- Carballa, M., Regueiro, L., Lema, J.M., 2015. Microbial management of anaerobic digestion: exploiting the microbiome-functionality nexus. *Curr. Opin. Biotechnol., Environmental biotechnology • Energy biotechnology* 33, 103–111. doi:10.1016/j.copbio.2015.01.008
- Cavaleiro, A.J., Pereira, M.A., Alves, M., 2008. Enhancement of methane production from long chain fatty acid based effluents. *Bioresour. Technol.* 99, 4086–4095. doi:10.1016/j.biortech.2007.09.005
- Cavaleiro, A.J., Pereira, M.A., Guedes, A.P., Stams, A.J.M., Alves, M.M., Sousa, D.Z., 2016. Conversion of C<sub>n</sub>-Unsaturated into C<sub>n-2</sub>-Saturated LCFA Can Occur Uncoupled from Methanogenesis in Anaerobic Bioreactors. *Environ. Sci. Technol.* 50, 3082–3090. doi:10.1021/acs.est.5b03204
- Cavaleiro, A.J., Salvador, A.F., Alves, J.I., Alves, M., 2009. Continuous High Rate Anaerobic Treatment of Oleic Acid Based Wastewater is Possible after a Step Feeding Start-Up. *Environ. Sci. Technol.* 43, 2931–2936. doi:10.1021/es8031264

- Chauhan, A., Ogram, A., 2006. Fatty Acid-Oxidizing Consortia along a Nutrient Gradient in the Florida Everglades. *Appl. Environ. Microbiol.* 72, 2400–2406. doi:10.1128/AEM.72.4.2400-2406.2006
- Chemerys, A., Pelletier, E., Cruaud, C., Martin, F., Violet, F., Jouanneau, Y., 2014. Characterization of Novel Polycyclic Aromatic Hydrocarbon Dioxygenases from the Bacterial Metagenomic DNA of a Contaminated Soil. *Appl. Environ. Microbiol.* 80, 6591–6600. doi:10.1128/AEM.01883-14
- Chen, I.-M.A., Markowitz, V.M., Chu, K., Palaniappan, K., Szeto, E., Pillay, M., Ratner, A., Huang, J., Andersen, E., Huntemann, M., Varghese, N., Hadjithomas, M., Tennesen, K., Nielsen, T., Ivanova, N.N., Kyrpides, N.C., 2016. IMG/M: integrated genome and metagenome comparative data analysis system. *Nucleic Acids Res.* gkw929. doi:10.1093/nar/gkw929
- Chen, Y., Murrell, J.C., 2010. When metagenomics meets stable-isotope probing: progress and perspectives. *Trends Microbiol.* 18, 157–163. doi:10.1016/j.tim.2010.02.002
- Chong, S.C., Liu, Y., Cummins, M., Valentine, D.L., Boone, D.R., 2002. *Methanogenium marinum* sp. nov., a H<sub>2</sub>-using methanogen from Skan Bay, Alaska, and kinetics of H<sub>2</sub> utilization. *Antonie Van Leeuwenhoek* 81, 263–270. doi:10.1023/A:1020535222281
- Christodoulou, A.P., Rosano, H.L., 1968. Effect of pH and nature of monovalent cations on surface isotherms of saturated C16 to C22 soap monolayers. *Adv Chem Ser* 84, 210–234.
- Cirne, D.G., Paloumet, X., Björnsson, L., Alves, M.M., Mattiasson, B., 2007. Anaerobic digestion of lipid-rich waste—Effects of lipid concentration. *Renew. Energy* 32, 965–975. doi:10.1016/j.renene.2006.04.003
- Cole, J.R., Wang, Q., Cardenas, E., Fish, J., Chai, B., Farris, R.J., Kulam-Syed-Mohideen, A.S., McGarrell, D.M., Marsh, T., Garrity, G.M., Tiedje, J.M., 2009. The Ribosomal Database Project: improved alignments and new tools for rRNA analysis. *Nucleic Acids Res.* 37, D141–D145. doi:10.1093/nar/gkn879
- Conklin, A., Stensel, H.D., Ferguson, J., 2006. Growth Kinetics and Competition Between *Methanosarcina* and *Methanosaeta* in Mesophilic Anaerobic Digestion. *Water Environ. Res.* 78, 486–496. doi:10.2175/106143006X95393
- Coyotzi, S., Pratscher, J., Murrell, J.C., Neufeld, J.D., 2016. Targeted metagenomics of active microbial populations with stable-isotope probing. *Curr. Opin. Biotechnol., Analytical biotechnology* 41, 1–8. doi:10.1016/j.copbio.2016.02.017
- Dahle, H., Birkeland, N.-K., 2006. *Thermovirga lienii* gen. nov., sp. nov., a novel moderately thermophilic, anaerobic, amino-acid-degrading bacterium isolated from a North Sea oil well. *Int. J. Syst. Evol. Microbiol.* 56, 1539–1545. doi:10.1099/ijs.0.63894-0
- Davidsson, Å., Lövestedt, C., la Cour Jansen, J., Gruvberger, C., Aspegren, H., 2008. Co-digestion of grease trap sludge and sewage sludge. *Waste Manag.* 28, 986–992. doi:10.1016/j.wasman.2007.03.024
- DeSantis, T.Z., Hugenholtz, P., Larsen, N., Rojas, M., Brodie, E.L., Keller, K., Huber, T., Dalevi, D., Hu, P., Andersen, G.L., 2006. Greengenes, a Chimera-Checked 16S rRNA Gene Database and Workbench Compatible with ARB. *Appl. Environ. Microbiol.* 72, 5069–5072. doi:10.1128/AEM.03006-05
- Desbois, A.P., Smith, V.J., 2010. Antibacterial free fatty acids: activities, mechanisms of action and biotechnological potential. *Appl. Microbiol. Biotechnol.* 85, 1629–1642.
- De Vrieze, J., Regueiro, L., Props, R., Vilchez-Vargas, R., Jáuregui, R., Pieper, D.H., Lema, J.M., Carballa, M., 2016. Presence does not imply activity: DNA and RNA patterns differ

- in response to salt perturbation in anaerobic digestion. *Biotechnol. Biofuels* 9, 244. doi:10.1186/s13068-016-0652-5
- De Vrieze, J., Verstraete, W., Boon, N., 2013. Repeated pulse feeding induces functional stability in anaerobic digestion. *Microb. Biotechnol.* 6, 414–424. doi:10.1111/1751-7915.12025
- Dumont, M.G., Murrell, J.C., 2005. Stable isotope probing — linking microbial identity to function. *Nat. Rev. Microbiol.* 3, 499–504. doi:10.1038/nrmicro1162
- Eaton, A.D., Franson, M.A.H., 2005. *Standard Methods for Examination of Water & Wastewater*. Amer Public Health Assn.
- Edgar, R.C., 2013. UPARSE: highly accurate OTU sequences from microbial amplicon reads. *Nat. Methods* 10, 996–998. doi:10.1038/nmeth.2604
- Edgar, R.C., 2010. Search and clustering orders of magnitude faster than BLAST. *Bioinformatics* 26, 2460–2461. doi:10.1093/bioinformatics/btq461
- Edgar, R.C., Haas, B.J., Clemente, J.C., Quince, C., Knight, R., 2011. UCHIME improves sensitivity and speed of chimera detection. *Bioinformatics* 27, 2194–2200. doi:10.1093/bioinformatics/btr381
- Elsas, J.D. van, Chiurazzi, M., Mallon, C.A., Elhottová, D., Krištůfek, V., Salles, J.F., 2012. Microbial diversity determines the invasion of soil by a bacterial pathogen. *Proc. Natl. Acad. Sci.* 109, 1159–1164. doi:10.1073/pnas.1109326109
- Embree, M., Nagarajan, H., Movahedi, N., Chitsaz, H., Zengler, K., 2014. Single-cell genome and metatranscriptome sequencing reveal metabolic interactions of an alkane-degrading methanogenic community. *ISME J.* 8, 757–767. doi:10.1038/ismej.2013.187
- Eyice, Ö., Namura, M., Chen, Y., Mead, A., Samavedam, S., Schäfer, H., 2015. SIP metagenomics identifies uncultivated Methylophilaceae as dimethylsulphide degrading bacteria in soil and lake sediment. *ISME J.* 9, 2336–2348. doi:10.1038/ismej.2015.37
- Fujita, Y., Matsuoka, H., Hirooka, K., 2007. Regulation of fatty acid metabolism in bacteria. *Mol. Microbiol.* 66, 829–839. doi:10.1111/j.1365-2958.2007.05947.x
- Gan, Y., Qiu, Q., Liu, P., Rui, J., Lu, Y., 2012. Syntrophic Oxidation of Propionate in Rice Field Soil at 15 and 30°C under Methanogenic Conditions. *Appl. Environ. Microbiol.* 78, 4923–4932. doi:10.1128/AEM.00688-12
- Garcia, J.-L., Patel, B.K.C., Ollivier, B., 2000. Taxonomic, Phylogenetic, and Ecological Diversity of Methanogenic Archaea. *Anaerobe* 6, 205–226. doi:10.1006/anae.2000.0345
- Girault, R., Bridoux, G., Nauleau, F., Poullain, C., Buffet, J., Peu, P., Sadowski, A.G., Béline, F., 2012. Anaerobic co-digestion of waste activated sludge and greasy sludge from flotation process: Batch versus CSTR experiments to investigate optimal design. *Bioresour. Technol.* 105, 1–8. doi:10.1016/j.biortech.2011.11.024
- Goodwin, S., McPherson, J.D., McCombie, W.R., 2016. Coming of age: ten years of next-generation sequencing technologies. *Nat. Rev. Genet.* 17, 333–351. doi:10.1038/nrg.2016.49
- Gray, N.D., Sherry, A., Grant, R.J., Rowan, A.K., Hubert, C.R.J., Callbeck, C.M., Aitken, C.M., Jones, D.M., Adams, J.J., Larter, S.R., Head, I.M., 2011. The quantitative significance of Syntrophaceae and syntrophic partnerships in methanogenic degradation of crude oil alkanes. *Environ. Microbiol.* 13, 2957–2975. doi:10.1111/j.1462-2920.2011.02570.x
- Grob, C., Taubert, M., Howat, A.M., Burns, O.J., Dixon, J.L., Richnow, H.H., Jehmlich, N., von Bergen, M., Chen, Y., Murrell, J.C., 2015. Combining metagenomics with metaproteomics and stable isotope probing reveals metabolic pathways used by a

- naturally occurring marine methylotroph. *Environ. Microbiol.* 17, 4007–4018.  
doi:10.1111/1462-2920.12935
- Guo, M., Song, W., Buhain, J., 2015. Bioenergy and biofuels: History, status, and perspective. *Renew. Sustain. Energy Rev.* 42, 712–725. doi:10.1016/j.rser.2014.10.013
- Gustafson, W.G., Feinberg, B.A., McFarland, J.T., 1986. Energetics of beta-oxidation. Reduction potentials of general fatty acyl-CoA dehydrogenase, electron transfer flavoprotein, and fatty acyl-CoA substrates. *J. Biol. Chem.* 261, 7733–7741.
- Hanaki, K., Matsuo, T., Nagase, M., 1981. Mechanism of inhibition caused by long-chain fatty acids in anaerobic digestion process. *Biotechnol. Bioeng.* 23, 1591–1610.  
doi:10.1002/bit.260230717
- Hansen, K.H., Ahring, B.K., Raskin, L., 1999. Quantification of Syntrophic Fatty Acid- $\beta$ -Oxidizing Bacteria in a Mesophilic Biogas Reactor by Oligonucleotide Probe Hybridization. *Appl. Environ. Microbiol.* 65, 4767–4774.
- Hao, L., Bize, A., Conteau, D., Chapleur, O., Courtois, S., Kroff, P., Desmond-Le Quémener, E., Bouchez, T., Mazéas, L., 2016. New insights into the key microbial phylotypes of anaerobic sludge digesters under different operational conditions. *Water Res.* 102, 158–169. doi:10.1016/j.watres.2016.06.014
- Hatamoto, M., Imachi, H., Fukayo, S., Ohashi, A., Harada, H., 2007a. *Syntrophomonas palmitatica* sp. nov., an anaerobic, syntrophic, long-chain fatty-acid-oxidizing bacterium isolated from methanogenic sludge. *Int. J. Syst. Evol. Microbiol.* 57, 2137–2142.  
doi:10.1099/ijs.0.64981-0
- Hatamoto, M., Imachi, H., Ohashi, A., Harada, H., 2007b. Identification and Cultivation of Anaerobic, Syntrophic Long-Chain Fatty Acid-Degrading Microbes from Mesophilic and Thermophilic Methanogenic Sludges. *Appl. Environ. Microbiol.* 73, 1332–1340.  
doi:10.1128/AEM.02053-06
- Hatamoto, M., Imachi, H., Yashiro, Y., Ohashi, A., Harada, H., 2007c. Diversity of Anaerobic Microorganisms Involved in Long-Chain Fatty Acid Degradation in Methanogenic Sludges as Revealed by RNA-Based Stable Isotope Probing. *Appl. Environ. Microbiol.* 73, 4119–4127. doi:10.1128/AEM.00362-07
- Heijnen, J.J., Van Dijken, J.P., 1992. In search of a thermodynamic description of biomass yields for the chemotrophic growth of microorganisms. *Biotechnol. Bioeng.* 39, 833–858.  
doi:10.1002/bit.260390806
- He, X., Iasmin, M., Dean, L.O., Lappi, S.E., Ducoste, J.J., de los Reyes III, F.L., 2011. Evidence for fat, oil, and grease (FOG) deposit formation mechanisms in sewer lines. *Environ. Sci. Technol.* 45, 4385–4391.
- Hill, M.O., 1973. Diversity and Evenness: A Unifying Notation and Its Consequences. *Ecology* 54, 427–432. doi:10.2307/1934352
- Honda, T., Fujita, T., Tonouchi, A., 2013. *Aminivibrio pyruvatiphilus* gen. nov., sp. nov., an anaerobic, amino-acid-degrading bacterium from soil of a Japanese rice field. *Int. J. Syst. Evol. Microbiol.* 63, 3679–3686. doi:10.1099/ijs.0.052225-0
- Hori, T., Haruta, S., Ueno, Y., Ishii, M., Igarashi, Y., 2006. Dynamic Transition of a Methanogenic Population in Response to the Concentration of Volatile Fatty Acids in a Thermophilic Anaerobic Digester. *Appl. Environ. Microbiol.* 72, 1623–1630.  
doi:10.1128/AEM.72.2.1623-1630.2006
- Huson, D.H., Auch, A.F., Qi, J., Schuster, S.C., 2007. MEGAN analysis of metagenomic data. *Genome Res.* 17, 377–386. doi:10.1101/gr.5969107



- Hwu, C.-S., Lettinga, G., 1997. Acute toxicity of oleate to acetate-utilizing methanogens in mesophilic and thermophilic anaerobic sludges. *Enzyme Microb. Technol.* 21, 297–301. doi:10.1016/S0141-0229(97)00050-1
- Hwu, C.-S., Tseng, S.-K., Yuan, C.-Y., Kulik, Z., Lettinga, G., 1998. Biosorption of long-chain fatty acids in UASB treatment process. *Water Res.* 32, 1571–1579. doi:10.1016/S0043-1354(97)00352-7
- Ito, T., Yoshiguchi, K., Ariesyady, H.D., Okabe, S., 2011. Identification of a novel acetate-utilizing bacterium belonging to Synergistes group 4 in anaerobic digester sludge. *ISME J.* 5, 1844–1856. doi:10.1038/ismej.2011.59
- Jackson, B.E., Bhupathiraju, V.K., Tanner, R.S., Woese, C.R., McInerney, M.J., 1999. *Syntrophus aciditrophicus* sp. nov., a new anaerobic bacterium that degrades fatty acids and benzoate in syntrophic association with hydrogen-using microorganisms. *Arch. Microbiol.* 171, 107–114. doi:10.1007/s002030050685
- Johansson, I., Svensson, M., 2001. Surfactants based on fatty acids and other natural hydrophobes. *Curr. Opin. Colloid Interface Sci.* 6, 178–188. doi:10.1016/S1359-0294(01)00076-0
- Johnson, D.R., Lee, T.K., Park, J., Fenner, K., Helbling, D.E., 2014. The functional and taxonomic richness of wastewater treatment plant microbial communities are associated with each other and with ambient nitrogen and carbon availability. *Environ. Microbiol.* n/a–n/a. doi:10.1111/1462-2920.12429
- Jonsson, S., Borén, H., 2002. Analysis of mono- and diesters of o-phthalic acid by solid-phase extractions with polystyrene–divinylbenzene-based polymers. *J. Chromatogr. A* 963, 393–400. doi:10.1016/S0021-9673(02)00647-7
- Jost, L., 2006. Entropy and diversity. *Oikos* 113, 363–375. doi:10.1111/j.2006.0030-1299.14714.x
- Ju, F., Zhang, T., 2015. *Experimental Design and Bioinformatics Analysis for the Application of Metagenomics in Environmental Sciences and Biotechnology.* *Environ. Sci. Technol.* 49, 12628–12640. doi:10.1021/acs.est.5b03719
- Junicke, H., Feldman, H., Van Loosdrecht, M.C.M., Kleerebezem, R., 2016. Limitation of syntrophic coculture growth by the acetogen. *Biotechnol. Bioeng.* 113, 560–567. doi:10.1002/bit.25816
- Junicke, H., Loosdrecht, M.C.M. van, Kleerebezem, R., 2016. Kinetic and thermodynamic control of butyrate conversion in non-defined methanogenic communities. *Appl. Microbiol. Biotechnol.* 100, 915–925. doi:10.1007/s00253-015-6971-9
- Kabouris, J.C., Tezel, U., Pavlostathis, S.G., Engelmann, M., Dulaney, J.A., Todd, A.C., Gillette, R.A., 2009. Mesophilic and Thermophilic Anaerobic Digestion of Municipal Sludge and Fat, Oil, and Grease. *Water Environ. Res.* 81, 476–485. doi:10.2175/106143008X357192
- Kang, D.D., Froula, J., Egan, R., Wang, Z., 2015. MetaBAT, an efficient tool for accurately reconstructing single genomes from complex microbial communities. *PeerJ* 3, e1165. doi:10.7717/peerj.1165
- Kanicky, J.R., Poniatowski, A.F., Mehta, N.R., Shah, D.O., 2000. Cooperativity among Molecules at Interfaces in Relation to Various Technological Processes: Effect of Chain Length on the pKa of Fatty Acid Salt Solutions†. *Langmuir* 16, 172–177. doi:10.1021/la990719o

- Kanicky, J.R., Shah, D.O., 2002. Effect of Degree, Type, and Position of Unsaturation on the pKa of Long-Chain Fatty Acids. *J. Colloid Interface Sci.* 256, 201–207. doi:10.1006/jcis.2001.8009
- Karlsson, A., Einarsson, P., Schnürer, A., Sundberg, C., Ejlertsson, J., Svensson, B.H., 2012. Impact of trace element addition on degradation efficiency of volatile fatty acids, oleic acid and phenyl acetate and on microbial populations in a biogas digester. *J. Biosci. Bioeng.* 114, 446–452. doi:10.1016/j.jbiosc.2012.05.010
- Karlsson, A., Ejlertsson, J., Nezirevic, D., Svensson, B.H., 1999. Degradation of phenol under meso- and thermophilic, anaerobic conditions. *Anaerobe* 5, 25–35. doi:10.1006/anae.1998.0187
- Karst, S.M., Kirkegaard, R.H., Albertsen, M., 2016. mmgenome: a toolbox for reproducible genome extraction from metagenomes. bioRxiv 059121. doi:10.1101/059121
- Keener, K.M., Ducoste, J.J., Holt, L.M., 2008. Properties influencing fat, oil, and grease deposit formation. *Water Environ. Res.* 80, 2241–2246.
- Kim, S.-H., Han, S.-K., Shin, H.-S., 2004. Kinetics of LCFA Inhibition on Acetoclastic Methanogenesis, Propionate Degradation and  $\beta$ -Oxidation. *J. Environ. Sci. Health Part A* 39, 1025–1037. doi:10.1081/ESE-120028411
- Kleerebezem, R., Van Loosdrecht, M.C., 2010. A generalized method for thermodynamic state analysis of environmental systems. *Crit. Rev. Environ. Sci. Technol.* 40, 1–54.
- Klindworth, A., Pruesse, E., Schweer, T., Peplies, J., Quast, C., Horn, M., Glöckner, F.O., 2013. Evaluation of general 16S ribosomal RNA gene PCR primers for classical and next-generation sequencing-based diversity studies. *Nucleic Acids Res.* 41, e1–e1. doi:10.1093/nar/gks808
- Koster, I.W., Cramer, A., 1987. Inhibition of Methanogenesis from Acetate in Granular Sludge by Long-Chain Fatty Acids. *Appl. Environ. Microbiol.* 53, 403–409.
- Kuhn, M., 2008. Caret package. *J. Stat. Softw.* 28.
- Laban, N.A., Tan, B., Dao, A., Foght, J., 2015. Draft Genome Sequence of Uncultivated Toluene-Degrading Desulfobulbaceae Bacterium Tol-SR, Obtained by Stable Isotope Probing Using [ $^{13}\text{C}$ ]Toluene. *Genome Announc.* 3, e01423–14. doi:10.1128/genomeA.01423-14
- Labatut, R.A., Angenent, L.T., Scott, N.R., 2011. Biochemical methane potential and biodegradability of complex organic substrates. *Bioresour. Technol.* 102, 2255–2264. doi:10.1016/j.biortech.2010.10.035
- Lalman, J.A., Bagley, D.M., 2001. Anaerobic degradation and methanogenic inhibitory effects of oleic and stearic acids. *Water Res.* 35, 2975–2983. doi:10.1016/S0043-1354(00)00593-5
- Lalman, J.A., Bagley, D.M., 2000. Anaerobic degradation and inhibitory effects of linoleic acid. *Water Res.* 34, 4220–4228. doi:10.1016/S0043-1354(00)00180-9
- Lalman, J., Bagley, D.M., 2002. Effects of C18 long chain fatty acids on glucose, butyrate and hydrogen degradation. *Water Res.* 36, 3307–3313. doi:10.1016/S0043-1354(02)00014-3
- LaRowe, D.E., Dale, A.W., Amend, J.P., Van Cappellen, P., 2012. Thermodynamic limitations on microbially catalyzed reaction rates. *Geochim. Cosmochim. Acta* 90, 96–109. doi:10.1016/j.gca.2012.05.011
- Lee, C., Kim, J., Hwang, K., O’Flaherty, V., Hwang, S., 2009. Quantitative analysis of methanogenic community dynamics in three anaerobic batch digesters treating different wastewaters. *Water Res.* 43, 157–165. doi:10.1016/j.watres.2008.09.032

- Lee, I.-S., Parameswaran, P., Rittmann, B.E., 2011. Effects of solids retention time on methanogenesis in anaerobic digestion of thickened mixed sludge. *Bioresour. Technol.* 102, 10266–10272. doi:10.1016/j.biortech.2011.08.079
- Lee, M.J., Zinder, S.H., 1988. Isolation and Characterization of a Thermophilic Bacterium Which Oxidizes Acetate in Syntrophic Association with a Methanogen and Which Grows Acetogenically on H<sub>2</sub>-CO<sub>2</sub>. *Appl. Environ. Microbiol.* 54, 124–129.
- Li, D., Liu, C.-M., Luo, R., Sadakane, K., Lam, T.-W., 2015. MEGAHIT: an ultra-fast single-node solution for large and complex metagenomics assembly via succinct de Bruijn graph. *Bioinformatics* 31, 1674–1676. doi:10.1093/bioinformatics/btv033
- Li, H., Chang, J., Liu, P., Fu, L., Ding, D., Lu, Y., 2015. Direct interspecies electron transfer accelerates syntrophic oxidation of butyrate in paddy soil enrichments. *Environ. Microbiol.* 17, 1533–1547. doi:10.1111/1462-2920.12576
- Li, H., Handsaker, B., Wysoker, A., Fennell, T., Ruan, J., Homer, N., Marth, G., Abecasis, G., Durbin, R., Subgroup, 1000 Genome Project Data Processing, 2009. The Sequence Alignment/Map format and SAMtools. *Bioinformatics* 25, 2078–2079. doi:10.1093/bioinformatics/btp352
- Liu, P., Qiu, Q., Lu, Y., 2011. Syntrophomonadaceae-Affiliated Species as Active Butyrate-Utilizing Syntrophs in Paddy Field Soil. *Appl. Environ. Microbiol.* 77, 3884–3887. doi:10.1128/AEM.00190-11
- Long, J.H., Aziz, T.N., Reyes III, F.L. de los, Ducoste, J.J., 2012. Anaerobic co-digestion of fat, oil, and grease (FOG): A review of gas production and process limitations. *Process Saf. Environ. Prot., Special Issue on Energy from Waste* 90, 231–245. doi:10.1016/j.psep.2011.10.001
- Lorowitz, W.H., Zhao, H., Bryan, M.P., 1989. *Syntrophomonas wolfei* subsp. *saponavida* subsp. nov., a Long-Chain Fatty-Acid-Degrading, Anaerobic, Syntrophic Bacterium; *Syntrophomonas wolfei* subsp. *wolfei* subsp. nov.; and Emended Descriptions of the Genus and Species. *Int. J. Syst. Evol. Microbiol.* 39, 122–126. doi:10.1099/00207713-39-2-122
- Louca, S., Doebeli, M., 2015. Calibration and analysis of genome-based models for microbial ecology. *eLife* 4, e08208. doi:10.7554/eLife.08208
- Louca, S., Parfrey, L.W., Doebeli, M., 2016. Decoupling function and taxonomy in the global ocean microbiome. *Science* 353, 1272–1277. doi:10.1126/science.aaf4507
- Love, M.I., Huber, W., Anders, S., 2014. Moderated estimation of fold change and dispersion for RNA-seq data with DESeq2. *Genome Biol.* 15, 1.
- Lovley, D.R., 1985. Minimum Threshold for Hydrogen Metabolism in Methanogenic Bacteria. *Appl. Environ. Microbiol.* 49, 1530–1531.
- Lozupone, C., Knight, R., 2005. UniFrac: a New Phylogenetic Method for Comparing Microbial Communities. *Appl. Environ. Microbiol.* 71, 8228–8235. doi:10.1128/AEM.71.12.8228-8235.2005
- Lueders, T., Pommerenke, B., Friedrich, M.W., 2004. Stable-Isotope Probing of Microorganisms Thriving at Thermodynamic Limits: Syntrophic Propionate Oxidation in Flooded Soil. *Appl. Environ. Microbiol.* 70, 5778–5786. doi:10.1128/AEM.70.10.5778-5786.2004
- Luostarinen, S., Luste, S., Sillanpää, M., 2009. Increased biogas production at wastewater treatment plants through co-digestion of sewage sludge with grease trap sludge from a meat processing plant. *Bioresour. Technol.* 100, 79–85. doi:10.1016/j.biortech.2008.06.029

- Mabrouk, A.F., Jr, L.R.D., 1961. Solubility of linoleic acid in aqueous solutions and its reaction with water. *J. Am. Oil Chem. Soc.* 38, 9–13. doi:10.1007/BF02633110
- Mata, J.A., Martínez-Cánovas, J., Quesada, E., Béjar, V., 2002. A Detailed Phenotypic Characterisation of the Type Strains of Halomonas Species. *Syst. Appl. Microbiol.* 25, 360–375. doi:10.1078/0723-2020-00122
- McInerney, M.J., 1992. The genus *Syntrophomonas*, and other syntrophic bacteria. *Prokaryotes* Springer N. Y. NY 2048–2057.
- McInerney, M.J., Bryant, M.P., Pfennig, N., 1979. Anaerobic bacterium that degrades fatty acids in syntrophic association with methanogens. *Arch. Microbiol.* 122, 129–135. doi:10.1007/BF00411351
- McInerney, M.J., Sieber, J.R., Gunsalus, R.P., 2009. Syntrophy in Anaerobic Global Carbon Cycles. *Curr. Opin. Biotechnol.* 20, 623–632. doi:10.1016/j.copbio.2009.10.001
- McMahon, K., 2001. Anaerobic codigestion of municipal solid waste and biosolids under various mixing conditions—II: microbial population dynamics. *Water Res.* 35, 1817–1827. doi:10.1016/S0043-1354(00)00438-3
- McMahon, K.D., Martin, H.G., Hugenholtz, P., 2007. Integrating ecology into biotechnology. *Curr. Opin. Biotechnol., Energy biotechnology / Environmental biotechnology* 18, 287–292. doi:10.1016/j.copbio.2007.04.007
- McMahon, K.D., Zheng, D., Stams, A.J.M., Mackie, R.I., Raskin, L., 2004. Microbial population dynamics during start-up and overload conditions of anaerobic digesters treating municipal solid waste and sewage sludge. *Biotechnol. Bioeng.* 87, 823–834. doi:10.1002/bit.20192
- Menes, R.J., Travers, D., 2006. Detection of fatty acid beta-oxidizing syntrophic bacteria by fluorescence in situ hybridization. *Water Sci. Technol.* 54, 33. doi:10.2166/wst.2006.483
- Mulat, D.G., Jacobi, H.F., Feilberg, A., Adamsen, A.P.S., Richnow, H.-H., Nikolausz, M., 2016. Changing Feeding Regimes To Demonstrate Flexible Biogas Production: Effects on Process Performance, Microbial Community Structure, and Methanogenesis Pathways. *Appl. Environ. Microbiol.* 82, 438–449. doi:10.1128/AEM.02320-15
- Narihiro, T., Terada, T., Ohashi, A., Kamagata, Y., Nakamura, K., Sekiguchi, Y., 2012. Quantitative detection of previously characterized syntrophic bacteria in anaerobic wastewater treatment systems by sequence-specific rRNA cleavage method. *Water Res.* 46, 2167–2175. doi:10.1016/j.watres.2012.01.034
- Neufeld, J.D., Dumont, M.G., Vohra, J., Murrell, J.C., 2006. Methodological Considerations for the Use of Stable Isotope Probing in. *Microb. Ecol.* 53, 435–442. doi:10.1007/s00248-006-9125-x
- Nielsen, H.B., Ahring, B.K., 2006. Responses of the biogas process to pulses of oleate in reactors treating mixtures of cattle and pig manure. *Biotechnol. Bioeng.* 95, 96–105. doi:10.1002/bit.20963
- Noutsopoulos, C., Mamais, D., Antoniou, K., Avramides, C., Oikonomopoulos, P., Fountoulakis, I., 2013. Anaerobic co-digestion of grease sludge and sewage sludge: The effect of organic loading and grease sludge content. *Bioresour. Technol.* 131, 452–459. doi:10.1016/j.biortech.2012.12.193
- Oksanen, J., Kindt, R., Legendre, P., O’Hara, B., Stevens, M.H.H., Oksanen, M.J., Suggests, M., 2007. The vegan package. *Community Ecol. Package* 631–637.

- Palatsi, J., Affes, R., Fernandez, B., Pereira, M.A., Alves, M.M., Flotats, X., 2012. Influence of adsorption and anaerobic granular sludge characteristics on long chain fatty acids inhibition process. *Water Res.* 46, 5268–5278. doi:10.1016/j.watres.2012.07.008
- Palatsi, J., Illa, J., Prenafeta-Boldú, F.X., Laureni, M., Fernandez, B., Angelidaki, I., Flotats, X., 2010. Long-chain fatty acids inhibition and adaptation process in anaerobic thermophilic digestion: Batch tests, microbial community structure and mathematical modelling. *Bioresour. Technol.* 101, 2243–2251. doi:10.1016/j.biortech.2009.11.069
- Palatsi, J., Laureni, M., Andrés, M.V., Flotats, X., Nielsen, H.B., Angelidaki, I., 2009. Strategies for recovering inhibition caused by long chain fatty acids on anaerobic thermophilic biogas reactors. *Bioresour. Technol.* 100, 4588–4596. doi:10.1016/j.biortech.2009.04.046
- Parada, A.E., Needham, D.M., Fuhrman, J.A., 2016. Every base matters: assessing small subunit rRNA primers for marine microbiomes with mock communities, time series and global field samples. *Environ. Microbiol.* 18, 1403–1414. doi:10.1111/1462-2920.13023
- Parks, D.H., Imelfort, M., Skennerton, C.T., Hugenholtz, P., Tyson, G.W., 2015. CheckM: assessing the quality of microbial genomes recovered from isolates, single cells, and metagenomes. *Genome Res.* 25, 1043–1055. doi:10.1101/gr.186072.114
- Pereira, M.A., Cavaleiro, A.J., Mota, M., Alves, M.M., 2003. Accumulation of long chain fatty acids onto anaerobic sludge under steady state and shock loading conditions: effect on acetogenic and methanogenic activity.
- Pereira, M. a., Pires, O. C., Mota, M., Alves, M. M., 2005. Anaerobic biodegradation of oleic and palmitic acids: Evidence of mass transfer limitations caused by long chain fatty acid accumulation onto the anaerobic sludge. *Biotechnol. Bioeng.* 92, 15–23. doi:10.1002/bit.20548
- Pereira, M.A., Pires, O.C., Mota, M., Alves, M.M., 2002. Anaerobic degradation of oleic acid by suspended and granular sludge: identification of palmitic acid as a key intermediate. *Water Sci. Technol. J. Int. Assoc. Water Pollut. Res.* 45, 139–144.
- Pereira, M. A., Sousa, D. Z., Mota, M., Alves, M. M., 2004. Mineralization of LCFA associated with anaerobic sludge: Kinetics, enhancement of methanogenic activity, and effect of VFA. *Biotechnol. Bioeng.* 88, 502–511. doi:10.1002/bit.20278
- Phelps, T.J., Conrad, R., Zeikus, J.G., 1985. Sulfate-Dependent Interspecies H<sub>2</sub> Transfer between *Methanosarcina barkeri* and *Desulfovibrio vulgaris* during Coculture Metabolism of Acetate or Methanol. *Appl. Environ. Microbiol.* 50, 589–594.
- Pramanik, A., Pawar, S., Antonian, E., Schulz, H., 1979. Five different enzymatic activities are associated with the multienzyme complex of fatty acid oxidation from *Escherichia coli*. *J. Bacteriol.* 137, 469–473.
- Props, R., Kerckhof, F.-M., Rubbens, P., Vrieze, J.D., Sanabria, E.H., Waegeman, W., Monsieurs, P., Hammes, F., Boon, N., 2016. Absolute quantification of microbial taxon abundances. *ISME J.* doi:10.1038/ismej.2016.117
- Quéménéur, M., Marty, Y., 1994. Fatty acids and sterols in domestic wastewaters. *Water Res.* 28, 1217–1226. doi:10.1016/0043-1354(94)90210-0
- Radajewski, S., Ineson, P., Parekh, N.R., Murrell, J.C., 2000. Stable-isotope probing as a tool in microbial ecology. *Nature* 403, 646–649. doi:10.1038/35001054
- Ralston, A.W., Hoerr, C.W., 1942. The Solubilities of the Normal Saturated Fatty Acids. *J. Org. Chem.* 07, 546–555. doi:10.1021/jo01200a013

- Regmi, P., Bunce, R., Miller, M.W., Park, H., Chandran, K., Wett, B., Murthy, S., Bott, C.B., 2015. Ammonia-based intermittent aeration control optimized for efficient nitrogen removal. *Biotechnol. Bioeng.* 112, 2060–2067.
- Regueiro, L., Lema, J.M., Carballa, M., 2015. Key microbial communities steering the functioning of anaerobic digesters during hydraulic and organic overloading shocks. *Bioresour. Technol.* 197, 208–216. doi:10.1016/j.biortech.2015.08.076
- Ren, Y., Aguirre, J., Ntamack, A.G., Chu, C., Schulz, H., 2004. An Alternative Pathway of Oleate  $\beta$ -Oxidation in *Escherichia coli* Involving the Hydrolysis of a Dead End Intermediate by a Thioesterase. *J. Biol. Chem.* 279, 11042–11050. doi:10.1074/jbc.M310032200
- Rinzema, A., Boone, M., Knippenberg, K. van, Lettinga, G., 1994. Bactericidal Effect of Long Chain Fatty Acids in Anaerobic Digestion. *Water Environ. Res.* 66, 40–49.
- Rittmann, B.E., Hausner, M., Löffler, F., Love, N.G., Muyzer, G., Okabe, S., Oerther, D.B., Peccia, J., Raskin, L., Wagner, M., 2006. A vista for microbial ecology and environmental biotechnology. *Environ. Sci. Technol.* 40, 1096–1103.
- Roy, F., Albagnac, G., Samain, E., 1985. Influence of Calcium Addition on Growth of Highly Purified Syntrophic Cultures Degrading Long-Chain Fatty Acids. *Appl. Environ. Microbiol.* 49, 702–705.
- Saidi-Mehrabad, A., He, Z., Tamas, I., Sharp, C.E., Brady, A.L., Rochman, F.F., Bodrossy, L., Abell, G.C., Penner, T., Dong, X., Sensen, C.W., Dunfield, P.F., 2013. Methanotrophic bacteria in oilsands tailings ponds of northern Alberta. *ISME J.* 7, 908–921. doi:10.1038/ismej.2012.163
- Salvador, A.F., Cavaleiro, A.J., Sousa, D.Z., Alves, M.M., Pereira, M.A., 2013. Endurance of methanogenic archaea in anaerobic bioreactors treating oleate-based wastewater. *Appl. Microbiol. Biotechnol.* 97, 2211–2218. doi:10.1007/s00253-012-4061-9
- Schink, B., 1997. Energetics of syntrophic cooperation in methanogenic degradation. *Microbiol. Mol. Biol. Rev.* 61, 262–280.
- Schmidt, A., Müller, N., Schink, B., Schleheck, D., 2013. A Proteomic View at the Biochemistry of Syntrophic Butyrate Oxidation in *Syntrophomonas wolfei*. *PLoS ONE* 8, e56905. doi:10.1371/journal.pone.0056905
- Schnürer, A., Schink, B., Svensson, B.H., 1996. *Clostridium ultunense* sp. nov., a Mesophilic Bacterium Oxidizing Acetate in Syntrophic Association with a Hydrogenotrophic Methanogenic Bacterium. *Int. J. Syst. Bacteriol.* 46, 1145–1152. doi:10.1099/00207713-46-4-1145
- Segata, N., Börnigen, D., Morgan, X.C., Huttenhower, C., 2013. PhyloPhlAn is a new method for improved phylogenetic and taxonomic placement of microbes. *Nat. Commun.* 4. doi:10.1038/ncomms3304
- Sekiguchi, Y., Kamagata, Y., Nakamura, K., Ohashi, A., Harada, H., 2000. *Syntrophothermus lipocalidus* gen. nov., sp. nov., a novel thermophilic, syntrophic, fatty-acid-oxidizing anaerobe which utilizes isobutyrate. *Int. J. Syst. Evol. Microbiol.* 50, 771–779. doi:10.1099/00207713-50-2-771
- Shade, A., 2016. Diversity is the question, not the answer. *ISME J.* doi:10.1038/ismej.2016.118
- Shigematsu, T., Tang, Y., Mizuno, Y., Kawaguchi, H., Morimura, S., Kida, K., 2006. Microbial diversity of mesophilic methanogenic consortium that can degrade long-chain fatty acids in chemostat cultivation. *J. Biosci. Bioeng.* 102, 535–544. doi:10.1263/jbb.102.535

- Sieber, J.R., Crable, B.R., Sheik, C.S., Hurst, G.B., Rohlin, L., Gunsalus, R.P., McInerney, M.J., 2015. Proteomic analysis reveals metabolic and regulatory systems involved in the syntrophic and axenic lifestyle of *Syntrophomonas wolfei*. *Front. Microbiol.* 6.
- Sieber, J.R., Le, H.M., McInerney, M.J., 2014. The importance of hydrogen and formate transfer for syntrophic fatty, aromatic and alicyclic metabolism. *Environ. Microbiol.* 16, 177–188. doi:10.1111/1462-2920.12269
- Sieber, J.R., McInerney, M.J., Gunsalus, R.P., 2012. Genomic Insights into Syntrophy: The Paradigm for Anaerobic Metabolic Cooperation. *Annu. Rev. Microbiol.* 66, 429–452. doi:10.1146/annurev-micro-090110-102844
- Sieber, J.R., Sims, D.R., Han, C., Kim, E., Lykidis, A., Lapidus, A.L., McDonnald, E., Rohlin, L., Culley, D.E., Gunsalus, R., McInerney, M.J., 2010. The genome of *Syntrophomonas wolfei*: new insights into syntrophic metabolism and biohydrogen production. *Environ. Microbiol.* 12, 2289–2301. doi:10.1111/j.1462-2920.2010.02237.x
- Silva, S.A., Cavaleiro, A.J., Pereira, M.A., Stams, A.J.M., Alves, M.M., Sousa, D.Z., 2014. Long-term acclimation of anaerobic sludges for high-rate methanogenesis from LCFA. *Biomass Bioenergy* 67, 297–303. doi:10.1016/j.biombioe.2014.05.012
- Silva, S.A., Salvador, A.F., Cavaleiro, A.J., Pereira, M.A., Stams, A.J.M., Alves, M.M., Sousa, D.Z., 2016. Toxicity of long chain fatty acids towards acetate conversion by *Methanosaeta concilii* and *Methanosarcina mazei*. *Microb. Biotechnol.* 9, 514–518. doi:10.1111/1751-7915.12365
- Silvestre, G., Illa, J., Fernández, B., Bonmatí, A., 2014. Thermophilic anaerobic co-digestion of sewage sludge with grease waste: Effect of long chain fatty acids in the methane yield and its dewatering properties. *Appl. Energy* 117, 87–94. doi:10.1016/j.apenergy.2013.11.075
- Silvestre, G., Rodríguez-Abalde, A., Fernández, B., Flotats, X., Bonmatí, A., 2011. Biomass adaptation over anaerobic co-digestion of sewage sludge and trapped grease waste. *Bioresour. Technol.* 102, 6830–6836. doi:10.1016/j.biortech.2011.04.019
- Singh, P., Kansal, A., Carliell-Marquet, C., 2016. Energy and carbon footprints of sewage treatment methods. *J. Environ. Manage.* 165, 22–30. doi:10.1016/j.jenvman.2015.09.017
- Smith, A.L., Skerlos, S.J., Raskin, L., 2015. Anaerobic membrane bioreactor treatment of domestic wastewater at psychrophilic temperatures ranging from 15° C to 3° C. *Environ. Sci. Water Res. Technol.* 1, 56–64.
- Soliva, C.R., Meile, L., Cieślak, A., Kreuzer, M., Machmüller, A., 2004. Rumen simulation technique study on the interactions of dietary lauric and myristic acid supplementation in suppressing ruminal methanogenesis. *Br. J. Nutr.* 92, 689–700. doi:10.1079/BJN20041250
- Sousa, D.Z., Pereira, M.A., Smidt, H., Stams, A.J.M., Alves, M.M., 2007a. Molecular assessment of complex microbial communities degrading long chain fatty acids in methanogenic bioreactors. *FEMS Microbiol. Ecol.* 60, 252–265. doi:10.1111/j.1574-6941.2007.00291.x
- Sousa, D.Z., Salvador, A.F., Ramos, J., Guedes, A.P., Barbosa, S., Stams, A.J.M., Alves, M.M., Pereira, M.A., 2013. Activity and Viability of Methanogens in Anaerobic Digestion of Unsaturated and Saturated Long-Chain Fatty Acids. *Appl. Environ. Microbiol.* 79, 4239–4245. doi:10.1128/AEM.00035-13

- Sousa, D.Z., Smidt, H., Alves, M.M., Stams, A.J.M., 2009. Ecophysiology of syntrophic communities that degrade saturated and unsaturated long-chain fatty acids. *FEMS Microbiol. Ecol.* 68, 257–272. doi:10.1111/j.1574-6941.2009.00680.x
- Sousa, D.Z., Smidt, H., Alves, M.M., Stams, A.J.M., 2007b. *Syntrophomonas zehnderi* sp. nov., an anaerobe that degrades long-chain fatty acids in co-culture with *Methanobacterium formicum*. *Int. J. Syst. Evol. Microbiol.* 57, 609–615. doi:10.1099/ijs.0.64734-0
- Stams, A.J.M., Plugge, C.M., 2009. Electron transfer in syntrophic communities of anaerobic bacteria and archaea. *Nat. Rev. Microbiol.* 7, 568–577. doi:10.1038/nrmicro2166
- Stams, A.J.M., Sousa, D.Z., Kleerebezem, R., Plugge, C.M., 2012. Role of syntrophic microbial communities in high-rate methanogenic bioreactors. *Water Sci. Technol.* 66, 352. doi:10.2166/wst.2012.192
- Sundberg, C., Al-Soud, W.A., Larsson, M., Alm, E., Yekta, S.S., Svensson, B.H., Sørensen, S.J., Karlsson, A., 2013. 454 pyrosequencing analyses of bacterial and archaeal richness in 21 full-scale biogas digesters. *FEMS Microbiol. Ecol.* 85, 612–626. doi:10.1111/1574-6941.12148
- Svetlitsnyi, V., Rainey, F., Wiegel, J., 1996. *Thermosyntropha lipolytica* gen. nov., sp. nov., a Lipolytic, Anaerobic, Alkalitolerant, Thermophilic Bacterium Utilizing Short- and Long-Chain Fatty Acids in Syntrophic Coculture with a Methanogenic Archaeum. *Int. J. Syst. Bacteriol.* 46, 1131–1137. doi:10.1099/00207713-46-4-1131
- Thauer, R.K., Jungermann, K., Decker, K., 1977. Energy conservation in chemotrophic anaerobic bacteria. *Bacteriol. Rev.* 41, 100–180.
- Treu, L., Campanaro, S., Kougias, P.G., Zhu, X., Angelidaki, I., 2016a. Untangling the Effect of Fatty Acid Addition at Species Level Revealed Different Transcriptional Responses of the Biogas Microbial Community Members. *Environ. Sci. Technol.* 50, 6079–6090. doi:10.1021/acs.est.6b00296
- Treu, L., Kougias, P.G., Campanaro, S., Bassani, I., Angelidaki, I., 2016b. Deeper insight into the structure of the anaerobic digestion microbial community; the biogas microbiome database is expanded with 157 new genomes. *Bioresour. Technol.* 216, 260–266. doi:10.1016/j.biortech.2016.05.081
- Urakawa, H., Martens-Habbena, W., Stahl, D.A., 2010. High Abundance of Ammonia-Oxidizing Archaea in Coastal Waters, Determined Using a Modified DNA Extraction Method. *Appl. Environ. Microbiol.* 76, 2129–2135. doi:10.1128/AEM.02692-09
- U.S. DOE, 2010. Annual Energy Outlook.
- Vanwonterghem, I., Jensen, P.D., Ho, D.P., Batstone, D.J., Tyson, G.W., 2014. Linking microbial community structure, interactions and function in anaerobic digesters using new molecular techniques. *Curr. Opin. Biotechnol., Energy biotechnology • Environmental biotechnology* 27, 55–64. doi:10.1016/j.copbio.2013.11.004
- Vanwonterghem, I., Jensen, P.D., Rabaey, K., Tyson, G.W., 2016. Genome-centric resolution of microbial diversity, metabolism and interactions in anaerobic digestion. *Environ. Microbiol.* 18, 3144–3158. doi:10.1111/1462-2920.13382
- Verastegui, Y., Cheng, J., Engel, K., Kolczynski, D., Mortimer, S., Lavigne, J., Montalibet, J., Romantsov, T., Hall, M., McConkey, B.J., Rose, D.R., Tomashek, J.J., Scott, B.R., Charles, T.C., Neufeld, J.D., 2014. Multisubstrate Isotope Labeling and Metagenomic Analysis of Active Soil Bacterial Communities. *mBio* 5, e01157–14. doi:10.1128/mBio.01157-14



- Vital, M., Howe, A.C., Tiedje, J.M., 2014. Revealing the Bacterial Butyrate Synthesis Pathways by Analyzing (Meta)genomic Data. *mBio* 5, e00889–14. doi:10.1128/mBio.00889-14
- Vuono, D.C., Benecke, J., Henkel, J., Navidi, W.C., Cath, T.Y., Munakata-Marr, J., Spear, J.R., Drewes, J.E., 2015. Disturbance and temporal partitioning of the activated sludge metacommunity. *ISME J.* 9, 425–435. doi:10.1038/ismej.2014.139
- Wan, C., Zhou, Q., Fu, G., Li, Y., 2011. Semi-continuous anaerobic co-digestion of thickened waste activated sludge and fat, oil and grease. *Waste Manag.* 31, 1752–1758. doi:10.1016/j.wasman.2011.03.025
- Wang, L., Aziz, T.N., de los Reyes, F.L., 2013. Determining the limits of anaerobic co-digestion of thickened waste activated sludge with grease interceptor waste. *Water Res.* 47, 3835–3844. doi:10.1016/j.watres.2013.04.003
- Wang, Q., Garrity, G.M., Tiedje, J.M., Cole, J.R., 2007. Naïve Bayesian Classifier for Rapid Assignment of rRNA Sequences into the New Bacterial Taxonomy. *Appl. Environ. Microbiol.* 73, 5261–5267. doi:10.1128/AEM.00062-07
- Warikoo, V., McInerney, M.J., Robinson, J.A., Suflita, J.M., 1996. Interspecies acetate transfer influences the extent of anaerobic benzoate degradation by syntrophic consortia. *Appl. Environ. Microbiol.* 62, 26–32.
- Waterhouse, A.M., Procter, J.B., Martin, D.M.A., Clamp, M., Barton, G.J., 2009. Jalview Version 2—a multiple sequence alignment editor and analysis workbench. *Bioinformatics* 25, 1189–1191. doi:10.1093/bioinformatics/btp033
- Weng, C., Jeris, J.S., 1976. Biochemical mechanisms in the methane fermentation of glutamic and oleic acids. *Water Res.* 10, 9–18. doi:10.1016/0043-1354(76)90151-2
- Werner, J.J., Garcia, M.L., Perkins, S.D., Yarasheski, K.E., Smith, S.R., Muegge, B.D., Stadermann, F.J., DeRito, C.M., Floss, C., Madsen, E.L., Gordon, J.I., Angenent, L.T., 2014. Microbial Community Dynamics and Stability during an Ammonia-Induced Shift to Syntrophic Acetate Oxidation. *Appl. Environ. Microbiol.* 80, 3375–3383. doi:10.1128/AEM.00166-14
- Werner, J.J., Knights, D., Garcia, M.L., Scalfone, N.B., Smith, S., Yarasheski, K., Cummings, T.A., Beers, A.R., Knight, R., Angenent, L.T., 2011. Bacterial community structures are unique and resilient in full-scale bioenergy systems. *Proc. Natl. Acad. Sci.* 108, 4158–4163. doi:10.1073/pnas.1015676108
- Westerholm, M., Dolfing, J., Sherry, A., Gray, N.D., Head, I.M., Schnürer, A., 2011. Quantification of syntrophic acetate-oxidizing microbial communities in biogas processes. *Environ. Microbiol. Rep.* 3, 500–505. doi:10.1111/j.1758-2229.2011.00249.x
- Wiltsee, G., 1998. Urban waste grease resource assessment. National Renewable Energy Laboratory.
- Wittebolle, L., Marzorati, M., Clement, L., Balloi, A., Daffonchio, D., Heylen, K., De Vos, P., Verstraete, W., Boon, N., 2009. Initial community evenness favours functionality under selective stress. *Nature* 458, 623–626. doi:10.1038/nature07840
- Wittebolle, L., Vervaeren, H., Verstraete, W., Boon, N., 2008. Quantifying Community Dynamics of Nitrifiers in Functionally Stable Reactors. *Appl. Environ. Microbiol.* 74, 286–293. doi:10.1128/AEM.01006-07
- Wittwer, C.T., Herrmann, M.G., Moss, A.A., Rasmussen, R.P., 1997. Continuous fluorescence monitoring of rapid cycle DNA amplification. *Biotechniques* 22, 130–139.
- Wu, C., Dong, X., Liu, X., 2007. *Syntrophomonas wolfei* subsp. *methylbutyratica* subsp. nov., and assignment of *Syntrophomonas wolfei* subsp. *saponavida* to *Syntrophomonas*

- saponavida sp. nov. comb. nov. Syst. Appl. Microbiol. 30, 376–380.  
doi:10.1016/j.syapm.2006.12.001
- Wu, C., Liu, X., Dong, X., 2006. Syntrophomonas erecta subsp. sporosyntropha subsp. nov., a spore-forming bacterium that degrades short chain fatty acids in co-culture with methanogens. Syst. Appl. Microbiol. 29, 457–462. doi:10.1016/j.syapm.2006.01.003
- Yalcinkaya, S., Malina, J.F., 2015. Anaerobic co-digestion of municipal wastewater sludge and un-dewatered grease trap waste for assessing direct feed of grease trap waste in municipal digesters. Int. Biodeterior. Biodegrad. 104, 490–497. doi:10.1016/j.ibiod.2015.08.007
- Yamada, T., Sekiguchi, Y., 2009. Cultivation of Uncultured *Chloroflexi* Subphyla: Significance and Ecophysiology of Formerly Uncultured *Chloroflexi* “Subphylum I” with Natural and Biotechnological Relevance. Microbes Environ. 24, 205–216.  
doi:10.1264/jsme2.ME09151S
- Yu, Y., Lee, C., Kim, J., Hwang, S., 2005. Group-specific primer and probe sets to detect methanogenic communities using quantitative real-time polymerase chain reaction. Biotechnol. Bioeng. 89, 670–679. doi:10.1002/bit.20347
- Zamanzadeh, M., Parker, W.J., Verastegui, Y., Neufeld, J.D., 2013. Biokinetics and bacterial communities of propionate oxidizing bacteria in phased anaerobic sludge digestion systems. Water Res. 47, 1558–1569. doi:10.1016/j.watres.2012.12.015
- Zengler, K., Richnow, H.H., Rosselló-Mora, R., Michaelis, W., Widdel, F., 1999. Methane formation from long-chain alkanes by anaerobic microorganisms. Nature 401, 266–269.  
doi:10.1038/45777
- Zhang, C., Liu, X., Dong, X., 2005. Syntrophomonas erecta sp. nov., a novel anaerobe that syntrophically degrades short-chain fatty acids. Int. J. Syst. Evol. Microbiol. 55, 799–803. doi:10.1099/ijs.0.63372-0
- Zhang, C., Liu, X., Dong, X., 2004. Syntrophomonas curvata sp. nov., an anaerobe that degrades fatty acids in co-culture with methanogens. Int. J. Syst. Evol. Microbiol. 54, 969–973.  
doi:10.1099/ijs.0.02903-0
- Zhang, F., Liu, X., Dong, X., 2012. Thermosyntropha tengcongensis sp. nov., a thermophilic bacterium that degrades long-chain fatty acids syntrophically. Int. J. Syst. Evol. Microbiol. 62, 759–763. doi:10.1099/ijs.0.033456-0
- Zhang, T., Shao, M.-F., Ye, L., 2012. 454 Pyrosequencing reveals bacterial diversity of activated sludge from 14 sewage treatment plants. ISME J. 6, 1137–1147.  
doi:10.1038/ismej.2011.188
- Zhao, H., Yang, D., Woese, C.R., Bryant, M.P., 1993. Assignment of Fatty Acid- $\beta$ -Oxidizing Syntrophic Bacteria to Syntrophomonadaceae fam. nov. on the Basis of 16S rRNA Sequence Analyses. Int. J. Syst. Bacteriol. 43, 278–286. doi:10.1099/00207713-43-2-278
- Ziels, R.M., Beck, D.A.C., Martí, M., Gough, H.L., Stensel, H.D., Svensson, B.H., 2015. Monitoring the dynamics of syntrophic  $\beta$ -oxidizing bacteria during anaerobic degradation of oleic acid by quantitative PCR. FEMS Microbiol. Ecol. 91, fiv028.  
doi:10.1093/femsec/fiv028
- Ziels, R.M., Karlsson, A., Beck, D.A.C., Ejlertsson, J., Yekta, S.S., Bjorn, A., Stensel, H.D., Svensson, B.H., 2016. Microbial community adaptation influences long-chain fatty acid conversion during anaerobic codigestion of fats, oils, and grease with municipal sludge. Water Res. 103, 372–382. doi:10.1016/j.watres.2016.07.043

Zonta, Ž., Alves, M.M., Flotats, X., Palatsi, J., 2013. Modelling inhibitory effects of long chain fatty acids in the anaerobic digestion process. *Water Res.* 47, 1369–1380.  
doi:10.1016/j.watres.2012.12.007

# APPENDIX A

## Supplemental Information for Chapter 3:

### Monitoring the Dynamics of Syntrophic $\beta$ -Oxidizing Bacteria During Anaerobic Degradation of Oleic Acid by Quantitative PCR

**Number of Pages:** 13

**Number of Tables:** 2

**Number of Figures:** 11

#### Contents

Supplemental Table A1: Characteristics of qPCR primers and probes.....	A2
Supplemental Table A2: Intermediate metabolites of LCFA degradation.....	A3
Supplemental Figure A1: Specificity testing of <i>Syntrophomonas</i> qPCR assay.....	A4
Supplemental Figure A2: Specificity testing of <i>Syntrophus</i> qPCR assay.....	A5
Supplemental Figure A3: Calibration curve for <i>Syntrophomonas</i> qPCR assay.....	A6
Supplemental Figure A4: Calibration curve for <i>Syntrophus</i> qPCR assay.....	A6
Supplemental Figure A5: Spiked calibration curve for <i>Syntrophomonas</i> qPCR assay validation	A7
Supplemental Figure A6: Spiked bioreactor samples for <i>Syntrophomonas</i> qPCR assay validation..	A8
Supplemental Figure A7: Spiked calibration curve for <i>Syntrophus</i> qPCR assay validation..	A9
Supplemental Figure A8: qPCR of methanogenic archaeal targets.....	A10
Supplemental Figure A9: Community richness, evenness, and Unifrac distances.....	A11
Supplemental Figure A10: Phylogenetic tree of <i>Syntrophomonas</i> OTUs.....	A12
Supplemental Figure A11: Comparison of predictions by Illumina sequencing and qPCR...	A13

**Supplemental Table A1:** Characteristics and performance of all qPCR primer/probe sets used in this study

Oligo. Name <sup>1</sup>	Target Group	Sequence	Refs.	Reference Sequence <sup>2</sup>	Calibration Slope <sup>3</sup>	Calibration Intercept <sup>3</sup>
Sym-678 (F)	<i>Syntrophomonas</i>	CCWGGTGTAGCGGT	This study	<i>Syntrophomonas zehnderi</i> OL-4 (NR_044008.1)	-3.30	38.7
Sym-696 (P)		TGCGTAGAAATCAGGAGGAAYACCAGT				
Sym-738 (R)		TCAGGGYCAGTCCAG				
Syntr-441 (F)	<i>Syntrophus</i>	GGTGGGAAGAAATGTATKGA	This study	<i>Syntrophus aciditrophicus</i> SB (NR_102776.1)	-3.32	38.8
Syntr-462 (P)		TTAAYAGCCTTTGTACTTGACGGTAC				
Syntr-559 (R)		CTCTTTACGCCCAATGAT				
BAC-338 (F)	Bacteria	ACTCCTACGGGAGGCAG	Yu et al., 2005 <sup>4</sup>	<i>Methylocella silvestris</i> BL2 (NR_074237.1)	-3.41	39.1
BAC-516 (P)		TGCCAGCAGCCGCGGTAATAC				
BAC-805 (R)		GACTACCAGGGTATCTAATCC				
Msc-380 (F)	<i>Methanosarcinaceae</i>	GAAACCGYGATAAGGGGA	Yu et al., 2005	<i>Methanosarcina barkeri</i> DSM800 (NR_025303.1)	-3.51	39.3
Msc-492 (P)		TTAGCAAGGGCCGGGCAA				
Msc-828 (R)		TAGCGARCATCGTTTACG				
Mst-702 (F)	<i>Methanosaetaceae</i>	TAATCCTYGARGGACCACCA	Yu et al., 2005	<i>Methanosaeta concilii</i> Opfikon (NR_028242.1)	-3.58	41.1
Mst-753 (P)		ACGGCAAGGGACGAAAGCTAGG				
Mst-862 (R)		CCTACGGCACCRACMAC				
MBT-857 (F)	<i>Methanobacteriales</i>	CGWAGGGAAGCTGTAAAGT	Yu et al., 2005	<i>Methanobacterium formicicum</i> DSMZ1535 (NR_025028.1)	-3.49	38.9
MBT-929 (P)		AGCACCACAACGCGTGGA				
MBT-1196 (R)		TACCGTCGTCCACTCCTT				
MMB-282 (F)	<i>Methanomicrobiales</i>	ATCGRTACGGGTTGTGGG	Yu et al., 2005	<i>Methanoculleus bourgensis</i> MS2 (NR_042786.1)	-3.41	41.6
MMB-749 (P)		TYCGACAGTGAGGRACGAAAGCTG				
MMB-832 (R)		CACCTAACGCRCATHGTTTAC				
MCC-495 (F)	<i>Methanococcales</i>	TAAGGGCTGGGCAAGT	Yu et al., 2005	<i>Methanococcus voltae</i> (U38461.1)	-3.83	44.3
MCC-686 (P)		TAGCGGTGRAATGYGTTGATCC				
MCC-832 (R)		CACCTAGTYCGCARAGTTTA				

<sup>1</sup> F = forward primer; P = hydrolysis probe; R = reverse primer

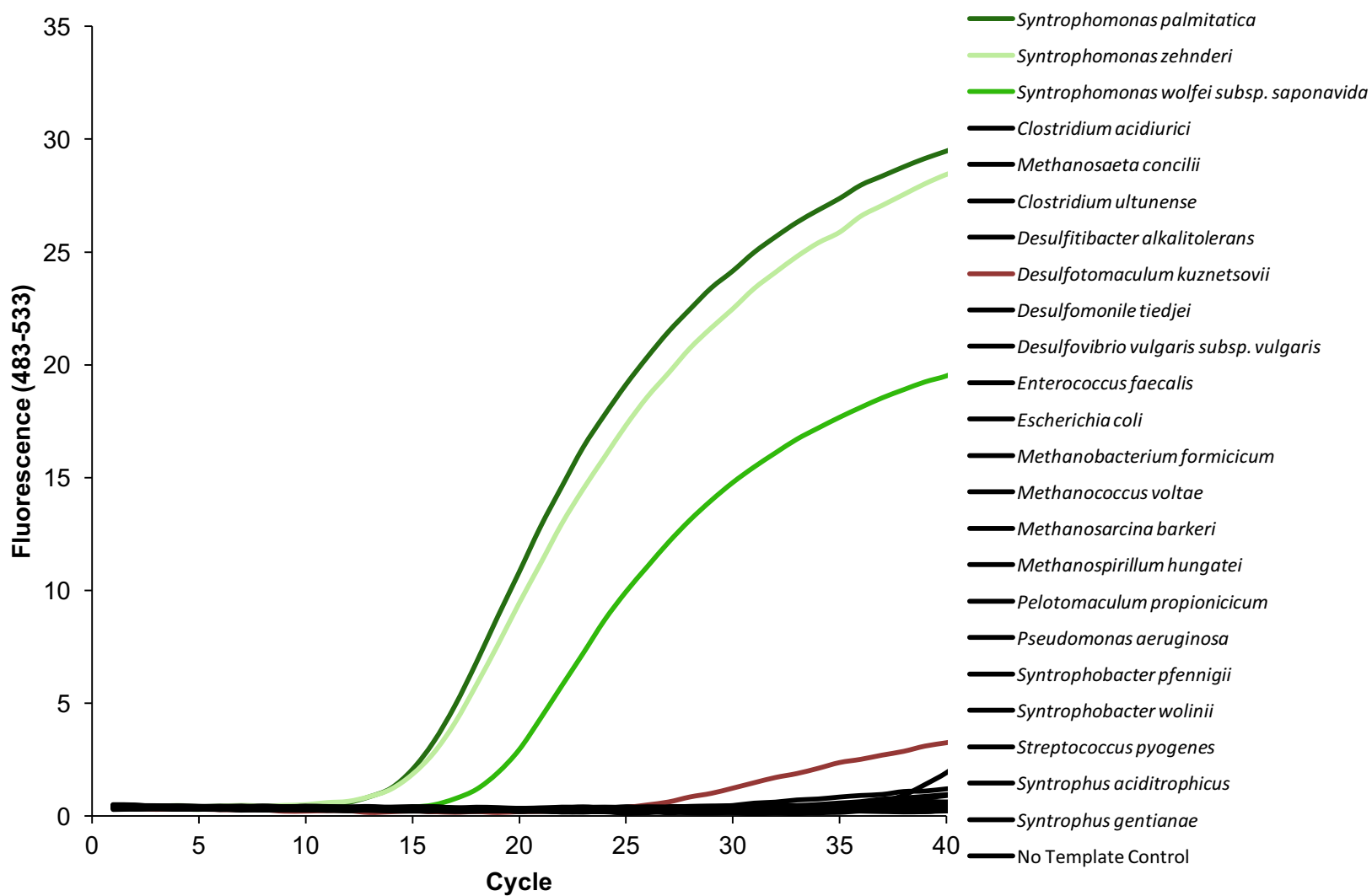
<sup>2</sup> Organism from which the 16S sequence for was derived for the construction of plasmids for calibration standards, followed by the accession number of the 16S sequence

<sup>3</sup> Calculated by performing linear regressions plots of  $C_t$  values versus the  $\log_{10}$  of the template concentrations.

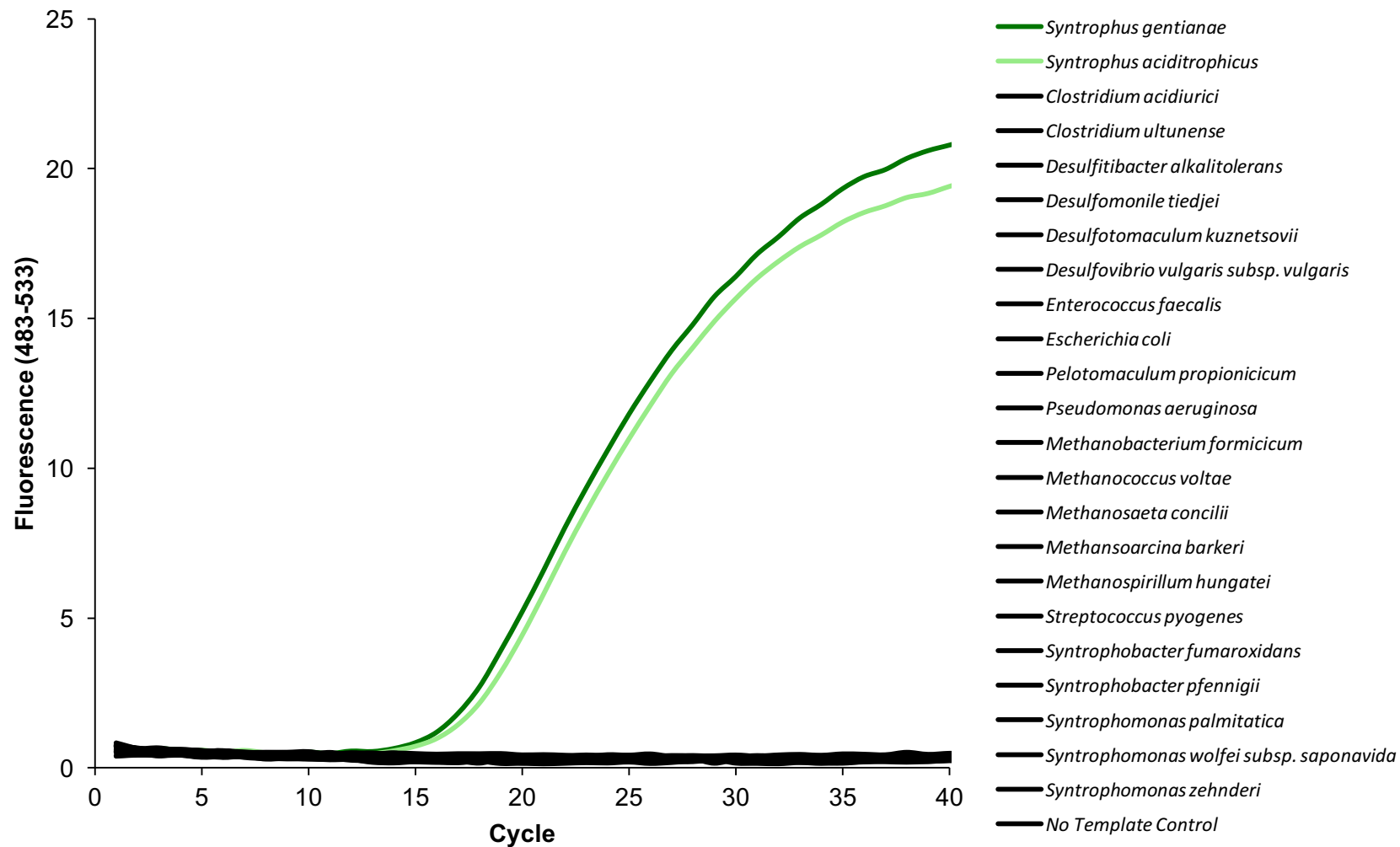
<sup>4</sup> Yu Y, Lee C, Kim J & Hwang S (2005). *Biotechnol. Bioeng.* 89: 670–679.

**Supplemental Table A2:** Concentration of intermediate metabolites based on samples taken at end of each batch cycle in fed-batch bioreactors degrading oleic acid. Error bars indicate one standard deviation based on biological replicates (n=3).

<b>Batch Cycle</b>	<b>Oleic Acid mM</b>	<b>Stearic Acid mM</b>	<b>Palmitic Acid mM</b>	<b>Acetic Acid mM</b>
1	0.08 ± 1E-3	0.12 ± 7E-4	0.09 ± 1E-2	0.11 ± 3E-2
2	0.10 ± 4E-4	0.13 ± 2E-3	0.24 ± 2E-2	0.32 ± 1E-1
3	0.09 ± 4E-3	0.12 ± 1E-3	0.15 ± 3E-2	2.02 ± 4E-1
4	0.13 ± 2E-3	0.14 ± 7E-4	0.09 ± 1E-3	1.84 ± 4E-1
5	0.08 ± 2E-3	0.12 ± 1E-3	0.07 ± 1E-2	2.21 ± 9E-1

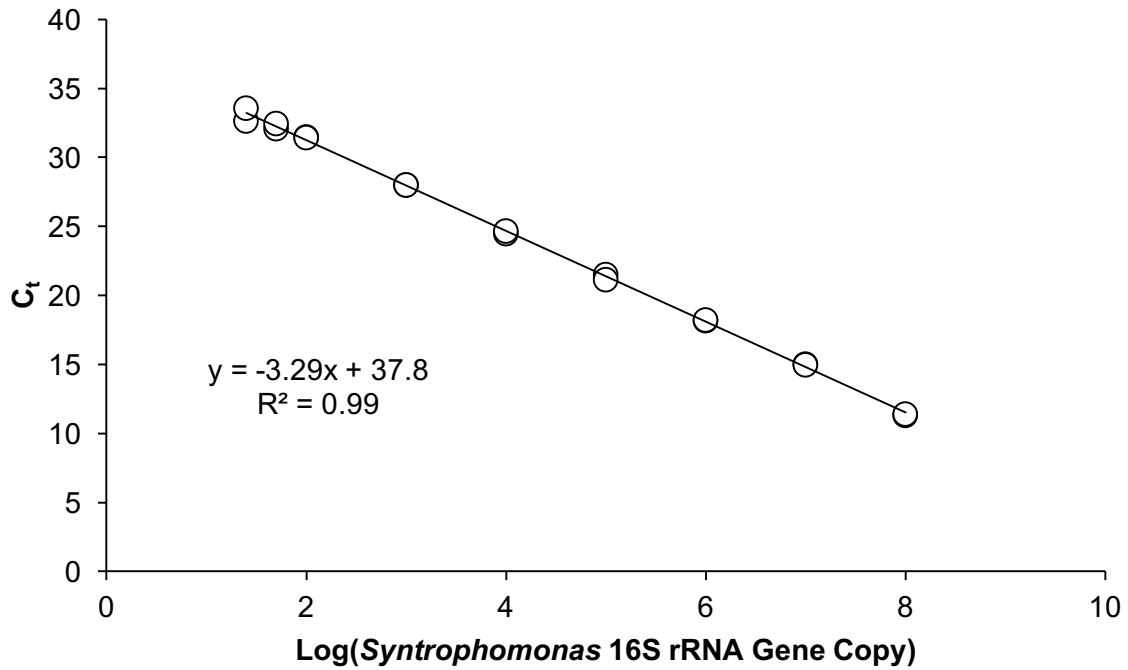


**Supplemental Figure A1:** Fluorescence response during specificity testing of the *Syntrophomonas* qPCR assay using pure-culture DNA samples. Approximately 0.5 to 2 ng of genomic DNA template was loaded in each qPCR reaction. The samples colored black did not produce a fluorescence signal at a  $C_t$  less than that of the lowest qPCR calibration standard ( $C_t$  of ~35 at 25 gene copies).

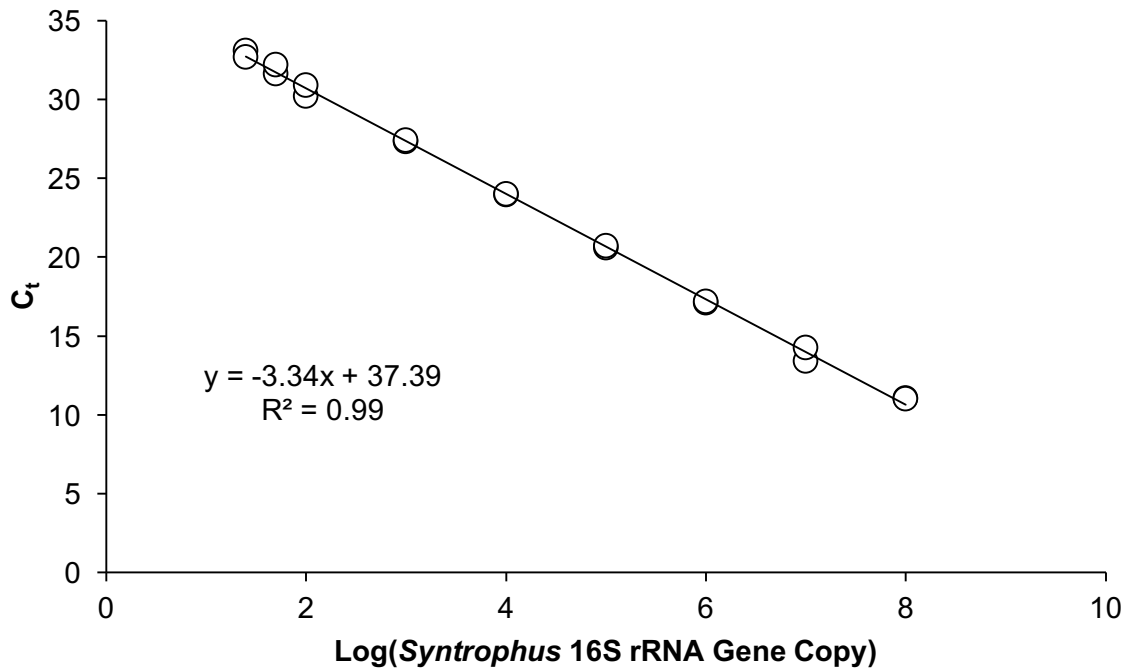


**Supplemental Figure A2:** Fluorescence response during specificity testing of the *Syntrophus* qPCR assay using pure-culture DNA samples. Approximately 0.5 to 2 ng of genomic DNA template was loaded in each qPCR reaction. The samples colored black did not produce a fluorescence signal at a  $C_t$  less than that of the lowest qPCR calibration standard ( $C_t$  of ~35 at 25 gene copies).

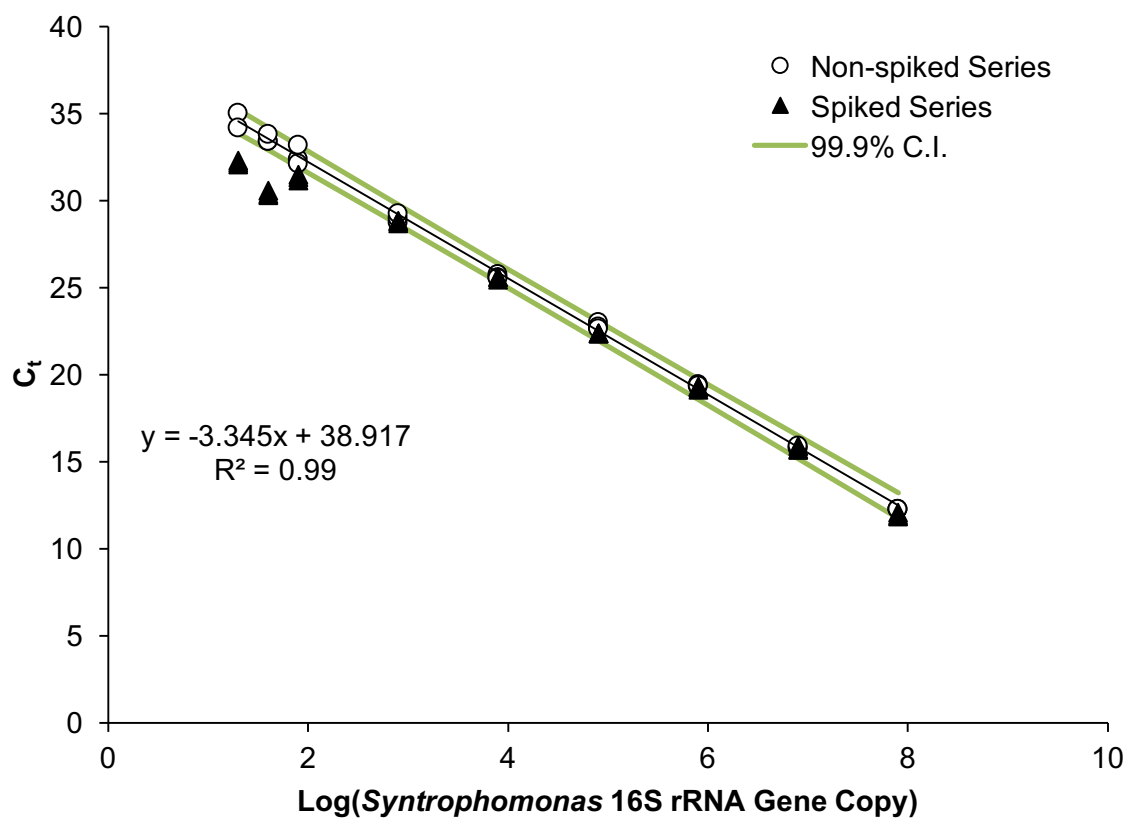




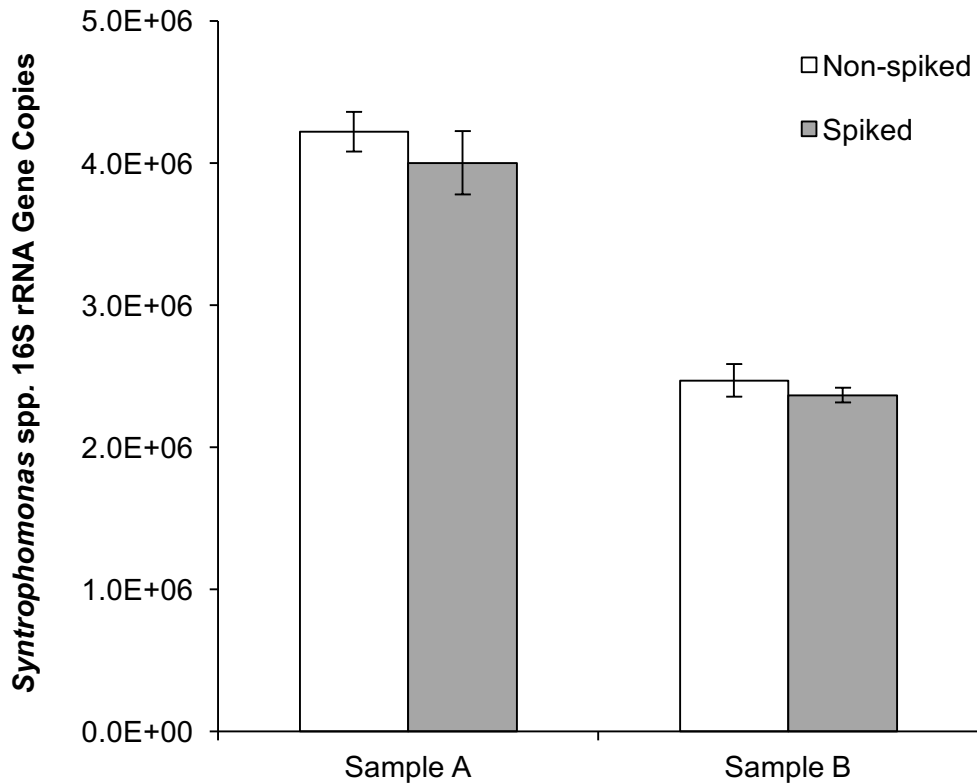
**Supplemental Figure A3:** Threshold cycles ( $C_t$ ) versus the log of the 16S rRNA gene copies of a typical standard calibration curve prepared for the *Syntrophomonas* primer/probe set. Duplicate points are shown for each standard dilution concentration.



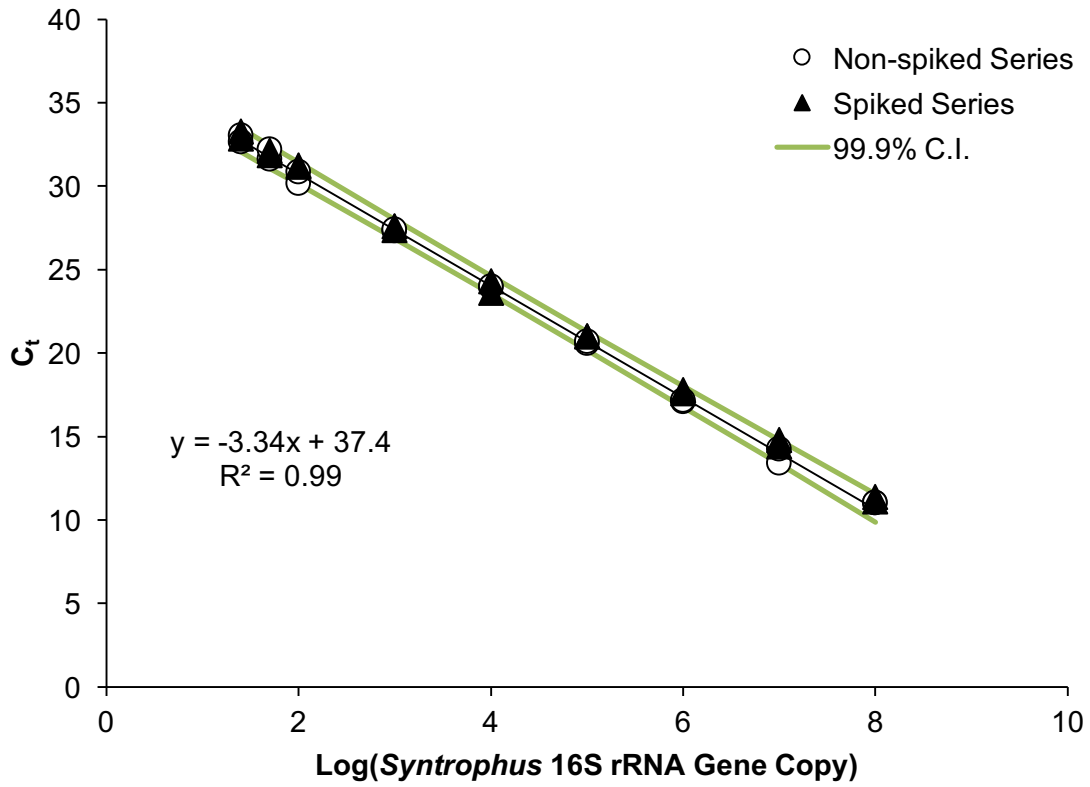
**Supplemental Figure A4:** Threshold cycles ( $C_t$ ) versus the log of the 16S rRNA gene copies of a typical standard calibration curve prepared for the *Syntrophus* primer/probe set. Duplicate points are shown for each standard dilution concentration.



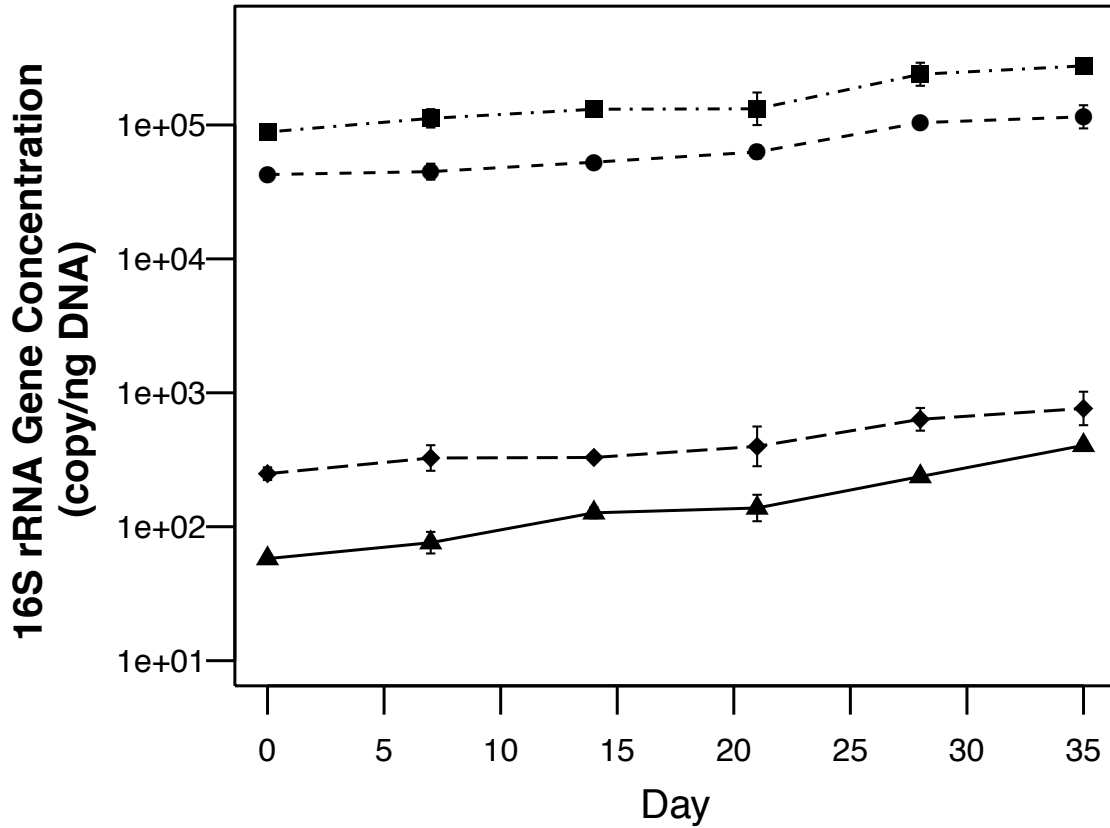
**Supplemental Figure A5:** Comparison of the linear dynamic range of samples in two *Syntrophomonas* standard dilution series that were either spiked or not spiked with  $\sim 10^6$  16S gene copies of *Desulfotomaculum kuznetsovii* DNA. The linear regression and 99.9% confidence intervals shown refer to the non-spiked standard dilution series of *Syntrophomonas* DNA.



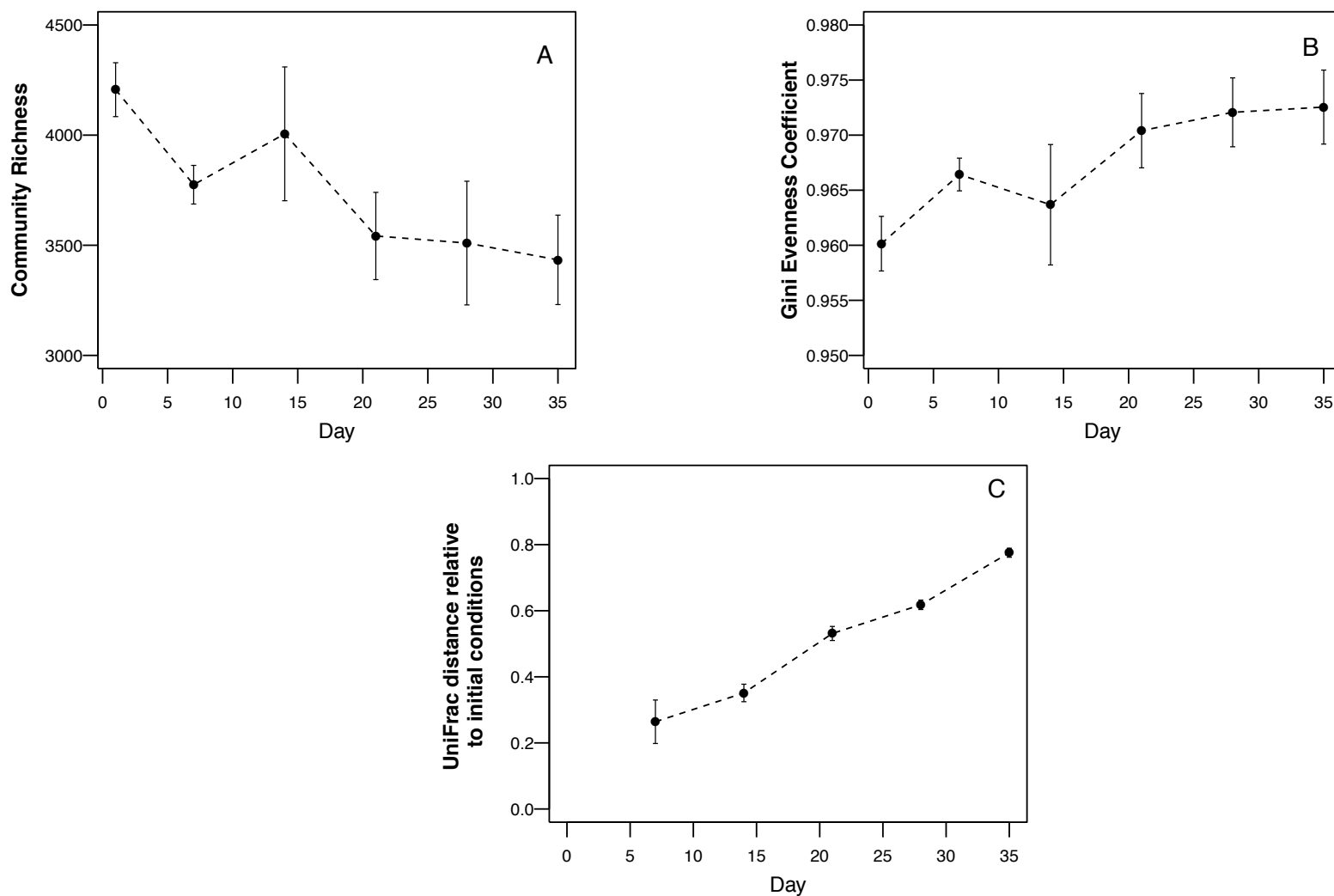
**Supplemental Figure A6:** Comparison of *Syntrophomonas* spp. 16S rRNA gene abundance in two random bioreactor DNA extracts quantified with and without spiking the qPCR mix with *Desulfotomaculum kuznetsovii* DNA. Sample A was spiked with 6 ng of *D. kuznetsovii* DNA, and Sample B was spiked with 0.6 ng *D. kuznetsovii* DNA. Error bars show 95% confidence intervals for triplicate technical replicates. Spiking *Desulfotomaculum kuznetsovii* DNA did not significantly impact the quantitative predictability of the *Syntrophomonas* qPCR primer/probe set applied to the experimental DNA samples ( $p > 0.1$ ).



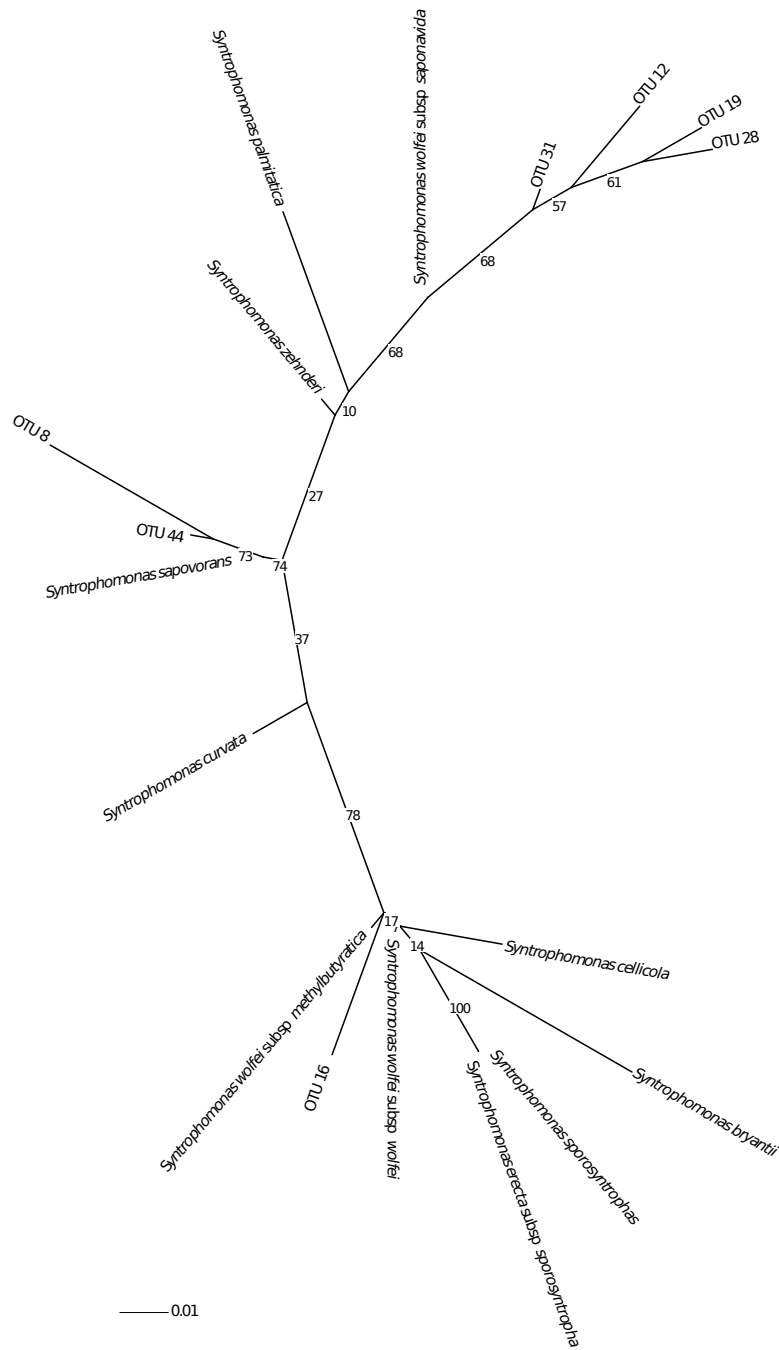
**Supplemental Figure A7:** Comparison of the linear dynamic range of samples in two *Syntrophus* standard dilution series that were either spiked or not spiked with  $\sim 10^6$  16S gene copies of *Desulfomonile tiedje* DNA. The linear regression and 99.9% confidence intervals shown refer to the non-spiked standard dilution series of *Syntrophus* DNA.



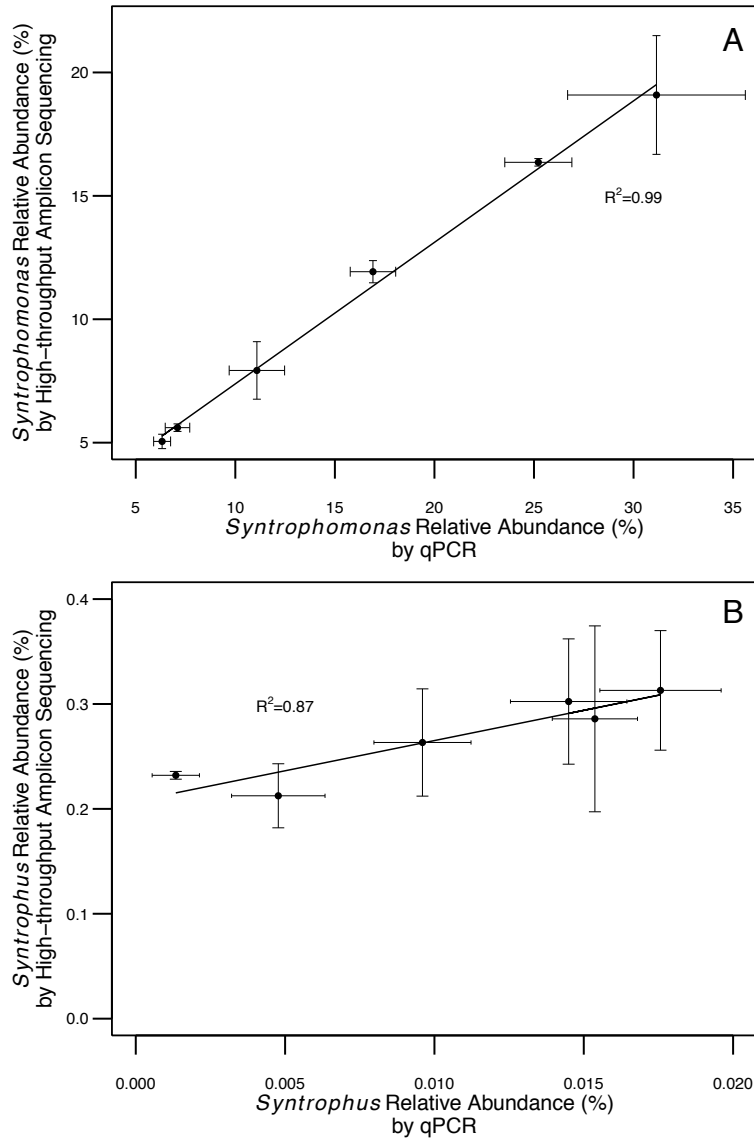
**Supplemental Figure A8:** Changes in the 16S rRNA gene concentration of each methanogenic archaeal target group in the bioreactors degrading oleic acid. (■) = *Methanomicrobiales*; (●) = *Methanosaetaceae*; (◆) = *Methanobacteriales*; (▲) = *Methanosarcinaceae*. *Methanococcales* were not detected by qPCR on the bioreactor samples. Error bars indicate one standard deviation based on the biological replicates (n=3) and technical replicates (n=2).



**Supplemental Figure A9:** (A) Species richness of the bacterial communities over time determined as number of OTU's by rarefaction of random subsamples of size 38,600 from the community OTU matrices, (B) Community evenness of the bacterial communities over time determined with the Gini coefficient (higher Gini coefficient values represent lower community evenness), (C) Weighted UniFrac distance values relative to the initial bioreactor communities (higher UniFrac distances represent greater divergence from initial community structure). Error bars indicate one standard deviation based on the triplicate biological replicates.



**Supplemental Figure A10:** A phylogenetic tree of 16S rRNA gene sequences of the 7 most abundant *Syntrophomonas* OTU's with that of characterized *Syntrophomonas* species. 16S rRNA sequences of characterized species were retrieved from the NCBI database. The sequences were aligned with MUSCLE v3.8.31 (Edgar, R.C. (2004) *Nucleic Acids Res*, 32(5), 1792-97) and the alignment was trimmed to the 300 bp length of the OTU sequence with BMGE v1.1 (<http://www.biomedcentral.com/1471-2148/10/210>). The tree was constructed with RAxML 7.7.2 using GTRGAMMA model and 100 bootstraps. Rendering was performed with iTOL (Letunic I. and Bork (2011) *Nucleic Acids Res*, doi: 10.1093/nar/gkr201).



**Supplemental Figure A11:** Comparison of the relative abundance predicted by high-throughput amplicon sequencing of the 16S rRNA gene by Illumina MiSeq and by the newly developed qPCR assays for (A) *Syntrophomonas* and (B) *Syntrophus*. Error bars for high-throughput amplicon sequencing data indicate one standard deviation based on biological replicates (n=3), while error bars for qPCR data indicate one standard deviation based on biological replicates (n=3) and technical replicates (n=2).



## APPENDIX B

### Supplemental Information for Chapter 4:

#### **Microbial community adaptation influences long-chain fatty acid conversion during anaerobic codigestion of fats, oils, and grease with municipal sludge**

**Number of Pages: 7**

**Number of Tables: 1**

**Number of Figures: 5**

#### **Contents:**

Supplemental Table B1: Characteristics of qPCR primers and probes.....	B2
Supplemental Figure B1: LCFA composition of codigester effluent.....	B3
Supplemental Figure B2: Diversity metrics for <i>Bacteria</i> communities.....	B4
Supplemental Figure B3: Bray-Curtis distances for <i>Bacteria</i> communities .....	B5
Supplemental Figure B4: Diversity metrics for <i>Archaea</i> communities.....	B6
Supplemental Figure B5: Bray-Curtis distances for <i>Bacteria</i> communities .....	B7

**Supplemental Table B1:** Characteristics and performance of all qPCR primer/probe sets used in this study

Oligo. Name <sup>1</sup>	Target Group	Sequence	Refs.	Reference Sequence <sup>2</sup>	Calibration Slope <sup>3</sup>	Calibration Intercept <sup>3</sup>
Sym-678 (F)	<i>Syntrophomonas</i>	CCWGGTGTAGCGGT	Ziels et al., 2015 <sup>4</sup>	<i>Syntrophomonas zehnderi</i> OL-4 (NR_044008.1)	-3.30	38.7
Sym-696 (P)		TGCGTAGAAATCAGGAGGAAYACCAGT				
Sym-738 (R)		TCAGGGYCAGTCCAG				
Syntr-441 (F)	<i>Syntrophus</i>	GGTGGGAAGAAATGTATKGA	Ziels et al., 2015	<i>Syntrophus aciditrophicus</i> SB (NR_102776.1)	-3.32	38.8
Syntr-462 (P)		TTAAYAGCCTTTGTACTTGACGGTAC				
Syntr-559 (R)		CTCTTTACGCCCAATGAT				
BAC-338 (F)	<i>Bacteria</i>	ACTCCTACGGGAGGCAG	Yu et al., 2005 <sup>5</sup>	<i>Methylocella silvestris</i> BL2 (NR_074237.1)	-3.41	39.1
BAC-516 (P)		TGCCAGCAGCCGCGGTAATAC				
BAC-805 (R)		GACTACCAGGGTATCTAATCC				
Msc-380 (F)	<i>Methanosarcinaceae</i>	GAAACCGYGATAAGGGGA	Yu et al., 2005	<i>Methanosarcina barkeri</i> DSM800 (NR_025303.1)	-3.51	39.3
Msc-492 (P)		TTAGCAAGGGCCGGGCAA				
Msc-828 (R)		TAGCGARCATCGTTTACG				
Mst-702 (F)	<i>Methanosaetaceae</i>	TAATCCTYGARGGACCACCA	Yu et al., 2005	<i>Methanosaeta concilii</i> Opfikon (NR_028242.1)	-3.58	41.1
Mst-753 (P)		ACGGCAAGGGACGAAAGCTAGG				
Mst-862 (R)		CCTACGGCACCRACMAC				
MBT-857 (F)	<i>Methanobacteriales</i>	CGWAGGGAAGCTGTAAAGT	Yu et al., 2005	<i>Methanobacterium formicicum</i> DSMZ1535 (NR_025028.1)	-3.49	38.9
MBT-929 (P)		AGCACCACAACGCGTGGA				
MBT-1196 (R)		TACCGTCGTCCACTCCTT				
MMB-282 (F)	<i>Methanomicrobiales</i>	ATCGRTACGGGTTGTGGG	Yu et al., 2005	<i>Methanoculleus bourgensis</i> MS2 (NR_042786.1)	-3.41	41.6
MMB-749 (P)		TYCGACAGTGAGGRACGAAAGCTG				
MMB-832 (R)		CACCTAACGCRCATHGTTTAC				
MCC-495 (F)	<i>Methanococcales</i>	TAAGGGCTGGGCAAGT	Yu et al., 2005	<i>Methanococcus voltae</i> (U38461.1)	-3.83	44.3
MCC-686 (P)		TAGCGGTGRAATGYGTTGATCC				
MCC-832 (R)		CACCTAGTYCGCARAGTTTA				

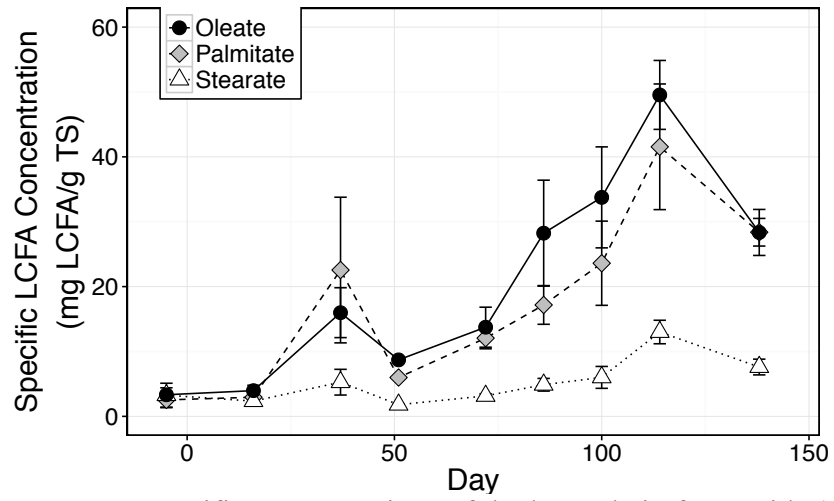
<sup>1</sup> F = forward primer; P = hydrolysis probe; R = reverse primer

<sup>2</sup> Organism from which the 16S sequence was derived for the construction of plasmids for calibration standards, followed by the accession number of the 16S sequence.

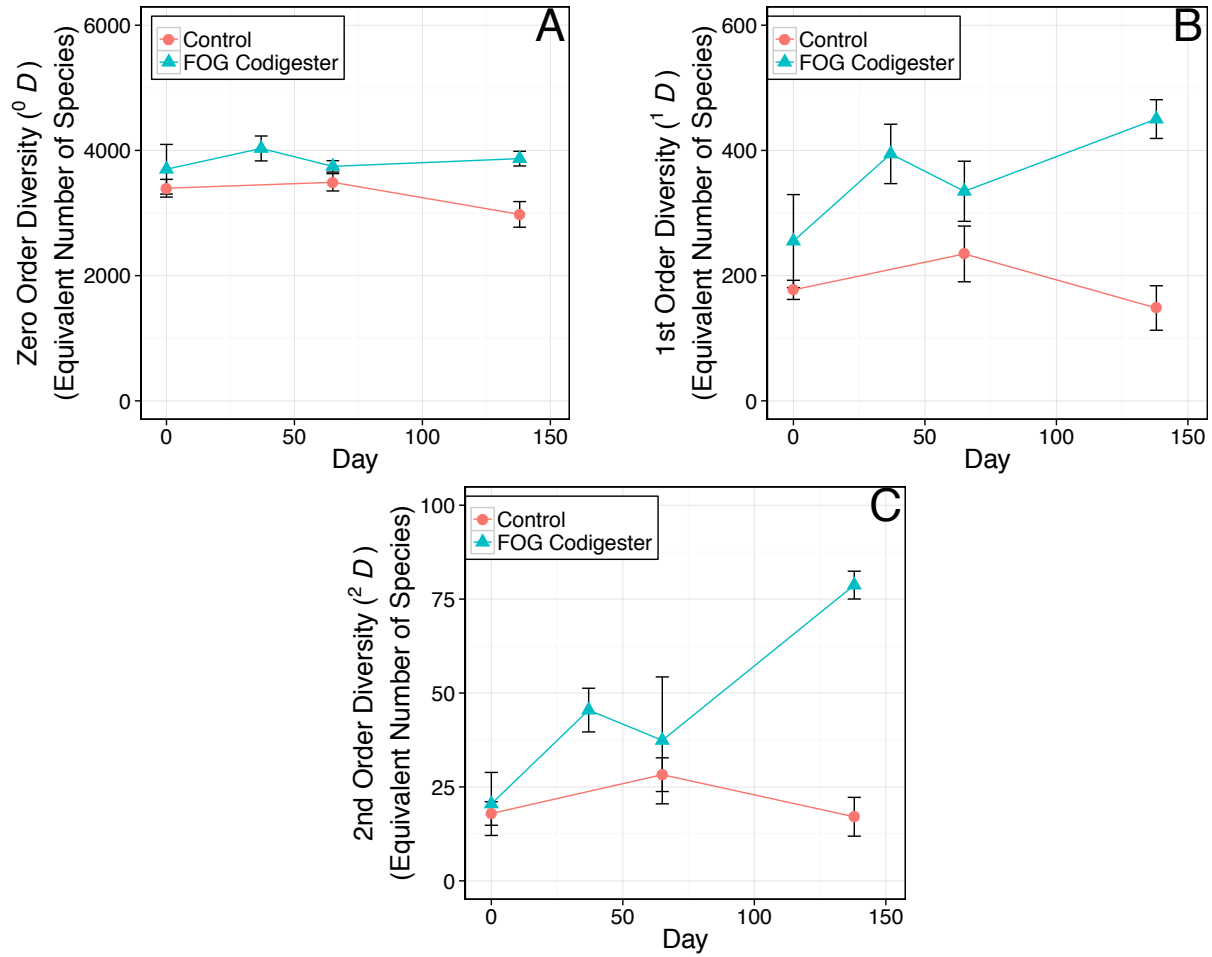
<sup>3</sup> Calculated by performing linear regressions plots of C<sub>t</sub> values versus the log<sub>10</sub> of the template concentrations.

<sup>4</sup> Ziels, R.M., et al., 2015. FEMS Microbiol. Ecol. 91

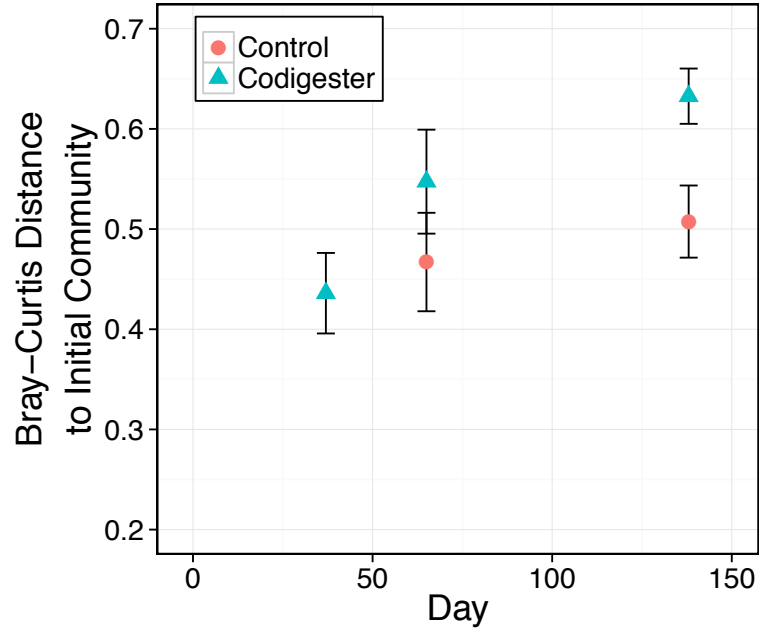
<sup>5</sup> Yu, Y., et al., 2005. Biotechnol. Bioeng. 89, 670–679.



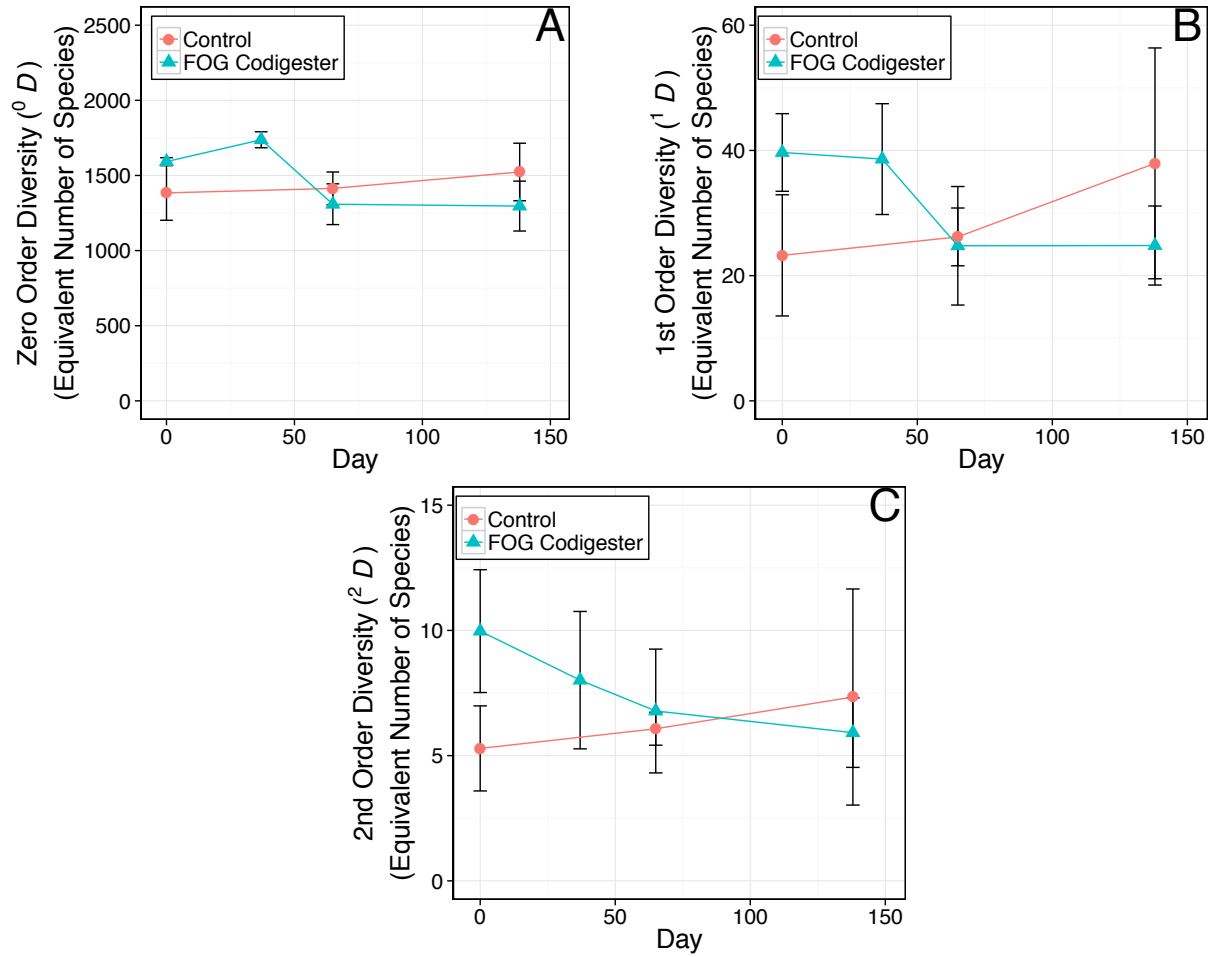
**Supplemental Figure B1:** Specific concentrations of the long-chain fatty acids (LCFAs) oleate, palmitate, and stearate in the FOG codigester effluent during the experimental period.



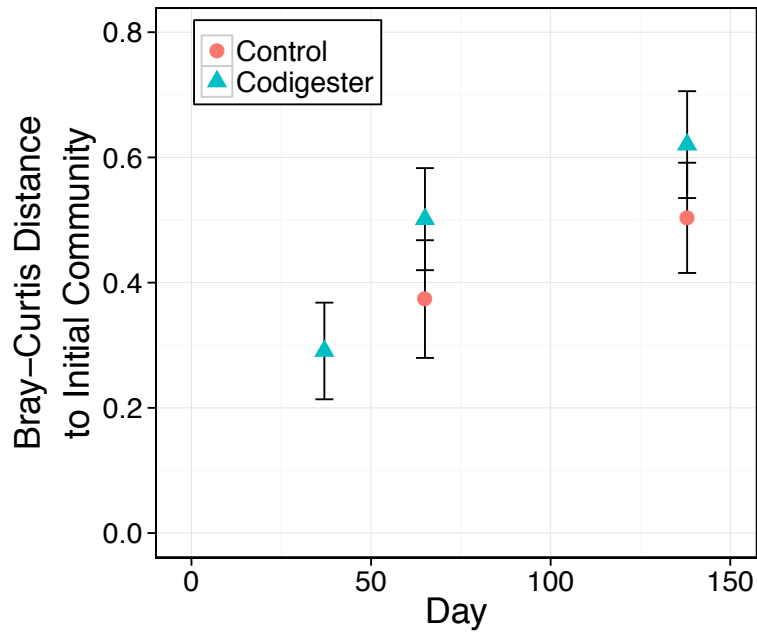
**Supplemental Figure B2:** Hill diversity numbers ( ${}^qD$ ) of orders (A)  $q=0$ , (B)  $q=1$ , and (C)  $q=2$  for the FOG codigester and control digester *Bacteria* communities over the course of the experimental period. Calculations were made based on Illumina MiSeq 16S amplicon sequencing data after rarefying to an equal number of reads for all samples to account for unequal sequencing depths. Error bars represent a standard deviation based on triplicate DNA extractions for each time point.



**Supplemental Figure B3** Bray-Curtis distance of the FOG codigester and control digester *Bacteria* communities relative to their respective initial communities at day=0. Calculations were made based on Illumina MiSeq 16S amplicon sequencing data after rarefying to an equal number of reads for all samples to account for unequal sequencing depths. Error bars represent a standard deviation based on triplicate DNA extractions for each time point.



**Supplemental Figure B4** Hill diversity numbers ( ${}^qD$ ) of orders (A)  $q=0$ , (B)  $q=1$ , and (C)  $q=2$  for the FOG codigester and control digester *Archaea* communities over the course of the experimental period. Calculations were made after rarefying to an equal number of reads for all samples to account for unequal sequencing depths. Error bars represent a standard deviation based on triplicate DNA extractions for each time point.



**Supplemental Figure B5** Bray-Curtis distance of the FOG codigester and control digester *Archaea* communities relative to their respective initial communities at day=0. Calculations were made based on Illumina MiSeq 16S amplicon sequencing data after rarefying to an equal number of reads for all samples to account for unequal sequencing depths. Error bars represent a standard deviation based on triplicate DNA extractions for each time point.

# APPENDIX C

## Supplemental Information for Chapter 5:

### Syntrophic community structure and biokinetics driven by long-chain fatty acid feeding strategy in anaerobic codigestion

**Number of Pages: 17**

**Number of Tables: 8**

**Number of Figures: 8**

#### Contents:

Supplemental Methods: Quantitative PCR	C2
Supplemental Methods: Substrate Inhibition Modeling	C3
Supplemental Table C1: Summary of the Phase I digester performances	C4
Supplemental Table C2: Summary of the Phase II co-digester performances	C5
Supplemental Table C3: Batch test maximum acetate conversion rates ( $q_{max,acetate}$ )	C6
Supplemental Table C4: Effluent LCFA concentrations in the Phase I digesters	C7
Supplemental Table C5: Effluent LCFA concentrations in the Phase II digesters	C7
Supplemental Table C6: Oleate conversion rates ( $q_{oleate}$ ) with the digester sludges	C8
Supplemental Table C7: Results nonlinear substrate inhibition model fitting	C9
Supplemental Table C8: Summary of the multiple linear regression model for $q_{max,oleate}$	C10
Supplemental Figure C1: A schematic of the experimental manure digesters	C11
Supplemental Figure C2: Inferred absolute abundance of the genus <i>Methanosaeta</i>	C12
Supplemental Figure C3: Correspondence analysis (CA) plot for <i>Syntrophomonas</i> reads	C12
Supplemental Figure C4: Relative fractions of the 5 most abundant <i>Methanosaeta</i> OTUs	C13
Supplemental Figure C5: Hill diversity numbers ( ${}^qD$ ) for <i>Bacteria</i>	C14
Supplemental Figure C6: Hill diversity numbers ( ${}^qD$ ) for <i>Archaea</i>	C15
Supplemental Figure C7: A phylogenetic tree 6 <i>Syntrophomonas</i> OTUs	C16
Supplemental Figure C8: Linear regression of observed $q_{max,acetate}$ values	C17



## ***Supplemental Materials and Methods:***

### **Quantitative PCR (qPCR)**

qPCR analysis on syntrophic LCFA  $\beta$ -oxidizing bacteria was conducted targeting 16S rRNA genes of the genus *Syntrophomonas* using the primers Synm-678-F (CCWGGTGTAGCGGT) and Synm-738-F (TCAGGGYCAGTCCAG) and probe Synm-696-P (TGCGTAGAAATCAGGAGGAAYACCAGT), developed by Ziels et al. (2015). Additionally, qPCR was conducted targeting the domain *Bacteria* with the primers BAC-338-F (ACTCCTACGGGAGGCAG) and BAC-805-R (GACTACCAGGGTATCTAATCC) and probe BAC-516-P (TGCCAGCAGCCGCGGTAATAC), as well as the domain *Archaea* with the primers ARC-787-F (ATTAGATACCCSBGTAGTCC) and ARC-1059-R (GCCATGCACCWCCTCT) and probe ARC-915-P (AGGAATTGGCGGGGGAGCAC) (Yu et al., 2005). All hydrolysis probes were labeled with 6-FAM at the 5' end and BHQ-1 at the 3' end.

qPCR was performed using a MasterCycler Realplex4 (Eppendorf). Each 20  $\mu$ L reaction mix contained 5  $\mu$ L DNA template, 2  $\mu$ L PCR-grade water, 500 nM of each forward and reverse primers, 200 nM of hydrolysis probe and 10  $\mu$ L TaqMan™ Fast Advanced Master Mix (2X, Applied Biosystems). All samples were analyzed in duplicate. No-template controls (NTCs) were included with each qPCR run. Extracted DNA from the digester biomass samples was diluted 1:10 in nuclease-free water to prevent PCR inhibition. Calibration standards for the qPCR assays were prepared as described by Ziels et al. (2015), and were included in duplicate in each qPCR run for all target groups. Calibration standards included  $10^8$ ,  $10^7$ ,  $10^6$ ,  $10^5$ ,  $10^4$ ,  $10^3$ , and  $10^2$  gene copies per reaction. Average slopes of calibration curves were -3.30 for *Bacteria* (101% PCR efficiency), -3.56 for *Archaea* (91% PCR efficiency), and -3.39 (97% PCR efficiency) for *Syntrophomonas*.  $R^2$  values of calibration curves were always above 0.99 for all targets.

### Biokinetic Modeling of Oleate Conversion:

Biokinetic parameters for oleate conversion were determined by fitting a modified form of the Michaelis-Menten model that was empirically derived to account for substrate inhibition on microbial growth and substrate utilization kinetics (Aiba et al., 1968). The inclusion of the inhibition term,  $K_I$ , accounted for substrate inhibition at high oleate concentrations.

$$q = q_{max} \frac{S}{K_s + S} \cdot \exp\left(-\frac{S}{K_I}\right)$$

where:  $q$  is the specific methane production rate ( $\text{mL CH}_4 \text{ g VS}^{-1} \text{ d}^{-1}$ ) at oleate concentration,  $S$  ( $\text{mg/L}$ );  $q_{max}$  is the maximum specific methane production rate ( $\text{mL CH}_4 \text{ g VS}^{-1} \text{ d}^{-1}$ );  $K_s$  is the half-saturation constant ( $\text{mg/L}$ ); and  $K_I$  is the substrate inhibition term ( $\text{mg/L}$ ).

The biokinetic parameters,  $q_{max}$ ,  $K_s$ , and  $K_I$  were determined by nonlinear regression of the specific methane production rates versus the initial oleate concentration using the nls package in R version 3.2.1. The triplicate specific rate measurements at each oleate concentration were pooled to obtain a single set of biokinetic parameters. The resulting biokinetic parameters are shown in Table C7, and an example model fit for the Day 84 batch tests is shown below in Methods Figure S-M1.

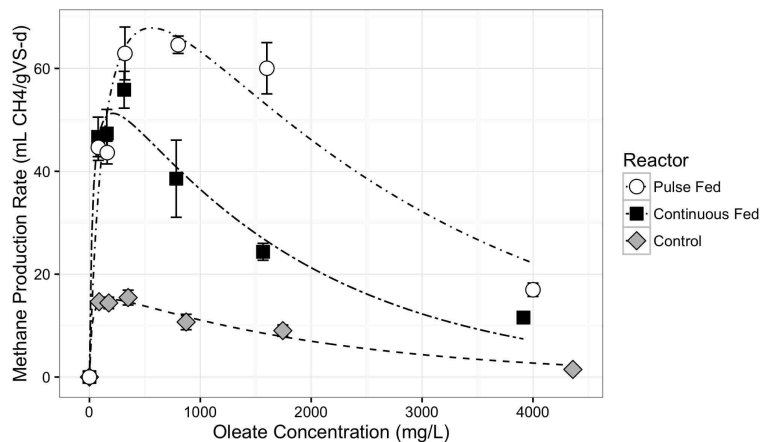


**Figure C-Methods-1:** Example substrate inhibition model fit for the day 84 oleate batch tests.

**Supplemental Table C1.** Summary of the Phase I digester performances based on effluent VS, effluent COD, COD removal, pH, digester methane production, and specific methane yield during the transient increases in LCFA loading. Values in parentheses represent one standard deviation.

Days	Reactor	Feed VSLR		Feed OLR		% Feed VS as LCFA	% Feed COD as LCFA	Effluent VS		Effluent COD		Digester pH		COD removal (%)		Daily Methane Production (@ STP)		Specific Methane Yield	
		(g VS/L-d)	(g VS/L-d)	(g COD/L-d)	(g COD/L-d)			(g/L)	(g/L)	(g/L)	(g/L)	(%)	(%)	(mL/d)	(mL/d)	(mL/g VS)	(mL/g VS)		
-50 -0	Control	1.3	(0.1)	2.4	(0.7)	0%	0%	16.7	(1.5)	29.5	(6.2)	7.11	(0.04)	37%	(6%)	994	(126)	195	(31)
	Continuous Fed	1.3	(0.1)	2.4	(0.7)	0%	0%	17.0	(0.9)	28.0	(5.0)	7.10	(0.04)	41%	(5%)	968	(112)	192	(33)
	Pulse Fed	1.3	(0.1)	2.4	(0.7)	0%	0%	16.7	(0.8)	31.2	(7.1)	7.10	(0.04)	34%	(7%)	994	(107)	195	(30)
1 - 20	Control	1.3	(0.1)	2.3	(0.3)	0%	0%	17.3	(0.6)	26.8	(3.4)	7.12	(0.02)	39%	(3%)	960	(55)	176	(22)
	Continuous Fed	1.26	(0.1)	2.2	(0.3)	3%	5%	16.8	(2.2)	25.7	(4.2)	7.12	(0.03)	34%	(5%)	946	(68)	187	(14)
	Pulse Fed	1.26	(0.1)	2.2	(0.3)	3%	5%	16.0	(2.4)	24.4	(3.4)	7.12	(0.03)	37%	(7%)	996	(151)	201	(33)
21 - 45	Control	1.4	(0.1)	3.1	(0.4)	0%	0%	18.3	(0.8)	38.0	(4.6)	7.11	(0.02)	40%	(4%)	975	(134)	181	(30)
	Continuous Fed	1.31	(0.1)	3.0	(0.4)	6%	7%	16.8	(0.7)	35.1	(3.0)	7.11	(0.02)	45%	(5%)	1104	(84)	214	(29)
	Pulse Fed	1.31	(0.5)	3.0	(0.4)	6%	7%	16.6	(0.6)	36.0	(5.3)	7.10	(0.02)	44%	(3%)	1194	(84)	229	(29)
46 - 65	Control	1.3	(0.1)	2.1	(0.4)	0%	0%	17.5	(0.6)	28.7	(5.9)	7.13	(0.02)	33%	(5%)	1004	(79)	193	(26)
	Continuous Fed	1.27	(0.1)	2.3	(0.4)	10%	16%	16.0	(0.3)	26.0	(3.0)	7.15	(0.03)	43%	(2%)	1239	(105)	237	(26)
	Pulse Fed	1.27	(0.2)	2.3	(0.4)	10%	16%	15.5	(0.4)	25.8	(2.1)	7.14	(0.03)	44%	(6%)	1392	(453)	265	(68)
66 - 86	Control	1.4	(0.2)	2.1	(0.2)	0%	0%	17.5	(0.7)	26.6	(1.7)	7.13	(0.02)	39%	(3%)	1046	(108)	198	(25)
	Continuous Fed	1.53	(0.2)	2.7	(0.2)	16%	27%	16.1	(0.8)	26.3	(2.4)	7.16	(0.02)	54%	(4%)	1726	(242)	290	(29)
	Pulse Fed	1.53	(0.3)	2.7	(0.2)	16%	27%	16.1	(0.9)	24.7	(3.6)	7.17	(0.03)	54%	(9%)	1749	(842)	282	(80)

**Supplemental Table C2.** Summary of the Phase II co-digester performances based on effluent VS, effluent COD, COD removal, pH, digester methane production, and specific methane yield during the transient increases in LCFA loading. Values in parentheses represent one standard deviation.

Days	Feed		Feed OLR		% Feed VS	% Feed COD	Effluent VS		Effluent COD		Digester pH		COD removal (%)		Daily Methane Production (@ STP)		Specific Methane Yield	
	(g VS/L-d)	(g COD/L-d)	(g VS/L-d)	(g COD/L-d)	as LCFA	as LCFA	(g/L)	(g/L)	(g/L)	(g/L)			(%)	(%)	(mL/d)	(mL/d)	(mL/g VS)	(mL/g VS)
<i>Phase II: Continuous-Fed Co-digester</i>																		
87-106	1.7	(0.2)	3.5	(0.2)	22%	32%	16.8	(0.9)	53	(4)	7.2	(0.04)	58%	(3%)	2071	(243)	312	(44)
107-126	1.8	(0.2)	3.7	(0.3)	32%	47%	16.0	(0.5)	43	(6)	7.3	(0.04)	63%	(2%)	2809	(309)	390	(59)
127 - 149	2.1	(0.2)	5.1	(0.3)	45%	54%	17.9	(3.5)	52	(7)	7.4	(0.07)	70%	(3%)	4354	(615)	480	(53)
150 - 183	2.6	(0.2)	6.0	(0.3)	50%	64%	18.3	(1.0)	58	(8)	7.4	(0.04)	74%	(2%)	5214	(404)	503	(55)
184 - 200	2.3	(0.1)	5.2	(0.4)	48%	62%	18.6	(1.1)	52	(10)	7.4	(0.04)	70%	(1%)	4482	(364)	499	(27)
<i>Phase II: Pulse-Fed Co-digester</i>																		
0 - 103	1.4	(0.2)	2.3	(0.5)	0%	0%	17.7	(0.8)	52	(12)	7.1	(0.02)	39%	(5%)	991	(106)	185	(28)
104-116	1.4	(0.2)	2.3	(0.3)	5%	10%	17.9	(0.6)	45	(2)	7.1	(0.02)	40%	(2%)	1236	(292)	226	(18)
117-126	1.3	(0.3)	2.4	(0.5)	13%	22%	17.3	(0.6)	41	(8)	7.2	(0.02)	45%	(2%)	1409	(559)	262	(16)
127-137	1.7	(0.4)	3.0	(1.0)	18%	30%	18.0	(1.2)	56	(9)	7.2	(0.05)	53%	(4%)	1947	(836)	286	(58)
138-149	1.9	(0.7)	3.9	(2.2)	36%	52%	18.3	(1.4)	49	(2)	7.3	(0.05)	66%	(2%)	3396	(1723)	465	(19)
150-183	2.6	(1.4)	6.0	(3.9)	50%	64%	18.3	(1.2)	58	(8)	7.4	(0.09)	74%	(2%)	5707	(1309)	545	(71)
184-200	2.3	(1.2)	5.2	(3.3)	48%	62%	18.8	(0.9)	52	(11)	7.5	(0.09)	70%	(1%)	4754	(1157)	526	(17)

**Supplemental Table C3:** Batch test maximum acetoclastic conversion rates ( $q_{max,acetate}$ ) with digester sludges throughout Phases I and II, at increasing initial oleate concentrations from 0 to 16 g/L. Values in parentheses indicate one standard deviation based on triplicate batch vials.

Reactor	Day	Observed $q_{max, acetate}$ (mL CH <sub>4</sub> /g VS-d) at initial oleate concentration:					
		0 g /L	0.8 g/L	4 g /L	8 g/L	12 g/L	16 g/L
<i>Phase I Digesters</i>							
Control	0	45 (4)	46 (2)	42 (6)	6 (5)	0 (2)	0 (2)
	41	35 (4)	32 (5)	28 (1)	11 (3)	2 (1)	0 (1)
	84	39 (1)	46 (1)	36 (1)	20 (1)	6 (1)	1 (1)
Continuous-Fed	0	47 (5)	38 (6)	43 (5)	7 (2)	0 (2)	0 (6)
	41	40 (3)	49 (2)	44 (2)	12 (2)	0 (2)	0 (2)
	84	64 (6)	92 (5)	79 (5)	24 (2)	5 (1)	0 (1)
Pulse-Fed	0	37 (3)	34 (4)	36 (3)	7 (4)	0 (3)	0 (3)
	41	32 (2)	30 (2)	34 (3)	12 (2)	1 (2)	0 (1)
	84	61 (8)	84 (11)	66 (11)	19 (5)	6 (2)	1 (1)
<i>Phase II Digesters</i>							
Continuous-Fed	129	137 (11)	168 (9)	143 (6)	10 (4)	1 (3)	0 (3)
	170	111 (13)	139 (9)	120 (23)	1 (8)	0 (8)	0 (8)
	204	52 (8)	95 (5)	38 (6)	0 (2)	0 (2)	0 (2)
Pulse-Fed	129	88 (5)	93 (6)	89 (5)	17 (4)	2 (4)	0 (4)
	148	142 (19)	182 (16)	102 (13)	5 (2)	0 (1)	0 (2)
	170	104 (9)	146 (9)	98 (25)	12 (5)	2 (5)	0 (5)
	204	70 (8)	106 (5)	19 (11)	1 (3)	0 (2)	0 (1)

**Supplemental Table C4.** Effluent LCFA concentrations in the Phase I digesters during the step increases in LCFA loading. Note that oleate was not detected above the LOQ in any effluent samples during Phase I. Values in parentheses are one standard deviation.

Days	Reactor	% Feed VS as LCFA	% Feed COD as LCFA	Palmitate (mg/L)	Stearate (mg/L)
-50 -0	Control	0%	0%	19 (16)	14 (11)
	Continuous Fed	0%	0%	16 (4)	13 (6)
	Pulse Fed	0%	0%	16 (7)	ND
1 - 20	Control	0%	0%	32 (10)	18 (7)
	Continuous Fed	3%	5%	29 (12)	17 (7)
	Pulse Fed	3%	5%	39 (23)	17 (6)
21 - 45	Control	0%	0%	27 (13)	13 (4)
	Continuous Fed	6%	7%	17 (8)	10 (3)
	Pulse Fed	6%	7%	19 (11)	10 (2)
46 - 65	Control	0%	0%	36 (21)	14 (2)
	Continuous Fed	10%	16%	24 (11)	12 (1)
	Pulse Fed	10%	16%	22 (9)	13 (2)
66 - 86	Control	0%	0%	19 (6)	12 (1)
	Continuous Fed	16%	27%	20 (10)	12 (3)
	Pulse Fed	16%	27%	14 (10)	11 (5)

ND = not detected

**Supplemental Table C5.** Effluent LCFA concentrations in the Phase II digesters during the step increases in LCFA loading. Values in parentheses represent one standard deviation.

Days	% Feed VS LCFA	% Feed COD LCFA	Palmitate (mg/L)	Stearate (mg/L)	Oleate (mg/L)
<i>Phase II: Continuous-Fed Co-digester</i>					
87 - 106	22%	32%	12.2 (4.3)	10.2 (0.6)	ND
107 - 126	32%	47%	16.3 (3.8)	10.5 (1.3)	10.6 (2.9)
127 - 149	45%	54%	ND	ND	ND
150 - 183	50%	64%	17.1 (2.8)	14.1 (2.1)	14.5 (2.0)
184 - 200	48%	62%	22.6 (1.3)	18.2 (0.4)	13.1 (0.4)
<i>Phase II: Pulse-Fed Co-digester</i>					
0 - 103	0%	0%	28 (14)	14 (5)	7 (4)
104-116	5%	10%	23 (11)	12 (3)	6 (0)
117-126	13%	22%	18 (5)	13 (0)	7 (1)
127-137	18%	30%	ND	ND	ND
138-149	36%	52%	ND	ND	ND
150-183	50%	64%	43 (37)	39 (18)	121 (120)
184-200	48%	62%	18 (0)	22 (0)	15 (0)

ND = not detected

**Supplemental Table C6:** Initial oleate conversion rates ( $q_{oleate}$ ) with the digester sludges for experimental Phases I and II at increasing initial oleate concentrations from 0 to 4500 mg/L. Green highlighted cells indicate the maximum observed oleate conversion rate ( $q_{max,oleate}$ ). Values in parentheses indicate one standard deviation based on triplicate batch vials.

Reactor	Day	Observed $q_{oleate}$ (mL CH <sub>4</sub> /g VS-d) at initial oleate concentration of:											
		100 mg /L		175 mg /L		350 mg /L		875 mg/L		1800 mg/L		4500 mg/L	
<b>Phase I Digesters</b>													
Control	0	23	(1)	24	(2)	22	(1)	18	(3)	14	(1)	1	(0)
	41	8	(0)	11	(0)	10	(1)	7	(1)	5	(1)	1	(1)
	84	15	(0)	14	(1)	15	(1)	11	(1)	9	(1)	1	(0)
Continuous-Fed	0	25	(1)	27	(2)	23	(3)	24	(1)	13	(3)	3	(1)
	41	34	(1)	29	(1)	34	(1)	20	(1)	11	(0)	3	(0)
	84	47	(4)	47	(5)	56	(4)	39	(7)	24	(2)	12	(1)
Pulse-Fed	0	24	(3)	22	(0)	25	(4)	16	(3)	12	(0)	2	(1)
	41	18	(1)	23	(1)	23	(1)	13	(0)	9	(1)	4	(1)
	84	45	(3)	44	(2)	63	(5)	65	(2)	60	(5)	17	(1)
<b>Phase II Digesters</b>													
Continuous-Fed	129	37	(6)	60	(3)	130	(2)	161	(16)	167	(0)	158	(14)
	170	49	(3)	61	(4)	89	(5)	113	(2)	144	(5)	57	(10)
	204	17	(1)	46	(3)	70	(4)	81	(2)	59	(9)	10	(1)
Pulse-Fed	129	26	(3)	39	(3)	49	(1)	27	(1)	15	(1)	6	(0)
	148	35	(2)	75	(7)	101	(5)	123	(7)	124	(9)	38	(7)
	170	64	(6)	94	(6)	135	(2)	155	(5)	168	(4)	12	(5)
	204	24	(4)	69	(6)	84	(4)	104	(5)	108	(1)	14	(3)

**Supplemental Table C7:** Biokinetic parameters obtained with nonlinear regression fitting of the Aiba et al. (1968) substrate inhibition model to observed methane production rates at various initial oleate concentrations using experimental digester sludges throughout Phases I and II (see *Supplemental Materials and Methods*). Values in parentheses indicate the parameter standard error based on the model fit.

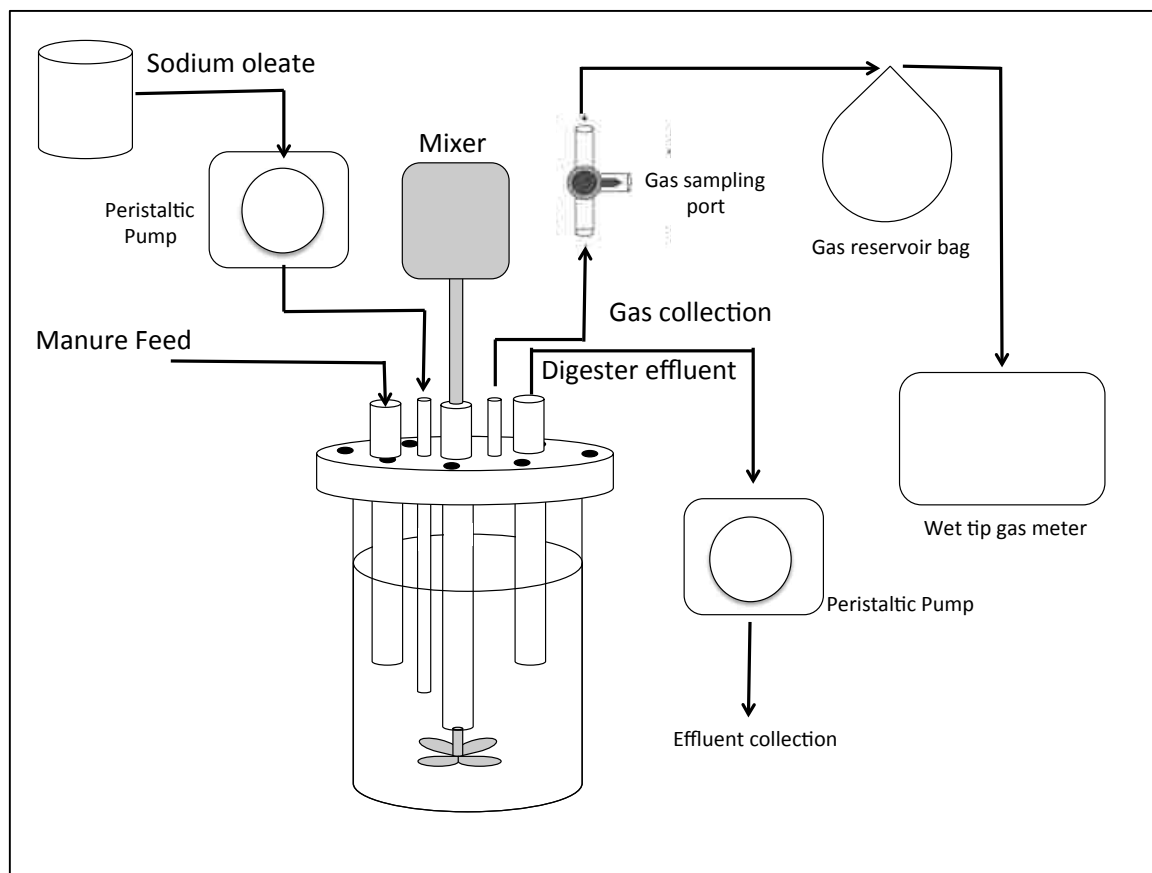
<b>Reactor</b>	<b>Day</b>	<b><math>K_s</math> (mg/L)</b>	<b><math>K_i</math> (mg/L)</b>	<b><math>q_{max}</math> (mL CH<sub>4</sub>/g VS-d)</b>
<b><i>Phase I Digesters</i></b>				
Control	0	17 (14)	2027 (249)	28 (1)
	41	68 (32)	1494 (185)	15 (1)
	84	18 (15)	2114 (282)	18 (1)
Continuous-Fed Co-digester	0	26 (16)	1994 (261)	33 (2)
	41	11 (9)	1388 (116)	40 (1)
	84	28 (18)	1804 (265)	65 (3)
Pulse-Fed Co-digester	0	18 (20)	1676 (294)	30 (2)
	41	44 (21)	1356 (154)	31 (1)
	84	153 (45)	2599 (302)	107 (5)
<b><i>Phase II Digesters</i></b>				
Pulse-Fed Co-digester	129	277 (123)	783 (61)	127 (7)
	148	628 (184)	2530 (217)	318 (15)
	170	893 (429)	1592 (143)	603 (36)
	204	1486 (931)	1622 (130)	540 (34)
Continuous-Fed Co-digester	129	373 (108)	10332 (2326)	250 (12)
	170	686 (250)	3347 (403)	299 (17)
	204	1450 (894)	1344 (85)	426 (22)



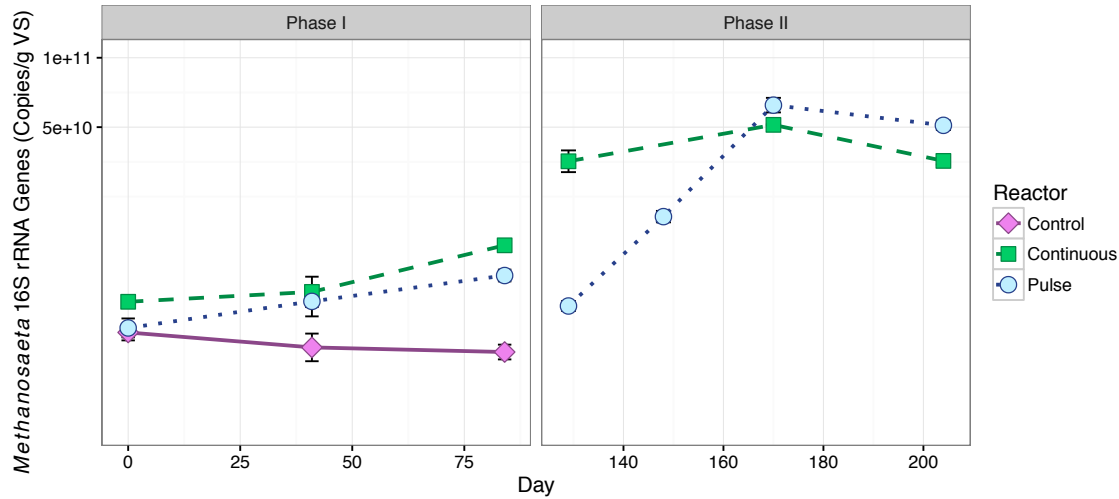
**Supplemental Table C8.** Summary results of the cross-validated multiple linear regression model for predicting  $q_{max,oleate}$  values based on the absolute abundance of 6 Syntrophomonas OTUs. The parameter estimate for the OTUs represents their contributions towards the overall model slope, and  $p$  represents the probability of a t value greater than the one obtained. Values for the residual standard error,  $R^2$ , and model F statistic are also given.

<b>Parameter</b>	<b>Estimate</b>	<b>Std. Error</b>	<b>t value</b>	<b><math>p</math></b>
Intercept	1.6E+01	7.6E+00	2.13	3.9E-02
seq_34	3.2E-09	6.2E-10	5.19	6.0E-06
seq_35	8.8E-10	1.8E-10	4.81	2.1E-05
seq_58	2.0E-09	5.2E-10	3.75	5.4E-04
seq_154	2.4E-09	1.1E-09	2.17	3.6E-02
seq_1083	2.3E-08	6.2E-09	3.70	6.4E-04
seq_7128	-7.0E-08	3.0E-08	-2.34	2.4E-02

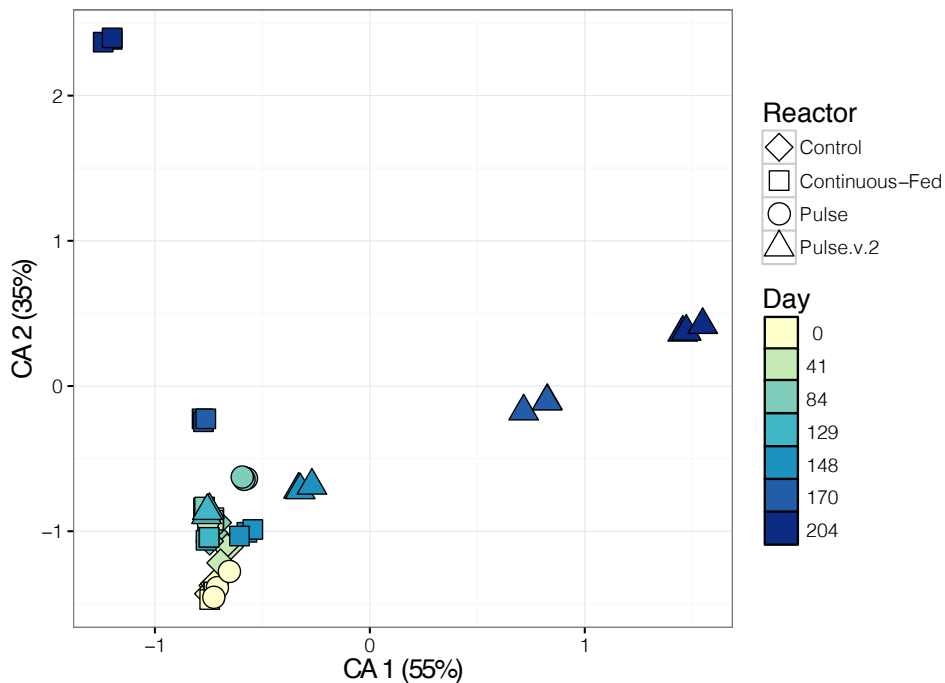
Residual standard error: 17.31 on 41 degrees of freedom  
Multiple  $R^2$ : 0.9112, Adjusted  $R^2$ : 0.8982  
F-statistic: 70.11 on 6 and 41 DF, p-value: < 2.2e-16



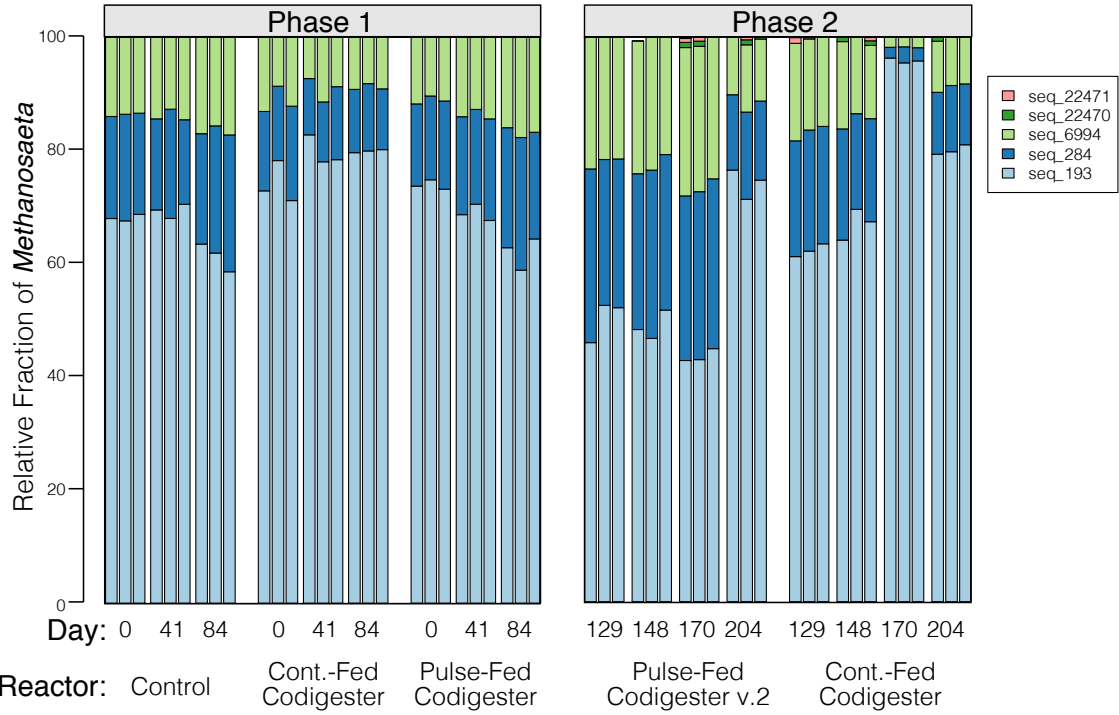
**Supplemental Figure C1:** A schematic showing the configuration of the experimental manure digesters. Note the sodium oleate feed line was only included in the codigesters.



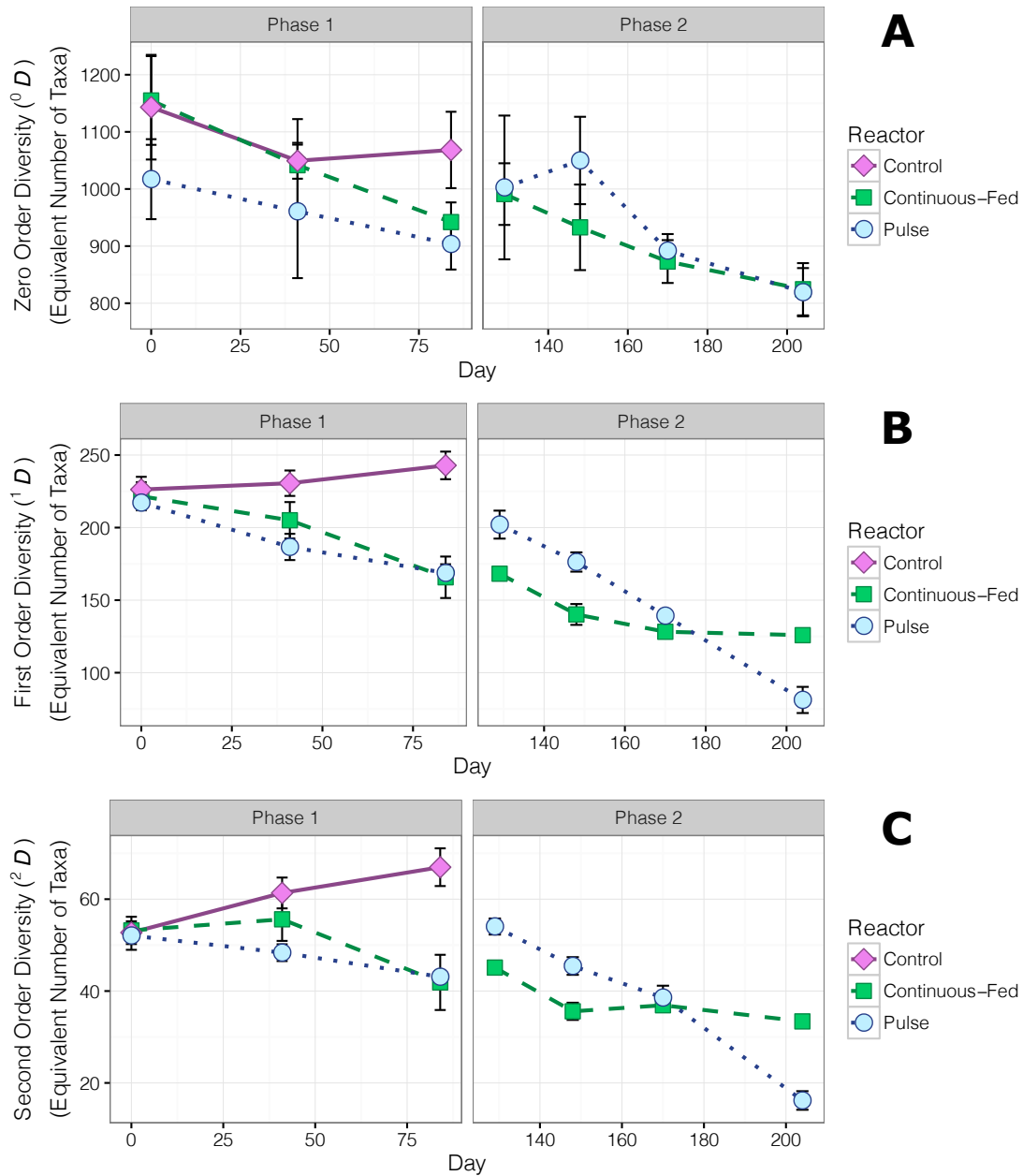
**Supplemental Figure C2:** Inferred absolute abundance of the genus *Methanoseta* over time in the experimental codigesters. Inferred abundance values were estimated by multiplying total *Archaea* 16S rRNA concentrations by the fraction of *Archaea* 16S amplicons classified to *Methanoseta*.



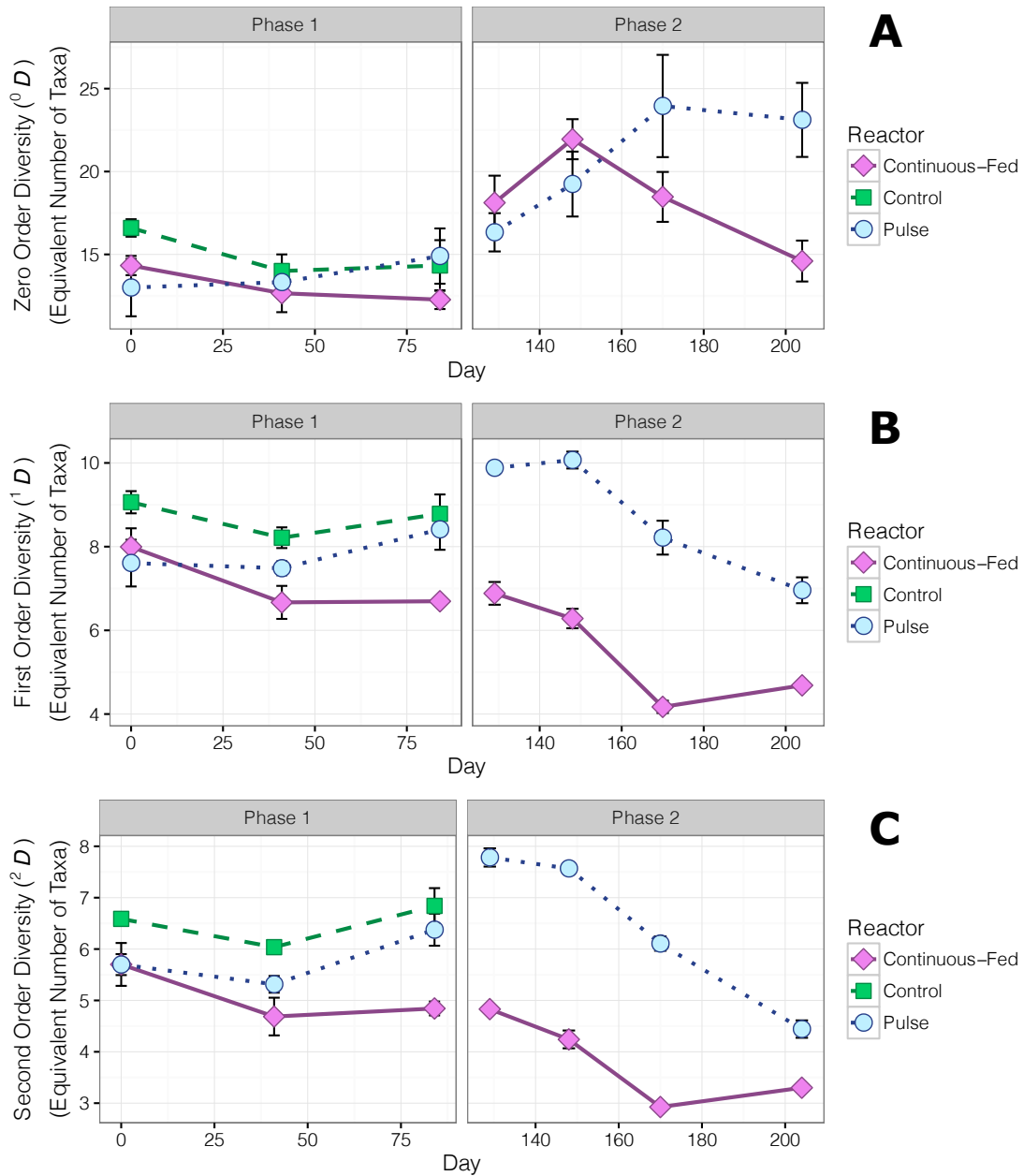
**Supplemental Figure C3:** Correspondence analysis (CA) plot based on *Syntrophomonas* normalized OTU sequence counts in the codigester and control digester samples collected throughout Phases I and II. The color of each marker represents the sample collection day and the shape of each marker represents the digester sludge source. The triplicate samples shown for each sample day are from replicate DNA extractions.



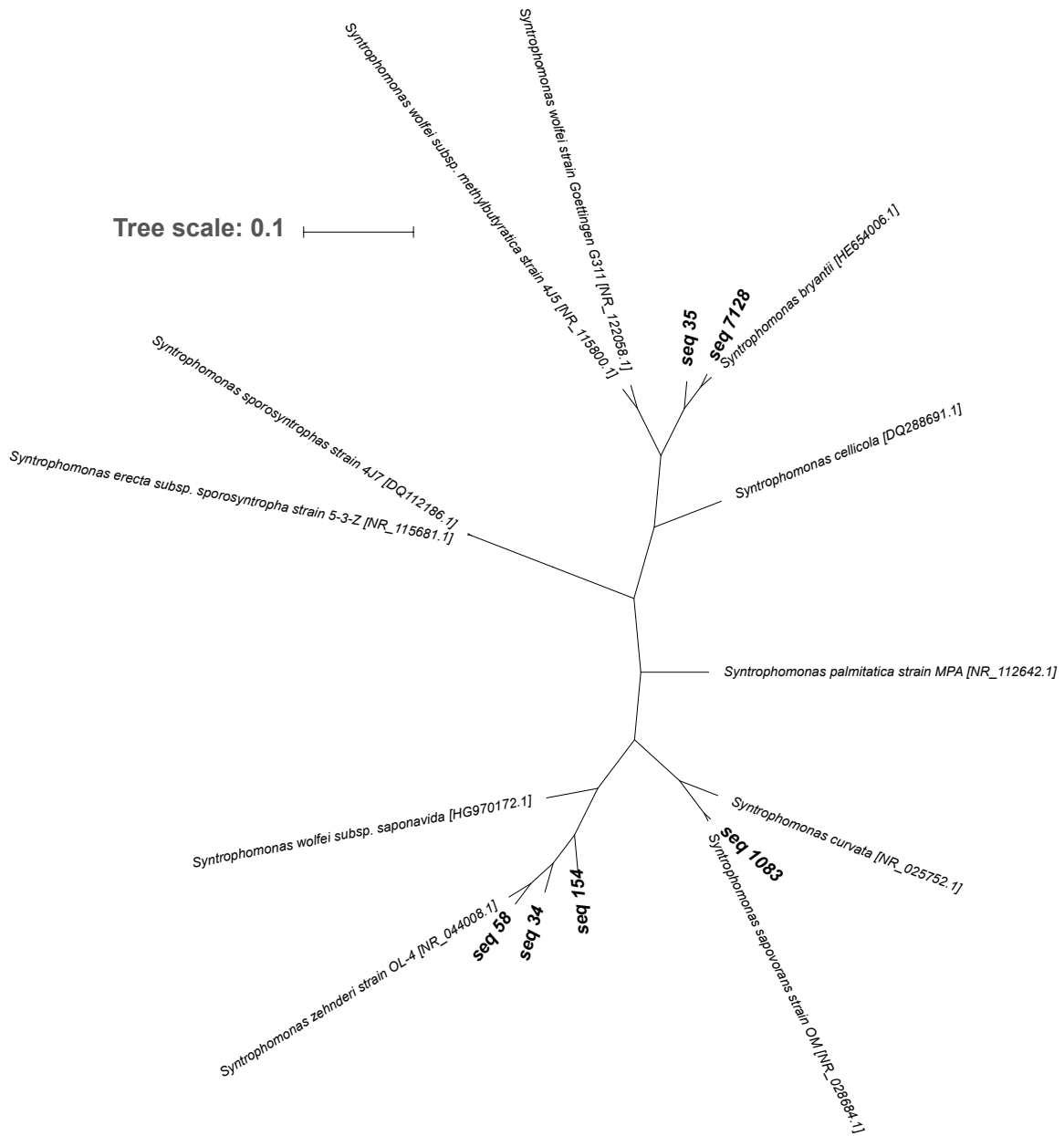
**Supplemental Figure C4:** Relative fractions of the 5 most abundant *Methanosaeta* OTUs within the *Methanosaeta* genus of the digesters during Phases I and II based on 16S rRNA amplicon sequencing.



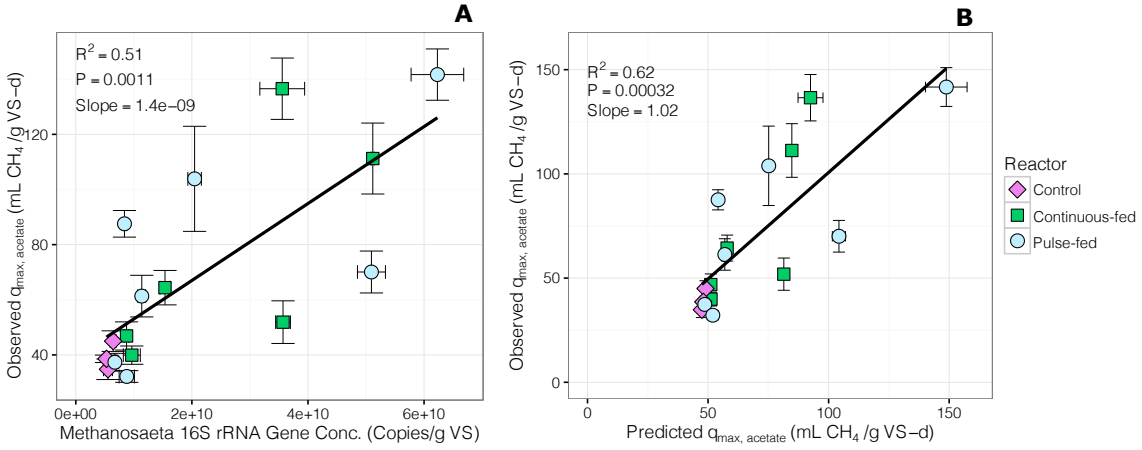
**Supplemental Figure C5:** Hill diversity numbers ( ${}^qD$ ) of orders (A)  $q=0$ , (B)  $q=1$ , and (C)  $q=2$  for the experimental digester *Bacteria* 16S rRNA sequence libraries throughout Phases I and II. Calculations were made after normalizing read counts with DESeq2 to account for unequal sequencing depths. Error bars represent a standard deviation based on triplicate DNA extractions for each time point.



**Supplemental Figure C6:** Hill diversity numbers ( ${}^qD$ ) of orders (A)  $q=0$ , (B)  $q=1$ , and (C)  $q=2$  for the experimental digester *Archaea* 16S rRNA sequence libraries throughout Phases I and II. Calculations were made after normalizing read counts with DESeq2 to account for unequal sequencing depths. Error bars represent a standard deviation based on triplicate DNA extractions for each time point.



**Supplemental Figure C7:** A phylogenetic tree of partial 16S rRNA gene sequences of the 6 *Syntrophomonas* OTUs selected in the multiple linear regression, along with other characterized *Syntrophomonas* species. 16S rRNA sequences of characterized species were retrieved from the NCBI database. The sequences were aligned with MUSCLE v3.8.31 (Edgar, R.C. (2004) *Nucleic Acids Res*, 32(5), 1792-97). The tree was constructed with ClustalW2 using the neighbor-joining method. Rendering was performed with iTOL (Letunic I. and Bork (2011) *Nucleic Acids Res*, doi: 10.1093/nar/gkr201).



**Supplemental Figure C8:** Linear regression of observed  $q_{max, acetate}$  values versus (A) the total *Methanosaeta* 16S rRNA gene concentration; and (B) the 16S rRNA gene concentration of 2 selected *Methanosaeta* OTUs (seq\_193 and seq\_284 from Fig. S4).



## APPENDIX D

### Supplemental Information for Chapter 6:

**DNA-stable isotope probing based metagenomics identifies key long-chain fatty acid degrading populations in parallel anaerobic codigesters with different oleate feeding strategies**

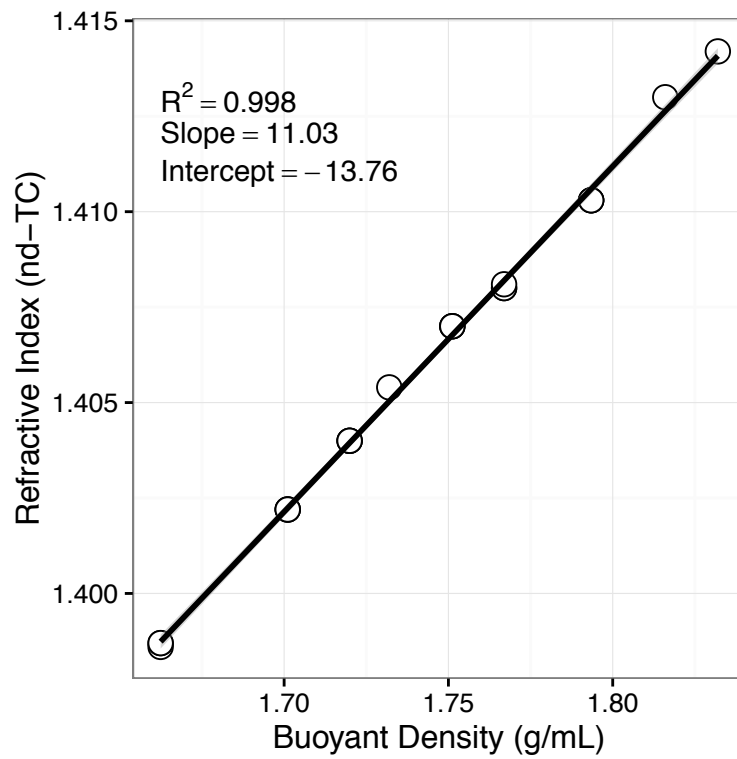
**Number of Pages: 11**

**Number of Tables: 3**

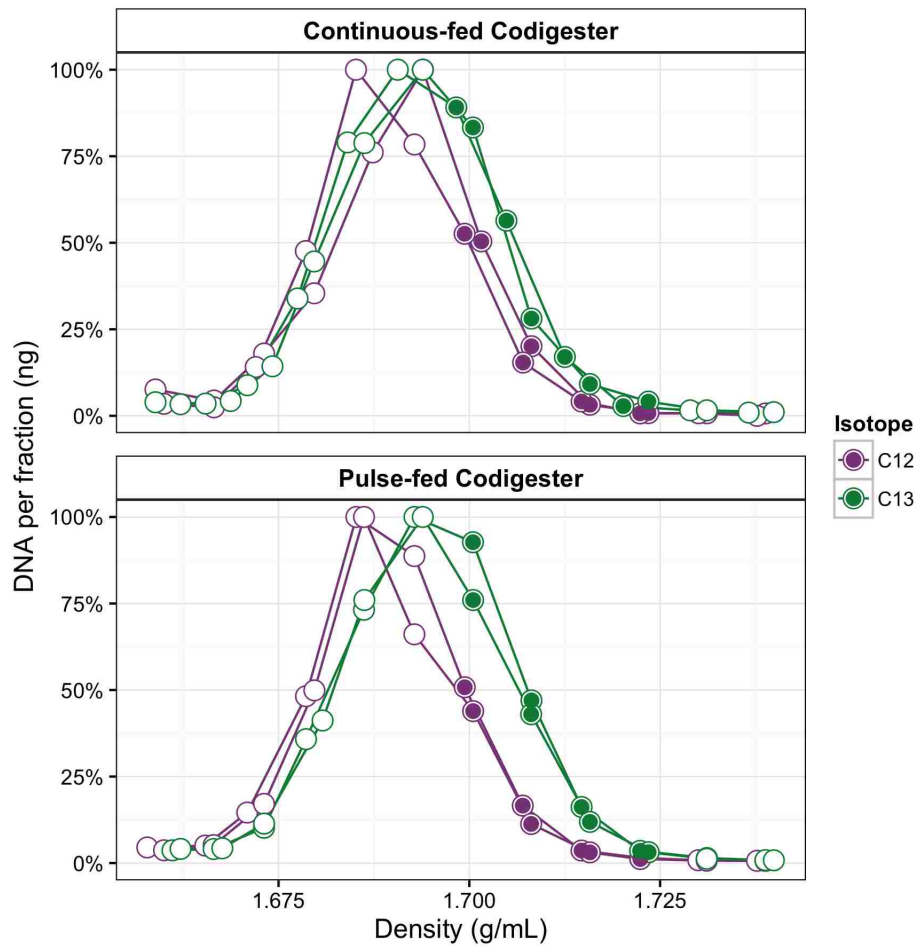
**Number of Figures: 6**

#### **Contents:**

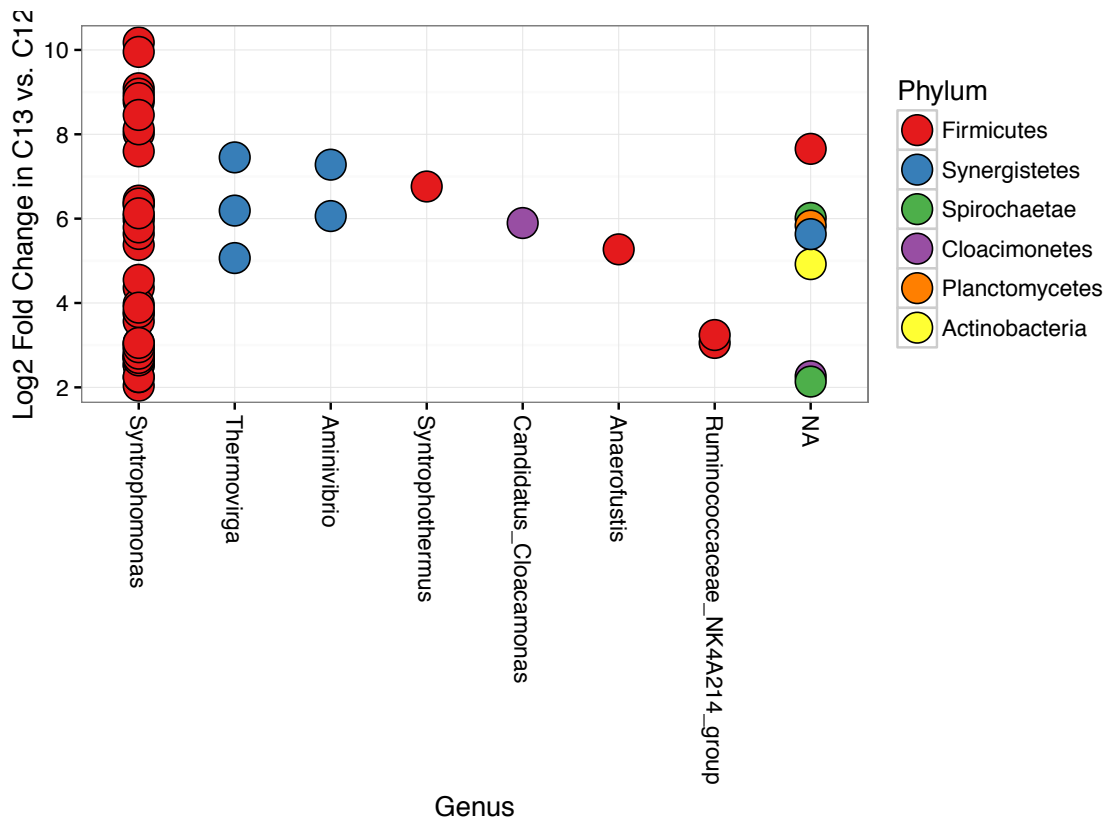
Supplemental Figure D1: Calibration curve of nd-TC versus the buoyant density	D2
Supplemental Figure D2: Total DNA concentration for each density gradient fraction	D3
Supplemental Figure D3: Genus and phylum level taxonomic assignments of 16S rRNA amplicon OTUs in the pulse-fed codigester that were significantly enriched in <sup>13</sup> C	D4
Supplemental Figure D4: Genus and phylum level taxonomic assignments of 16S rRNA amplicon OTUs in the continuous-fed codigester that were significantly enriched in <sup>13</sup> C	D5
Supplemental Figure D5: Venn-diagram of <sup>13</sup> C enriched <i>Syntrophomonas</i> OTUs	D5
Supplemental Figure D6: A phylogenetic tree of metagenomic GBs based on UPGMA clustering of <i>in-situ</i> DNA-DNA hybridization distances	D6
Supplemental Figure D7: Coverage values of KEGG ECs involved in interspecies hydrogen or formate transfer	D7
Supplemental Methods: Quantitative PCR	D8
Supplemental Methods: Modeling Methane Production Kinetics	D8
Supplemental Table D1: Summary of modeled methane production kinetic parameters	D9
Supplemental Table D2: Characteristics of all genome bins enriched in <sup>13</sup> C metagenomes	D10
Supplemental Table D3: Read coverage values for all KEGG EC's in Pathway Map 00071	D11



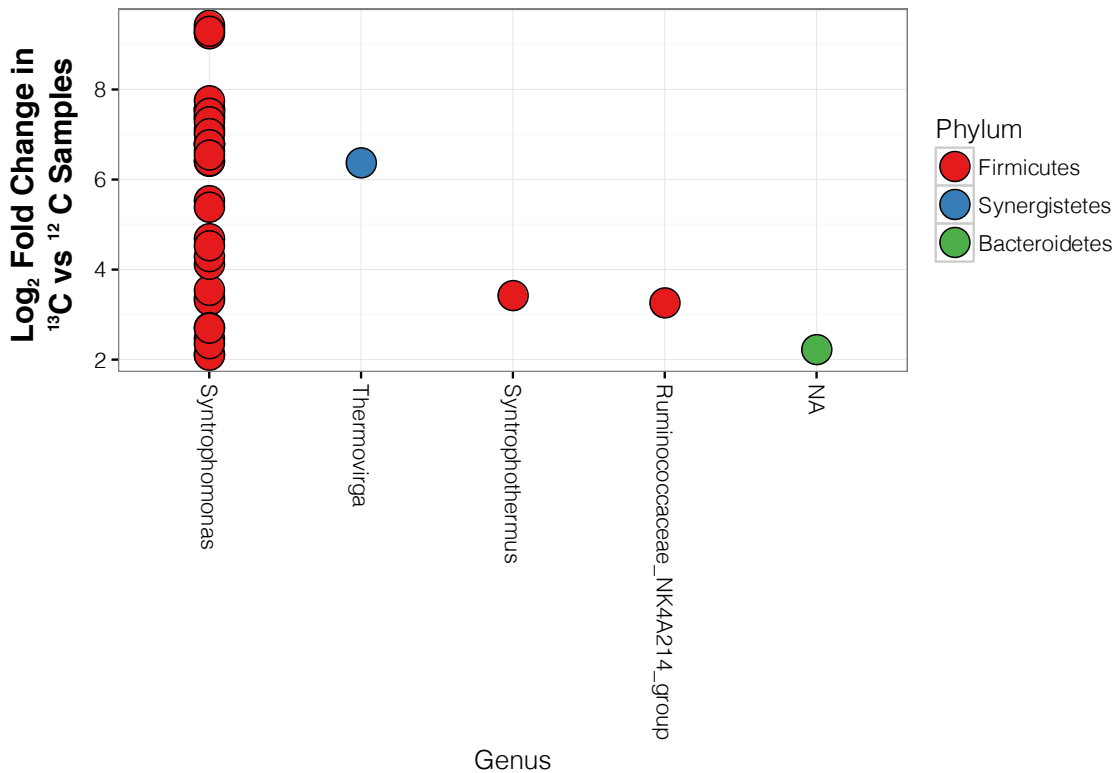
**Supplemental Figure D1:** Calibration curve of temperature-corrected refractive index (nd-TC) versus the buoyant density of the CsCl/TE solution used during isopycnic separation of DNA.



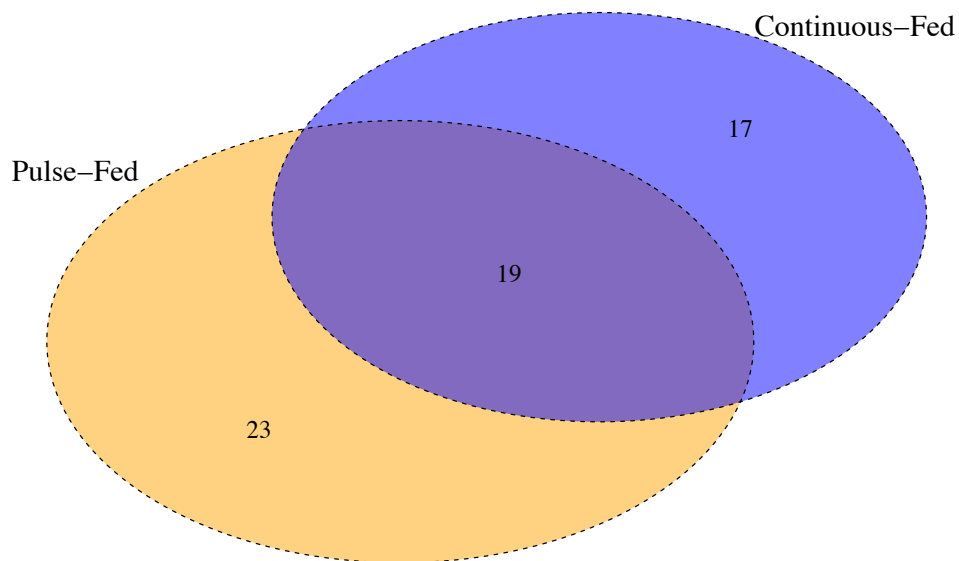
**Supplemental Figure D2:** Total DNA concentration measured by Qubit for each density gradient fraction recovered after isopycnic separation of DNA from the  $^{13}\text{C}$ -incubated microcosms and  $^{12}\text{C}$ -controls for both anaerobic codigester samples. The filled circles indicate gradient fractions that were selected and pooled for subsequent 16S rRNA amplicon sequencing and metagenomic sequencing. Each point represents an average of duplicate technical replicates.



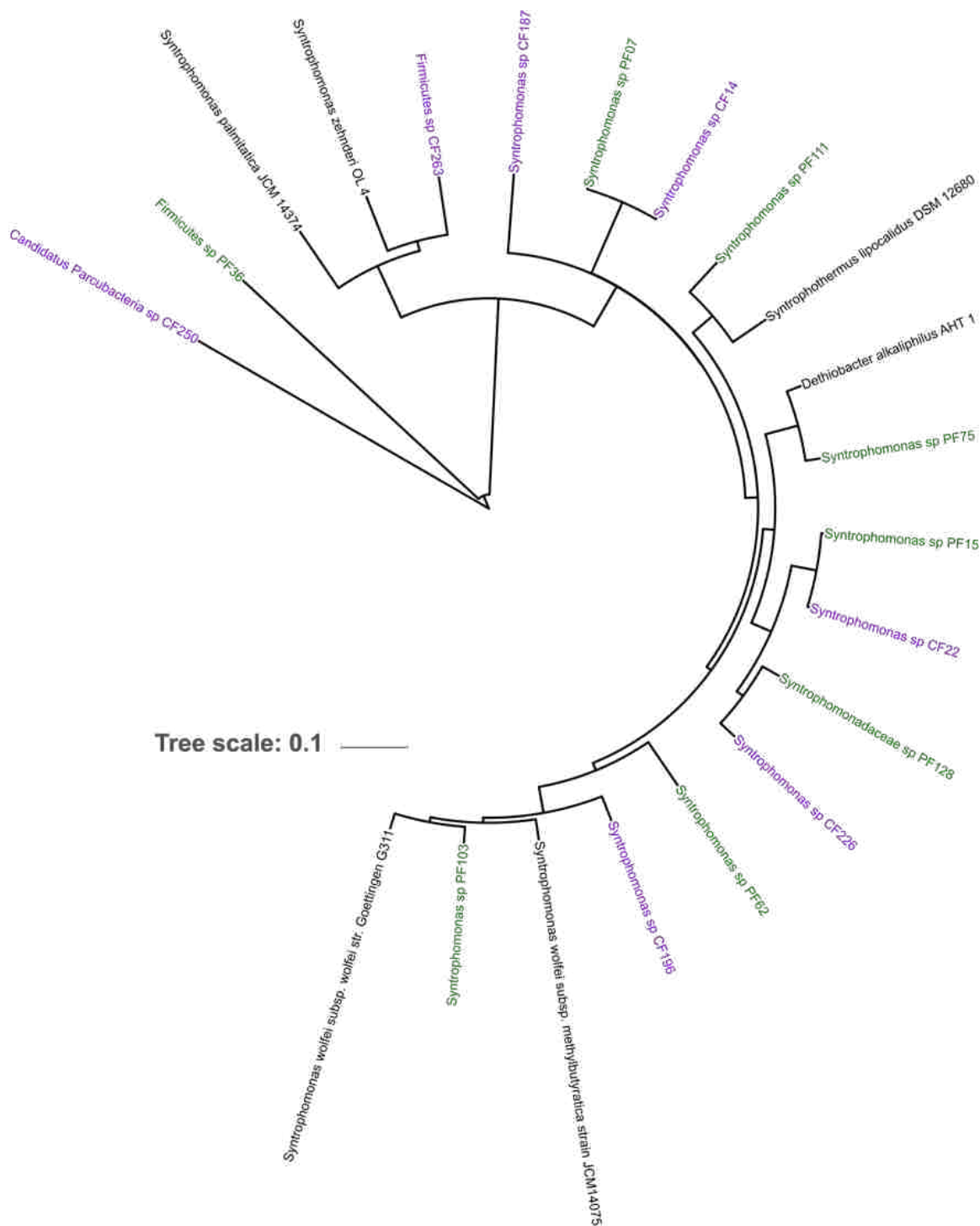
**Supplemental Figure D3:** Genus and phylum level taxonomic assignments of 16S rRNA amplicon OTUs in the pulse-fed codigester that were identified as significantly enriched in <sup>13</sup>C samples versus <sup>12</sup>C samples using DESeq2 (Love et al., 2014), along with their log<sub>2</sub> fold change.



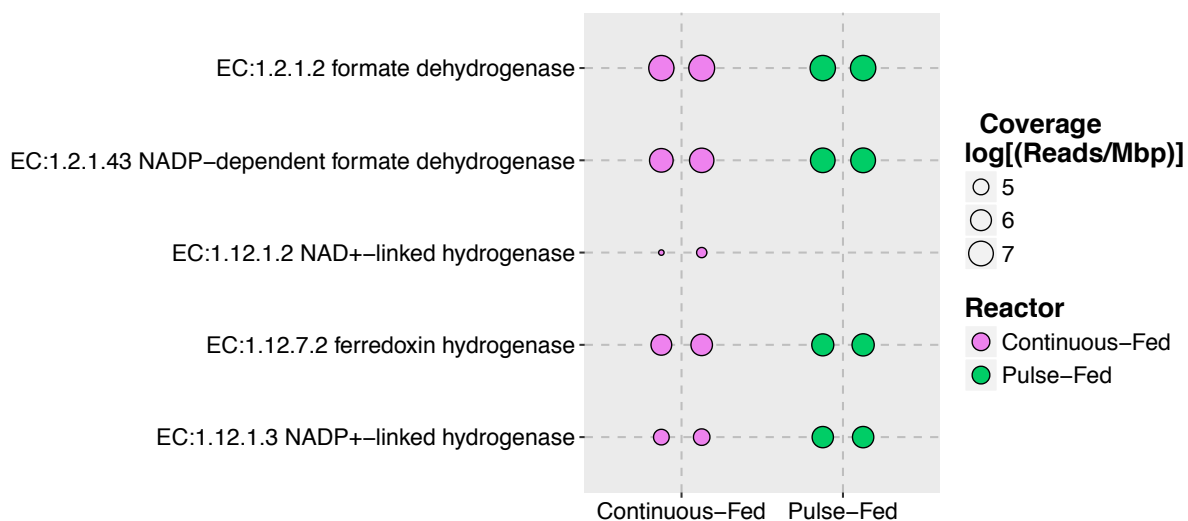
**Supplemental Figure D4:** Genus and phylum level taxonomic assignments of 16S rRNA amplicon OTUs in the continuous-fed codigester that were identified as significantly enriched in <sup>13</sup>C samples versus <sup>12</sup>C samples using DESeq2 (Love et al., 2014), along with their log<sub>2</sub> fold change.



**Supplemental Figure D5:** Venn-diagram of *Syntrophomonas* 16S rRNA OTUs that were significantly enriched in <sup>13</sup>C samples versus <sup>12</sup>C samples for both codigesters.



**Supplemental Figure D6:** A phylogenetic tree of metagenomic GBs based on UPGMA clustering of *in-situ* DNA-DNA hybridization distances calculated with GGDC (<http://ggdc.dsmz.de/>)



**Supplemental Figure D7:** Cumulative coverage values of KEGG ECs potentially involved in interspecies hydrogen or formate transfer based on all significantly enriched genome bins in the <sup>13</sup>C-incubated samples for both codigester metagenome sets. Values from duplicate microcosms are shown for both codigesters, and the size of the marker is proportional to the  $\log_{10}$  of the EC coverage.

## Supplemental Methods

### **Quantitative PCR:**

qPCR analysis on 16S rRNA genes of the genus *Syntrophomonas* using the primers Synm-678-F (CCWGGTGTAGCGGT) and Synm-738-F (TCAGGGYCAGTCCAG) and probe Synm-696-P (TGCGTAGAAATCAGGAGGAAYACCAGT), developed by Ziels et al. (2015). The hydrolysis probe was labeled with 6-FAM at the 5' end and BHQ-1 at the 3' end. qPCR was performed using a MasterCycler Realplex4 (Eppendorf). Each 20  $\mu$ L reaction mix contained 5  $\mu$ L DNA template, 2  $\mu$ L PCR-grade water, 500 nM of each forward and reverse primers, 200 nM of hydrolysis probe and 10  $\mu$ L TaqMan™ Fast Advanced Master Mix (2X, Applied Biosystems). All samples were analyzed in duplicate. No-template controls (NTCs) were included with each qPCR run. Precipitated DNA from each CsCl density gradient fraction was diluted 1:10 in nuclease-free water to prevent PCR inhibition. Calibration standards for the qPCR assays were prepared as described by Ziels et al. (2015), and were included in duplicate in each qPCR run for all target groups. Calibration standards included  $10^8$ ,  $10^7$ ,  $10^6$ ,  $10^5$ ,  $10^4$ ,  $10^3$ , and  $10^2$  gene copies per reaction. The average slope of the calibration curve was -3.39 (97% PCR efficiency) for *Syntrophomonas*, and the  $R^2$  value was above 0.99.

### **Modeling Methane Production Kinetics:**

A modified Gompertz equation was used to describe the inoculum-corrected methane production kinetics in the samples incubated with  $^{13}\text{C}$ -labeled oleate and the  $^{12}\text{C}$ -controls:

$$M(t) = P \cdot \exp \left[ -\exp \left[ \frac{q_{\max} \cdot e}{P} (\lambda - t) + 1 \right] \right]$$

where  $M$  is the accumulated methane (mL  $\text{CH}_4$ ) minus the blank control at time =  $t$  (days),  $P$  is the maximum cumulative methane production (mL  $\text{CH}_4$ ),  $q_{\max}$  is the maximum methane production rate (mL  $\text{CH}_4/\text{hr}$ ),  $e$  is 2.7182818, and  $\lambda$  is the lag-phase time (hr). The model fitting



and parameter standard error estimation was conducted with nonlinear regression in R version 3.0.2.

**Supplemental Table D1:** Summary of modeled methane production kinetic parameters determined by fitting the modified Gompertz equation to observed cumulative methane curves using nonlinear regression.

Feed Round	Pulse-Fed Codigester						Continuous-Fed Codigester					
	$P$ (mL CH <sub>4</sub> )		$q_{max}$ (mL CH <sub>4</sub> /hr)		$\lambda$ (hr)		$P$ (mL CH <sub>4</sub> )		$q_{max}$ (mL CH <sub>4</sub> /hr)		$\lambda$ (hr)	
1	24.9	0.7	0.85	0.05	3.3	0.9	25.7	1.0	0.67	0.03	2.3	0.8
2	26.3	0.5	1.02	0.05	3.7	0.6	25.3	0.5	0.84	0.03	1.8	0.5
3	27.8	0.4	1.14	0.04	3.6	0.4	26.3	0.5	0.98	0.04	2.3	0.5

**Supplemental D2:** Read coverage, taxonomic classification, and other characteristics of all genome bins that were significantly enriched in <sup>13</sup>C metagenomes relative to <sup>12</sup>C controls for both codigester sample sets. This set includes genome bins with less than 40% completeness.

Genome Bin I.D.	Coverage in 12-C Metagenomes (reads/Mbp) <sup>a</sup>		Coverage in 13-C Metagenomes (reads/Mbp) <sup>a</sup>		Log2 fold-change <sup>b</sup>	p-value <sup>b</sup>	Taxonomy <sup>c</sup>	Completeness <sup>d</sup>	GC	Size (Mbp)	Coding Density <sup>d</sup>
	A	B	A	B							
<b>Pulse-fed Codigester Genome Bins</b>											
bin.19	3.41E+04	2.83E+04	9.94E+05	1.11E+06	5.05	4E-224	<i>Syntrophomonas</i>	14%	39.8%	0.26	90%
bin.15	4.56E+04	3.95E+04	1.09E+06	1.24E+06	4.75	2E-207	<i>Syntrophomonas</i>	47%	41.4%	1.21	86%
bin.11	7.36E+04	6.67E+04	1.37E+06	1.59E+06	4.37	5E-180	<i>Syntrophomonas</i>	38%	43.7%	1.01	87%
bin.86	5.23E+03	3.59E+03	9.41E+04	8.51E+04	4.31	3E-119	Unresolved	0%	38.3%	0.25	88%
bin.75	1.12E+04	8.92E+03	1.84E+05	1.91E+05	4.20	1E-152	<i>Syntrophomonas</i>	90%	41.2%	2.10	89%
bin.62	1.31E+04	9.59E+03	1.61E+05	1.48E+05	3.75	3E-103	<i>Syntrophomonas</i>	97%	43.5%	2.66	87%
bin.137	5.48E+03	4.64E+03	6.56E+04	6.14E+04	3.63	1E-123	<i>Syntrophomonas</i>	23%	40.6%	1.08	86%
bin.103	1.11E+04	8.26E+03	1.13E+05	9.55E+04	3.41	5E-83	<i>Syntrophomonas</i>	57%	44.6%	1.12	85%
bin.36	3.16E+04	2.72E+04	2.97E+05	3.10E+05	3.35	1E-110	<i>Firmicutes</i>	85%	50.8%	1.60	90%
bin.87	1.77E+04	1.34E+04	1.53E+05	1.34E+05	3.19	5E-77	<i>Syntrophomonas</i>	18%	48.5%	0.53	89%
bin.111	1.13E+04	1.06E+04	9.55E+04	9.28E+04	3.09	3E-105	<i>Syntrophomonas</i>	89%	45.7%	3.38	88%
bin.2	3.48E+05	3.02E+05	2.54E+06	2.20E+06	2.85	9E-75	<i>Syntrophomonas</i>	39%	46.4%	0.70	91%
bin.7	1.61E+05	1.63E+05	1.04E+06	1.12E+06	2.73	2E-81	<i>Syntrophomonas</i>	74%	49.7%	1.27	89%
bin.128	9.25E+03	9.39E+03	5.86E+04	6.05E+04	2.66	8E-80	<i>Syntrophomonadaceae</i>	98%	46.4%	2.71	88%
bin.109	1.64E+04	1.48E+04	9.82E+04	9.11E+04	2.59	9E-69	<i>Syntrophomonas</i>	21%	47.4%	0.78	88%
bin.4	2.95E+05	2.92E+05	1.32E+06	1.52E+06	2.27	8E-53	<i>Syntrophomonas</i>	26%	53.3%	0.69	89%
<b>Continuous-Fed Genome Bins</b>											
bin.22	3.36E+04	4.79E+04	9.06E+05	1.40E+06	4.69	2E-60	<i>Syntrophomonas</i>	74%	41.4%	2.00	86%
bin.15	7.76E+04	9.67E+04	1.45E+06	2.24E+06	4.29	1E-54	<i>Syntrophomonas</i>	22%	44.4%	0.54	87%
bin.170	4.91E+03	6.25E+03	6.43E+04	7.49E+04	3.56	2E-46	<i>Syntrophomonas</i>	36%	45.6%	0.59	85%
bin.20	9.19E+04	6.91E+04	6.21E+05	1.25E+06	3.42	3E-27	<i>Syntrophomonas</i>	7%	44.2%	0.25	88%
bin.17	1.42E+05	9.77E+04	8.46E+05	1.70E+06	3.29	2E-24	<i>Syntrophomonas</i>	31%	46.2%	0.55	90%
bin.142	8.10E+03	1.08E+04	9.25E+04	1.09E+05	3.34	3E-39	<i>Syntrophomonas</i>	7%	49.2%	0.27	90%
bin.283	8.56E+02	8.79E+02	6.68E+03	1.03E+04	3.21	3E-31	Unresolved	13%	45.8%	0.54	88%
bin.13	2.16E+05	1.39E+05	1.13E+06	2.28E+06	3.14	8E-22	<i>Syntrophomonas</i>	23%	48.5%	0.46	92%
bin.196	4.98E+03	4.92E+03	3.72E+04	5.87E+04	3.19	5E-32	<i>Syntrophomonas</i>	72%	42.9%	2.41	87%
bin.226	4.45E+03	3.67E+03	2.31E+04	3.77E+04	2.82	1E-23	<i>Syntrophomonas</i>	98%	47.6%	3.18	88%
bin.14	1.81E+05	1.74E+05	9.92E+05	1.32E+06	2.65	1E-26	<i>Syntrophomonas</i>	63%	49.7%	0.78	89%
bin.171	9.70E+03	9.16E+03	4.44E+04	6.36E+04	2.46	2E-21	Unresolved	0%	44.0%	0.44	85%
bin.213	8.07E+03	7.50E+03	3.63E+04	4.99E+04	2.42	3E-21	Unresolved	0%	39.0%	0.28	86%
bin.263	1.12E+03	1.22E+03	5.27E+03	7.88E+03	2.43	4E-20	<i>Firmicutes</i>	83%	50.6%	4.81	92%
bin.12	2.97E+05	3.06E+05	1.34E+06	1.92E+06	2.38	3E-20	<i>Syntrophomonas</i>	28%	52.9%	0.61	90%
bin.193	1.08E+03	7.62E+02	4.45E+03	4.89E+03	2.29	8E-17	<i>Syntrophus</i>	32%	53.4%	0.29	89%
bin.250	5.63E+02	4.61E+02	1.83E+03	2.85E+03	2.12	1E-11	<i>Candidatus Parcubacteria</i>	40%	30.8%	0.25	91%
bin.187	7.45E+03	8.50E+03	3.47E+04	3.78E+04	2.14	1E-19	<i>Syntrophomonas</i>	86%	45.6%	2.12	89%

<sup>a</sup> Based on normalized read counts with DESeq2; <sup>b</sup> Determined with DESeq2; <sup>c</sup> Based on LCA of BLAST output;

<sup>d</sup> Based on CheckM output

**Supplemental Table D3:** Read coverage values (in reads/Mbp) for all KEGG EC's in the Pathway Map 00071 for significantly enriched genome bins in each <sup>13</sup>C and <sup>12</sup>C DNA-SIP metagenome, along with auxiliary genes for LCFA double bond degradation (EC's 5.3.3.8, 5.3.3.-, 1.3.1.34). Coverage values of ECs across samples were calculated as the sum of each significantly enriched genome bin coverage value multiplied by the EC frequency within the genome bin.

EC Number	Name	Pulse-fed Codigester Samples				Continuous-fed Codigester Samples			
		12-C		13-C		12-C		13-C	
EC:6.2.1.3	long-chain fatty acid-CoA ligase	2.38E+06	2.16E+06	3.16E+07	3.43E+07	1.93E+06	1.93E+06	2.51E+07	4.10E+07
EC:2.3.1.21	carnitine O-palmitoyltransferase	0	0	0	0	0	0	0	0
EC:1.3.3.6	fatty acyl-coenzyme A oxidase	0	0	0	0	0	0	0	0
EC:1.3.8.8	long-chain acyl-CoA dehydrogenase	0	0	0	0	0	0	0	0
EC:1.3.8.7	medium-chain acyl-CoA dehydrogenase	1.29E+06	1.17E+06	1.05E+07	1.04E+07	9.77E+05	8.69E+05	7.61E+06	1.29E+07
EC:1.3.8.9	very long-chain acyl-CoA dehydrogenase	0	0	0	0	0	0	0	0
EC:1.3.99.-	acyl-CoA dehydrogenase	1.13E+04	1.06E+04	9.55E+04	9.28E+04	0	0	0	0
EC:1.3.8.1	short-chain acyl-CoA dehydrogenase	1.54E+06	1.50E+06	1.14E+07	1.23E+07	1.25E+06	1.18E+06	8.18E+06	1.25E+07
EC:4.2.1.17	enoyl-CoA hydratase	4.31E+06	3.93E+06	3.75E+07	3.72E+07	2.94E+06	2.49E+06	2.30E+07	3.91E+07
EC:4.2.1.74	long-chain-enoyl-CoA hydratase	0	0	0	0	0	0	0	0
EC:1.1.1.35	3-hydroxyacyl-CoA dehydrogenase	1.10E+05	1.05E+05	8.40E+05	8.59E+05	1.08E+03	7.62E+02	4.45E+03	4.89E+03
EC:1.1.1.36	(R)-3-hydroxyacyl-CoA dehydrogenase	2.14E+04	1.64E+04	3.19E+05	2.93E+05	4.98E+03	4.92E+03	3.72E+04	5.87E+04
EC:1.1.1.211	long-chain-3-hydroxyacyl-CoA dehydrogenase	0	0	0	0	0	0	0	0
EC:2.3.1.16	acetyl-CoA acyltransferase	3.00E+05	2.93E+05	2.20E+06	2.28E+06	1.48E+05	1.40E+05	1.66E+06	2.84E+06
EC:2.3.1.9	acetyl-CoA acyltransferase	3.77E+06	3.47E+06	2.77E+07	2.72E+07	2.16E+06	1.93E+06	1.50E+07	2.50E+07
EC:2.7.2.1	acetate kinase	6.53E+05	5.89E+05	5.68E+06	5.56E+06	5.39E+04	6.86E+04	1.02E+06	1.55E+06
EC:2.7.2.12	acetate kinase (diphosphate)	0	0	0	0	0	0	0	0
EC:2.3.1.8	phosphate acetyltransferase	6.53E+05	5.89E+05	5.68E+06	5.56E+06	2.32E+05	2.40E+05	2.00E+06	2.86E+06
EC:5.3.3.8	delta-3,delta-2-enoyl-CoA isomerase	0	0	0	0	0	0	0	0
EC:5.3.3.-	delta-3,5,delta-2,4-dienoyl-CoA isomerase	0	0	0	0	0	0	0	0
EC:1.3.1.34	delta-2,delta-4-dienoyl-CoA reductase	1.72E+05	1.74E+05	1.14E+06	1.21E+06	1.49E+04	1.70E+04	6.93E+04	7.57E+04

# Ryan Ziels

## Curriculum Vitae

---

Phone: (360) 739-9143

Email: ziels@uw.edu

### **CURRICULUM VITAE IN SHORT (FOR MORE DETAILS, PLEASE SEE FULL CV)**

Ryan Ziels was raised within the Pacific Northwest in the city of Bellingham, Washington. Having developed a deep respect for the inspiring environment in the northwest region, Ryan sought an undergraduate degree in Environmental Resource Engineering (ERE) at Humboldt State University (HSU) in Arcata, California. During his undergraduate tenure, he was supported by the National Oceanic and Atmospheric Science's Hollings Fellowship, which also provided him with his first research experience in environmental science and engineering. He graduated at the top of his class at HSU in 2011, receiving both the ERE Roscoe Schenler Award and Outstanding Graduate in ERE Award, as well as the Academic Excellence Award for the entire College of Natural Resources and Science. Having developed research skills in biological water treatment technologies through an NSF-funded undergraduate program, Ryan sought to further advance the field of environmental biotechnology by joining the graduate program in Civil and Environmental Engineering at the University of Washington (UW) in the group of Dr. David Stensel. He was awarded the prestigious NSF Graduate Research Fellowship in 2011 to support his graduate endeavors at the UW. He conducted his Master's research at the UW on biodegradation of pharmaceutical estrogens during wastewater treatment, which resulted in several peer reviewed papers and international conference presentations. In 2013, Ryan commenced his PhD at the UW on anaerobic conversion of fats, oils, and greases for renewable methane production, which was supported by a U.S. EPA grant proposal that he primarily drafted. He was the recipient of the NSF Graduate Research Opportunities Worldwide (GROW) fellowship and UW Valle Scholarship in 2013, which supported his 8-month research exchange to the Biogas Research Center at Linköping University in Sweden. He received further support for his PhD research with a Department of Energy (DOE) Joint Genome Institute grant that he solely drafted. He was also the recipient of the prestigious Water Environment Foundation Canham Award in 2015. He received the NSF GROW fellowship a second time, to support his research exchange to the Laboratory of Microbiology at Wageningen University in the spring of 2016. Ryan expects to receive his PhD degree in Civil and Environmental Engineering from the UW in the fall of 2016.

# Ryan Ziels

## Curriculum Vitae

---

Phone: (360) 739-9143

Email: ziels@uw.edu

### Educational History

---

*June 2013-Current* *University of Washington* *Seattle, WA*

#### **PhD Candidate in Civil and Environmental Engineering**

Advisor: H. David Stensel

*Thesis:* Microbial ecology and degradation kinetics of fats, oils, and grease (FOG) in anaerobic digestion systems.

*Sept. 2011 – June 2013* *University of Washington* *Seattle, WA*

#### **MSE in Civil and Environmental Engineering**

Advisor: H. David Stensel

*Thesis:* Influence of Kinetic and Metabolic Selection on 17 $\alpha$ -ethinylestradiol Biodegradation in Activated Sludge Wastewater Treatment Systems

*Aug. 2006 – May 2011* *Humboldt State University* *Arcata, CA*

#### **BS in Environmental Resources Engineering**

Summa Cum Laude

### Professional History

---

*Sept. 2011- Current* *University of Washington* *Seattle, WA*

#### **Graduate Research Assistant**

*Research:* Biological treatment processes:

(1) Ecophysiology of syntrophic microorganisms degrading lipids and long-chain fatty acids in biogas processes

- Designed and operated anaerobic biogas reactors for converting fats, oils, and greases into renewable methane
- Developed molecular microbiology approaches for assessing microbial ecology in bioreactors
  - Metagenomics, transcriptomics, amplicon sequencing, bioinformatics quantitative PCR, stable isotope probing
- Conducted bioassays to measure methane production rates and inhibition

kinetics from long-chain fatty acids

- Developed GC-FID method for detecting free fatty acids in reactor samples

(2) Pharmaceutical biodegradation during activated sludge wastewater treatment processes

- LC-MS/MS method development for quantification of steroid estrogens in water samples
- Designed and operated pilot treatment units at King County treatment plant.
- Conducted kinetic bioassays for measuring estrogen removal rates by bacterial communities.
- Analyzed treatment process performance of pilot systems

*March 2016-July 2016*

*Laboratory of Microbiology  
Wageningen University*

*Wageningen,  
Netherlands*

**Visiting Researcher / NSF Graduate Research Opportunities Worldwide (GROW) Fellow**

*Research:* Develop bioinformatics techniques to analyze metagenomic and transcriptomic sequencing datasets from stable-isotope probing experiments on syntrophic anaerobic communities degrading fatty acids.

*June 2013-Feb. 2014*

*Linköping University  
Biogas Research Center*

*Linköping, Sweden*

**Visiting Researcher / NSF Graduate Research Opportunities Worldwide (GROW) Fellow**

*Research:* Developed quantitative PCR (qPCR) assays and metagenomic approaches to target syntrophic bacterial populations responsible for converting waste fats, oils, and grease into substrates for methane in full-scale anaerobic digesters.

*May-August 2010*

*Clarkson University*

*Potsdam, NY*

**National Science Foundation REU Fellow**

*Research:* Operated lab-scale anaerobic digesters to investigate the performance and economic feasibility of anaerobic co-digestion of glycerol and whey with manure.

*May -August 2009*

*National Oceanic and Atmospheric Administration  
Northwest Fisheries Science Center*

*Seattle, WA*

### **Ernest F. Hollings Research Fellow**

*Research:* Modeled juvenile salmon migration through the nearshore Skagit River delta in an effort to design and model effective habitat restoration strategies.

*January –August 2008*

*Redwood Coast Energy Authority*

*Eureka, CA*

### **Energy Efficiency Intern**

Implemented Energy Watch Program

Provided and designed energy conservation measures to commercial buildings

*September 2006-May 2007*

*Humboldt State University*

*Arcata, CA*

### **Energy Management Intern**

Planned and performed energy audits on campus buildings

Implemented energy-saving programs to reduce greenhouse gas emissions

---

## **Teaching Experience**

---

*2013-Current*

*University of Washington*

*Seattle, WA*

### **Guest Lecturer**

Taught lectures for the courses:

- *Biological Treatment Systems (CEE 541)*
- *Wastewater Treatment and Reuse (CEE 482)*

*2008-2011*

*Humboldt State University*

*Arcata, CA*

### **Instructional Student Assistant**

Classes Taught (under supervision of professor):

*Water Quality Laboratory*

*Computational Methods for Environmental Engineering Laboratory*

*Introduction to Environmental Science and Engineering Laboratory*

---

## **Peer-Refereed Publications**

---

**Ziels, R.M.,** Karlsson, A., Beck, D. A. C., Ejlertsson, J., Yekta S., Bjorn A., Stensel, H. D., Svensson, B. H. (2016) Microbial community adaptation influences long-chain fatty acid conversion during anaerobic codigestion of fats, oils, and grease with municipal sludge. *Water Research*. 103, 372-382 doi: 10.1016/j.watres.2016.07.04

---

Yekta S., **Ziels R.M.**, Björn A., Skyllberg U., Ejlertsson J., Karlsson A., Svedlund M., Wilen M., Svensson B.H. (2016) Effects of sulfide on anaerobic digestion of iron-rich primary and activated sewage sludge. *Under Review at Water Research*

**Ziels, R.M.**, Beck, D. A. C., Marti, M., Gough, H. L., Stensel, H. D., Svensson, B. H. (2015) Monitoring the dynamics of syntrophic  $\beta$ -oxidizing bacteria during anaerobic degradation of oleic acid. *FEMS Microbiology Ecology*. 91(4) doi: 10.1093/femsec/fiv028

Lust, M. J., **Ziels, R. M.**, Strand, S. E., Gough, H. L., Stensel, H. D. (2015) Biodegradation kinetics of 17 $\alpha$ -ethinylestradiol in activated sludge treatment processes. *Environmental Engineering Science*. 32(7) doi:10.1089/ees.2014.0467

**Ziels, R. M.**, Lust, M. J., Gough, H. L., Strand, S. E., & Stensel, H. D. (2014). Influence of Bioselector Processes on 17 $\alpha$ -Ethinylestradiol Biodegradation in Activated Sludge Wastewater Treatment Systems. *Environmental science & technology*, 48(11), 6160-6167. doi: 10.1021/es405351b

---

## Conference Proceedings and Other Non-Journal Articles

---

### **Reviewed by Abstract Only:**

**Ziels, R. M.**, Karlsson A., Ejlertsson, J., Yekta, S., Bjorn, A., Stensel, H.D., Svensson, B. H. Dynamics Of Syntrophic LCFA-degrading Bacteria During Co-digestion Of FOG With Municipal Sludge. *Proceedings of the 14<sup>th</sup> IWA World Congress on Anaerobic Digestion (AD14)*, Viña del Mar, Chile, November 2015. (Oral presentation)

**Ziels, R. M.**, Karlsson A., Ejlertsson, J., Yekta, S., Bjorn, A., Stensel, H.D., Svensson, B. H. Importance of Syntrophic Long-Chain Fatty Acid-Degrading Bacteria During Anaerobic Co-Digestion of FOG With Municipal Wastewater Sludge. *Proceedings of the Water Environment Federation*, Chicago, September 2015. (Oral presentation).

**Ziels, R.M.**, Beck, D. A. C., Marti, M., Gough, H. L., Stensel, H. D., Svensson, B. H. Quantitative importance of syntrophic  $\beta$ -oxidizing bacteria during anaerobic degradation of oleic acid. *2nd International Conference on Biogas Microbiology (ICBM)*, Uppsala, Sweden, June 2014. (Oral Presentation)

**Ziels, R.M.**, Ojong, P, Yekta, S.S., Gustavsson, K., Svensson, B.H., Björn, A., Ejlertsson, J., Karlsson, A. Impacts of co-digesting waste vegetable oil with primary and waste activated sludge on microbial community and process performance. *Green Gas Sweden Research Outlook*, March 2014. (Oral Presentation)

**Ziels, R.M.**, Lust, M. J., Strand, S. E., Gough, H. L., Stensel, H. D. Influence of Kinetic and Metabolic Selection on 17 $\alpha$ -ethinylestradiol Biodegradation in Activated Sludge Wastewater Treatment Systems. *Proceedings of the 8th IWA Specialized Conference on Assessment and control of micropollutants and hazardous substances in water: Micropol & Ecohazard*, Zurich, Switzerland, June 2013. (Oral Presentation)



**Ziels, R. M.**, K. Venkiteshwaran, S. J. Grimberg. Organic loading effects on acidification during the two-phased anaerobic co-digestion of lactose with dairy manure, *37<sup>th</sup> North East Regional Meeting (NERM) of the American Chemical Society (ASC)*, Potsdam, NY, June 2010. (Poster Presentation)

**Ziels, R. M.**, K. Venkiteshwaran, S. J. Grimberg. Effect of substrate and organic loading on the two-phased anaerobic co-digestion of glycerol and lactose with dairy manure. *Symposium for Undergraduate Research Experience*, Potsdam, NY, July 2010. (Oral Presentation).

**Ziels, R. M.**, and C. Greene. Modelling juvenile salmon migration through the nearshore using individual-based modeling techniques. *NOAA Science and Education Symposium*, Silver Spring, MD, July 2009. (Poster Presentation).

---

## Honors and Awards

- Water Environment Foundation (WEF) Canham Scholar Award (2015)
- National Science Foundation (NSF) Graduate Research Opportunities Worldwide Awardee; Laboratory of Microbiology, Wageningen University, Netherlands (2015)
- Garr M. Jones Scholarship, Brown & Caldwell (2014)
- University of Washington Valle Fellowship (2013)
- National Science Foundation (NSF) Graduate Research Opportunities Worldwide Awardee; Biogas Research Center, Linköping University, Sweden (2013)
- National Science Foundation (NSF) Graduate Research Fellowship (2011)
- Academic Excellence in the College of Natural Resources and Science, Humboldt State University (2011)
- Outstanding Graduate in Environmental Resource Engineering, Humboldt State University (2011)
- National Oceanic and Atmospheric Administration (NOAA) Ernest E. Hollings Scholarship Award (2008-2010)
- American Council of Engineering Companies (ACEC) California Scholarship Award (2010)
- Roscoe & Schenler Engineering Excellence Scholarship Award, Humboldt State University (2009)

---

## Funded Research Proposals

- Community Science Program – Small scale Metagenome Project (U.S. DOE, Joint Genome Institute, \$90,000 worth of sequencing granted, 2015-2016) (Co-PI, solely drafted research proposal)
- Water Environment Research Federation National Research Center for Resource Recovery and Nutrient Management (U.S. EPA, STAR\_N3R14A, \$218,348, 2013-2016) (was a major contributor to drafting research proposal)

## **Professional and Academic Societies**

---

Water Environment Federation (WEF), Member

American Society of Civil Engineers, Member

California Water Environment Association (CWEA), North Coast Chapter, Student Liaison  
(2008-2011)

Renewable Energy Student Union, Humboldt State University (2006-2011)

Campus Center for Appropriate Technology, Humboldt State University (2006-2011)

## **Professional Certifications**

---

Engineer in Training (EIT)